Idealized Models of Intrinsic Midlatitude Atmosphere-Ocean Interaction

by

Joseph J. Barsugli

A dissertation submitted in partial fulfillment of
the requirements for the degree of

Doctor of Philosophy

University of Washington

1995

In presenting this dissertation in partial fulfillment of the requirements for the Doctoral degree at the University of Washington, I agree that the library shall make its copies freely available for inspection. I further agree that extensive copying of this dissertation is allowable only for scholarly purposes, consistent with "fair use" as prescribed in the U.S. Copyright Law. Requests for copying or reproduction of this dissertation may be referred to University Microfilms, 1490 Eisenhower Place, P.O. Box 975, Ann Arbor, MI 48106, to whom the author has granted "the right to reproduce and sell (a) copies of the manuscript in microform and/or (b) printed copies of the manuscript made from microform."

Signature_____

Date _____

University of Washington

Abstract

Idealized Models of Intrinsic Midlatitude
Atmosphere-Ocean Interaction

by Joseph J. Barsugli
Chairperson of Supervisory Committee:Prof. Dennis Hartmann
Department of Atmospheric Sciences

An efficient two-level global general circulation model with simplified physical parameterizations is coupled to a 50 m constant-depth mixed-layer ocean. This model is used to study the effect of coupling on the intraseasonal and interannual variability of the atmosphere-ocean system in the midlatitudes on an all-ocean planet in the absence of tropical forcing. The coupled model circulation is compared with the atmosphere model forced by constant zonal mean sea surface temperatures (SST's) and prescribed time-dependent SSTs. Multidecadal integrations with constant annual-mean insolation are used for simplicity of interpretation and to ensure statistical significance of the results. It is found that coupling enhances SST anomaly variance and persistence, and leads to slow eastward propagation. These effects cannot be explained solely by the direct forcing of the atmosphere by SST anomalies. Linear regressions are used to diagnose a possible mechanism for these phenomena. The natural nolinear variability of the atmosphere is the main source of low frequency variability in this model. The feedback due to coupling with SST anomalies localizes this variabilty in such a way as to markedly enhance persistence, and produce propagation. The tentative explanation for the localization is found in the interaction between the barotropic structure of the natural variability and the baroclinic response of the atmosphere to low-level heating in this model. In order to simply explain the role of coupling in the three numerical model runs, a one-dimensional stochastically-forced coupled energy balance model is developed. SST and atmosphere spectra, total variance, and lag correlations are predicted.

TABLE OF CONTENTS

Page

List of Figures ii

List of Tables vii

Chapter 1: Introduction 1

Chapter 2: Model Description 12

Chapter 3: Coupling and Low Frequency Variability on an All-Ocean Planet: Experiment Design and Climatology. 30

Chapter 4: Effects of Coupling on Variance, Persistence, and Propagation of Low-Frequency Anomalies 59

Chapter 5: Coupling and Low-Frequency V ariability on an All-Ocean Planet: Discussion 138

Chapter 6: Variance and Coupling in a Stochastically Forced Energy Balance Model 150

Chapter 7: Conclusion 175

Bibliography 178

Appendix A: Persistence Algorithm 183

Appendix B: Budgets Using Linear Regression 185

Appendix C: Derivation of the Energy Balance Model 187

LIST OF FIGURES

Figure 2.1 Comparison longwave radiative parameterizations.

Figure 2.2. Moist convective adjustment function.

Figure 2.3. Fraction of insolation absorbed .

Figure 3.1. Schematic of experimental design.

Figure 3.2. Adjustment of COUPLED ocean temperature at selected latitudes.

Figure 3.3. Zonal mean climatology of winds, divergence, and temperatures.

Figure 3.4. Zonal mean climatology of SST and ocean-atmosphere temperature difference.

Figure 3.5. Zonal mean climatology of surface fluxes .

Figure 3.6. Zonal mean climatology of quadratic quantities.

Figure 3.7. RMS amplitude of spherical harmonic coefficients for model variable $\bar{\zeta}$ in the COUPLED run.

Figure 3.8 Same as in figure 3.7, except for model variable $\hat{\zeta}$.

Figure 3.9. Same as in figure 3.7, except for model variable $\hat{D}$

Figure 3.10. Same as in figure 3.7, except for model variable $\bar{\theta}$.

Figure 3.11. Same as in figure 3.7, except for model variable $\hat{\theta}$

Figure 3.12. Same as the top panel in figure 3.7, except for difference of between runs.

Figure 3.13. Same as the top panel in figure 3.8, except for difference of between runs.

Figure 3.14. Same as the top panel in figure 3.9, except for difference of between runs.

Figure 3.15. Same as the top panel in figure 3.10, except for difference of between runs.

Figure 3.16. Same as the top panel in figure 3.11,

Figure 4.1. Time-longitude plos for Southern Hemisphere SST index.

Figure 4.2. Time-longitude plots for Northern Hemisphere SST index

Figure 4.3. Snapshots of typical SST anomalies.

Figure 4.4. Variance of SST, $\bar{\theta}$, and $\bar{\zeta}$ as a function of latitude.

Figure 4.5. Variance of SST as a function of zonal wavenumber.

Figure 4.6. Power spectrum for midlatitude SST index.

Figure 4.7. Power spectrum for $\bar{\theta}$ at latitudes 41.5 N and 41.5 S.

Figure 4.8. Power spectrum for $\bar{\zeta}$ at latitudes 41.5 N and 41.5 S.

Figure 4.9. Power spectrum for total surface fluxes.

Figure 4.10. Power spectrum for total surface fluxes in MOGA and UNCOUPLED runs separately.

Figure 4.11. RMS amplitude in frequency-wavenumber domain of SST.

Figure 4.12. As in figure 4.11 except for differences between runs.

Figure 4.13. Normalized measure of SST anomaly persistence.

Figure 4.14. Unnormalized measure of SST anomaly persistence.

Figure 4.15. Lag regression maps for COUPLED run surface latent heat flux.

Figure 4.16. Lag regressions for COUPLED run surface sensible heat flux.

Figure 4.17. Lag regressions for COUPLED run surface net longwave flux.

Figure 4.18. Lag Regression maps for COUPLED run total surface heat flux.

Figure 4.19. As in Figure 4.18 except for UNCOUPLED run total surface heat flux.

Figure 4.20. As in Figure 4.18 except for MOGA run total surface heat flux

Figure 4.21. As in Figure 4.18 except for MOGA-RESPONSE run total surface heat flux

Figure 4.22. Lag regression maps for COUPLED 250 mb streamfunction.

Figure 4.23. Lag regression maps for COUPLED 750 mb streamfunction.

Figure 4.24. Lag regression maps for COUPLED 250 mb divergence.

Figure 4.25. Lag regression maps for COUPLED vertical mean potential temperature.

Figure 4.26. Lag regression maps for COUPLED vertical difference potential temperature .

Figure 4.27. Lag regression maps for COUPLED 250 mb eddy vorticity flux convergence.

Figure 4.28. Lag regression maps for MOGA 250 mb streamfunction.

Figure 4.29. Lag regression maps for MOGA 750 mb streamfunction.

Figure 4.30. Lag regression maps for MOGA vertical mean potential temperature.

Figure 4.31. Lag regression maps for UNCOUPLED 250 mb streamfunction.

Figure 4.32. Lag regression maps for UNCOUPLED 750 mb streamfunction.

Figure 4.33. Lag regression maps for UNCOUPLED vertical mean potential temperature,

Figure 4.34. Lag regression maps for MOGA-RESPONSE 250 mb streamfunction.

Figure 4.35. Lag regression maps for MOGA-RESPONSE 750 mb streamfunction.

Figure 4.36. Lag regression maps for MOGA-RESPONSE vertical mean potential temperature,

Figure 4.37. Lag regression maps for MOGA-RESPONSE vertical difference potential temperature.

Figure 4.38. Lag regression maps for MOGA-RESPONSE 250 mb divergence.

Figure 4.39. Lag regression maps for MOGA-RESPONSE 250 mb eddy vorticity flux convergence.

Figure 4.40. Steady LINEAR response to coupled sea surface temperature forcing. First set of variables.

Figure 4.41. Steady LINEAR response to coupled sea surface temperature forcing. Second set of variables.

Figure 4.42. 750 mb heat budget using linear regression for COUPLED run

Figure 4.43. As in figure 4.42 except for MOGA DIAGNOSTIC rregressions.

Figure 4.44. As in figure 4.42 except for UNCOUPLED DIAGNOSTIC regressions.

Figure 4.45. As in figure 4.42 except for MOGA-RESPONSE.

Figure 4.46. 250 mb vorticity budget for COUPLED run

Figure 4.47. Same as figure 4.46 except for MOGA DIAGNOSTIC run

Figure 4.48. Same as figure 4.46 except for UNCOUPLED DIAGNOSTIC run.

Figure 4.49. Same as figure 4.46 except for MOGA-RESPONSE

Figure 4.50. Same as figure 4.46 except for difference between COUPLED and UNCOUPLED DIAGNOSTIC runs.

Figure 4.51. Same as figure 4.46 except for difference between COUPLED and MOGA DIAGNOSTIC runs.

Figure 5.1. Coupled and uncoupled random walks.

Figure 5.2. Close-up of COUPLED run simultaneous regression maps.

Figure 5.3. Close-up of UNCOUPLED run simultaneous regression maps.

Figure 5.4. Close-up of MOGA run simultaneous regression maps

Figure 5.5. Close-up of MOGA RESPONSE run simultaneous regression maps.n

Figure 6.1. Predicted lag-correlation for stochastic SST equation with simple atmospheric feedback.

Figure 6.2. Diagram of simple energy balance model.

Figure 6.3. Averaged power spectrum of stochastic forcing term from UNCOUPLED run.

Figure 6.4. Stochastic model power spectra for white noise forcing with unit amplitude.

Figure 6.5. Ratio of power in SST in the limit as the frequency approaches zero.

Figure 6.6. Ratio of total power between COUPLED and UNCOUPLED runs.

Figure 6.7. Estimate of heat flux proportionality constant.

LIST OF TABLES

Table 2.1. Longwave Radiation Coefficients from Held, Linder, and Suarez (1981)

Table 2.2. Longwave Radiation Coefficients from OGI Model

Table 2.3. Cloudiness in Longwave Models.

Table 4.1. Total Variance for Pentad Means

Table 4.2. Mean Power in Midlatitudes at Lowest Frequencies

Table 6.1 . Standard Parameters for Stochastic Model

ACKNOWLEDGMENTS

The author would like to acknowledge the unique contribution of the stormy relationship and love of Robert Schmitt, and the continuing support and friendship of Mark Daley. Throughout the years technical assistance and moral support was received from Ileana Blade, Mark Borges, Marc Michelson, Jin-Yi Yu, Matt Newman, and a host of others. I would like to give special thanks to Prof. David Battisti, who helped enormously to bring this project to completion, and to Prof. Dennis Hartmann for his perseverence.

DEDICATION

To those I have lost -- Melba, Michael, and Mia; and to those I have found -- Bob, Whipple, Henry, June, and myself, during the long process of completing this degree. And to my father, Nick.

... Iff shrugged. ‘A P2C2E.’
‘And what is that?’
‘Obvious,’ said the Water Genie with a wicked grin. ‘It’s a Process Too Complicated To Explain.’

Salman Rushdie, **Haroun and the Sea of Stories**

Chapter 1 Introduction

The Earth’s climate is the product of a complicated web of interconnected physical and dynamical processes. Interactions among these processes can lead to changes in certain aspects of the climate on various space and time scales. For example average wintertime temperatures in a geographical region may vary from year to year. The large-scale patterns of climate variability at the seasonal to interannual time scales are often referred to as “low-frequency variability” by atmospheric scientists. In the past two decades there has been an explosion of observational and theoretical research into low-frequency variability, due in part to the increasing availability of large observational data sets and the increasing power and sophistication of numerical models. However our understanding of low-frequency variability is far from complete, and there are many basic questions thatremain to be answered.

One of these unanswered questions regards the role of the oceans in the midlatitudes. It is clear that the large-scale dynamics of the midlatitude atmosphere alone can generate low-frequency variability (Hendon and Hartmann, 1985). The ocean is also able to generate low-frequency anomalies simply due to the large heat capacity of its well-mixed upper layer acting as a low-pass time filter of atmospheric forcing. (Hasselmann 1976). The question remains: Is the interaction between these two processes important in determining the nature of low-frequency variability. The focus of this dissertation is on

using idealized models to enhance our theoretical understanding of the role of coupling between atmospheric dynamics and oceanic mixed-layer thermodynamics in the generation and spatial organization of low-frequency variability in the midlatitudes.

The research presented in this dissertation has applications to two of the major outstanding questions in the atmospheric sciences: extended-range prediction and the detection of anthropogenic climate change. Extended-range prediction is based on the hypothesis that, although we cannot predict the weather more than two weeks in advance, we can predict some statistical aspects of the climate out to a season or more in advance. The main focus of research into extended-range prediction has been on the response of the midlatitudes to tropical diabatic forcing, and in particular the response to large-scale tropical anomalies associated with the El Niño-Southern Oscillation (ENSO) phenomenon. The focus on tropical-extratropical interaction seems reasonable because ENSO is predictable several seasons in advance, and because there are statistically significant correlations between indices of ENSO and climate anomalies in certain midlatitude locations. Nevertheless, these correlations explain less than 50% of the seasonal mean 500 mb height variance and less than 25% of the monthly mean 500 mb height variance, even over the most sensitive regions. (Wallace, 1983). A better understanding of midlatitude atmosphere-ocean interaction may improve our understanding of tropical-extratropical interaction beyond the level of linear correlations, or at least lead to better theoretical limits on midlatitude predictability.

The application to climate change detection is less immediate, but nevertheless important. In order to determine the likelihood that an observed climate trend is or is not the result of anthropogenic sources, such as the increase in “greenhouse” gases due to industrialization, it is essential to understand the natural level of climate variability on

many different time and space scales. Unfortunately, the historical record is insufficient to establish a global picture of this variability, which leaves numerical modeling as the only option presently available. The trend has been to use ever more complicated numerical models, including coupled atmospheric and oceanic general circulation models (GCMs). Current research involves long runs of these coupled models -- on the order of 1000 years -- in order to investigate natural variability (e.g. Manabe and Stoufer (in press), and Schneider and Kinter (1994)). The advent of these long runs brings with it new interpretive problems, the primary one of which is determining the robustness of model results to details of the model architecture and choice of parameters. Mechanistic studies can be used to investigate possible interactions among different physical subsystems of the coupled model which might not be expected from studying the individual subsystems in isolation. Because these large coupled model runs take enormous amounts of computer time and generate enormous amounts of output, it is difficult to perform mechanistic studies. To this end, the use of idealized models such as the one used in this study can shed light on the important processes in the current and next generation of coupled GCMs.

1.1 The Role of Midlatitude SST Anomalies

Two conflicting views of the role of midlatitude sea surface temperature (SST) anomalies are prevalent. One is that the SST anomalies are an almost completely passive response to the atmosphere. The success of SST hindcasts in the midlatitudes by prognostic-depth mixed-layer models (Haney 1985, Gaspar 1988) is certainly an indication that a mixed-layer model can capture the essence of midlatitude ocean thermodynamics on seasonal time scales away from dynamically active regions such as the western boundary currents. This approach completely avoids any questions of coupling, as the atmospheric

fields used to force the ocean are themselves a product of the coupling. Another expression of the view of the passivity of the ocean is the claim of success for stochastic models in reproducing observed spectra, such as in Hasselmann (1976), and Frankignoul and Hasselmann (1977). The same criticism as above holds true. It is extremely difficult, if not impossible, to separate forcing from response using the observational data. However it is possible, by using an atmospheric GCM, to generate an “uncoupled” model atmosphere for comparison with a coupled model and ocean. Such a comparison forms a substantial part of the work presented in chapters 3-5 of this dissertation.

In contrast to the view of the ocean as passive, there is the view that the primary role of SST anomalies is to provide a crucial lower boundary condition to the atmosphere, determining the statistical properties of the overlying flow. Many experiments have looked at the response of the atmosphere to prescribed forcing, some of which are described in the following section. But these studies overlook a crucial point -- that the observed covariance between midlatitude SST anomalies and atmospheric anomalies includes forcing of SST anomalies by atmospheric patterns as well as the atmospheric response to SST forcing. Once again the problem of separating forcing from response is central and left unanswered. In order to investigate the role of direct forcing, I performed a numerical experiment in which an atmospheric GCM was forced by prescribed, time-dependent SST anomalies. The comparison of the direct forcing experiment with the coupled and uncoupled model runs is presented in chapters 3-5 of this dissertation. One result stands out in these simulations: the nature of low frequency variability in the coupled system is clearly different from that in the system in which time-dependent SST is prescribed, which is in turn different from that in the completely uncoupled system.

The theme that recurs throughout this dissertation is the following: the importance

of ocean mixed-layer thermodynamics in the midlatitudes lies both in the ability of SST anomalies to directly force the atmosphere, and in the ability of the ocean temperatures to adjust to the low frequency forcing from the atmosphere. The first depends on the *value* of the temperature at the lower boundary, while the second depends crucially on the *nature* of the boundary conditions. I will demonstrate that the two aspects of atmosphere-ocean interaction have qualitatively different effects on low-frequency variability, and that in terms of their effect on the overall amplitude of SST variability, the two effects are of comparable importance.

1.2 Previous Modeling Studies

There has been much work on various aspects of the coupled ocean-atmosphere problem in midlatitudes. The most recent general review article on midlatitude coupled ocean-atmosphere observations and modeling on seasonal time scales is Frankignoul (1985). This paper is highly recommended, particularly for its overview of stochastic models and for its discussion of the linear theory.

As mentioned before, Hendon and Hartmann (1985) demonstrated that nonlinear processes in a 2-level model atmosphere with zonally symmetric boundary conditions can generate low-frequency variability which is reasonable both in amplitude and structure. Numerous other studies have focused on the variability in two-level models. Most relevant to the present study are those by Robinson (1991a) and Qin and Robinson (1992). In the former, Robinson determines that feedback from high-frequency eddies reinforces low-frequency anomalies and slows their eastward propagation. In the latter the authors put forth barotropic mechanisms for the maintenance of low-frequency midlatitude circulation anomalies. The “in-phase” feedback mechanism, which reinforces the low-frequency

anomalies, results primarily from an modulation of meridional eddy vorticity flux by the deformation of high-frequency eddies. The “quadrature” feedback mechanism, which reinforces westward zonal propagation of the low-frequency anomalies relative to the mean flow, results from the modulation of the zonal eddy vorticity flux due to the deformation of the high-frequency eddies. The “in-phase” feedback is dominant at very long zonal wavelengths, while the “quadrature” feedback is dominant for shorter zonal wavelengths.

Numerous numerical experiments have been done to study the response of the atmosphere to prescribed SST anomalies or to prescribed atmospheric heating anomalies. Only a few will be mentioned, concentrating on those involving two-level models. Egger (1976) was the first to consider explicitly forcing by SST anomalies in a two-level model with spherical geometry. However he makes the fundamental error of assuming that the atmospheric heating is completely in phase with the SST anomaly (in general, heating in linear models is located one-quarter wavelength upstream from a maximum in SST). Phillips (1982) investigated the linear and nonlinear response to prescribed, constant SST anomalies in a quasigeostrophic, beta-plane, channel model. His model showed an equivalent barotropic response to SST forcing, but his runs were far too short to get good statistics. In fact, I suspect that what he calls the “nonlinear” response may be just a sampling of the natural variability.

Hoskins and Karoly (1983) investigated the linear response of a multi-level, linear, primitive-equation model on the sphere to idealized midlatitude atmospheric heating anomalies. They focused particularly on the dynamic balance in the region of heating and on the far-field response. For low-level heating in the midlatitudes they found that the heating is balanced mainly by anomalous meridional temperature advection. An argument

based on scale analysis supports this result. The far-field response is a barotropic wave-train. Hendon and Hartmann (1982) extended this work to include the effects of surface heat fluxes induced by the linear response to atmospheric heating. They found that the effect of surface fluxes is to enhance the low-level atmospheric heating and therefore to enhance the far-field response.

Some modeling studies with realistic GCMs (Palmer and Sun 1985, Pitcher et al. 1988) indicate that prescribed SST anomalies can influence the atmosphere, but exact nature of this is still unclear (Kushnir and Lau, 1992). Nevertheless, the magnitudes of the atmospheric anomalies associated with the midlatitude SST anomalies in these models indicate that these anomalies can have a substantial effect on the large scale atmospheric flow. More recently Lau and Nath (1994) have investigated the relative roles of tropical and midlatitude SST anomalies in affecting the midlatitude atmospheric variability by prescribing the time-dependent history of observed SSTs over restricted regions of the world's oceans while prescribing the climatological SSTs over the remainder of the ocean surface. Their experiments were labeled according to the region of prescribed SSTs: TOGA (Tropical Ocean, Global Atmosphere), MOGA (Midlatitude Ocean, Global Atmosphere) and GOGA (Global Ocean, Global Atmosphere). The MOGA experiment is particularly relevant to the work presented in this dissertation. They found that the MOGA run exhibited a "much weaker and less reproducible response" than the TOGA and GOGA runs.

Some work has been done on understanding the role of the midlatitude ocean mixed-layer in the response to ENSO forcing, most notably that of Alexander (1992a, 1992b). Using a predictive-depth mixed-layer coupled to the NCAR Community Climate Model (CCM), he established that the model captures the main pattern of Northern Pacific

SST variability associated with tropical ENSO forcing, and that the atmospheric circulation serves as the link between the tropical and extratropical ocean. He also compared the coupled model to an “uncoupled” model in which the ocean model is forced with CCM surface fluxes computed based on climatological SSTs. The coupled model exhibited a 25 to 50 percent reduction in the midlatitude SST anomalies associated with ENSO forcing compared to an uncoupled mode. The SST variance is also reduced. Coupling has a similar effect on the atmospheric thermal fields. Based on this result he concludes that atmosphere-ocean interaction acts primarily as a thermal damping process. His runs were too short to investigate with any certainly the feedback from the midlatitude SST anomalies back onto the atmospheric circulation.

Mechanistic studies of midlatitude variability involving coupling of atmospheric models to simple mixed-layer models have been few. Frankignoul (1985) presents analytical results from a 2-level linear quasigeostrophic model which are quite illuminating. He finds damped linear modes that propagate slowly eastward with phase speeds on the order of 5 - 10 cm s^{-1}. Salmon and Henderschott (1976) investigated the role of transients and static stability in composites centered around SST maxima. They used a simple, two-level quasigeostrophic GCM coupled to a shallow (10 meter) slab mixed-layer. The entire surface of the planet was ocean covered. The control run climatology was derived from the coupled run climatology, and no flux corrections were used. They then used the control run atmosphere to force a slave ocean model. While their integrations were too short to accumulate meaningful statistics, the results do show a tendency for coupling to cause slow eastward propagation (seen in their figure 8, though this is not mentioned in the text). The work in Chapters 3-5 of this thesis is indebted to their experimental design.

Miller and Roads (1990) investigated the extended range predictability in a simple

coupled model. They found that for 30 - 60 day prediction, using a coupled model is no better than using persistence of the original atmospheric field. However, specifying the "true" time-dependent SST field derived from the coupled run did improve forecast skill. Miller (1992) included geostrophic and Ekman flow and a 50 meter fixed-depth mixed layer in their ocean model, and did mechanistic studies of the variability in his model. He found a potential feedback mediated by anomalous temperature advection the Ekman flow in the ocean. In a linear analysis of a coupled model, Roads (1989) did find a linearly unstable coupled mode in the midlatitudes, but its significance is unclear. However, Alexander (1992a) found that Ekman flow had a minor effect on the coupled system in the midlatitudes, except perhaps near the oceanic polar front (approximately 40°N latitude). Ekman flow in the mixed-layer will not be considered in the present study.

There is some current research that points to subtle effects of coupling in organizing the natural low-frequency variability of the atmosphere. A recent study by N.-C. Lau (pers. comm.) compared two simulations involving the global atmosphere response to tropical SST forcing. In one the midlatitude SSTs were specified to be the climatological values (TOGA), and in the other a 50 m slab mixed-layer was used in the midlatitudes (TOGA-ML). In both simulations the time-dependent history of tropical SST was prescribed and a small ensemble of runs was performed with different atmospheric initial conditions. Although the Pacific North America (PNA) pattern of midlatitude variability as determined from an EOF analysis was essentially the same in both experiments, the time series of the PNA index was strikingly different. During the simulated 1982-3 ENSO warm event the TOGA-ML runs strongly favored one polarity of the PNA pattern whereas the TOGA runs showed a more nearly equal distribution of PNA polarity. Dymnikov (pers. comm.) has suggested the possibility of similar effect in the North Atlantic. He took

the first EOF of circulation over the North Atlantic from a GCM run, and modeled its time dependence as consisting of two regimes, which are determined in the course of the analysis to be a blocking ridge and a zonal flow state. As in Lau's research, he compared two runs--one in which the SST was prescribed, and the other in which SST was determined by a 50 m mixed layer. There was no anomalous tropical forcing in Dymnikov's simulation. His regime analysis indicated that when the mixed layer was included, the probability of being in the blocking state vs. the zonal flow state was altered in favor of the blocking state. I have been informed that Dymnikov's results are very sensitive to the parameters used and should be considered preliminary. Nevertheless, the above results are tantalizing and point to the need for simple experiments to provide a theoretical basis for the behavior of the atmosphere when coupled to even the simplest of ocean models.

1.3 Road Map of the Dissertation

This dissertation presents two approaches to investigate the simplest effect of coupling of the atmosphere to the ocean in the midlatitudes. First, simulations with a 2-level atmosphere GCM with simplified physics and an all-ocean geometry are used to investigate the effects of coupling. Second, a stochastically forced energy-balance model is used to investigate some properties of the spectra of the coupled systems.

The thesis is organized as follows. Chapter 2 is a description of the coupled numerical model used in this study. Chapter 3 presents the experiment design and climatologies of the model runs. Chapter 4 presents the phenomenology of the effects of coupling and direct forcing in these experiments. These results are then discussed and interpreted in Chapter 5. Chapter 6 develops and presents a simple, stochastically-forced, energy balance model which captures some of the features of midlatitude variability seen in the experi-

ments with the nonlinear numerical model. Finally, Chapter 7 summarizes the main points from the previous chapters and points the direction to future research.

All is for the best in the best of all possible worlds.

Voltaire, **Candide**

Chapter 2: Model Description

2.1 Introduction

The atmosphere model can best be described as combining the numerics of Hendon and Hartmann (1985, henceforth HH) with the physics of Held and Suarez (1978, henceforth HS), with some modifications to both. The result is a 2-level, global, spectral transform, primitive equation model with reasonably complete physics which runs with acceptable speed at T21 (triangular - 21) truncation on a workstation for long integrations[1]. This model is intended for mechanistic studies. The many idealizations involved in formulating the physics and dynamics can be seen as assets because they simplify interpretation, even though they may reduce the fidelity of the model output to the climatology of the atmosphere. The model was originally coded to include an arbitrary distribution of land and ocean with zonally asymmetric physics, lower-level moisture advection and a simple precipitation parameterization, as in Semtner's (1984) version of the HS model. The current study only uses a "dry" version of this model in which there is no advection of moisture. Instead, latent heat is released immediately and locally, and the atmosphere is convectively adjusted to a moist-neutral profile.

The present model was coded from scratch, using the HH code as a rough guide. One great strength of this model as it is presently coded is its modularity and therefore its flexibility. The time stepping scheme and the physical parameterizations can be easily

1. On a single processor of a Sparcserver 1000 the "dry" model simulates 500 days per hour of CPU time, and occupies approximately 300 K of memory.

changed. Coupling to more complex ocean models would be relatively easy. The two main areas of inflexibility are the horizontal discretization, which must remain spectral (though different resolution and rhomboidal truncation are supported) and the vertical discretization, which must remain 2-level. In addition, the atmosphere model is coded to evaluate nonlinear terms and physics one latitude belt at a time, and any proposed changes which require changing this structure are cumbersome, but straightforward.

2.2 Model Equations and Vertical Discretization

As in HH, the primitive equations in pressure coordinates on the sphere can be written:

$$\frac{\partial \zeta}{\partial t} = -\nabla\bullet(\underset{\sim}{\mathbf{v}}(\zeta + f)) - k \bullet \nabla\times\left(\omega\frac{\partial}{\partial p}\underset{\sim}{\mathbf{v}} + \underset{\sim}{F}\right), \qquad \text{(EQ 2.1a)}$$

$$\frac{\partial D}{\partial t} = k \bullet \nabla\times(\underset{\sim}{\mathbf{v}}(\zeta + f)) - \nabla\bullet\left(\omega\frac{\partial}{\partial p}\underset{\sim}{\mathbf{v}} + \underset{\sim}{F}\right) - \nabla^2\left(\phi + \frac{\underset{\sim}{\mathbf{v}} \bullet \underset{\sim}{\mathbf{v}}}{2}\right), \qquad \text{(EQ 2.1b)}$$

$$\frac{\partial \theta}{\partial t} = -\nabla\bullet(\underset{\sim}{\mathbf{v}}\theta) - \frac{\partial}{\partial p}(\omega\theta) + \Pi Q, \qquad \text{(EQ 2.1c)}$$

$$\nabla\bullet\underset{\sim}{\mathbf{v}} + \frac{\partial \omega}{\partial p} = 0, \qquad \text{(EQ 2.1d)}$$

$$\frac{\partial \phi}{\partial p} = -\frac{R\theta}{p\Pi}, \qquad \text{(EQ 2.1e)}$$

where the prognostic variables are vorticity, ζ, divergence, D, and potential temperature, θ. The other variables in the above equations are: horizontal velocity, $\underset{\sim}{\mathbf{v}}$, vertical (pressure) velocity, ω, and geopotential ϕ. The mechanical and thermal forcings are represented by $\underset{\sim}{F}$ and Q respectively. The Coriolis parameter is f, and the proportionality between temperature and potential temperature is given by

$$\Pi = \left(\frac{p_s}{p}\right)^{R/c_p},$$

where R is the gas constant for dry air, c_p is the specific heat of dry air, and $p_s = 1000\ \text{mb}$. In addition to the above we have the sea surface temperature (SST) equation:

$$c_e \frac{dT_o}{dt} = F_S, \qquad \text{(EQ 2.1f)}$$

where c_e is the effective specific heat of a column of water in the mixed layer and F_s is the net surface heat flux.

The model is discretized in the vertical following HH. The two model levels are denoted by numeric subscripts: $(\ )_1$ for the upper level at 250 mb and $(\ )_2$ for the lower level at 750 mb. An overbar ($\overline{\ }$) represents the vertical mean of the two levels, and a hat, ($\hat{\ }$) represents half the difference between upper and lower levels. Equations 2.1a-e become:

$$\frac{\partial}{\partial t}\bar{\zeta} = -\nabla\bullet(\bar{\underset{\sim}{\mathbf{v}}}(\bar{\zeta} + f) + \hat{\underset{\sim}{\mathbf{v}}}\hat{\zeta}) - k \bullet \nabla\times(\hat{\underset{\sim}{\mathbf{v}}}\hat{D}) + K_D\nabla^4\bar{\zeta} - C_D\zeta_2/2\ , \qquad \text{(EQ 2.2a)}$$

$$\frac{\partial}{\partial t}\hat{\zeta} = -\nabla\bullet(\hat{\underset{\sim}{\mathbf{v}}}(\bar{\zeta} + f) + \bar{\underset{\sim}{\mathbf{v}}}\hat{\zeta}) + K_D\nabla^4\hat{\zeta} + C_D\zeta_2/2, \qquad \text{(EQ 2.2b)}$$

$$\frac{\partial}{\partial t}\hat{D} = -k \bullet \nabla\times(\hat{\underset{\sim}{\mathbf{v}}}(\bar{\zeta} + f) + \bar{\underset{\sim}{\mathbf{v}}}\hat{\zeta}) - \nabla^2(\bar{\underset{\sim}{\mathbf{v}}} \bullet \hat{\underset{\sim}{\mathbf{v}}}) \qquad \text{(EQ 2.2c)}$$
$$- c_p\hat{\Pi}\nabla^2\bar{\theta} + K_D\nabla^4\hat{D} + C_D\hat{D}/2,$$

$$\frac{\partial}{\partial t}\bar{\theta} = -\nabla\bullet(\bar{\underset{\sim}{\mathbf{v}}}\bar{\theta} + \hat{\underset{\sim}{\mathbf{v}}}\hat{\theta}) + K_D\nabla^4\bar{\theta} + \overline{\Pi Q} + \bar{Q}_{CONV}, \qquad \text{(EQ 2.2d)}$$

$$\frac{\partial}{\partial t}\hat{\theta} = -\nabla\bullet(\hat{\mathbf{v}}\bar{\theta} + \bar{\underset{\sim}{\mathbf{v}}}\hat{\theta}) + \bar{\theta}\hat{D} + K_D\nabla^4\hat{\theta} + \widehat{\Pi Q} + \hat{Q}_{CONV}. \qquad \text{(EQ 2.2e)}$$

Here we have included biharmonic diffusion of momentum and temperature, with diffusion coefficient K_D, and linear surface drag, with coefficient C_D. Q_{CONV} is the heating

due to convective adjustment. The thermal forcing at each level of the atmosphere is the sum of shortwave heating (SW), net longwave heating (LW), turbulent sensible heat flux convergence (SH) and latent heat release (LH):

$$Q = Q_{\mathrm{SW}} + Q_{\mathrm{LW}} + Q_{\mathrm{SH}} + Q_{\mathrm{LH}}.$$

The equation for ocean temperature, 2.1f, becomes:

$$c_e \frac{dT_o}{dt} = F_{SW} - (F_{LW} + F_{SH} + F_{LH}), \qquad \text{(EQ 2.2f)}$$

where the effective specific heat of the surface, $c_e = \rho_o c_o h$ is that of a $h = 50$ m slab of water at ocean gridpoints. The right hand side is the sum of the various surface heat fluxes. With the exception of the surface shortwave flux, all fluxes will be defined so that a positive value denotes a net upward flux.

2.3 Physical Parameterizations

2.3.1 Longwave Radiation

The longwave radiative fluxes are computed using the same method as in HS. They applied this parameterization in the zonal mean only, applying linear damping to the zonal eddies. In order to accommodate a zonally asymmetric surface I calculate the longwave fluxes at each gridpoint as in Semtner (1984). Because this results in a thermal damping of the eddies, the linear eddy damping used in HS is turned off. One result is that the time scale of damping in the polar regions, where temperatures are cold, is relatively slow compared to that for uniform linear eddy damping of HS, or for that matter of most other simple two-level models driven by relaxation to a thermal equilibrium. I find this to be a more realistic aspect of this model. I should emphasize that the parameterization assumes the same distribution of clouds at every point on the globe. The gross effects of water-vapor,

however, are implicitly included through the dependence of the parameterization on the atmospheric temperatures.

The longwave parameterization is based on look-up tables from which one calculates the net flux of longwave radiation at the surface, 500mb and the top of the atmosphere (TOA) based on the temperatures at the two atmospheric levels and on the difference between the surface air temperature and the SST. The convergence of the longwave flux into each layer is then used as the heating rate for that layer. The surface is assumed to act as a perfect blackbody. The look-up table of coefficients can be found in Held, Linder and Suarez (1981, henceforth HLS) and are reproduced here in Table 2.1. The meaning of the coefficients a_1, b_1, etc. in this table is as described in in HS and HLS. As noted in HLS, the original table in HS contains several errors. These values are derived from a Rogers and Walshaw (1967)-type longwave radiation model as described in HS.

Since these coefficients were derived from a 1970's-era radiation model, I was curious how they would compare to coefficients derived from a more recent model. To this end I repeated the derivation of the coefficients using the radiation code from the Oregon Graduate Institute's 1D RCM model (MacKay and Khalil, 1991). The new coefficients are shown in Table 2.2. The OGI model includes a more modern treatment of the water vapor continuum and includes the effects of trace gases. The average cloud distribution could not be handled in exactly the same manner as in HS, but the levels were approximated as closely as possible. The cloud levels and amounts are shown in Table 2.3. The original HS (and Manabe and Wetherald) calculation assumed random overlap of colouds at different levels. For example, it was assumed that the fraction of time that middle and low clouds were simultaneously present was the product of the the fractions for middle and low cloud occurrance given in the rows of Table 2.3 denoted by the abbreviation "HS". Since only a

single cloud layer in one of the OGI model's 18 fixed model layers could be included at a time, cloud overlap was handled in the following, somewhat arbitrary manner. Individual runs of the OGI radiation code were done for clear sky conditions and for high, middle, and low cloudiness, with cloud heights as specified in Table 2.3. The average longwave fluxes were computed using a weighted average of the fluxes from the individual runs. The weights were determined from the cloud amounts used in HS (which in turn were taken from Manabe and Strickler, 1964) by adding up the fraction of time when only a single cloud layer was present with partial contributions from times when a given cloud layer is present simultaneously with another layer or layers. This choice of what is meant by "partial contribution" was rather arbitrary, and is indicated schematically in the "comments" column of Table 2.3. In this column, H, M and L stand for the fraction of high, middle, and low cloud amount as shown in the first three rows of this table. As in Manabe and Wetherald, the high clouds were assumed to have an emissivity of 0.5 in the infrared. This was approximated by treating the clouds as blackbodies, but reducing the high cloud amount by a factor of 0.5. The reduced cloud amounts for high clouds is shown in parentheses in Table 2.3. The original Manabe and Wetherald (1967) vertical profile of relative humidity was used in the new radiative calculations.

The look-up table coefficients calculated using the OGI model (Table 2.2) differ somewhat from those in HLS (Table 2.1), but for the range of temperatures seen in this model, the radiative fluxes are remarkably similar. This agreement in radiative fluxes is seen in plots of net radiation at the TOA, 500mb level and surface as a function of vertical mean potential temperature $\bar{\theta}$, shown in figure 2.1a-c. The difference between the fluxes derived from the new model and those from the HS model are shown in figure 2.1d. In all the plots in figure 2.1 we have fixed the air-sea temeprature difference to be 1.8 K and the

vertical “stability”, $\hat{\theta}$ to be 10 K, but allowed $\bar{\theta}$ to vary. The primary differences due to the new parametrization are as follows: a reduction in TOA net upward flux which is greatest for large mean atmospheric potential temperature $\bar{\theta}$, a reduction in upward flux at 500 mb for $\bar{\theta} < 35$ K and an increase in 500 mb flux for $\bar{\theta} > 35$ K, a decrease in downward flux at the surface for most values of $\bar{\theta}$. The comparison of the climatologies of test runs using the two parameterizations (now shown) revealed a 1K increase in the tropical temperatures when the new radiative parameters were used, which is a small improvement in the climatology. However, in a simple numerical model used for mechanistic studies, differences of this magnitude are insignificant. The runs described in the following three chapters were done using the new longwave coeficients. However, a previous set of analogous runs of 6000 days each using the HLS coefficients showed the same phenomena.

2.3.2 Shortwave Radiation

The shortwave fluxes are also calculated using the parameterization of HS, which is described in detail in HLS. The shortwave parameterization is derived from the model of Manabe and Strickler (1964), using their estimated global mean high, middle and low cloudiness. Since the shortwave fluxes are remarkably insensitive to the temperature variations typically found around a latitude circle in the midlatitudes, in the present model the shortwave fluxes are calculated only for the zonal mean. The only free parameter in the HS radiative calculations is the surface albedo, for which both HS and the present study use a value of 0.1 globally. If land is included in the model, it is specified to have a higher albedo than ocean, usually 0.3, then two values of shortwave forcing are calculated at each latitude circle, one for land and one for ocean. Diagnostic plots for shortwave radiation for the range of typical model temperatures is shown in Figure 2.2, making the same assump-

tions as in figure 2.1. In panel 2.2a we have plotted the fraction of TOA insolation that is absorbed in the upper layer of the atmosphere (0 - 500 mb) as a function of mean atmospheric temperature and the cosine of the zenith angle. In panels 2.2b and 2.2c the same is shown for the lower layer of the atmosphere(500 - 1000mb) and the surface, assuming a surface albedo of 0.1. Since the solar heating is only applied in the zonal mean in the runs shown in this dissertation, it is only capable of contributing to the zonal mean variability.

2.3.3 Surface Fluxes

The surface fluxes of heat and moisture are computed using bulk aerodynamic formulas:

$$F_{\mathrm{SH}} = \rho_a C V_c c_p (T_o - T_s), \qquad \text{(EQ 2.3a)}$$

$$F_{\mathrm{LH}} = \rho_a C V_c L (q_s(T_o) - r_o q_s(T_s)) \ . \qquad \text{(EQ 2.3b)}$$

The surface quantities which go into the above formulas are calculated as follows:

$$V_c = \max(5\ \mathrm{m}/s, |\mathbf{v}_2|), \qquad \text{(EQ 2.4a)}$$

$$T_s = 0.986\ \bar{\theta} - 1.337\ \hat{\theta}. \qquad \text{(EQ 2.4b)}$$

V_c is the surface wind speed for flux computations, and is set to a minimum of 5 m/s. T_s is the surface air temperature, linearly extrapolated in log-pressure coordinates from the upper and lower level temperatures. The surface relative humidity is set to a constant value of $r_o = 0.8$. In the above, only the determination of the surface wind speed differs from HS.

In the “dry” version of the model used in the present study, the latent heat is released immediately and locally. The surface fluxes are deposited in the lowest 500 mb of the atmosphere, therefore:

$$(Q_{\mathrm{SH}})_2 = \frac{g}{c_p \Delta p} F_{\mathrm{SH}}$$

$$(Q_{\mathrm{LH}})_2 = \frac{g}{L \Delta p} F_{\mathrm{LH}}$$

where $\Delta p = 500\ \mathrm{mb}$.

2.3.4 Moist Convective Adjustment

Immediately after the spectral atmospheric variables are transformed to the physical space grid, the atmosphere is adjusted to a moist-neutral profile. In addition to adjusting the physical space variables, the convective heating rates are saved, and later transformed to spectral space along with the other nonlinear and physical forcings for use in time-stepping the spectral space variables. The adjustment procedure closely follows HS, but in the present "dry" model the adjustment to a moist adiabatic profile is unconditional.[1] The convective adjustment conserves $c_p(T_1 + T_2)$. To do this, we first calculate the vertical mean atmospheric temperature $\bar{T} = (T_1 + T_2)/2$. We then calculate $\hat{\theta}_{\mathrm{crit}}(\bar{T})$, which is the value of $\hat{\theta}$ for a moist adiabatic profile with mean temperature $\bar{T}$. A plot of $\hat{\theta}_{\mathrm{crit}}$ as a function of $\bar{T}$ is shown in figure 2.3 (see HS figure 3 for comparison). As in HS, the convective adjustment is performed by relaxation to the convectively adjusted temperature with a time scale of $\tau_{conv} = 8$ hours This is implemented in the current model as follows: When $\hat{\theta} < \hat{\theta}_{crit}$,

$$\bar{Q}_{conv} = \frac{\bar{\theta}_{crit} - \bar{\theta}}{\tau_{conv}},$$

$$\hat{Q}_{conv} = \frac{\hat{\theta}_{crit} - \hat{\theta}}{\tau_{conv}},$$

and in physical space,

1. In contrast, HS adjust to a constant value of $\hat{\theta} = 2.5\ \mathrm{K}$ in their "dry" model.

$$\hat{\theta} \rightarrow \hat{\theta} + \hat{Q}_{conv}\Delta t\,,$$
$$\bar{\theta} \rightarrow \bar{\theta} + \bar{Q}_{conv}\Delta t\,.$$

Previous simulations with the moist version of this model required special measures to suppress variance in the tropics due to unstable convective-dynamical modes. The simplest method is to put all the convective heating into the zonal mean. The present “dry” model requires no such special efforts.

2.3.5 Diffusion and Surface Drag

As indicated above, biharmonic diffusion of heat and momentum are included in order to compensate for the buildup of enstrophy at the limits of the horizontal truncation. The diffusive time scale is equivalent to a damping time of 2 days at total wavenumber N=21. This is a relatively low value of diffusion for a T21 truncation (cf. Yu and Hartmann, 1993). The time scale of the linear drag in the lower level is 5 days.

2.4 Numerics

The atmospheric equations are formulated using the spectral-transform method -- all nonlinear terms are calculated on a Gaussian grid in physical space with 64 gridpoints in the zonal direction and 32 in the meridional direction. Thus the gridpoints are located roughly every 5.5 degrees in latitude and longitude. The nonlinear terms and are then transformed to spectral space for time stepping.

I calculate the time change in the linear terms involving gravity waves, diffusion and drag in the equations of motion using a semi-implicit time scheme. As in HH, the zonal-mean internal gravity waves are treated fully implicitly to help damp them out. Unlike either HH or HS, I use a third-order Adams-Bashforth time scheme (Durran, 1990) for the

nonlinear terms in the atmospheric equations. All advective terms are treated this way, as are all thermal forcing terms (including the convective heating). This scheme was chosen because of its 3-rd order accuracy in amplitude and 4-th order accuracy in phase, and because of its stability, robustness and simplicity. The general form is:

$$X_{n+1} = X_n + \frac{\Delta t}{12}(23F_n - 16F_{n-1} + 5F_{n-2}) .$$

In general there is no advantage to using this scheme in a model with semi-implicit timestepping of fast-wave terms. However, the fact that this model is non-divergent means that the fastest wave speed (the equatorial internal Kelvin wave, approximately 60 m s^{-1}) is approximately the same as the fastest advective time scales of the midlatitude westerly jet (50-70 m s^{-1}). Therefore the maximum time step determined by the Courant-Friedrichs-Levy (CFL) criterion is usually set by the maximum advective speed, and there is no disadvantage to using the Adams-Bashforth scheme.

The surface temperature equations are handled in a simpler manner. For the fixed-depth mixed-layer the time stepping is a simple forward difference. This gives the exact solution to a piecewise constant forcing. Over land (not used in this study), the instantaneous surface energy balance is solved by a Newton-Raphson iteration as in the NCAR CCM (Williamson et al., 1987). The method is iterated until the change in surface temperature from the previous iteration is less than 0.01 K. This iteration usually converges in one or two steps.

2.5 Discussion

From a dynamical point of view, the coarse vertical discretization is the most serious shortcoming of the model. The 2-level discretization in the vertical is able to capture the character of midlatitude variability surprisingly well. However, one might expect ocean-

atmosphere interaction in the real world to involve, at least in part, the interaction of shallow, surface-forced, disturbances with the dynamics of the free atmosphere. Any such effects would be poorly modeled in the present study. In effect, the highly damped lower level of the model acts as a hybrid of the 750 mb level in the real atmosphere and the planetary boundary layer, and shares characteristics of both. In addition, the reader is advised to exercise caution in the interpretation of these results due to the possible effects of the rigid lid upper boundary condition. This condition prohibits the upward propagation of large-scale baroclinic waves that would otherwise take place, leading to the possibility of resonance or instability which is artificial. However for zonal wavenumber 5, which is roughly the equivalent-barotropic stationary wavenumber in the midlatitude waveguide in the model runs which will be presented, we should be well within the range where the tropopause acts as a significant wave reflector (Held, 1983).

Geophysical models almost invariably involve a trade-off between simplicity and realism. I have chosen a middle course in the choice of numerical model. The two-level atmospheric model presented here is quite idealized -- particularly in the vertical structure and the absence of land and the omission of moisture advection and precipitation -- and this involves a sacrifice of realism. Yet, I believe the big picture of the Earth's circulation remains recognizable in these model results, and I hope that the reader, in the course of reading this dissertation, can implicitly take into account the model's distortions of reality.

Table 2.1: Longwave Radiation Coefficients from Held, Linder, and Suarez (1981)

$\bar{\theta}$	a_1	b_1	c_1	a_2	b_2	c_2	a_3	b_3
-30.	109.0	-1.10	1.00	121.3	-2.18	1.26	104.3	-1.72
-25.	118.0	-1.16	1.01	131.0	-2.29	1.25	119.1	-2.06
-20.	127.4	-1.22	1.01	140.8	-2.28	1.25	134.7	-2.37
-15.	136.9	-1.26	1.01	150.6	-2.47	1.25	150.9	-2.65
-10.	146.8	-1.30	1.01	160.0	-2.52	1.26	167.8	-2.91
-5.	156.8	-1.34	1.01	168.3	-2.55	1.26	185.7	-3.17
0.	167.2	-1.37	1.01	176.4	-2.60	1.26	204.9	-3.44
5.	177.6	-1.40	1.01	183.7	-2.64	1.25	225.7	-3.74
10.	188.3	-1.42	0.99	190.6	-2.68	1.24	248.1	-4.06
15.	199.2	-1.43	0.97	197.0	-2.72	1.21	271.9	-4.40
20.	210.0	-1.44	0.95	202.8	-2.74	1.18	297.1	-4.74
25.	221.0	-1.44	0.92	208.1	-2.75	1.15	323.6	-5.08
30.	232.1	-1.43	0.88	213.1	-2.76	1.10	351.8	-5.45
35.	243.2	-1.41	0.83	217.6	-2.75	1.04	382.4	-5.85
40.	254.2	-1.39	0.77	221.7	-2.73	0.96	415.7	-6.32
45.	265.0	-1.35	0.68	225.0	-2.69	0.85	452.0	-6.85
50.	275.6	-1.30	0.59	227.8	-2.65	0.74	491.4	-7.43
55.	286.1	-1.24	0.48	230.2	-2.60	0.61	533.7	-8.04
60.	296.2	-1.16	0.39	231.9	-2.53	0.48	578.3	-8.66
65.	306.0	-1.08	0.30	233.0	-2.45	0.37	624.7	-9.25
70.	315.6	-0.98	0.24	233.6	-2.36	0.29	672.2	-9.79

Table 2.2: Longwave Radiation Coefficients from OGI Model

$\bar{\theta}$	a_1	b_1	c_1	a_2	b_2	c_2	a_3	b_3
-30	114.8	-1.32	0.80	122.0	-2.10	1.03	105.1	-2.04
-25	123.4	-1.36	0.82	130.8	-2.17	1.05	118.4	-2.29
-20	132.1	-1.39	0.84	139.6	-2.24	1.08	132.4	-2.53
-15	141.2	-1.42	0.85	148.8	-2.31	1.10	147.2	-2.75
-10	150.5	-1.45	0.86	156.9	-2.35	1.12	162.8	-2.96
-5	160.1	-1.47	0.87	165.2	-2.41	1.14	179.2	-3.18
0	170.0	-1.50	0.89	173.2	-2.48	1.17	196.6	-3.40
5	180.0	-1.52	0.90	180.9	-2.55	1.19	215.2	-3.63
10	190.5	-1.54	0.91	188.5	-2.62	1.21	235.3	-3.91
15	200.9	-1.55	0.91	195.8	-2.69	1.23	257.3	-4.24
20	211.3	-1.53	0.91	202.7	-2.73	1.23	282.0	-4.65
25	221.7	-1.50	0.89	209.1	-2.76	1.21	309.6	-5.15
30	232.1	-1.46	0.85	215.2	-2.77	1.18	339.9	-5.69
35	242.5	-1.42	0.80	220.8	-2.77	1.12	372.6	-6.25
40	253.0	-1.37	0.75	226.0	-2.75	1.06	408.7	-6.88
45	263.1	-1.31	0.70	230.9	-2.73	1.00	450.6	-7.73
50	272.7	-1.21	0.65	235.0	-2.67	0.92	499.2	-8.79
55	282.0	-1.09	0.59	238.4	-2.60	0.83	550.0	-9.74
60	291.3	-0.97	0.53	241.3	-2.52	0.74	596.6	-10.21
65	300.8	-0.87	0.49	244.0	-2.47	0.66	636.8	-10.19
70	310.6	-0.79	0.48	246.4	-2.45	0.63	674.2	-10.02

Table 2.3: Cloudiness in Longwave Models.

	height(km)	Amount	Comments
High (HS)	10	.228 (.114)	
Middle (HS)	4.1	.090	
Low (HS)	1.7-2.7	.313	
High (New)	8.4-10.2	.18 (.09)	H only + 1/2 HL
Middle (New)	3.4-4.4	.08	M only + HM + 1/2 LM
Low (New)	1.7-2.5	.28	L only + 1/2 HL + 1/2 LM

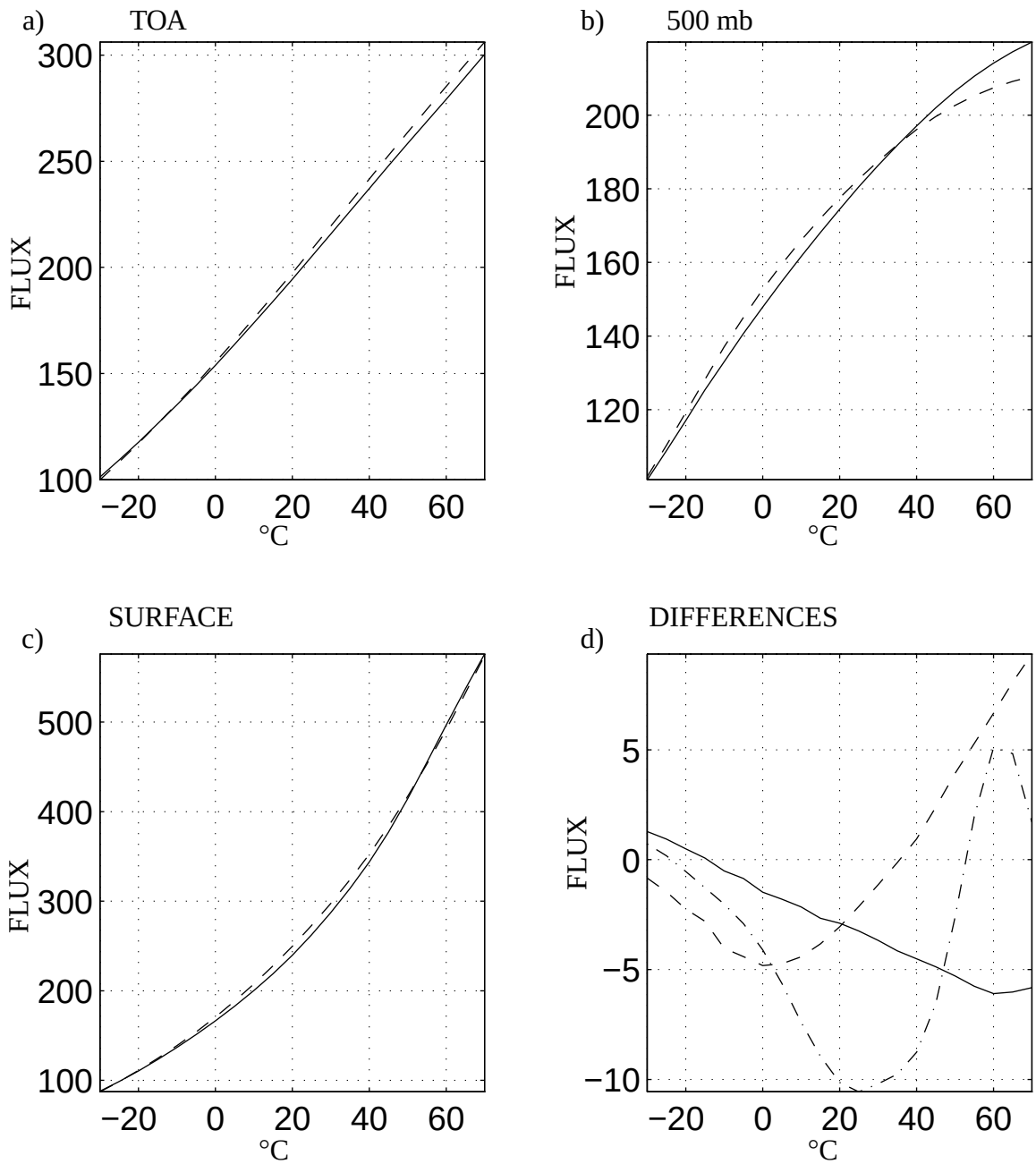

Figure 2.1 Comparison of new longwave radiative parameterization (New) with Held and Suarez (HS) model as a function of mean potential temperature for the following parameter choice: Air-sea temperature difference, $T_o - T_s$ = 1.8 K , stability, $\hat{\theta}$ = 10 K. a) Top of atmosphere (TOA) upward flux. b) 500 mb upward flux. c) Surface downward flux. New (solid lines), HS (dashed lines) in figures a-c. d) Differences: New- HS. TOA (solid line), 500 mb (dashed line), surface (dash-dot line). Units of flux are Wm^{-2}.

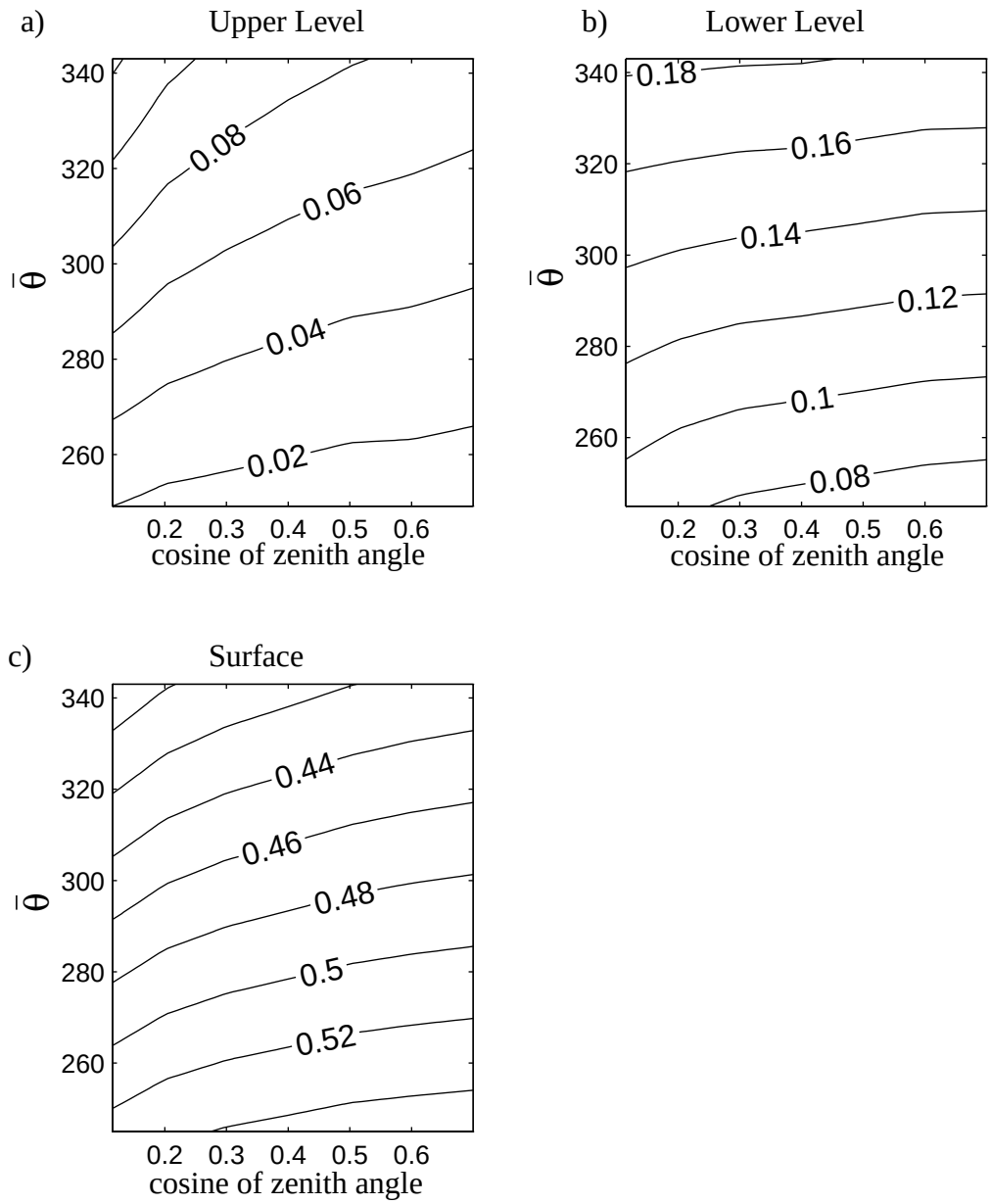

Figure 2.2. Fraction of insolation at the top of the atmosphere which is absorbed a) in the upper layer, b) in the lower layer, c) at the surface, as a function of $\bar{\theta}$ and of the cosine of the zenith angle. Surface albedo = .1, $\hat{\theta}$ = 10 K.

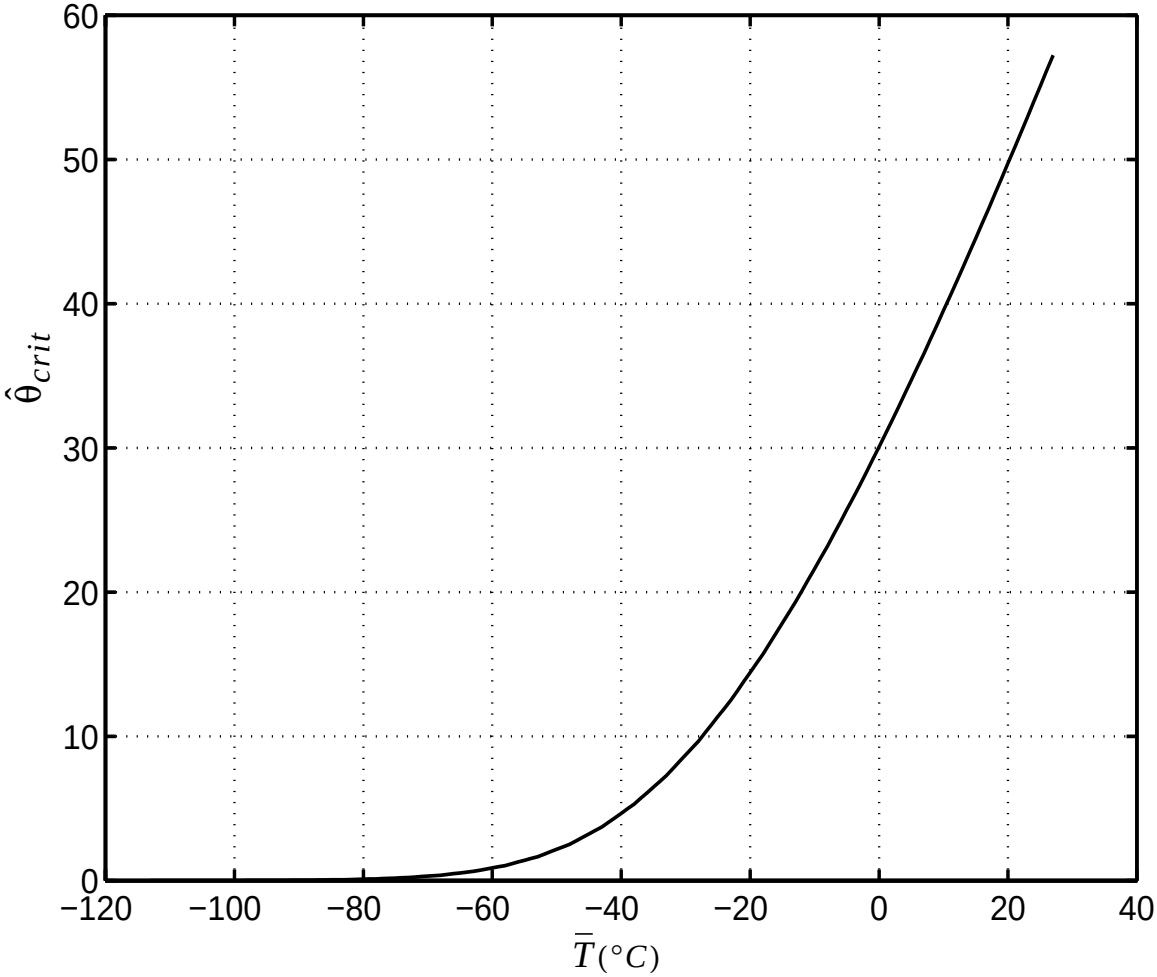

Figure 2.3. Moist convective adjustment function $\hat{\theta}_{crit}(\bar{T})$ as described in text.

He had bought a large map representing the sea,
Without the least vestige of land:
And the crew were much pleased when they found it to be
A map they could all understand.

Lewis Carroll, **The Hunting of the Snark**

Chapter 3: Coupling and Low-Frequency Variability on an All-Ocean Planet: Experiment Design and Climatology

3.1 Goals

In this chapter and in the following two chapters, the coupled model described in Chapter 2 is used to study the effect of coupling on low-frequency variability on an all-ocean planet with constant, annual-mean insolation. The numerical simulations will answer, in the context of the model, the following questions:

- Does coupling enhance low-frequency variability? If so, by how much, in which model variables, and at which frequencies and wavenumbers.
- Does coupling increase the persistence of low-frequency anomalies?
- Are any new modes of variability introduced by the coupling? If so, can a simple linear or nonlinear mechanism be deduced?
- What is the relative importance of the feedback loop allowed by coupling compared to the direct forcing of the atmosphere by SST anomalies.

This chapter begins with a detailed description of the methodology used in the numerical experiments and a presentation of the climatology of the model runs. Chapter 4 presents the results of the numerical integrations focusing in turn on the variance and

power spectra of SST and other selected variables, the propagation of SST anomalies and the associated frequency-wavenumber spectra, and the persistence of SST anomalies. A more detailed examination of the horizontal and vertical structure of the atmospheric anomalies associated with SST anomalies is presented. Chapter 5 contains a discussion of possible mechanisms for interpreting some of the results of Chapter 4.

3.2 Description of the Numerical Experiments: COUPLED, MOGA, and UNCOUPLED[1]

The goal of the experiment design is to create a set of runs with nearly identical time-mean climatologies which enable us to separate i) the effect of feedback due to atmosphere-ocean interaction from ii) the natural variability of the atmosphere alone and from iii) the effect of direct forcing of the atmosphere by SST anomalies. Since the climatology of the atmosphere is strongly dependent on the SST, the most practical way of assuring comparable atmosphere climatologies is to do the COUPLED model run first, and then use the SST from that run to derive the lower boundary condition for the control runs.

I will choose two different prescriptions for the control run SSTs. The first is to use the *zonal mean* of the climatological SST from the COUPLED run as the constant lower boundary condition on the atmosphere. I will refer to this run as the UNCOUPLED run. (Note that the climatology of the COUPLED run should be zonally symmetric, but due to sampling errors there is a slight departure from zonal symmetry). The second prescription uses the time-varying SST from the COUPLED run as the lower boundary condition on the atmosphere. In reference to similar experiments by Lau (1994) I will refer to this as the MOGA (Midlatitude Ocean, Global Atmosphere) run.[2]

---

1. The numerical experiments, COUPLED, MOGA, and UNCOUPLED, and in later sections, MOGA RESPONSE and LINEAR, will be referred to throughout the text in ALL-CAPITAL type.

The ocean model is then run in diagnostic mode, using the atmospheric variables from the MOGA and UNCOUPLED runs as input. I will refer to these as the MOGA DIAGNOSTIC ocean run and UNCOUPLED DIAGNOSTIC ocean run, respectively. Using this method I can diagnose what the SST would be if the ocean were forced by an "uncoupled" atmosphere -- that is, by an atmosphere which receives no feedback from anomalous SST it is forcing. Because the ocean model is so simple one can think of the ocean runs, whether COUPLED, MOGA DIAGNOSTIC of UNCOUPLED DIAGNOSTIC, as a time filtered view of the atmospheric low-frequency variability.

The UNCOUPLED run sets a baseline for atmospheric low-frequency variability -- what would happen in the case where there is no forcing of the atmosphere by SST anomalies and no adjustment of the SST to atmospheric anomalies. Comparison of the MOGA run to the UNCOUPLED run allows us to estimate the effect of direct forcing by SST anomalies on low-frequency variability. Comparison of the COUPLED run to the MOGA run allows us to determine whether there is any effect of coupling above and beyond that caused by the direct forcing. A schematic diagram of the ocean-atmosphere interactions in the COUPLED, MOGA, and UNCOUPLED runs is shown in Figure 3.1.

The above choices of lower boundary condition are similar to what is used in large atmospheric GCM climate simulations, except in that case the prescribed SSTs are usually taken from the observed SSTs rather than from a coupled model run. Because present-day large coupled atmosphere-ocean GCMs are not able to correctly simulate the climatology, a flux correction scheme is sometimes used to nudge the model climate back toward the observations. Sausen and Lunkeit (1990) give a particularly illuminating discussion of the

---

2. Since the global SSTs are specified in this run, the parallel might seem closer to Lau's GOGA (Global Ocean, Global Atmosphere) runs. Because the tropical SST variability is essentially nil in the present simulations, the acronym MOGA captures the spirit of these runs better.

meaning of flux correction in an idealized model. Since the above choices of control runs in this study result in nearly identical climatologies in the COUPLED, MOGA and UNCOUPLED runs, no flux correction scheme is needed or used in these experiments.

The “dry” model is used with the standard parameter values, as described in the previous chapter. Some salient features of the model are summarized here for convenience. The pseudo-spectral (spectral transform) model is run at T21 truncation, using a physical-space grid of 64 equally spaced longitudes, and 32 nearly equally spaced Gaussian latitudes. The model has biharmonic diffusion of momentum and heat with a 2-day time scale at total wavenumber 21, and linear frictional damping at the lower layer with a 5-day time scale. The time step is 30 minutes, yielding 48 timesteps per model day. Surface fluxes are parameterized using bulk aerodynamic formulae with transfer coefficient $C = 10^{-3}$ and surface relative humidity of 0.8. Latent heat flux into the atmosphere is released immediately and locally at the lower level in the geographic location where the evaporation took place. Longwave radiation is taken from a look-up table based on the model temperatures, and shortwave absorption is calculated in the zonal mean only and is nearly constant in time. The tropics are quiescent in these runs. Convective adjustment to a moist adiabat maintains the tropical vertical temperature structure.

The atmosphere model was first spun up for over 1000 days in an “all-land”[1] configuration, starting from rest with isothermal conditions at each level and $\hat{\theta} = 15\mathrm{K}$. The zonal mean of the surface air temperature T_s from the last 500 days of this run were used as the initial conditions for the ocean temperature in the coupled run. The coupled model, in an “all-ocean” configuration, was then run for 6000 days to study the approach to the thermal and dynamical statistical steady state. Because of the range of time scales inherent

1. Instantaneous surface energy balance at all locations. All other properties the same as for the ocean.

in the longwave parametrization due to the equator-to-pole temperature difference, is was difficult to predict from first principles the global equilibration time scale. However, one would expect that the slow radiative time scales of the polar regions would dominate the global statistical equilibration. Plots of the equilibration (not shown) indicate that the time scales are indeed slowest in the polar region, reflecting not only the slow radiative time scales, but also the adjustment of the horizontal eddy heat flux into the polar region. The equatorial adjustment is somewhat faster, due to the faster radiative time scales there and due to the fast (almost instantaneous) time scale of convective adjustment. The midlatitudes lie somewhere in-between and reflect both the global adjustment of the general circulation and the local radiative and mixed-layer time scales. After approximately 1500 days the coupled system zonal mean temperatures have all adjusted to values which are within the range of the natural variability for the rest of the run, which is interpreted to mean that the coupled system has adjusted statistically to its steady zonal climatology.

The COUPLED model was run for 18,000 model days or 50 360-day model years, of which the last 15,000 days will be analyzed for reasons stated below. For comparison to other simulations and to observational analyses it useful to note that 15,000 days is approximately equivalent to either 42 years, 500 months, or 167 3-month seasons. Because of the symmetry about the equator in the model's boundary conditions, the sampling period can be effectively doubled to 84 years by assuming that the Northern and Southern Hemispheres represent independent realizations of the same physical processes and pooling the statistics from the two hemispheres. The COUPLED atmospheric initial condition was that at the end of the spin-up run, but the ocean initial condition was set to the zonal mean of the last 3000 days of the spin-up run. The atmosphere model variables $\bar{\zeta}$, $\hat{\zeta}$, $\hat{D}$, $\bar{\theta}$ and $\hat{\theta}$, and the ocean temperature T_o were sampled daily. The net fluxes of

shortwave radiation, longwave radiation, sensible heat and latent heat were accumulated over all timesteps for each day and output daily.

The UNCOUPLED atmosphere was run for 18,000 days using the zonal mean of the climatology from the first 6000 days of the COUPLED run as the prescribed, time-independent, lower boundary condition. The initial condition for the atmosphere was the same as for the COUPLED atmosphere run. The initial condition for the UNCOUPLED DIAGNOSTIC ocean was the zonal mean state prescribed in the UNCOUPLED run. This was done so as not to bias the SST data due to initial conditions. The model state variables were sampled daily. At each timestep, the atmospheric state variables were used to force a slave ocean. Therefore the numerical aspects of the slave and coupled ocean models are identical. The following surface heat fluxes are dependent on T_o: upward longwave radiation, sensible heat, and latent heat. The shortwave radiation and downward longwave radiation are independent of T_o. The UNCOUPLED run produces two sets of surface fluxes, the fluxes that force the atmosphere, calculated using the prescribed, fixed SST, and the fluxes that force the diagnostic ocean, calculated using the time-varying, diagnostic ocean SST. Both sets of fluxes are accumulated at each timestep and output daily.

The MOGA run was integrated for 50 model years using the history of SST from the COUPLED run as the lower boundary condition. Note that the lower boundary condition depends both on time and space. The MOGA DIAGNOSTIC ocean initial condition was the same as in the UNCOUPLED DIAGNOSTIC ocean run (as above, to eliminate possible bias due to the initial conditions). The atmospheric initial condition was taken from an unrelated run of the coupled model. As in the UNCOUPLED run, two sets of surface fluxes are generated.

During the final editing and double-checking of this thesis it was discovered that an

error was made in specifying the UNCOUPLED boundary condition and the initial conditions for all the ocean simulations. Inadvertently, the zonal mean SSTs from a previous run using the HS radiative code was used instead of the zonal mean of the COUPLED run SSTs. The erroneous SSTs were approximately a degree colder than the true SSTs, resulting in atmospheric temperatures that were cold compared to the COUPLED and MOGA runs. It is believed that correction of this error will lead to only minor quantitative changes in the main results of this dissertation. The evidence for this assertion is that all the results of this thesis were originally found in a set of three runs, COUPLED, MOGA, and UNCOUPLED of 6000 days each which were completely consistent in their execution. The present set of runs of 18,000 days each was done solely for the purpose of increasing the statistical significance of the previous results. The climatologies for the earlier, consistent runs did not show the discrepancies which are present in the current runs.[1]

In order to be consistent and to avoid any bias in the diagnostic ocean runs based on the initial condition, the COUPLED ocean, MOGA DIAGNOSTIC ocean, and UNCOUPLED DIAGNOSTIC ocean in the runs described above were all initialized with the same zonally symmetric initial conditions derived from a previous set of runs. Each of these model runs undergoes an adjustment period during which the mean temperatures adjust and zonally asymmetric variability builds up to a statistically steady level. Figure 3.2a shows the zonal mean SST at selected latitudes as a function of time for the first 12,000 days of the COUPLED model run (sampled every 10 days). Figure 3.2b shows the spatial standard deviation of SST at the specified latitudes as a function of time. Based on this plot and on similar ones for other latitudes and runs, it was decided to exclude the first 3000 days of all the runs from analysis. After this time period, the mean and spatial stan-

1. The UNCOUPLED run will be redone using the correct boundary condition before the results presented in thie dissertation are submitted for publication in a refereed journal.

dard deviation of the midlatitude SST was clearly well within the range it would occupy for the rest of the run.

3.3 Model Climatology

In this section I will present the zonal mean climatology of the three runs described above. Because of the zonally symmetric boundary conditions, one expects the statistics of these runs to be zonally homogeneous. This is not strictly the case for the COUPLED and MOGA runs as the SST exhibits variance at even the lowest resolvable frequencies and therefore the lower boundary conditions are not strictly zonally symmetric. However, the departures from the zonal mean are small and only zonal mean statistics will be presented in this section. Note that when calculating SST anomalies as well as anomalies for other variables in the following work, I use the actual (zonally and meridionally varying) time mean as the climatology. I will first present zonal means of the model variables, followed by surface heat fluxes, and then present zonal mean eddy fluxes of heat and momentum in the atmosphere, along with atmospheric eddy kinetic energy.

The zonal-mean climatology of the model winds is shown in figures 3.3ab. The upper level (250 mb) zonal winds show a midlatitude jet of approximately 35 m s^{-1} centered at 41.5° latitude, with a full width at half-maximum of about 30 degrees of latitude. The lower level (750 mb) zonal winds show a jet of approximately 13 m s^{-1} centered at about 47° latitude, one gridpoint poleward of the upper level jet. Lower level easterlies extend to about 25° latitude, while significant upper level easterlies are confined to the deep tropics. The mean meridional circulation, consisting of three cells, is seen in the plots of meridional wind (figure 3.3c) and upper level divergence (figure 3.3d, which is also proportional to upward motion at 500 mb). The Hadley cell is rather weak, a common fea-

ture of models in which the forcing is symmetric about the equator, and consistent with the theoretical results of Lindzen and Hou (1988). Runs with this model using insolation with north-south asymmetry (not shown) produce a stronger Hadley cell. Perhaps the most unusual feature of the model climatology is the strong narrow downward branch of the Hadley cell in subtropics. The reason for this phenomenon is not known, but is probably related to the model physics, as this phenomenon does not occur in a version of this model forced via linear relaxation to a radiative equilibrium temperature profile.

The model temperatures, shown in figures 3.3ef are nearly constant between the equator and 20° latitude. The vertical mean potential temperature, $\bar{\theta}$, shows a sharp meridional gradient in the midlatitudes, which coincides with the strongly baroclinic westerly jet and is consistent with the thermal wind relation. The static stability, represented by $\hat{\theta}$ decreases from a value of approximately 14K at the equator to 12.5 K in the midlatitudes, and then increases to over 16 K at the poles. Radiative convective equilibrium maintains the equatorial stability in the model close to the moist adiabat, so the equatorial static stability is pegged to the vertical mean temperature. The polar values of static stability are determined primarily by radiative effects. If radiation and convective adjustment were the only processes present, then the midlatitudes would have very low $\hat{\theta}$. However the stabilizing effect of the baroclinic eddies and, in the subtropics, of the mean meridional circulation keep the mean stability well above moist adiabatic. One is advised to see Held and Suarez (1978, 1976) for further detail on the maintenance of static stability in two-level models with simplified physics.

The climatology of the zonal mean sea surface temperature, T_o, is shown in figure 3.4a. The climatoloby of the ocean-atmosphere temperature difference is shown in figure 3.4b. In the time mean, the ocean is everywhere warmer than the overlying atmosphere.

The temperature difference ranges from about 1K at the latitudes of strong surface easterlies or westerlies, to values above 2K at latitudes of weaker winds. This approximate inverse relationship between climatological temperature difference and mean surface winds can be understood in terms of the time mean surface energy balance. In the time mean, the insolation is balanced by a combination of longwave, sensible heat, and latent heat fluxes. The insolation and longwave flux are insensitive to surface wind speed, so the sum of sensible and latent heat fluxes must also be insensitive to wind speed. Since these are parameterized by bulk aerodynamic formulae, and are determined essentially by the product of wind speed and air-sea temperature difference, the inverse relationship follows naturally. Such a relationship is not readily observed in the real world. In the winter, the thermal contrasts provided by continental sources of cold air juxtaposed with oceanic western boundary currents (Gulf Stream, Kuroshio) results in localized regions of strong air-sea interaction. The all-ocean model is free of these strong zonally asymmetric effects. Observed mid-ocean air-sea temperature differences are typically 0.5 - 1 K, much smaller than in the model. The discrepancy arises from the fact that the atmospheric boundary layer over the ocean is typically shallower than the lower layer of the model, and thus can provide more rapid negative thermal feedback. For low frequency anomalies which are the focus of this thesis, atmospheric temperature anomalies tend to be deep, and the boundary layer adjusts rapidly to conditions imposed by the free atmospheric flow. Put another way, it is not likely that in the region of the storm track that the boundary layer is the bottleneck in determining climatological and low-frequency heat fluxes. The processes in the midlatitudes which accomplish this vertical redistribution, primarily adiabatic heating and eddy heat flux, but also longwave radiation, are reasonably well modeled by the two-level model. Therefore, I expect this model to reasonably represent perturbations from climatol-

ogy.

Despite the unrealistically large air-sea temperature differences, the model fluxes, shown in figure 3.5, are similar to observations, at least for the purpose of idealized model studies. (See for example, Esbensen and Kushnir, 1981). The net upward longwave flux about 25 Wm^{-2} too large compared to observed Southern Hemisphere annual mean open-ocean values, probably a result of the large air-sea temperature differences. The model's latitudinal distribution of longwave flux is also quite flat from equator to pole, even flatter than in the Esbensen and Kushnir observations. A possible explanation for the latter is that a major determinant of net longwave flux -- cloudiness -- has the same value everywhere on the globe in this model. And although moisture effects are included in the longwave parametrization, the relatively cool tropical temperatures achieved in this model limit the magnitude of downward longwave flux at the surface. By the same standard of comparison, model latent heat flux is too small by about 20 - 25 W m^{-2} except in the subtropical highs where the discrepancy is greater. The overall discrepancy is partly the result of the somewhat cool climatology of model temperatures. The discrepancy in the subtropical highs is most likely associated with the absence of cloudiness effects in this model. Model sensible heat flux is too large by 5 - 10 W $m^{-2.}$

The zonal mean eddy fluxes of heat and momentum and the eddy kinetic energy are shown in figures 3.6 a-d. The momentum flux is concentrated almost entirely at 250 mb and peaks just equatorward of the westerly jet. There is strong eddy flux convergence and hence westerly acceleration at the core of the jet and on its northern flank. In contrast to momentum flux, the 750 mb eddy heat flux is 50 percent larger than the upper level eddy heat flux. The 750 mb heat flux peaks about 10 degrees of latitude poleward of the jet, while the 250 mb heat flux has its peak slightly equatorward of the jet.

The position of the westerly jet is farther north than in observations, which also is seen in the climatology of Hendon and Hartmann (1985). When the current model is run using a prognostic moisture equation and the moisture parametrizations of Held and Suarez (1976), the jet is located closer to the equator, consistent with the HS climatology (not shown).

A comparison of the COUPLED, MOGA, and UNCOUPLED run climatologies reveals only minor differences among the runs. The COUPLED and MOGA runs are almost identical in their zonal mean statistics. Only the UNCOUPLED run shows significant differences. The most striking difference is in the model temperatures. This is a consequence of the error in lower boundary conditions described in section 3.2. The atmospheric dynamics of the UNCOUPLED run are in general a slight bit weaker than in the other two runs, with differences of about 5 percent in momentum flux, heat flux, and eddy kinetic energy, and differences of less than 5 percent in the mean winds. The climatologies of a set of consistent runs (not shown) without the erroneous boundary conditions do not exhibit the discrepancies in the SST, atmospheric temperature and eddy fields which are seen in the present set of runs.

Greater detail on the overall similarity and differences in the runs can be obtained by looking at the spectrum in terms of the root-mean-square (RMS) amplitude of each spherical harmonic coefficient (sampled daily). These are shown for the COUPLED run atmospheric variables in figures 3.7 - 3.11. Panel *a* of each of these figures shows the RMS amplitude for spectral coefficients for all zonal wavenumbers except the zonal mean. Panel *b* shows the zonal mean coefficients. The jagged appearance of the plots in panel *b* is a result of the alternation spherical harmonics with odd and even symmetry about the equator.

The barotropic component of vorticity $\bar{\zeta}$, (Fig. 3.7) exhibits a variance maximum at zonal wavenumbers 5 and 6 and large meridional scale, with relatively large amplitudes extending to about zonal wavenumber 10. The variance maxima for higher zonal wavenumbers is found at relatively small meridional scales. The baroclinic component of vorticity, $\hat{\zeta}$, (Fig 3.8) peaks at zonal wavenumbers 5 - 7 and in contrast to the barotropic vorticity has significant amplitude in the smaller meridional scales for these zonal wavenumbers. Presumably this difference represents the signature of baroclinic processes as compared to barotropic processes.

The differences between COUPLED, MOGA, and UNCOUPLED spectral amplitudes are shown in figure 3.12-3.16 for the model variables. The most striking feature is found in the barotropic vorticity field (Fig. 3.12). The COUPLED and MOGA runs both show a deficit of variance along the elongated maximum compared to the UNCOUPLED run, and an enhancement of variance for other coefficients. The enhancement is particularly strong for zonal wavenumber 4. In addition, the COUPLED run shows a deficit with respect to the MOGA at zonal wavenumbers 6-10 for total wavenumbers less than 15, and an enhancement of variance for lower zonal wavenumbers. For total wavenumbers greater than 15 or for zonal wavenumbers greater than ten, there is little difference between COUPLED and MOGA runs. The difference between the COUPLED and MOGA runs is presumably the result of feedback due to coupling.

In conclusion, the methodology succeeds in creating a set of comparable runs with very similar zonal mean climatologies with which the effects of coupling can be investigated.

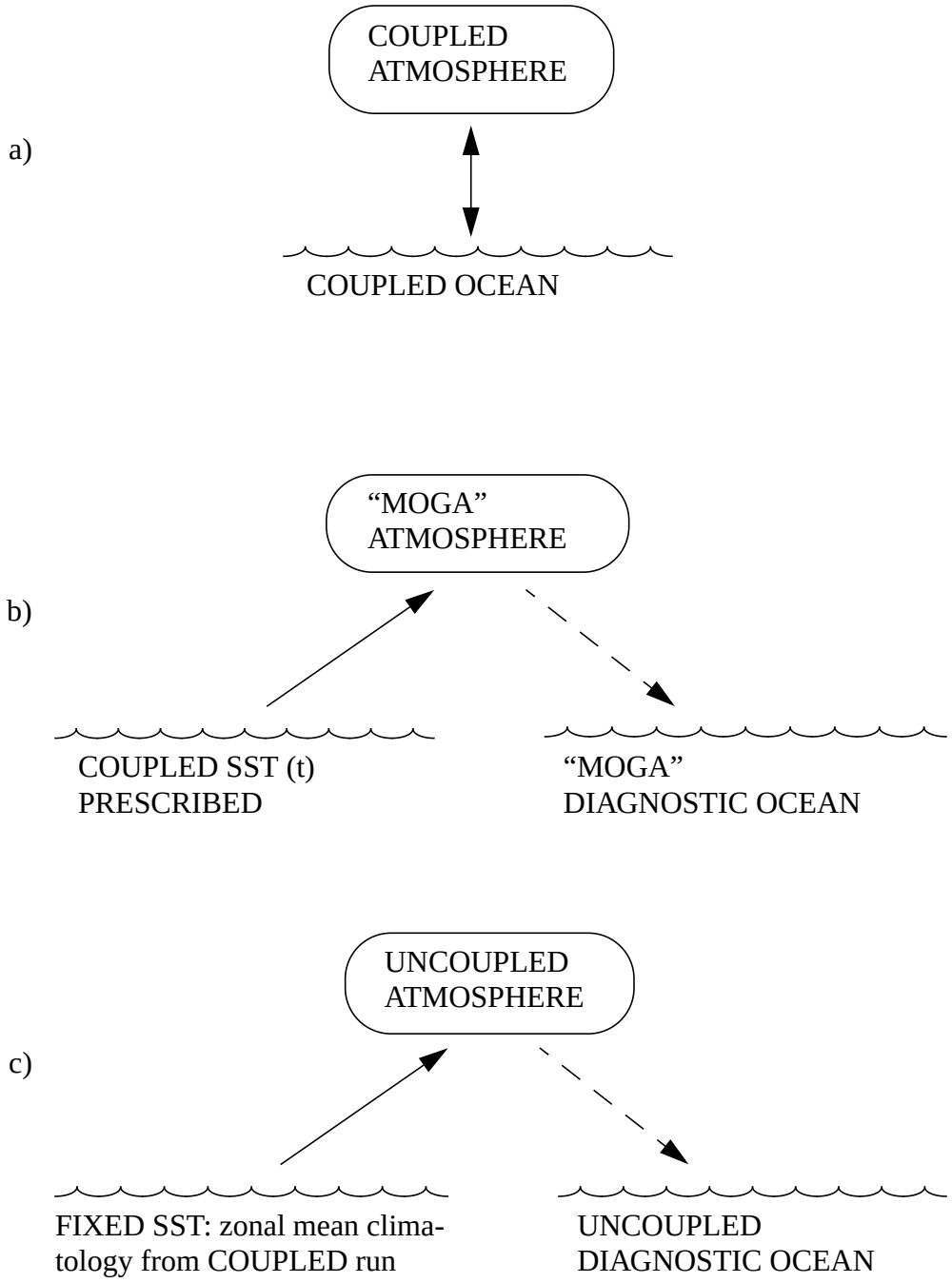

Figure 3.1. Schematic of experimental design. a) COUPLED run in which atmosphere and ocean interact. b) MOGA run in which the atmosphere is forced by the SST history from COUPLED run. The MOGA atmospheric variables are then used to force a mixed-layer ocean model in diagnostic mode. c) same as b) except that the SST is fixed to be the zonal mean climatology from the COUPLED run. In all cases, the fluxes that force the atmosphere are indicated by solid arrows. In the MOGA and UNCOUPLED runs, the fluxes which force the diagnostic ocean are indicated by dashed arrows.

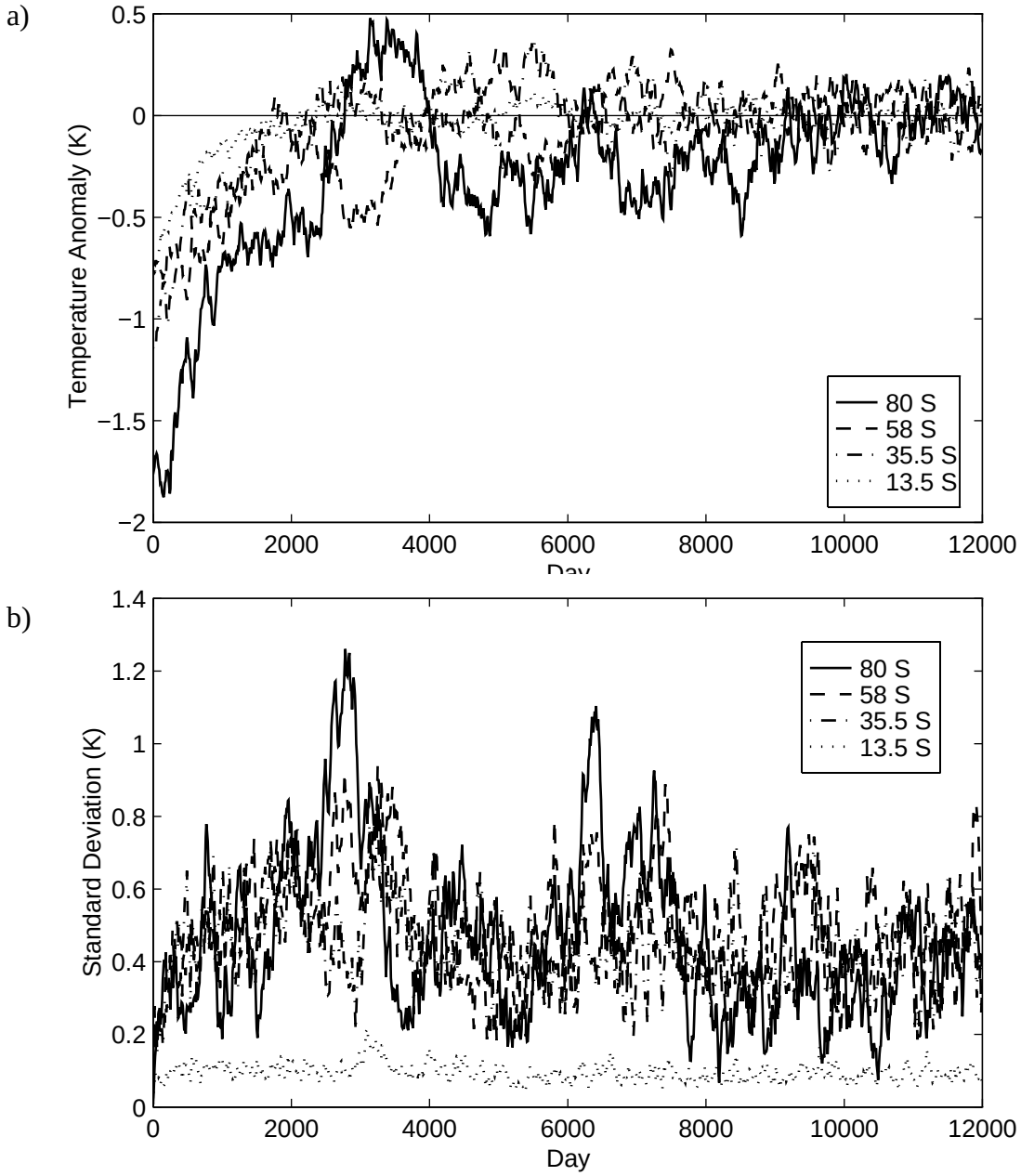

Figure 3.2. Adjustment of COUPLED ocean temperature at selected latitudes. a) zonal mean temperature anomaly relative to mean of days 10,000 - 12,000, b) spatial standard deviation of temperature along the specified latitude circle. Latitudes are indicated in legend.

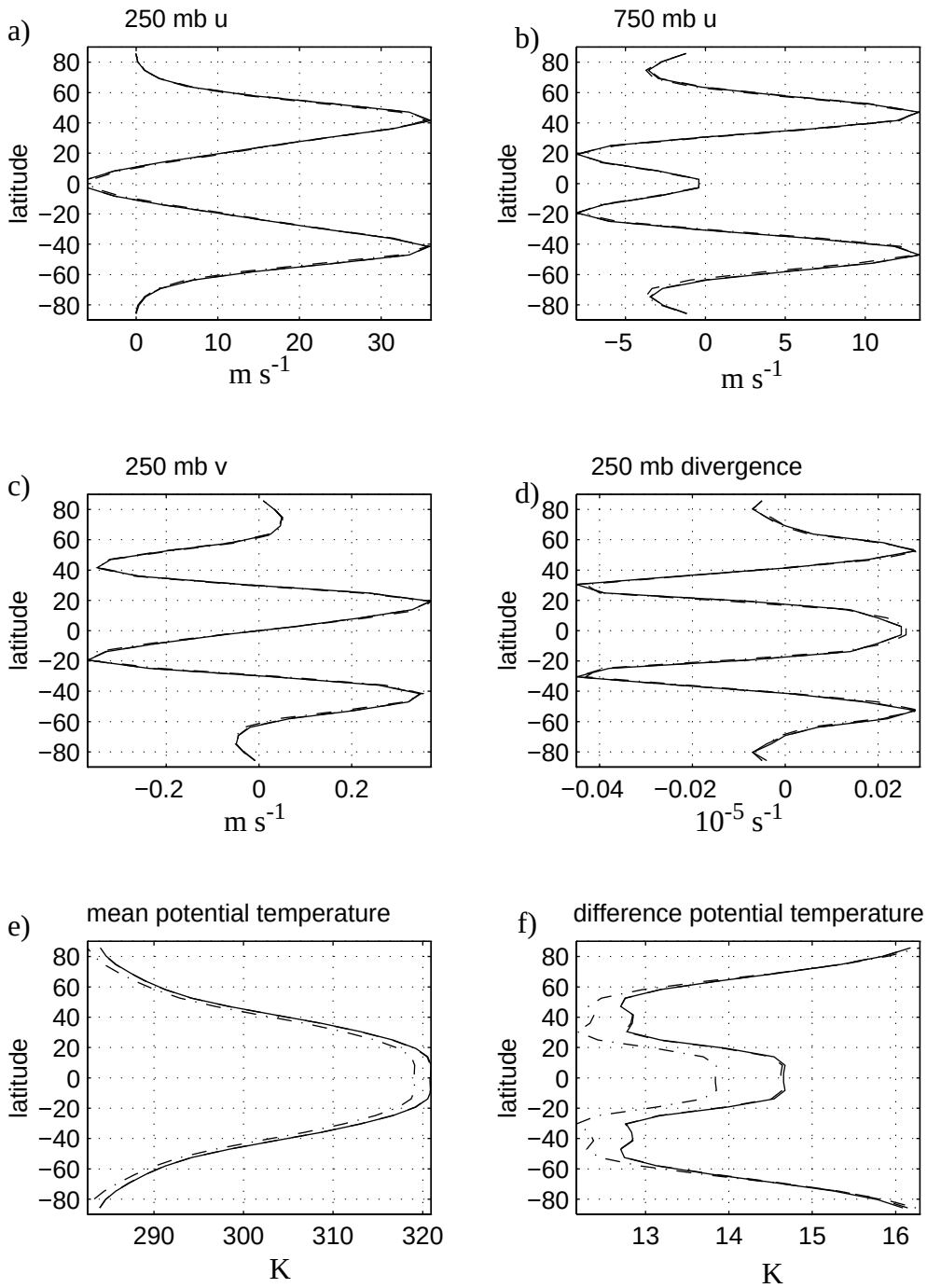

Figure 3.3. Zonal mean climatology of a) 250 mb zonal wind, b) 750 mb zonal wind, c) 250 mb meridional wind, d) 250 mb divergence, e) vertical mean potential temperature $\bar{\theta}$, f) vertical difference potential temperature $\hat{\theta}$, in the COUPLED (solid lines), MOGA (dashed lines), and UNCOUPLED (dash-dot lines) runs. In most cases only the COUPLED and MOGA climatologies are indistinguishable from one another, and in some cases all three are indistinguishable.

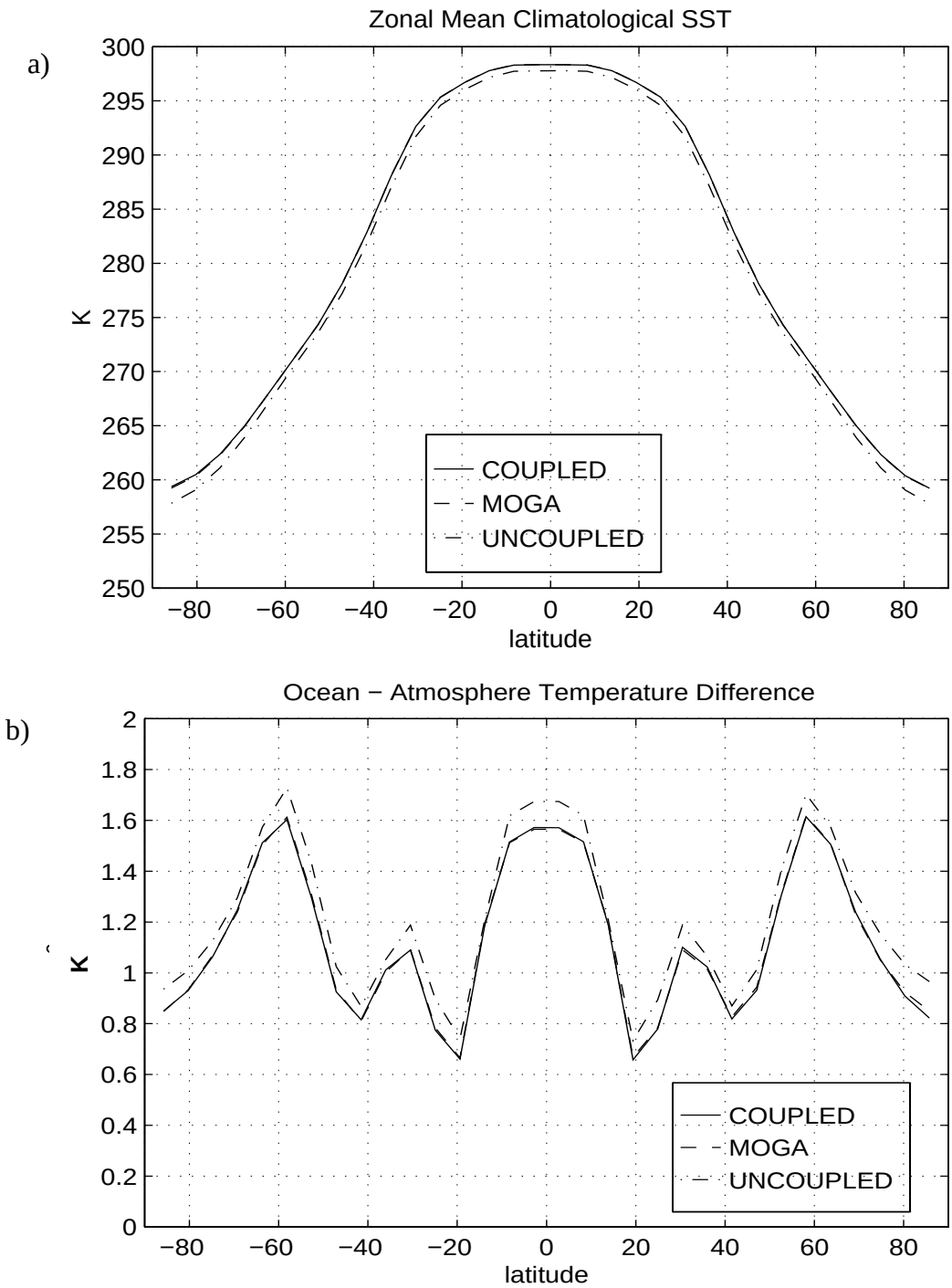

Figure 3.4. Zonal mean climatology of a) SST and b) Ocean-atmosphere temperature difference. In both plots the individual runs are indicated as follows: COUPLED (solid lines), MOGA (dashed lines), and UNCOUPLED (dash-dot lines). The COUPLED and MOGA runs are nearly indistinguishable.

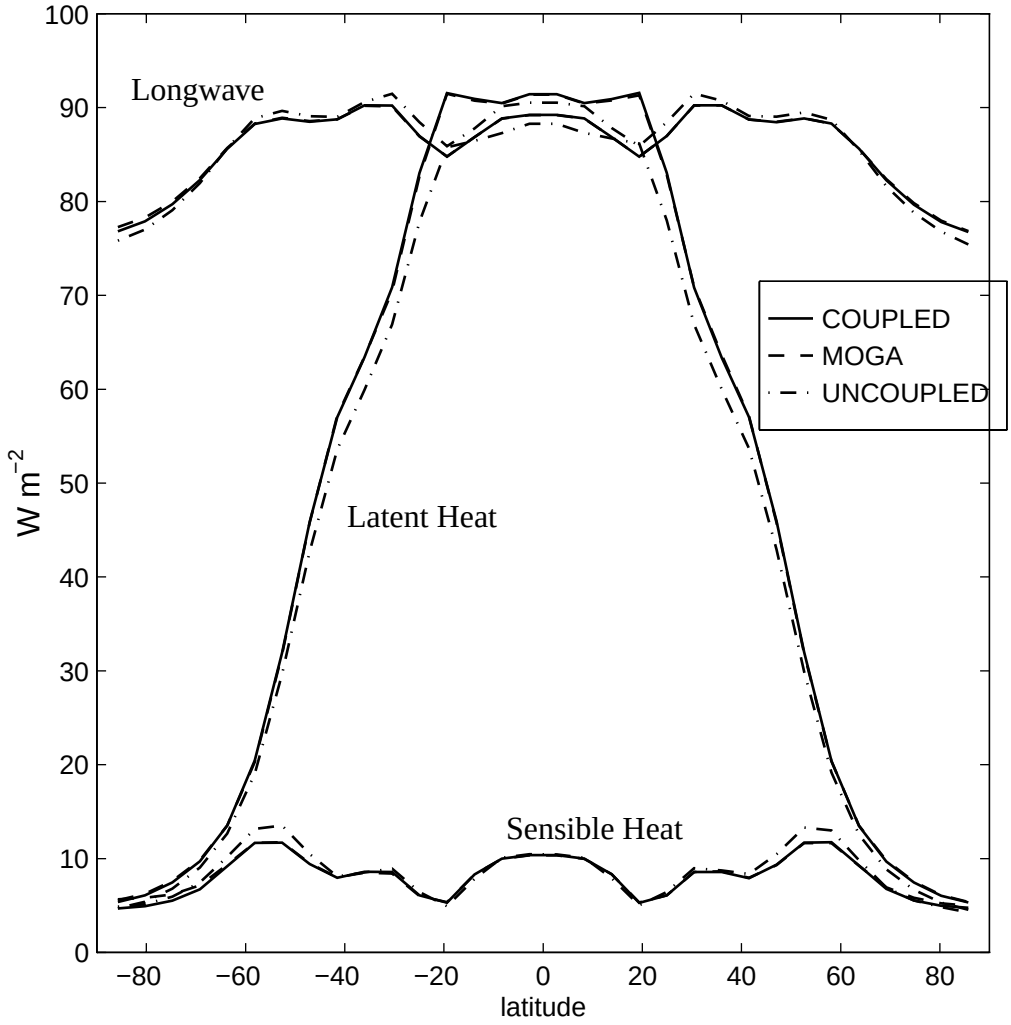

Figure 3.5. Zonal mean climatology of surface fluxes which force the atmosphere in the COUPLED (solid lines), MOGA (dashed lines), and UNCOUPLED (dash-dot lines) runs. The sets of lines which correspond to the longwave, latent heat, and sensible heat fluxes are labeled on the plot. Fluxes are positive-upwards. COUPLED and MOGA runs are nearly indistinguishable.

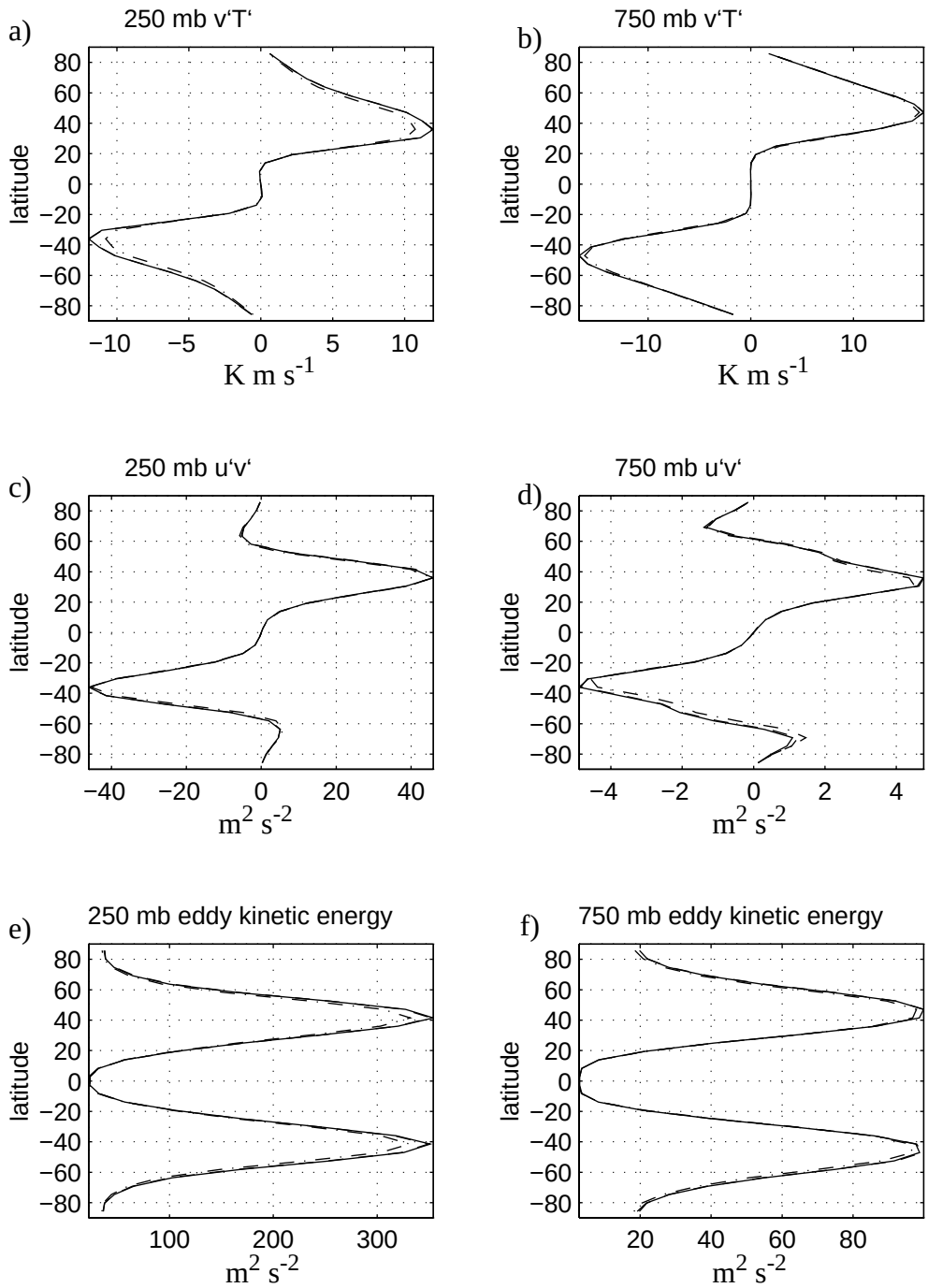

Figure 3.6. Zonal mean climatology of a) 250 mb eddy heat flux, b) 750 mb eddy heat flux, c) 250 mb momentum flux, d) 750 mb momentum flux, e) 250 mb eddy kinetic energy, f) 750 mb eddy kinetic energy, in the COUPLED (solid lines), MOGA (dashed lines), and UNCOUPLED (dash-dot lines) runs. In most cases only the COUPLED and MOGA climatologies are indistinguishable from one another, and in some cases all three are indistinguishable.

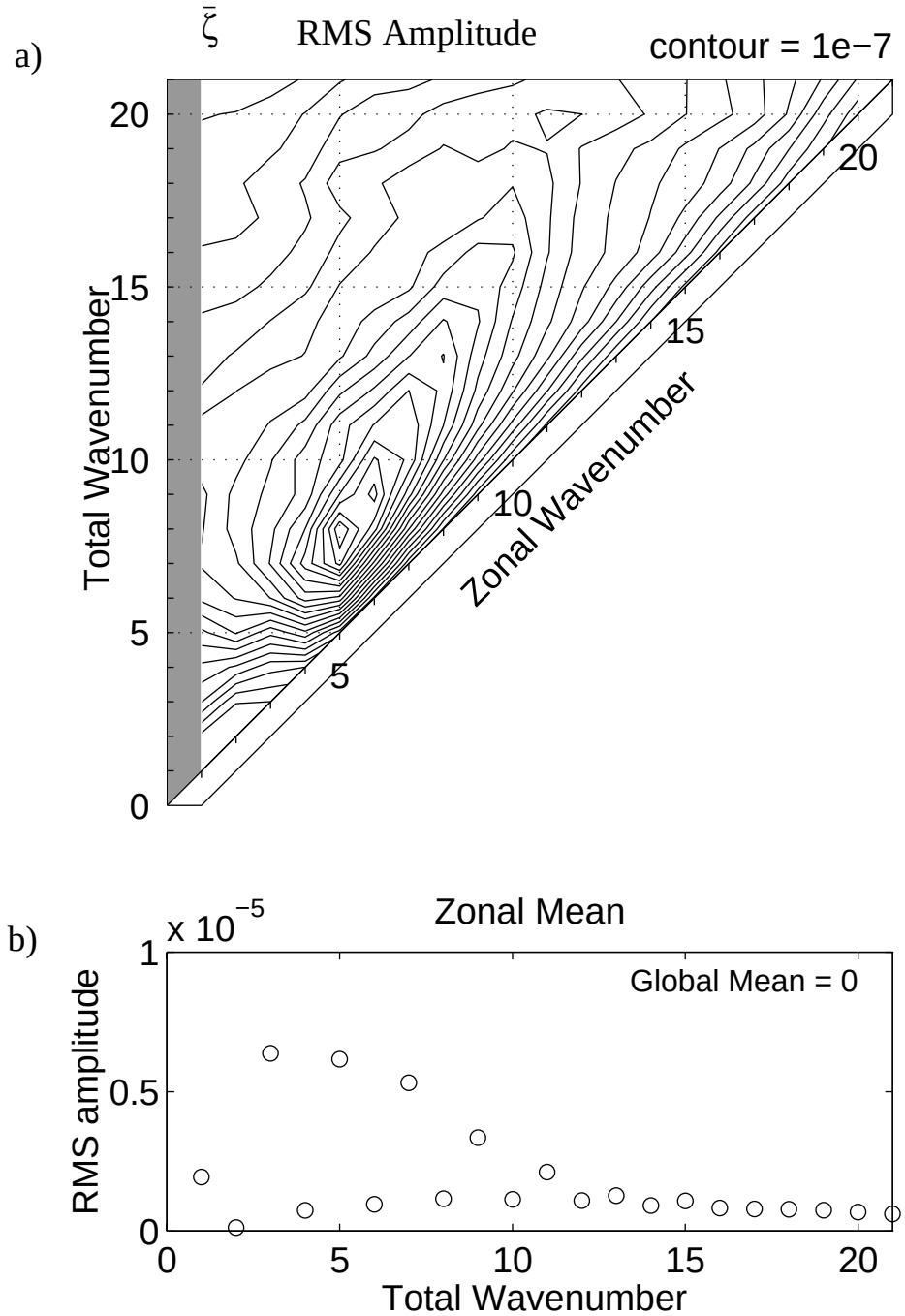

Figure 3.7. RMS amplitude of spherical harmonic coefficients for model variable $\bar{\zeta}$ in the COUPLED run for days 3001 - 18000. a) all coefficients except zonal mean coefficients, b) zonal mean coefficients. Global mean (the (0,0) spectral coefficient) is indicated in text in the lower panel. Units are s^{-1}.

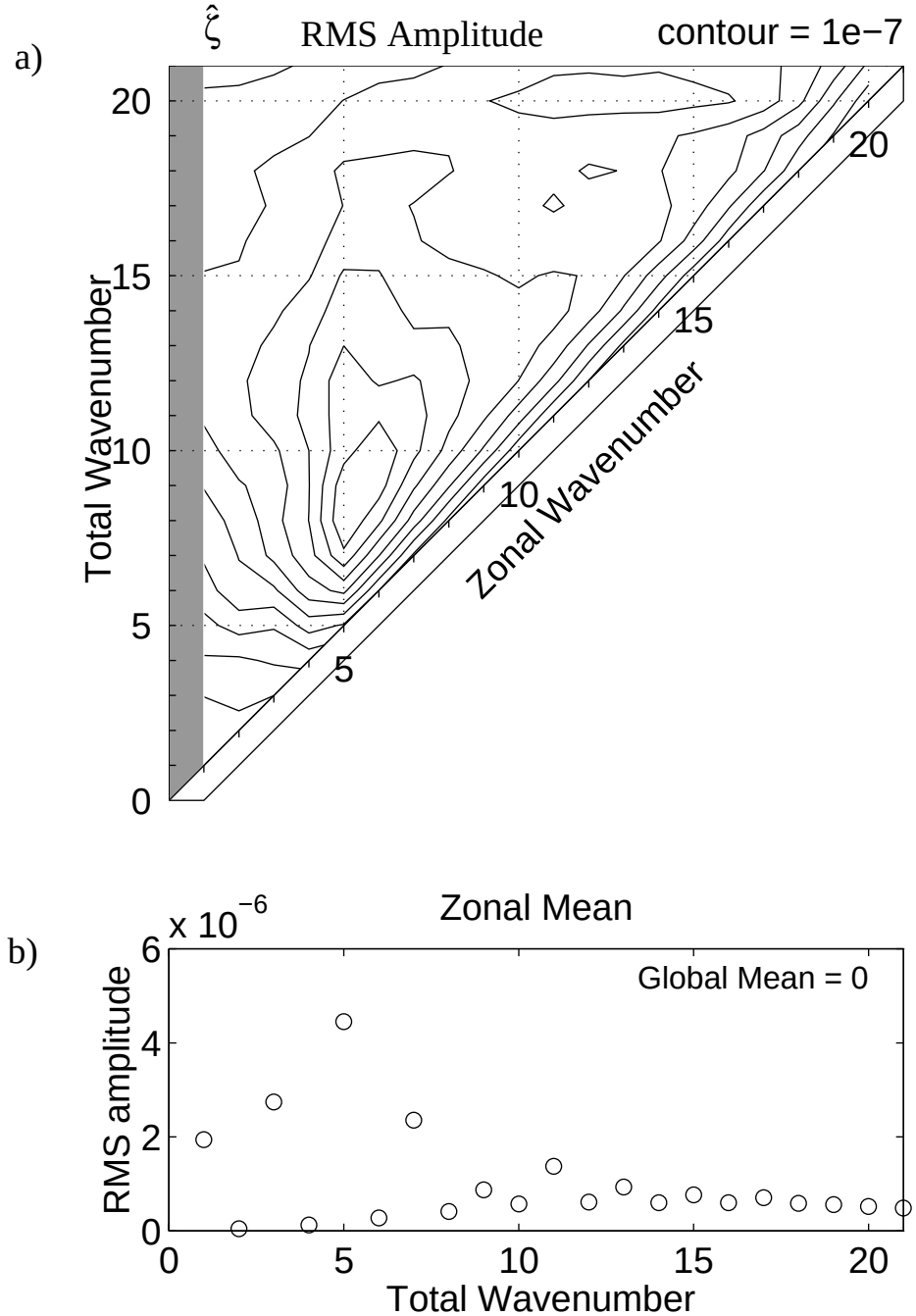

Figure 3.8 Same as in figure 3.7, except for model variable $\hat{\zeta}$. Units are s^{-1}.

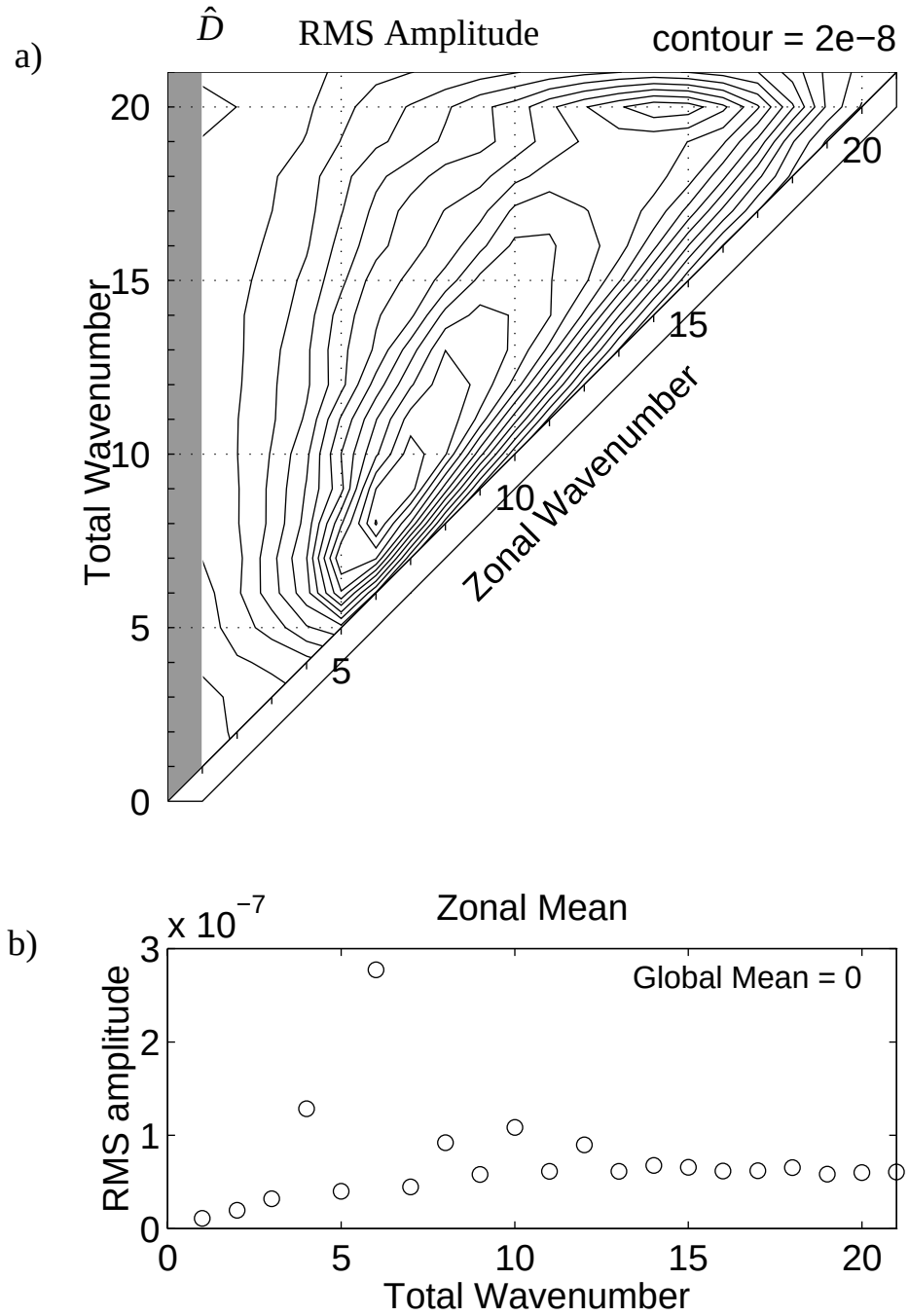

Figure 3.9. Same as in figure 3.7, except for model variable $\hat{D}$. Units are s^{-1}.

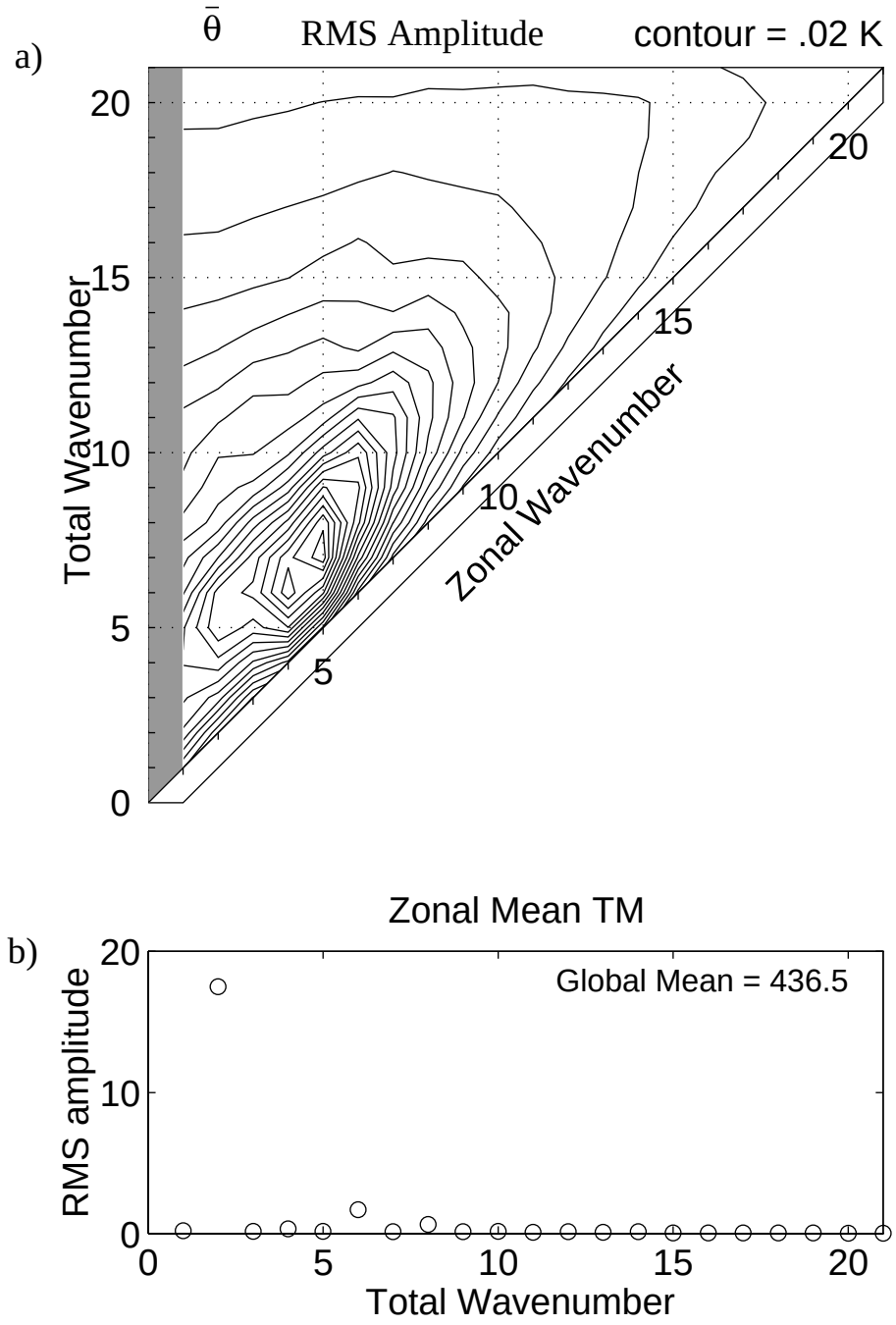

Figure 3.10. Same as in figure 3.7, except for model variable $\bar{\theta}$. Units are K.

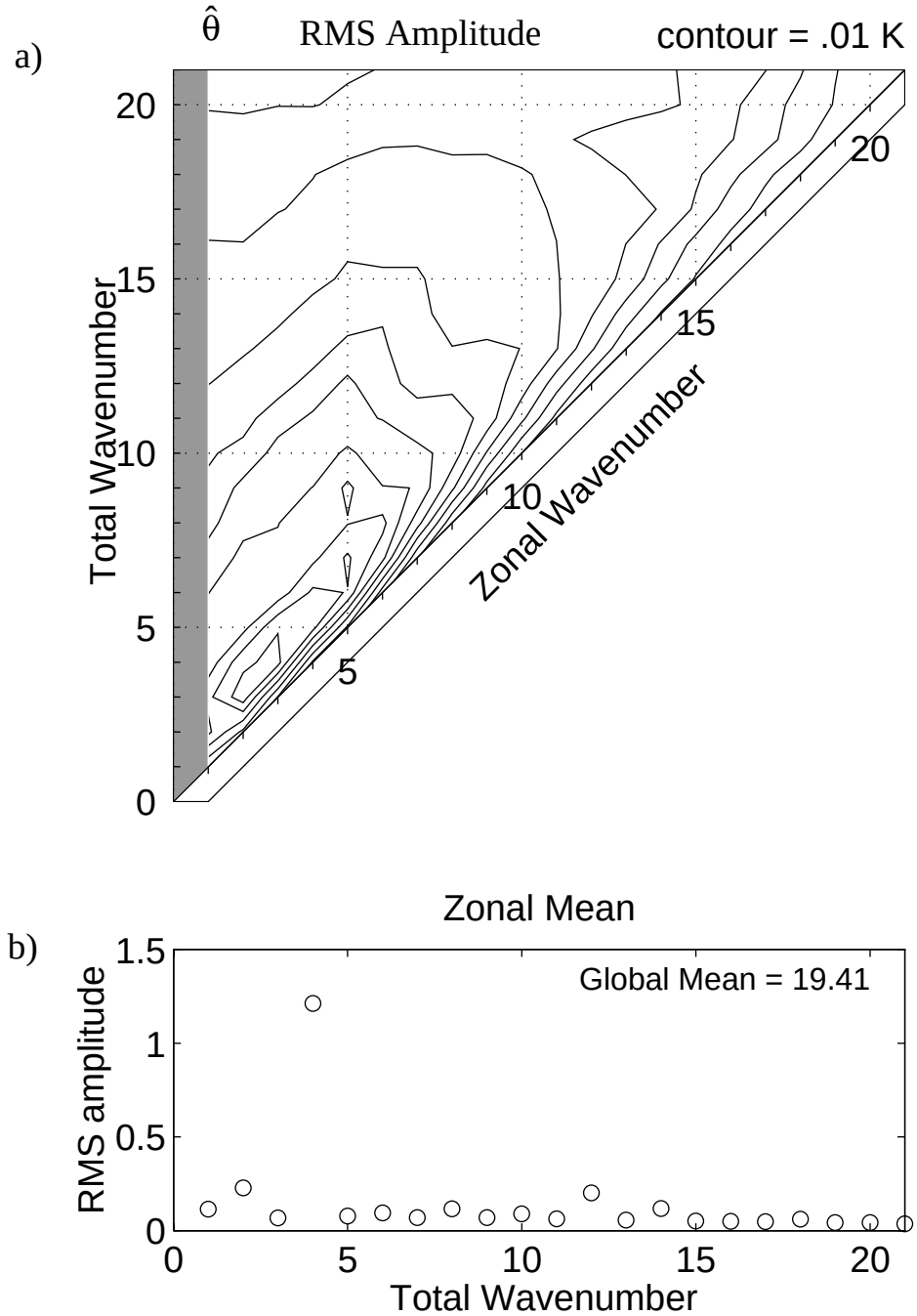

Figure 3.11. Same as in figure 3.7, except for model variable $\hat{\theta}$. Units are K.

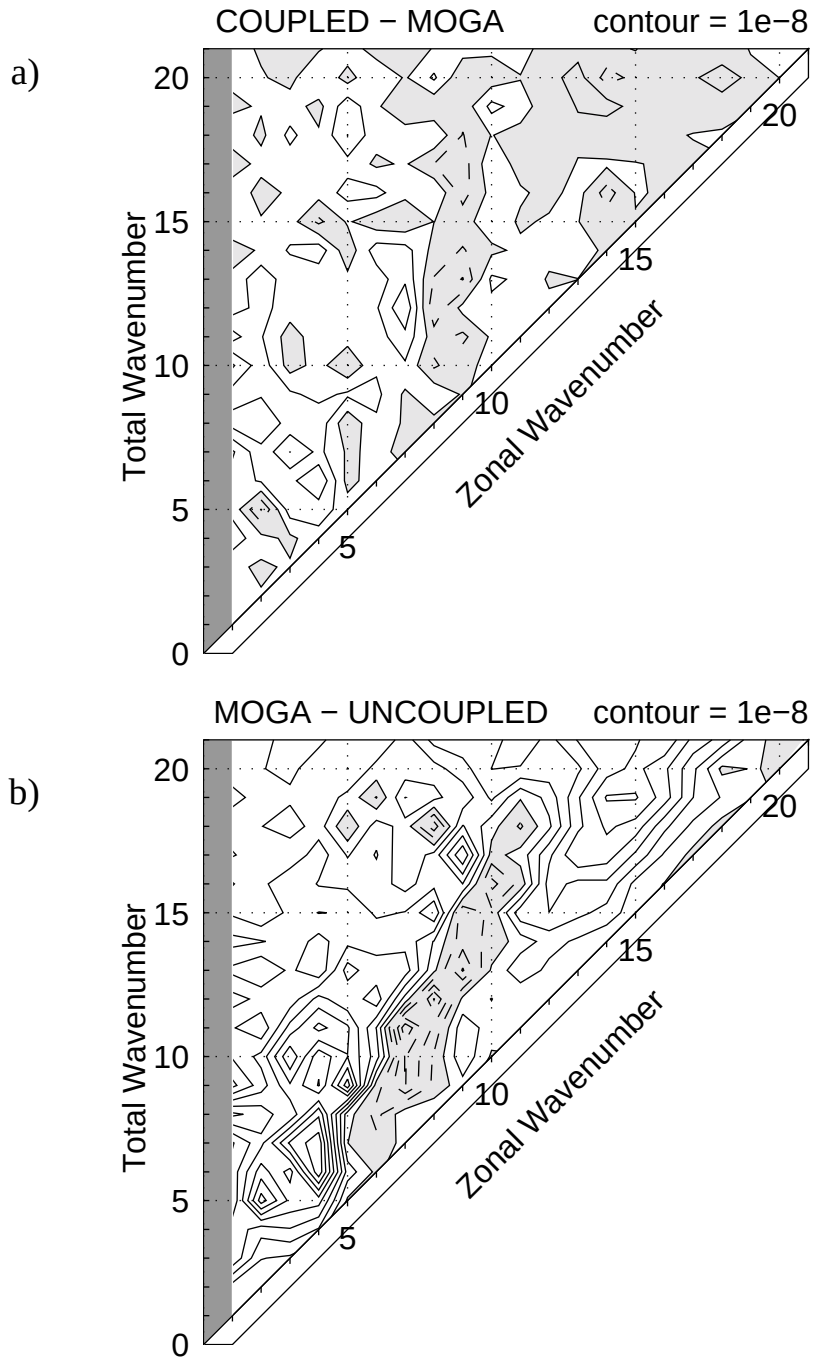

Figure 3.12. Same as the top panel in figure 3.7, except for difference of $\bar{\zeta}$ between runs. a) COUPLED - MOGA, b) MOGA - UNCOUPLED. Light gray shading indicates negative values.

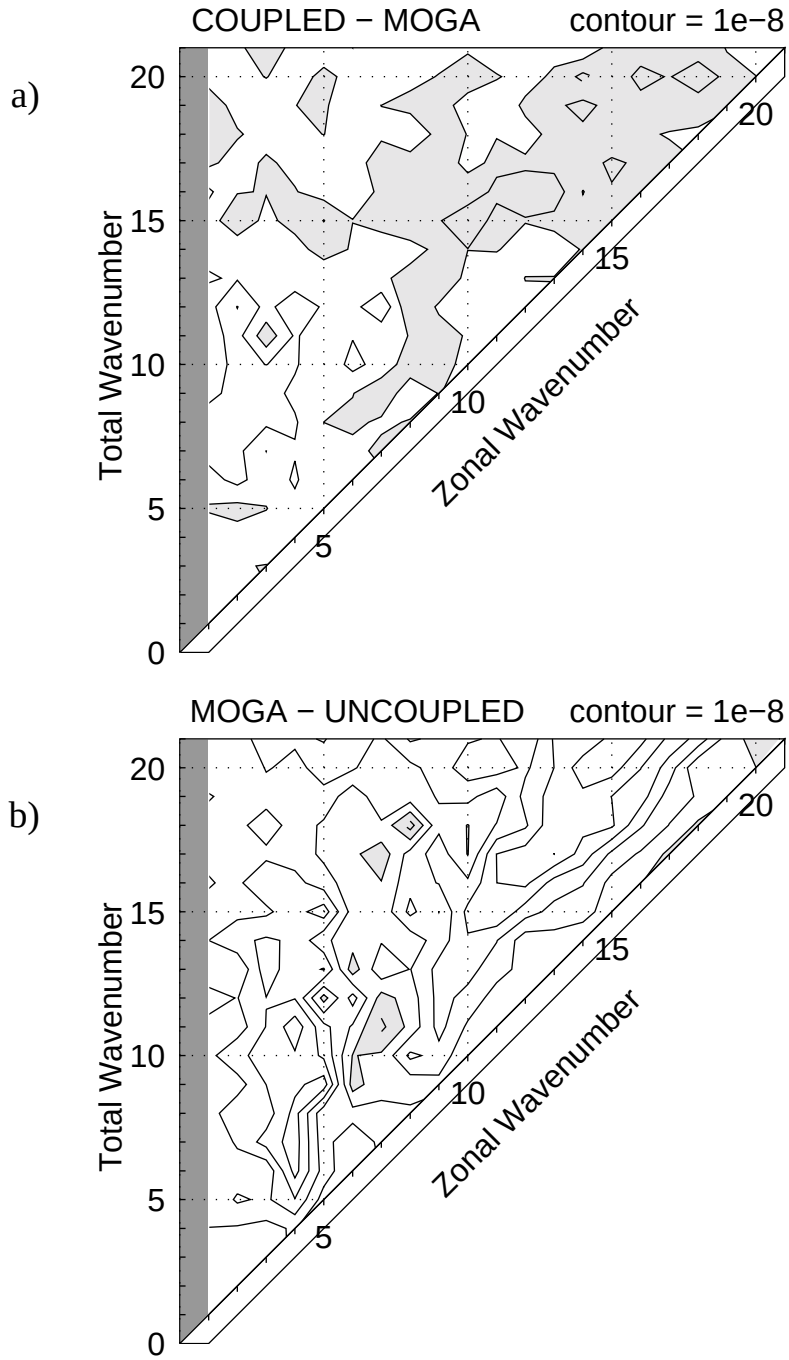

Figure 3.13. Same as the top panel in figure 3.7, except for difference of $\hat{\zeta}$ between runs. a) COUPLED - MOGA, b) MOGA - UNCOUPLED.

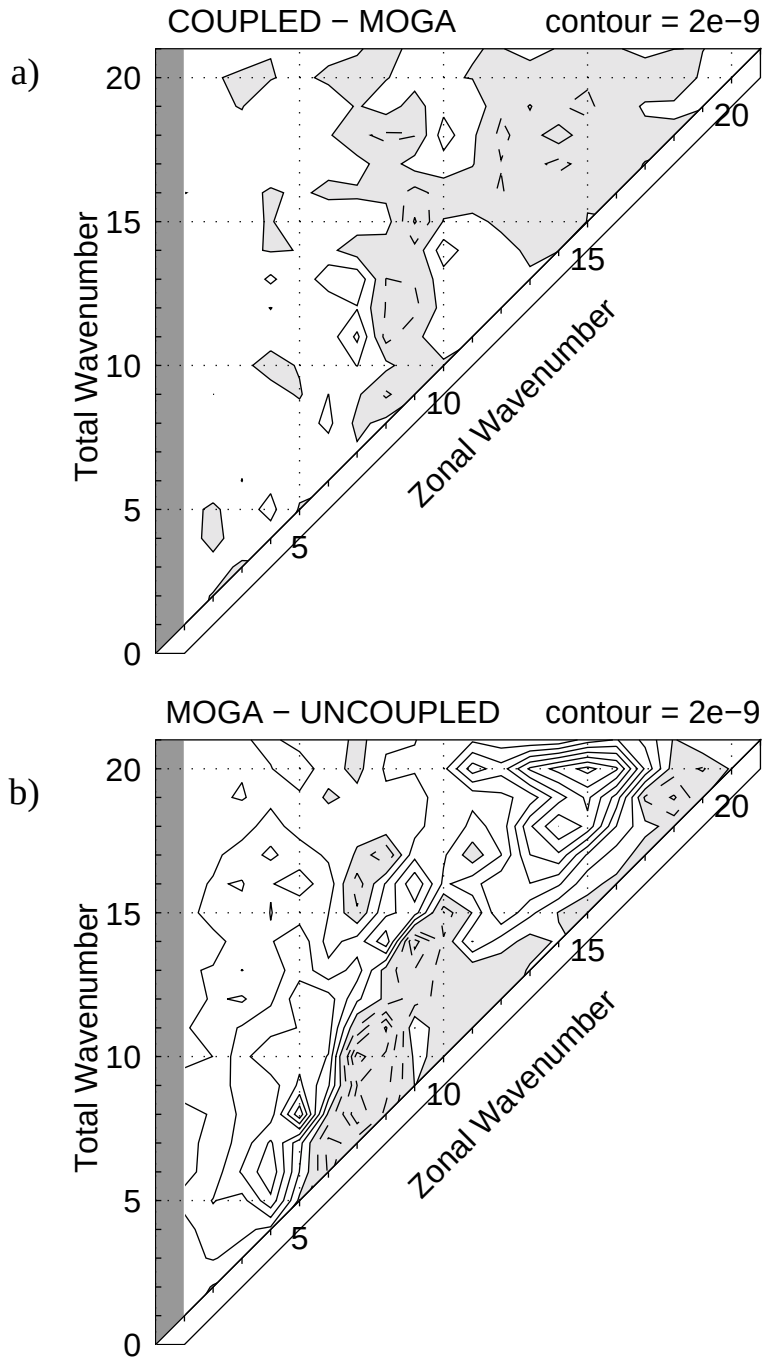

Figure 3.14. Same as the top panel in figure 3.7, except for difference of $\hat{D}$ between runs. a) COUPLED - MOGA, b) MOGA - UNCOUPLED.

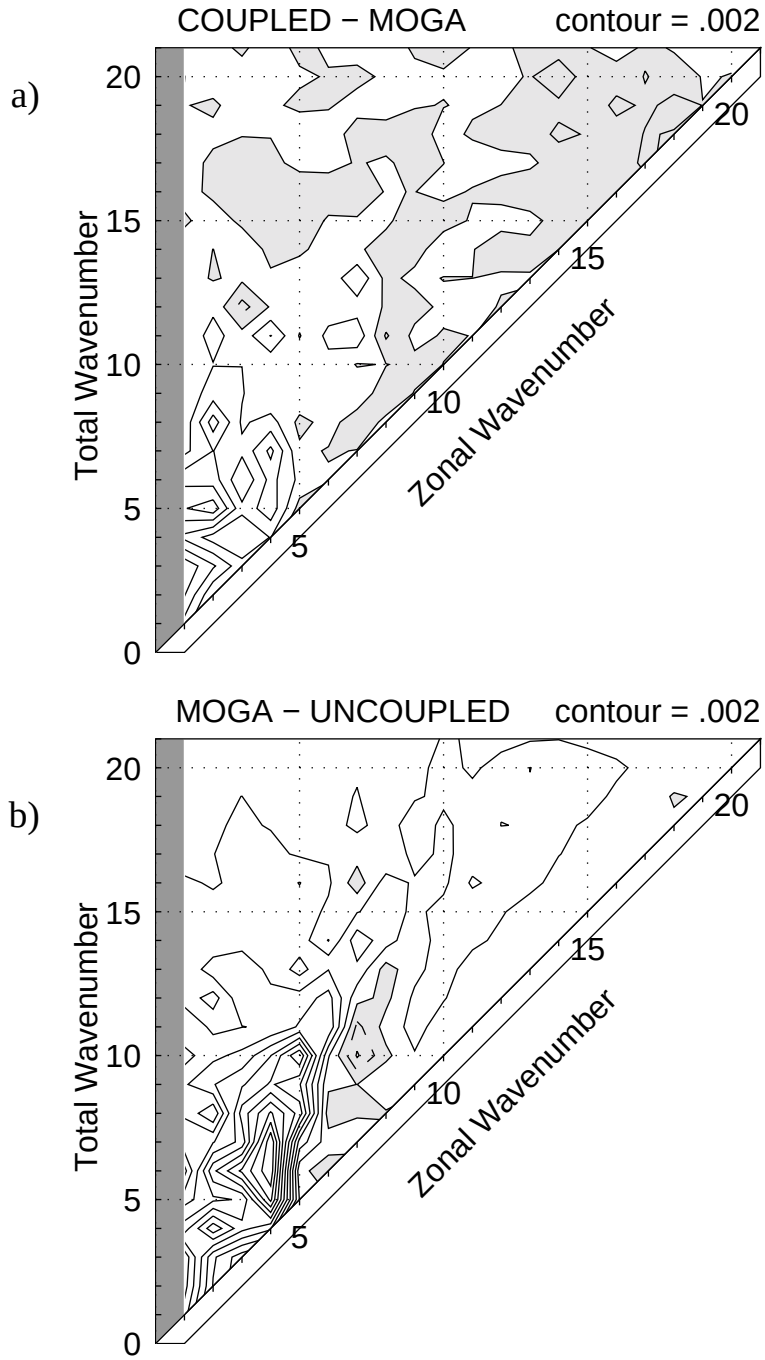

Figure 3.15. Same as the top panel in figure 3.7, except for difference of $\bar{\theta}$ between runs. a) COUPLED - MOGA, b) MOGA - UNCOUPLED. Units are K.

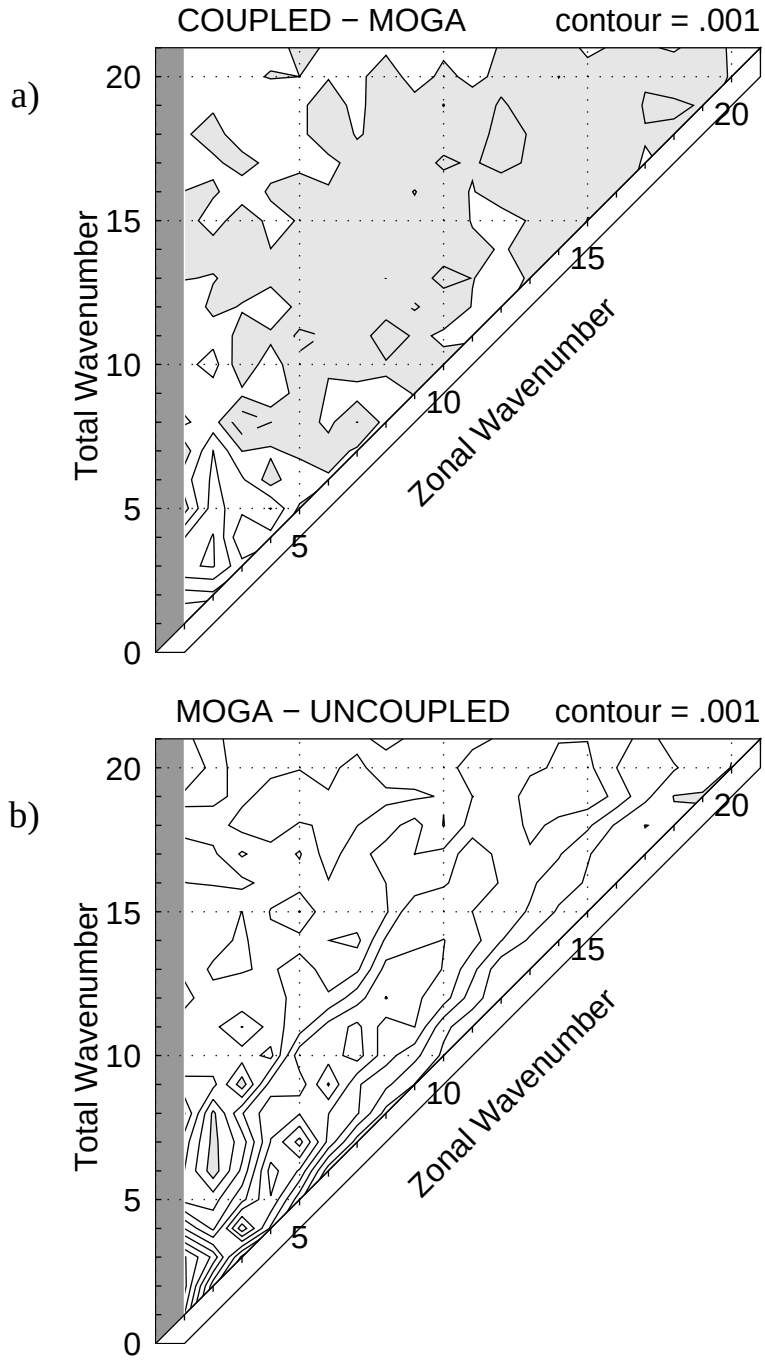

Figure 3.16. Same as the top panel in figure 3.7, except for difference of $\hat{\theta}$ between runs. a) COUPLED - MOGA, b) MOGA - UNCOUPLED. Units are K.

Chapter 4: Effects of Coupling on Variance, Persistence and Propagation of Low-Frequency Anomalies

4.1 Definition of Sea Surface Temperature Anomalies and SST Index

In all the following analysis, sea surface temperature (SST) anomalies are computed by subtracting the time mean SST at each gridpoint from the actual SST. For convenience of analysis, time series of pentad means (5-day means) were computed of the model variables and of quadratic quantities such as eddy kinetic energy, eddy heat flux and eddy momentum flux. (For the sake of clarity I reiterate that for the quadratic quantities I computed the time average of the products, not the product of the time averages). This averaging procedure acts as a low-pass filter. Unless explicitly stated otherwise, all analyzed quantities were computed from the pentad-mean time series.

To focus on the midlatitudes, an index time series of Southern Hemisphere midlatitude SST anomaly was created for every gridpoint in longitude by averaging the SST anomalies at latitudes 47°S, 41.5°S and 36°S for that longitude. The same was done for the Northern Hemisphere at latitudes 47°N, 41.5°N and 36°N. Recall that there should be no statistical difference between the model Northern and Southern Hemispheres.

Comparison among the model runs described in Chapter 3 will reveal three main effects of coupling relative to the UNCOUPLED and MOGA runs: increased total variance, increased persistence, and eastward propagation. In treating these subjects, the analysis proceeds sequentially from zero spatial dimensions (total variance and power spectra at a point), to one spatial dimension (time-longitude sections and wavenumber-frequency spectra along a latitude circle, which provide an indication of propagation and persis-

tence). Finally, the full spatial structure of the anomalies in two and three spatial dimensions is presented using one-point linear regression maps. Keep in mind that in the 2-level model the vertical structure of the atmospheric anomalies can be described completely either in terms of the upper and lower layers of the atmosphere, or in terms of the barotropic (vertical mean) and baroclinic (vertical difference) components.

4.2 Qualitative Description of SST Anomalies

Figures 4.1 (also color plate A) and 4.2 (also color plate B) present time-longitude sections of the midlatitude SST index for selected time periods of the COUPLED, MOGA DIAGNOSTIC, and UNCOUPLED diagnostic oceans. Figure 4.3 shows snapshots of SST anomalies for individual pentads which were selected to illustrate commonly occurring patterns. These choices were made after examining animated movies of SST anomaly and many individual SST maps. The plots I have chosen, along with the time-longitude sections, give a qualitative view of the typical space and time structure of midlatitude SST anomalies.

Maximum SST anomalies in the midlatitudes of the model are on the order of 1-2K, and tend to be of the same sign throughout the midlatitudes at a given longitude. Polar anomalies tend to have zonal wavenumber 1-2 as seen in figure 4.3b and 4.3c. Midlatitude events tend to have zonal wavenumbers 3 - 6. These midlatitude events often appear as wavetrains (figure 4.3a), global wavenumber 4-5 events (figure 4.3a), or localized anomalies (figure 4.3c, southern hemisphere). This categorization is not meant to be objective or definitive, but merely to serve as a guide to the quantitative analysis which will follow and to act as an anchor in reality when viewing more highly averaged fields. The time-longitude plots give an indication of the qualitative differences between the runs in the scale,

persistence and propagation characteristics of anomalies. It is indeed surprising that these modest SST anomalies are able to exert a significant influence on the low-frequency variability of the atmosphere in this model. The goal of the next several sections is to quantify these effects.

4.3 Spectra and Total Variance in the Midlatitudes

Even a cursory examination of the raw model output reveals that the COUPLED ocean exhibits larger SST variance than the UNCOUPLED DIAGNOSTIC ocean. A table of the total midlatitude variance is shown in Table 4.1 for SST, $\bar{\theta}$ and $\bar{\zeta}$. For SST the quantity shown is the mean of the temporal variances of each individual SST index time series (defined in section 4.1) over all longitudes and over both hemispheres. For the atmospheric variables the quantity shown is the mean variance at all longitudes for latitudes 41.5°N and 41.5°S. The COUPLED SST has approximately twice the total variance of the UNCOUPLED DIAGNOSTIC run, with the MOGA DIAGNOSTIC run lying in between. This hierarchy of variance occurs at all latitudes and for all zonal wavenumbers where there is significant variance, as shown in figure 4.4 and 4.5.

The corresponding variance ratios for the vertical mean atmospheric potential temperature, $\bar{\theta}$, are only on the order of 1.1, reflecting the fact that the model atmosphere has copious power at high and intermediate frequencies which are only weakly affected by coupling. A similar effect holds for the barclinic component of vorticity $\hat{\zeta}$, consistent with the thermal wind relation. The vertical mean vorticity, $\bar{\zeta}$, shows a 2% increase in variance due to coupling which may not be significant. We shall see in a later section that there is a strong wavelike signal in $\bar{\zeta}$ associated with anomalous SST in the COUPLED and both DIAGNOSTIC ocean runs. Because the enhancement of the total $\bar{\zeta}$ variance by the cou-

pling is so small. it can be inferred that $\bar{\zeta}$ signal must be primarily the result of a spatial reorganization of variability in the horizontal, rather than an overall enhancement of variability. The horizontal and vertical structure of these anomalies is discussed in more detail in section 4.6.

The power spectra of the midlatitude SST indices from the COUPLED, MOGA DIAGNOSTIC and UNCOUPLED DIAGNOSTIC runs is shown in figure 4.6. The power spectrum of $\bar{\theta}$ at selected latitudes is shown in figure 4.7. The spectra were computed from the pentad-mean data using 400-pentad Hanning window with a 200 day overlap for successive application of the window. The power spectrum at each longitude gridpoint was computed separately and then the spectra from all gridpoints at all longitudes in both hemispheres were averaged together. These spectra confirm that the main enhancement of atmospheric and oceanic temperature variance occurs only at very low frequencies, the same frequencies at which the SST has significant power. The spectrum of $\bar{\zeta}$ (figure 4.8) does not show much of a signal of the coupling effect, consistent with the small change in total variance. Note that the tendency for the spectral estimate at the lowest frequency in these plots to be much lower than at the second lowest frequency is probably an artifact of the spectral averaging which is implicit in the use of a Hanning window.

As an indication of the significance of the low-frequency enhancement of variance Table 4.2 shows the sum of the variance in the 10 lowest frequency bins along with the ratios of these quantities. For the spectra in question we can estimate the number of degrees of freedom per spectral estimate by dividing the total number of pentads (3000 from each hemisphere) by the total number of spectral estimates (200 for the window used here), yielding roughly 30 degrees of freedom per estimate. An individual spectral estimate has roughly twice this number of degrees of freedom due to the spectral averaging

effect of the Hanning window. For the 10-frequency average shown in Table 4.2 we get approximately 300 degrees of freedom (the effect of the Hanning window is inconsequential for a band-averaged spectral estimate). This is probably a conservative estimate of the number of degrees of freedom as the compositing of the spectra over longitude, and in the case of the SST spectra the averaging over adjacent latitudes, probably increases the significance substantially. The F-test for significance of the ratio of two variances (F = larger variance / smaller variance) indicates an *a priori* 95% confidence level for F = 1.21 and a 99% confidence level for F = 1.31. By this measure the SST variance differences among all the runs is significant. The differences in atmospheric temperature are also all probably significant at this level. However the differences among the runs in the barotropic vorticity field do not fulfill this test of significance.

The power spectra of the total surface flux is shown in figure 4.9. Total surface flux is defined as the sum of latent heat flux, sensible heat flux, and net longwave flux. Recall that the MOGA and UNCOUPLED runs each have two sets of fluxes associated with them. The first set consists of the fluxes which force the atmosphere, determined by the atmospheric variables and the prescribed SST. The power spectrum for these fluxes is shown in figure 4.9a. The second set consists of the fluxes which force the diagnostic ocean model, determined by the atmospheric variables and the time-dependent diagnostic ocean temperature. Their power spectra are shown in figure 4.9b. The COUPLED power spectrum is shown in both plots, as in this run the fluxes which the atmosphere feels and the fluxes which the ocean feels are identical.

A simple calculation yields some insight into relationship between the two types of fluxes in the UNCOUPLED run. To the extent that the effect of varying wind speed on the surface fluxes can be ignored, we can write

$$\frac{dT_{ocean}}{dt} = F_{ocean} \approx F_{atmosphere} + \lambda(T_{ocean} - T_{prescribed}) \qquad \text{(EQ 4.1)}$$

where $F_{atmosphere}$ and F_{ocean} are the surface fluxes that force the atmosphere and diagnostic ocean respectively, $T_{prescribed}$ and T_{ocean} are the prescribed SST and the diagnostic ocean SST respectively, and λ is a proportionality constant. For the UNCOUPLED run, $T_{prescribed}$ is constant in time and does not contribute to the variance. In that case we can solve for the ratio of power in the two fluxes:

$$\frac{P(F_{ocean})}{P(F_{atmosphere})} = \frac{\omega^2}{\omega^2 + \lambda^2} \qquad \text{(EQ 4.2)}$$

where $P(\ )$ represents the power of the quantity in the parentheses and ω the frequency. The two power spectra for the UNCOUPLED run are shown on the same plot in figure 4.10b.

The power spectra of the surface fluxes indicate an obvious, but important point. Because the COUPLED mixed-layer ocean can adjust to a low-frequency atmospheric temperature anomaly, the power in the COUPLED surface flux goes to zero as the frequency goes to zero. In contrast the power in the surface fluxes that force the UNCOUPLED atmosphere remains large all the way to the lowest frequencies. It is plausible that the main effect of this surplus of surface flux at low frequencies is to damp UNCOUPLED atmospheric variance -- a hypothesis that is supported by the smaller total thermal variance in this run compared to the COUPLED run.

The spectrum of fluxes into the MOGA diagnostic ocean generally lies in-between the COUPLED and UNCOUPLED spectra. In marked contrast, the fluxes into the MOGA atmosphere have the largest power at low frequencies of all the fluxes shown in figure 4.9. The reason for this large variance is that surface fluxes act as both forcing and damping in

the MOGA run. For the sake of argument, assume that we can separate the low-frequency variability of the MOGA atmosphere into two parts -- the “direct response” to the prescribed SST anomalies, and the “natural variability” which is unaltered from the UNCOUPLED case by the prescribed SST anomalies. The “natural variability” of the atmosphere would then be subjected on average to the same damping fluxes as in the UNCOUPLED run. The fluxes due to the “direct response” would then add to the damping fluxes, creating the large values seen in figure 4.9a. But in reality the separation is not so simple. The “direct response” and the “natural variability” of the MOGA run are correlated, and the low-frequency “damping” and “forcing” fluxes are not independent. The magnitude of this correlation will determine the relative roles of direct forcing and damping in determining the low-frequency variability. In any case, the chaotic nature of the atmospheric circulation will presumably result in these correlations being far from perfect, ensuring that damping will play a major role. Because of imperfect correlation between SST anomalies and atmospheric circulation, one would also expect that only a part of the enhanced thermal variance in the COUPLED run compared to the UNCOUPLED run is due to direct forcing by the SST anomalies, a conclusion which is supported by the integrated variance figures in Tables 1 and 2.

In conclusion, total SST variance is enhanced by coupling. Variance in the thermal fields of the atmosphere and the associated baroclinic streamfunction is also enhanced. Based on the results of the MOGA experiment it is estimated that only half the increased variance in this model due to coupling is accounted for by direct forcing of the atmosphere by SST anomalies.

4.4 Zonal Propagation

For anomalies that are confined in the meridional direction, time-longitude plots (often referred to in the atmospheric literature as Hovmoller plots) are a useful diagnostic tool. Figure 4.1 (and color plate A) shows a time-longitude plot of the Southern Hemisphere SST index from the COUPLED run and from the two DIAGNOSTIC ocean runs, for a selected time period. Figure 4.2 (and color plate B) shows the same for a segment of the Northern Hemisphere index. Several striking features are apparent to the eye. The COUPLED run anomalies have larger amplitude (note that the SST anomaly color scale has a greater range), larger zonal scale, and greater persistence than those in the UNCOUPLED run. The time-longitude plots of COUPLED SST show a tendency for long-lasting, coherent SST anomalies with predominantly eastward propagation. The MOGA DIAGNOSTIC SST plots also show a hint of eastward propagation and a zonal scale of the anomalies comparable to that of the COUPLED anomalies. The UNCOUPLED DIAGNOSTIC SST anomalies seem to show no preferred direction of propagation.

To quantify anomaly propagation in these runs I will look at wavenumber-frequency spectra, calculated as follows. First, the zonal Fourier transform of the midlatitude SST indices was calculated. Then the power in the frequency domain was calculated as for the one-dimensional spectra shown in section 4.3, except using 5000 day (1000 pentad) long realizations. A 1-2-1 smoother was applied to the spectrum in the frequency direction only, the time mean power estimates were then removed for plotting purposes. The power for the Northern and Southern Hemisphere indices was averaged. A contour plot of the square root of the power (the root-mean-square, or RMS amplitude of each spectral component) is shown in figure 4.11[1]. Only the upper half-plane of the spectrum is shown; the lower half-plane is related to the upper-half-plane by reflection through the origin. For the

plots shown, $\omega < 0$ corresponds to eastward traveling waves and $\omega > 0$ to westward traveling waves. (Note that these plots are reversed from the usual convention in which $\omega > 0$ and $k > 0$ corresponds to eastward propagation). This spectrum can roughly be thought of as the result of a two-dimensional Fourier transform of time-longitude plots like those in Figure 4.1 and 4.2.

There is a pronounced asymmetry in the spectrum of the COUPLED SST (Fig. 4.11a) at zonal wavenumbers 1-4 which is absent in the UNCOUPLED DIAGNOSTIC SST spectrum (Fig. 4.11c). The contour plot of the difference of these two spectra (Fig. 4.12a) demonstrates that this difference is mainly the result of an enhancement of eastward-propagating signals over a range of wavenumbers and frequencies in the COUPLED run. The COUPLED SST spectrum also shows a suppression of the westward propagating wavenumber 5 signal relative to the UNCOUPLED DIAGNOSTIC SST spectrum.

Comparison of the MOGA and UNCOUPLED DIAGNOSTIC SST spectra yield information about the effect of direct forcing of the atmosphere by SST anomalies. The MOGA run has a strongly enhanced eastward traveling wavenumber 1 signal compared to the UNCOUPLED run, as is shown in figure 4.12c. The low-frequency eastward and westward propagating signal at other low zonal wavenumbers is also enhanced in the MOGA run compared to the UNCOUPLED run. The difference between the COUPLED run and the MOGA run spectra, figure 4.12b, reveals that coupling has an effect above and beyond the direct effect of forcing by SST anomalies. The COUPLED spectrum shows a large enhancement of eastward wavenumber 4 power, and a small suppression of westward, wavenumber-4 power relative to the MOGA spectrum. The net effect is to increase the total power at wavenumber 4 while favoring the eastward traveling signal.

---

1. The RMS amplitude was chosen over the power for display purposes because this choice allows a greater range of power to be shown in a single contour plot.

The question of statistical significance arises, and is particularly vexing in this case. Because each spectral estimate has only a few degrees of freedom associated with it (6 in this case), and because we have no *a priori* reason to expect a peak at a given frequency, it is very difficult to establish the significance of any individual peak. Intuitively it seems as though a region of enhanced variance in the plots should have several degrees of freedom. One could theoretically proceed by making combinatorial arguments about all the possible contiguous blocks of statistical estimates, and produce some sort of *a posteriori* significance estimate for the signal in question. However, a simpler qualitative argument for the statistical significance of these results is that they are reproduced qualitatively in each hemisphere of the model separately (not shown). Though the spectral peaks do not occur at exactly the same frequencies in both hemispheres, the sense of the progression from UNCOUPLED to MOGA to COUPLED spectra is qualitatively similar.

We can get an estimate of the sampling error for various statistical moments of model variables by considering the linear regression between the SST index in one hemisphere and model variables in the opposite hemisphere. In effect we are using the opposite hemisphere as an independent realization of midlatitude variability that we can use to form a Monte Carlo estimate of the sampling error. Such “opposite hemisphere” statistics were produced in the course of the linear regression analysis presented in section 4.6 (not shown). For first order statistical moments (means), the sampling errors are quite small, usually between 5% and 10% of the spatial standard deviation at the corresponding latitude in the other hemisphere. For second moment quantities (variances, covariances), such as appear in the eddy vorticity flux convergence, the sampling error is between 10% and 20%. Some of this inter-hemispheric covariance may be of dynamical origin rather than due to sampling error, so this procedure provides a conservative estimate of sampling

error. Using the second moment estimates as a guide to the significance of power spectral estimates, it seems reasonable that the broad features of the space-time spectra are not the result of sampling error, though individual details may be.

An estimate of the range of phase speeds of the COUPLED anomalies can be derived by inspection of the time-longitude plots. Typical phase speeds for the wavenumber 4-5 features are in the range of 0.05 - 0.20 m/s, corresponding to a drift of between 5 and 20 degrees of longitude in 100 days. This propagation shows up on the wavenumber-frequency spectrum as the enhanced power in wavenumber 4 at frequencies between -.001 and -.003 (day $^{-1}$). These estimated phase speeds are of the same order as for the (damped) coupled linear modes in the quasi-geostrophic channel models described by Frankignoul (1985). Further comments on the feasibility of a linear explanation for this phenomenon are given in Chapter 5.

4.5 Persistence

The time-longitude plots (Figs. 4.1 and 4.2) suggest an increase in the persistence of SST anomalies, and by implication an increase in the persistence of the low-frequency atmospheric anomalies that are their cause. Even for stationary anomalies, persistence can be difficult to quantify and dependent on how persistence is defined. The situation is even more ambiguous for intermittently coherent anomalies which propagate at a range of speeds, as do the SST anomalies in the COUPLED run. To quantify persistence I have chosen an *ad hoc* method involving a direct analysis of a contoured version of the time-longitude plots of midlatitude SST index. In this method, a closed contour on a time-longitude contour plot is defined to be a single SST “event”. The method is described in detail in Appendix B.

The result of such an analysis on the COUPLED, MOGA and UNCOUPLED run SST indices is shown in figure 4.13. In this plot the cumulative fraction of event duration is plotted, starting with the longest lasting events. The SST events in the two hemispheres have been pooled together for this analysis; positive and negative anomalies are treated separately. This plot shows that, for example, the 200 longest events in the COUPLED run account for almost 75% of the total event duration. The comparable figure for the MOGA DIAGNOSTIC SST is 65% and for the UNCOUPLED DIAGNOSTIC SST 50%. These results hold when the positive and negative anomalies are pooled together and the two hemispheres considered separately (not shown).

One may question whether the computation of the fraction of total duration rather than the total sum of duration biases the analysis. To check this, figure 4.14 shows a plot of the cumulative sum of anomaly duration versus anomaly rank. There are more UNCOUPLED events and they add up to a longer total duration than for the other two runs, so that eventually the UNCOUPLED curves will overtake the others. However, for the first hundred or more anomalies the results from figure 4.13 are reproduced. In fact this unnormalized measure of persistence admits a simple description: the 100 longest events average approximately 60 days in duration for the COUPLED run, 50 days for the MOGA run, and 40 days for the UNCOUPLED run. Therefore, for the definition I have chosen, coupling increases persistence of the longest-lasting anomalies.

4.6 Three Dimensional Structure of Atmospheric Fields Associated with SST Anomalies

In order to set the stage for the discussion of possible mechanisms we will present here a diagnosis of the horizontal and vertical structure of the atmospheric anomalies associated with SST anomalies in the various runs. We will make extensive use of zonally

composited one-point linear regression maps, to be defined below. This course of analysis was chosen over other possibilities such as EOF or SVD analysis which generally perform better with spatially localized variability. Compositing on individual events was attempted and rejected as a method as it seemed to be unduly sensitive to the presence or absence of neighboring anomalies. While compositing may better describe the evolution of an individual anomaly, the present analysis sacrifices detail to increase statistical significance.

We will first describe how we compute the linear regression maps. Then the results of this analysis are presented for the surface fluxes. This is followed by a description of the structure of the atmospheric fields associated with the COUPLED SST, MOGA DIAGNOSTIC SST and UNCOUPLED DIAGNOSTIC SST. The nonlinear and linear response of the atmosphere to prescribed SST forcing is then computed and discussed. In order to find the cause of the low-frequency surface air temperature, an anomaly heat budget is calculated for the lower level heat equation using linear regression. An anomaly vorticity budget of the upper layer is carried out to investigate whether this field due is affected by coupling.

It is important to recognize that there are two possible sets of linear regressions that one can perform using the MOGA atmosphere. The first is the linear regression of the MOGA atmosphere variables against the MOGA DIAGNOSTIC SST, and the second is the regression of the MOGA atmosphere against the COUPLED SST which was prescribed as the lower boundary condition for that atmosphere run. When it would otherwise be ambiguous, I will use the term MOGA DIAGNOSTIC OCEAN to identify the former and MOGA ATMOSPHERIC RESPONSE, or more concisely MOGA-RESPONSE to identify the latter.

4.6.1 Linear Regression Maps

A one-point linear regression map is the map of linear regression coefficients between a reference time series and the time series at each gridpoint of a target atmospheric or oceanic field. For example one may choose as the reference time series the SST anomaly at a given model gridpoint, and as the target field the 250 mb streamfunction field. This technique is analogous to the more commonly used diagnostic tool of one-point correlation maps. The regression maps have the advantage over correlation maps of quantifying the relationship between the reference time series and the corresponding variables. In our case the units of the regression maps are always in terms of the amplitude of the target field per degree of SST anomaly.

In this study, the midlatitude SST indices defined above are chosen as the reference time series. To obtain a zonally composited linear regression map, we first form the one-point regression maps for each separate reference time series along a latitude circle. Such maps for all gridpoints at a given latitude are then composited, centered on the reference latitude, to form the final composited regression maps. I will refer to these simply as "regression maps". A sense of the statistically averaged time evolution of these anomalies can be obtained by performing the linear regression using a lag between the SST time series and the target field. I will refer to these as "lag regression maps". For slowly varying SST anomalies it is fruitful to apply this technique to all the terms in one of the model equations to obtain a "regression anomaly budget" in the form of a set of maps. This technique is described in more detail Appendix A. The main result is that for quadratically nonlinear terms, represented using the generic variables X and Y, we have: $(\tilde{XY}) = \overline{X}\tilde{Y} + \tilde{X}\overline{Y} + (\tilde{X'Y'})$, where an overbar here is the time mean, a prime the deviation from the time mean, and a *tilde* the linear regression against some reference time

series. These maps should not be thought of as the response to SST forcing, except in the MOGA ATMOSPHERIC RESPONSE case below. The technique will be used primarily to isolate the spatial structures of the atmospheric anomalies associated with SST anomalies.

4.6.2 Surface Fluxes

In this model the only causes of SST anomalies are anomalous surface fluxes of latent heat F_{LH}, sensible heat F_{SH}, net longwave radiation F_{LW},and net shortwave radiationF_{SW}. One expects that the sensible and latent heat fluxes would be dominant, and indeed this is the case. Figures 4.15 - 4.17 shows the lag regression maps for F_{SH}, F_{LH} and F_{LW}, vs. the Southern Hemisphere SST index for the COUPLED run for the ocean lagging the atmosphere by 120, 60, 0, -60, and -120 days. Time increases downward in all the lag-regression plots. All fluxes are defined to be positive-upwards. The individual panels have been inverted in order to provide a Northern Hemisphere orientation. The anomalous insolation F_{SW} is not shown because it is computed only for the zonal mean and its variability is insignificant in this model. The simultaneous regression maps (the middle panel in each figure, with lag=0) indicate local maximum sensible and latent heat flux anomalies of approximately 8 W m^{-2} per degree K of SST anomaly. The anomalous longwave flux is approximately 2 W $m^{-2}K^{-1}$. It is important to keep in mind that these plots mainly show the anomalous fluxes that force the SST anomalies, and not the “response” to that anomaly. The individual anomalous fluxes are all in the same sense, with only the obvious geographic variations in the meridional direction due to the sensitivity of the latent flux parametrization to the mean temperature. Hence from here on only the total surface flux, shown in figure 4.18 will be considered. The time evolution of the total flux

anomalies is such that they force the SST anomaly for times preceding the simultaneous maps, and damp the SST anomaly for times following the simultaneous maps. In other words, the total surface fluxes show a lag-regression pattern that is antisymmetric in lag, which is a necessary consequence of their role as the sole forcing of SST anomalies in this model. The simultaneous regressions show a flux pattern in zonal quadrature with the SST anomaly. While one might want to interpret a surface flux pattern in quadrature with SST as a sign of propagation, this interpretation is only correct only if feedback between the fluxes and the SST anomaly is allowed -- that is, only for the COUPLED system.

The regression maps of the total surface flux vs. the DIAGNOSTIC SST from the UNCOUPLED and MOGA runs, shown in figure 4.19 and 4.20 respectively, differ only subtly from those for the COUPLED run (Fig. 4.18) with slight displacements of the surface fluxes relative to the SST anomaly in the COUPLED run compared to the other runs. The UNCOUPLED run also shows a much more prominent zonal wavenumber 5 pattern in the simultaneous regression map than either of the other runs. Note that figure 4.21, which will be discussed in section 4.7, is included here with the other surface flux regression maps for later convenience of comparison.

The anomalous surface fluxes can result from anomalous surface wind or from anomalous ocean-atmosphere temperature difference. In order to investigate the relative contributions of these terms, the surface fluxes were separated into the following terms:

$$F_{\mathrm{SH+LH}} = c_1\overline{u_s}(T_o' - T_a') + c_2 u_s'(\overline{T_o} - \overline{T_a}) + c_3 u_s'(T_o' - T_a') \qquad \text{(EQ 4.3)}$$

where the constants c_1, c_2, and c_3 take into account the various constants which go into the bulk aerodynamic formulae, as well as the linearization of the dependence of saturation mixing ratio on temperature. Here the anomalous wind speed is defined as the actual surface wind speed V_c (defined by Eq. 2.4a) minus the time mean of V_c. These regression

maps (not shown) indicate that anomalous ocean-atmosphere temperature difference provides the main forcing of anomalous SST in this model. The regressions are antisymmetric with respect to lag, with regressions for the atmosphere leading the ocean being of the opposite sign as regressions with the atmosphere lagging the ocean.

The forcing by anomalous surface wind, though weaker, exhibits a strong zonally symmetric pattern (not shown). In addition, the regressions are strongly one-sided with respect to lag -- much stronger for the atmosphere leading the ocean than *vice-versa.* Interestingly, the zonal mean of the simultaneous regression map for anomalous wind forcing has almost exactly the same meridional structure as the first rotated EOF of surface wind speed. (not shown). The above points indicate that the component of forcing due to anomalous surface wind speed is likely to be the surface expression of the atmospheric zonal index cycle in this model. See Robinson (1991b) for a discussion of the index cycle in a 2-level model, and Yu and Hartmann (1993) for analysis of the index cycle in a multi-level atmospheric GCM. Investigation of the coupling of index cycle variability to SST anomalies is beyond the scope of the present study.

4.6.3 Horizontal and Vertical Structure of the COUPLED, MOGA, and UNCOUPLED Atmospheric Anomalies in Relation to the SST Anomalies that They Force

The lag regression maps of COUPLED 250 mb and 750 mb streamfunction with COUPLED SST are shown in figures 4.22 and 4.23 respectively. The sense of the circulation in all regression maps of streamfunction shown in this dissertation is such that a maximum of streamfunction corresponds to an anticyclonic circulation. The maximum streamfunction anomalies correspond to height anomalies[1] (per degree K of SST anom-

1. Approximated by multiplying the streamfunction by f/g.

aly) of approximately 50 m K^{-1} at 250 mb and 20 m K^{-1} at 750 mb. The vertical structure for the first three lags shown (lag = 120, lag = 60, and lag = 0 days, as labeled on the individual panels) is strongly barotropic, though the simultaneous (lag = 0) regression shows a non-zero phase shift between upper and lower levels. The time evolution appears somewhat like a localized wavetrain trapped in a zonal waveguide, with slow eastward group velocity. The shape of the low-frequency streamfunction anomalies, and presumably the deformation field with which they are associated, is reminiscent of the patterns of low-frequency variability described in two-level and barotropic models of Robinson (1992) and Qin and Robinson (1991). This similarity is an indication that the structure of the atmospheric variability in the COUPLED runs that is associated with SST anomalies appears to be determined mainly by the natural, uncoupled variability of the 2-level atmosphere alone. The maps for the atmosphere lagging the ocean (Fig. lag = -60 and -120 days) are contoured using a smaller contour interval that for the other lags. These maps show a weak baroclinic structure which we will come to see is the model's nonlinear response to prescribed SST forcing.

The 250 mb divergence field (proportional in this model to the 500 mb vertical velocity) simultaneous regression map (Fig. 4.24) indicates a wave-like pattern of upward and downward motion with a local maximum of upward motion over and slightly west of the warmest water. The corresponding $\bar{\theta}$ anomalies (Fig. 4.25) also exhibit a wave-like pattern with the maximum warm anomaly located above or slightly east of the SST maximum. The $\hat{\theta}$ anomalies (Fig. 4.26) are much smaller than the $\bar{\theta}$ anomalies and do not exhibit a wave-like pattern. The eddy vorticity flux convergence (Fig. 4.27) acts in a sense to reinforce the anticyclonic vorticity anomaly located above the SST maximum. The streamfunction, divergence, and $\bar{\theta}$ regression maps are consistent with the interpretation

that the phenomenon captured in the analysis of the COUPLED run is primarily (but not entirely) the forcing of the ocean by the natural variability of the atmosphere.

The MOGA DIAGNOSTIC regression maps (Figs 4.28-4.30) and UNCOUPLED DIAGNOSTIC regression maps (Figs 4.31 - 4.33) are strikingly similar in structure to those for the COUPLED run. In the interest of conciseness, only the 250 mb streamfunction, 750 mb streamfunction, and mean potential temperature fields are shown. The difference among these runs in overall magnitude of the linear regressions is partly a by-product of the linear regression method itself. In computing the linear regressions, the covariance between SST and the target field is divided by the variance of SST. Because the variance of SST is largest in the COUPLED run, and smallest in the UNCOUPLED run, there is a tendency for the COUPLED regressions to be significantly smaller than the UNCOUPLED regressions, with the MOGA regressions lying somewhere in-between in amplitude. For the barotropic vorticity field, the actual variance is almost identical among the three runs, so the effect of dividing by the SST variance is very pronounced. The thermal fields, and the baroclinic component of the wind field, are much more closely tied to the SST. For example, while the lower level streamfunction regression coefficient varies by about a factor of 2 between the COUPLED and UNCOUPLED runs, the lower level potential temperature regression coefficient in the region of maximum SST remains roughly constant in all three runs.

The strong coupling of the thermal fields of the atmosphere to SST anomalies, and the relative insensitivity of the barotropic component of the flow indicates that the difference between the COUPLED and UNCOUPLED runs can be summarized as follows. The baroclinic component of the flow is weaker in the UNCOUPLED run than in the COUPLED run, while the barotropic component is roughly the same in the two runs. This

description is consistent with the effect of coupling on thermal damping discussed in section 4.3. Because the COUPLED thermal anomalies are damped less rapidly due to surface fluxes than the UNCOUPLED thermal anomalies, the COUPLED anomalies tend to be larger. One additional consequence of the difference in baroclinic structure is that the lower-level wind, and hence the frictional damping tends to be weaker in the COUPLED run than the UNCOUPLED run. This seems to indicate that reduced frictional damping and reduced thermal damping go hand-in-hand.

4.7 Nonlinear and Linear Response to SST forcing: MOGA-RESPONSE and LINEAR runs

The previous section emphasized the forcing of the ocean by the atmosphere. Here I will consider the problem of the response of the atmosphere to prescribed SST anomalies. For the nonlinear 2-level model we can do this within the framework of the runs already described. For this purpose we compute lag regression maps for MOGA atmosphere variables vs. the COUPLED midlatitude SST index. The resulting maps (Figs. 4.34 - 4.39) depict the response of the model atmosphere to prescribed, time-dependent SST forcing and will be referred to by the name MOGA ATMOSPHERE RESPONSE, or simply MOGA-RESPONSE. Three aspects of this set of plots stand out. The first is the small amplitude of the response compared to the amplitudes seen in the COUPLED, MOGA DIAGNOSTIC, and UNCOUPLED DIAGNOSTIC regressions for lags of 120, 60, or 0 days. The second is that the local response in the region of heating is baroclinic and looks qualitatively like the prediction of linear theory. The third is that the regression maps are nearly symmetric with respect to lag, indicating that the atmosphere is nearly in statistical equilibrium with the SST.

The question naturally arises: to what extent would the linear response to the simul-

taneous regression map of SST (shown as the background maps in the simultaneous lag regression plots) resemble the nonlinear response? To answer this, the two-level model, including all physics except for convective adjustment, was linearized about the zonal mean of the climatology of the COUPLED run. The steady linear response to forcing was computed using the method described in Hoskins and Karoly (HK, 1983). The 3-rd order Adams-Bashforth time-stepping scheme of the 2-level model was replaced by a simple forward difference time step for the determination of the system matrix.

Briefly, the method is as follows. The system matrix **A** was calculated one column at a time by setting one spherical harmonic coefficient of the atmospheric state variables, $\underset{\sim}{X}$ equal to one and the others to zero and calculating the time derivative of $\underset{\sim}{X}$. This results in a matrix equation:

$$\frac{d}{dt}\underset{\sim}{X} = \mathbf{A}\underset{\sim}{X} + \underset{\sim}{F}. \qquad \text{(EQ 4.4)}$$

where $\underset{\sim}{F}$ is the forcing to be specified. The simultaneous regression map of COUPLED SST anomaly is then used to calculate the linearized thermal forcing of the atmosphere, which was projected onto the spherical harmonics. Because of the model physics, there is some forcing at both levels of the atmosphere. Since the chosen basic state is zonally symmetric, the problem is separable in zonal wavenumber. Eq. 4.4 is solved, one zonal wavenumber at a time, and the results transformed to physical space. Together figures 4.40a-e and 4.41a-e show the linear response in several atmospheric variables, some of which will not be discussed.

The LINEAR response 250 mb streamfunction (Fig. 4.41a) and 750 mb streamfunction (Fig. 4.41b) is strikingly similar in horizontal structure to the corresponding MOGA-RESPONSE fields (Figs. 4.34 and 4.35, respectively), however the LINEAR response is about twice as large as the MOGA-RESPONSE near the SST maximum. In addition, the

far-field LINEAR response is less attenuated than the in the MOGA-RESPONSE regression maps. The MOGA-RESPONSE is similar to what the linear response would be in the presence of large damping or horizontal diffusion. There is also a far-field barotropic wave train to the north of the midlatitude waveguide in the LINEAR response that one is hard pressed to find in the MOGA-RESPONSE fields. The divergence fields (Fig 4.40e for the LINEAR response and Fig, 4.38 for the MOGA-RESPONSE), $\bar{\theta}$ fields (Fig. 4.40c and Fig. 4.36), and $\hat{\theta}$ fields (Fig. 4.40d and Fig. 4.37) also show a great deal of similarity in structure between the LINEAR response and MOGA-RESPONSE.

4.7.1 Linear Regression of 750 mb Heat Budget

One can compute an anomaly budget for an atmospheric variable by constructing the linear regression maps for the individual terms in the time tendency equation for that variable. For the sake of comparison between runs it is convenient to compute a budget with respect to a reference time series that has been normalized to have unit variance. This procedure is described in detail in Appendix B. All budgets presented here are computed using simultaneous (lag = 0) linear regressions.

The dominant terms in the 750 mb potential temperature (heat) anomaly budgets for the COUPLED (Fig. 4.42), MOGA DIAGNOSTIC (Fig 4.43), and UNCOUPLED DIAGNOSTIC (Fig 4.44) experiments are almost identical in structure. In all three cases, the largest terms are the zonal and meridional advection of temperature (panels a and b in the above figures). These two terms cancel one another out to a large extent, resulting in their sum (panel f) being of the same order of magnitude as the adiabatic heating term (panel c). The total dynamical heating (panel e), defined as the negative of the sum panels a, b, c, and d, nearly balances the surface flux. Diffusion, radiative fluxes at 500 mb, convective

adjustment, and the budget residual are not shown. From the similarity among the budgets we can infer that the structure of low-frequency variability in these three models is the same to lowest order.

In the MOGA- RESPONSE heat budget (Fig. 4.45) the zonal and meridional advection terms act in the same sense, so that the total horizontal advection is the dominant term in balancing the diabatic heating due to surface fluxes. The adiabatic heating term and eddy flux convergence play minor roles.

4.7.2 Linear Regression of 250 mb Vorticity Budget

The normalized 250 mb anomaly vorticity budgets are shown in figures 4.46 - 4.48. Once again the note the similarity in structure among the COUPLED (Fig. 4.46), MOGA DIAGNOSTIC (Fig 4.47) and UNCOUPLED DIAGNOSTIC (Fig 4.48) budgets. The three-way balance between zonal advection, meridional advection and vortex stretching is again due to the large cancellation between the individual horizontal advection terms. Eddy vorticity flux convergence, which acts to reinforce the anticyclonic vorticity anomaly that lies above the SST maximum, is necessary to balance the damping effect of Ekman pumping due to surface friction. As seen in the heat budgets above, the MOGA-RESPONSE 250 mb vorticity budget stands apart from the rest. In particular, the vortex stretching term (Fig 4.49c) shows a strong maximum to the west of the SST maximum which is a consequence of the downward motion there.

The difference between the normalized 250 mb vorticity budgets for the COUPLED and UNCOUPLED DIAGNOSTIC runs is shown in figure 4.50. The main difference lies in the zonal wavenumber 5 component of the horizontal advection terms. The difference between the COUPLED and MOGA DIAGNOSTIC budgets is shown in figure 4.51. In

the immediate neighborhood of the SST maximum the difference resembles the MOGA-RESPONSE budget in structure. The resemblance is particularly strong in the vortex stretching term, a reflection of anomalous downward motion to the west of the SST maximum and anomalous upward motion to the east of the SST maximum which is present in the COUPLED run.

The 250 mb vorticity budget, as well as the linear regression maps shown earlier, are consistent with a 750 mb vorticity budget (not shown) in which the main balance is between meridional advection of planetary vorticity, vortex stretching, and frictional damping. Such a balance is a slight variant of that described in the final section of Palmer and Sun (1985). They put forth this balance as a possible explanation for the equivalent barotropic response of the atmosphere to a prescribed SST anomaly that they observed in their numerical model. Instead we see that this balance does not represent the direct response of the atmosphere but rather reflects the natural low-frequency variability of the uncoupled atmosphere.

4.8 Summary of Results

We are now in a position to answer the questions posed at the beginning of Chapter 3, at least from a phenomenological standpoint. Taken in the same order as before:

- Coupling enhances variance in the thermal fields and the associated thermal wind field of the atmosphere-ocean system. This enhancement takes place for time scales longer than the mixed-layer time scale, and is seen at all latitudes and for all zonal wavenumbers. For the parameters in this model, the amplitude of SST anomalies at low frequencies is enhanced by approximately a factor of two.
- Coupling also leads to increased persistence of SST anomalies, and by infer-

ence of the atmospheric anomalies that force the SST anomalies, though this effect is difficult to quantify.

- Coupling has a substantial effect on the qualitative nature of low-frequency variability, even though the direct atmospheric response to SST forcing is small. Coupling favors the eastward propagation of SST anomalies.
- For both the increased variance and eastward propagation, and possibly the increased persistence as well, it appears that there is an effect due to atmosphere-ocean feedback which acts in addition to direct forcing of the atmosphere by the SST anomalies. The two effects are of comparable magnitude.

Several other results were obtained along the way to answering the above questions. The surface fluxes in this model all act in the same sense and can be considered in sum rather than individually. The main contribution to the forcing of low-frequency midlatitude SST anomalies in this model comes from the variability in air-sea temperature difference rather than the variability in wind speed. However, the wind speed effect, which has a substantial zonal mean component, is not entirely negligible.

The atmospheric anomaly associated with a COUPLED SST anomaly is equivalent barotropic in structure and consists of an anticyclone centered slightly eastward from a warm SST anomaly. The COUPLED structure is strikingly similar to the structure associated with the UNCOUPLED DIAGNOSTIC and MOGA DIAGNOSTIC SST, indicating that the natural variability of the atmosphere alone plays an important role in all three simulations. The primary difference among the runs lies in the amplitude of the thermal fields. Therefore it can be inferred that the amplitude of the baroclinic circulation relative to the barotropic circulation varies from run to run due to coupling.

A lower level anomaly heat budget and upper level anomaly vorticity budget confirm that the patterns of variability resemble that of a finite-amplitude near-stationary Rossby wave in a midlatitude waveguide. Horizontal and vertical advection are both

important, and eddy fluxes act to balance the anomaly against dissipation.

The MOGA atmosphere's response to prescribed SST forcing has a strongly baroclinic vertical structure in the atmosphere region of forcing, in striking contrast to the results of the COUPLED, MOGA DIAGNOSTIC, and UNCOUPLED DIAGNOSTIC experiments. The response of the fully nonlinear MOGA atmosphere to the prescribed SST anomalies (as seen in the MOGA-RESPONSE regressions) is similar in structure to the response of the linearized model to the regressed SST anomaly from the COUPLED run, but has only about half the amplitude of the linear response.

In conclusion, even a weak coupling between the natural atmospheric variability in the two-level atmosphere model and the simplest of ocean models leads to large changes in the nature of low-frequency variability. A discussion of possible mechanisms to explain the above phenomena is presented in the next chapter.

Table 4.1: Total Variance for Pentad Means GLOBAL

Variable	COUPLED	MOGA	UNC.	C/U	M/U
SST Index	0.24	0.19	0.11	2.07	1.62
$\bar{\zeta} \times 10^{10}$	1.67	1.67	1.63	1.02	1.02
$\bar{\theta}$	4.60	4.47	4.12	1.12	1.09

Representative midlatitude variance of selected variables. Variance is based on pentad mean data. The mean of Northern and Southern Hemisphere variance is shown. SST indicates the midlatitude SST indices defined in the text. $\bar{\zeta}$ is the relative vorticity at latitudes 41.5°N and 41.5° S. $\bar{\theta}$ is the vertical mean potential temperature at latitudes 41.5°N and 41.5°S.

Table 4.2: Mean Power in Midlatitudes at Lowest Frequencies

Variable	COUPLED	MOGA	UNC.	C/U	M/U
SST Index	35.0	25.2	14.6	2.40	1.73
$\bar{\zeta} \times 10^{10}$	27.1	26.2	25.4	1.06	1.03
$\bar{\theta}$	83.5	70.4	54.0	1.54	1.30

As in table 4.1 except for average power in lowest frequencies, defined as 5×10^{-4} day $^{-1}$ to 5×10^{-3} day^{-1}.

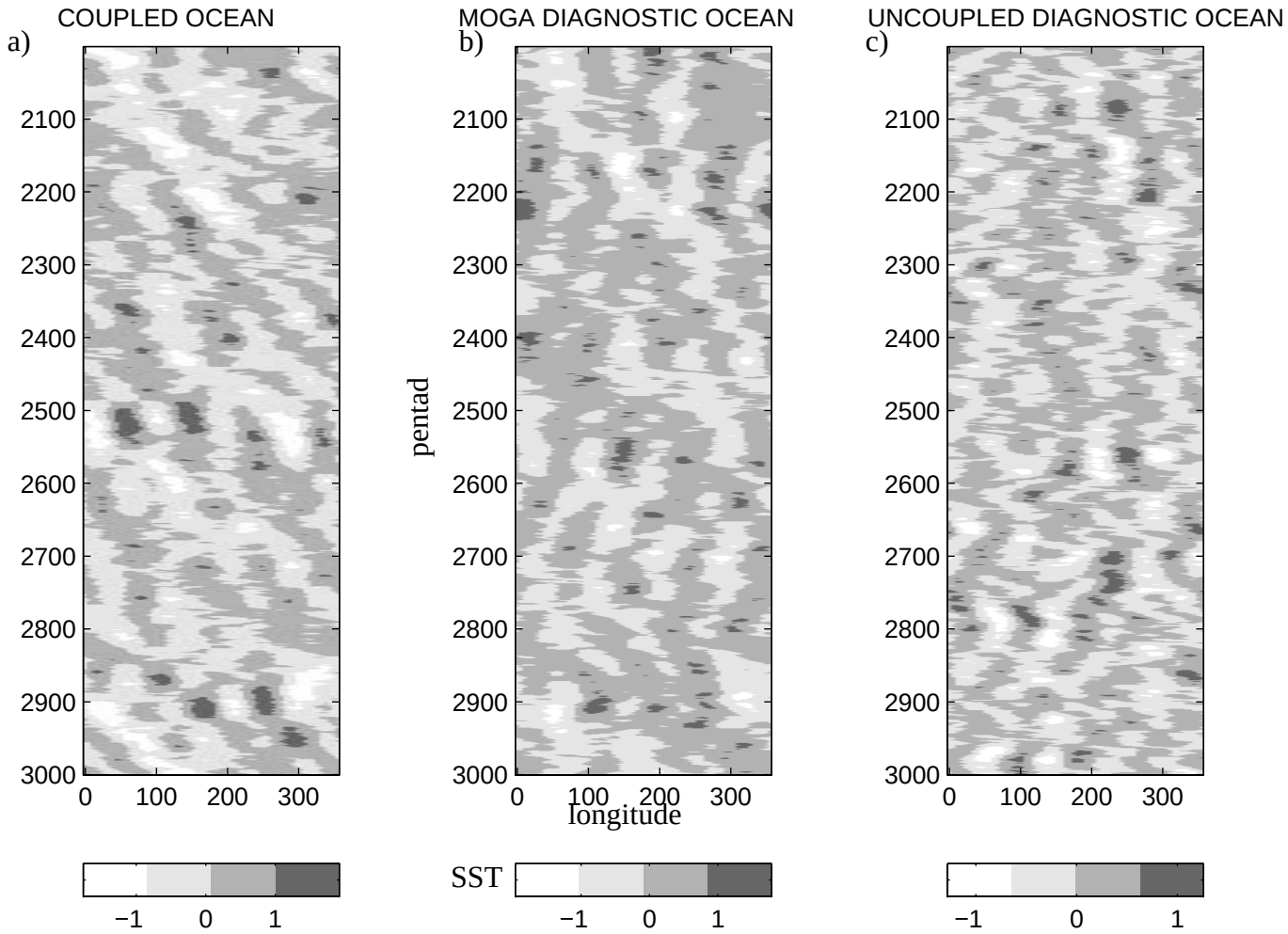

Figure 4.1. Time-longitude plot for Southern Hemisphere SST index as defined in text. SST anomaly (K) gray scale is shown beneath each figure. a) COUPLED ocean; b) MOGA diagnostic ocean; c) UNCOUPLED diagnostic ocean. Longitude is in degrees, time is in pentads.

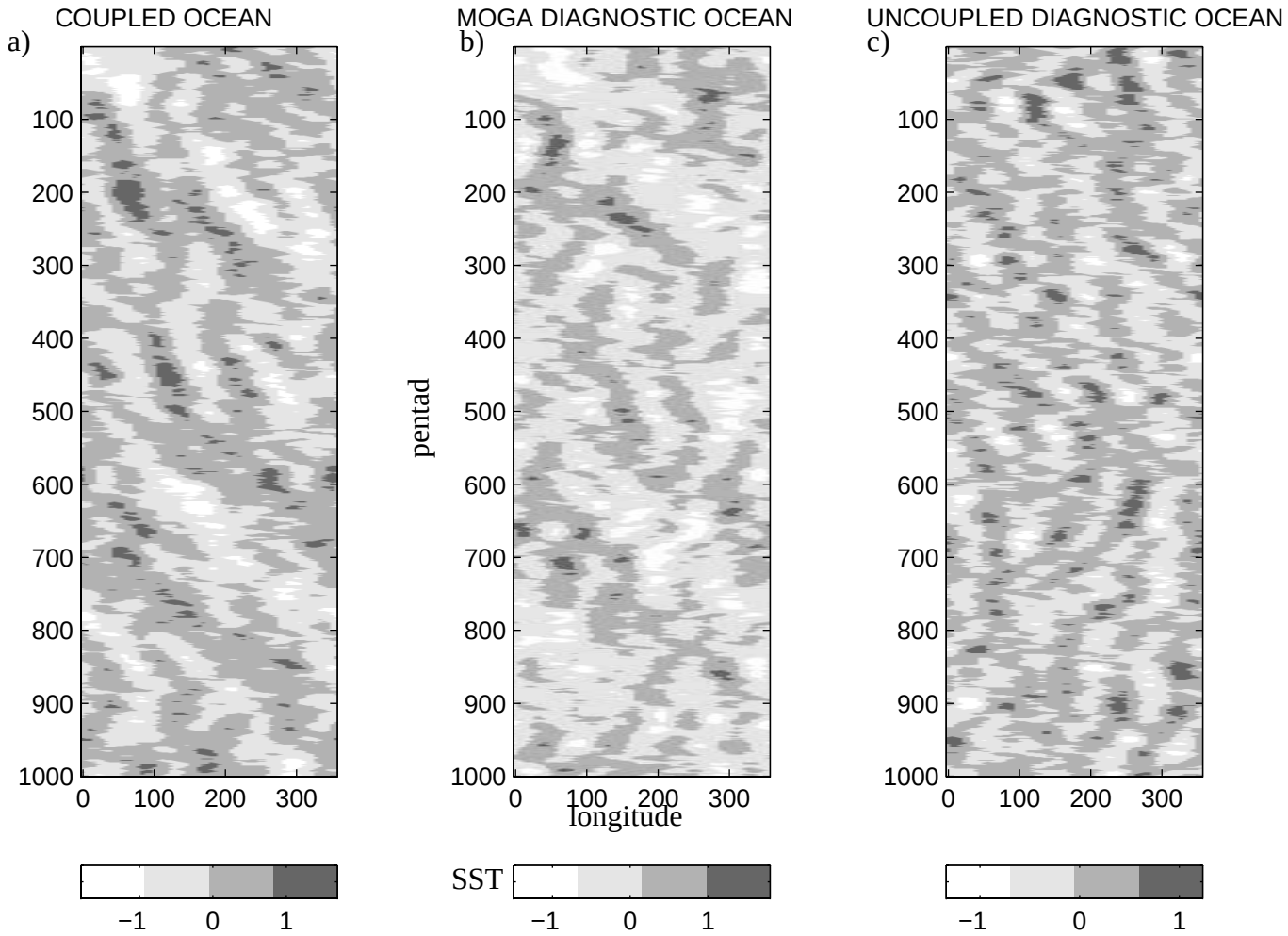

Figure 4.2. Time-longitude plot for Northern Hemisphere SST index as defined in text. SST anomaly (K) gray scale is shown beneath each figure. a) COUPLED ocean; b) MOGA diagnostic ocean; c) UNCOUPLED diagnostic ocean. Longitude is in degrees, time is in pentads.

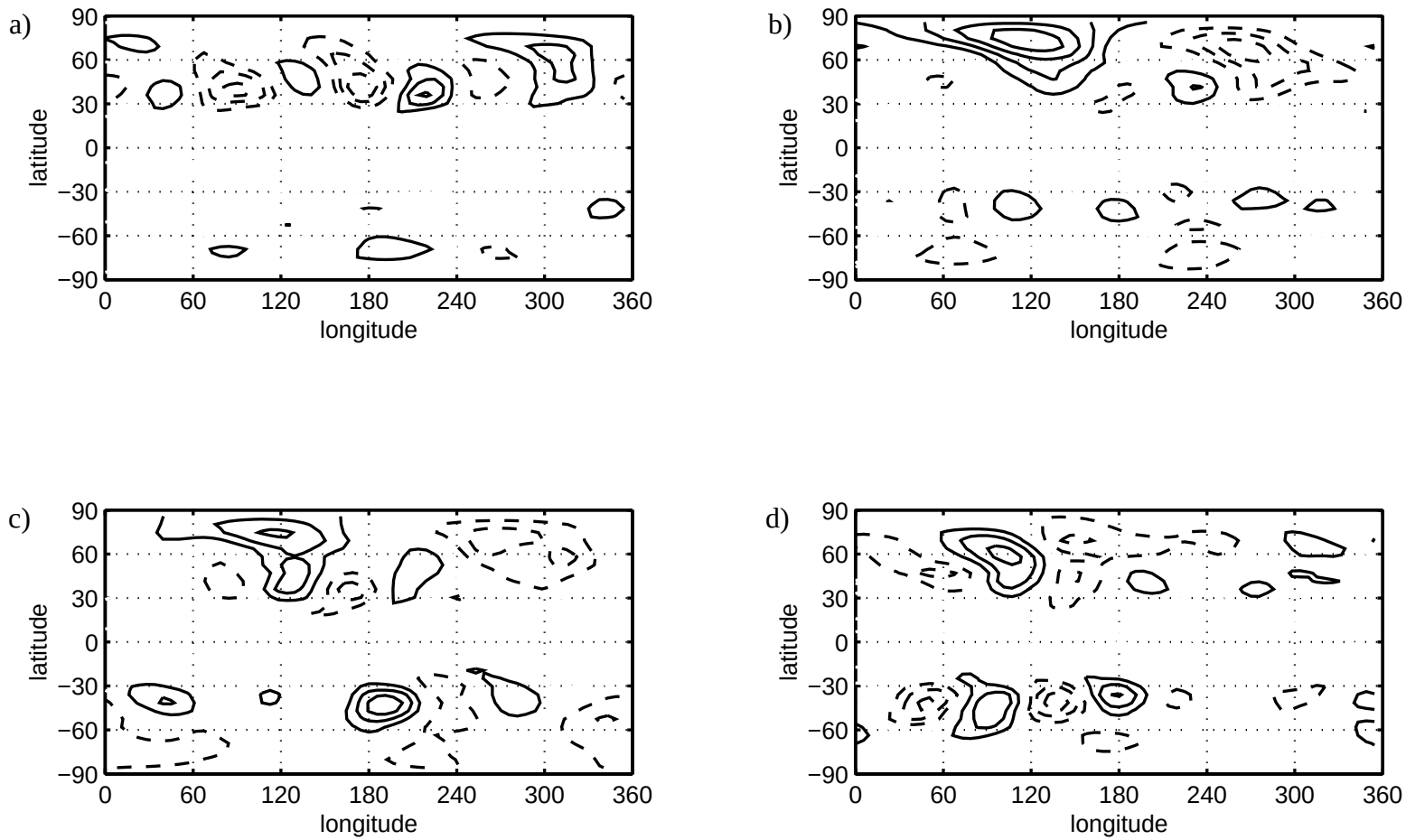

Figure 4.3. Sample SST pentad(5 day mean) anomaly for a) COUPLED pentad 1060 ; b) COUPLED pentad 475; c) COUPLED pentad 494; d) UNCOUPLED diagnostic ocean pentad 2980. Contour interval is .5 K in a) b) and c), .35K in d). Zero contour is suppressed.

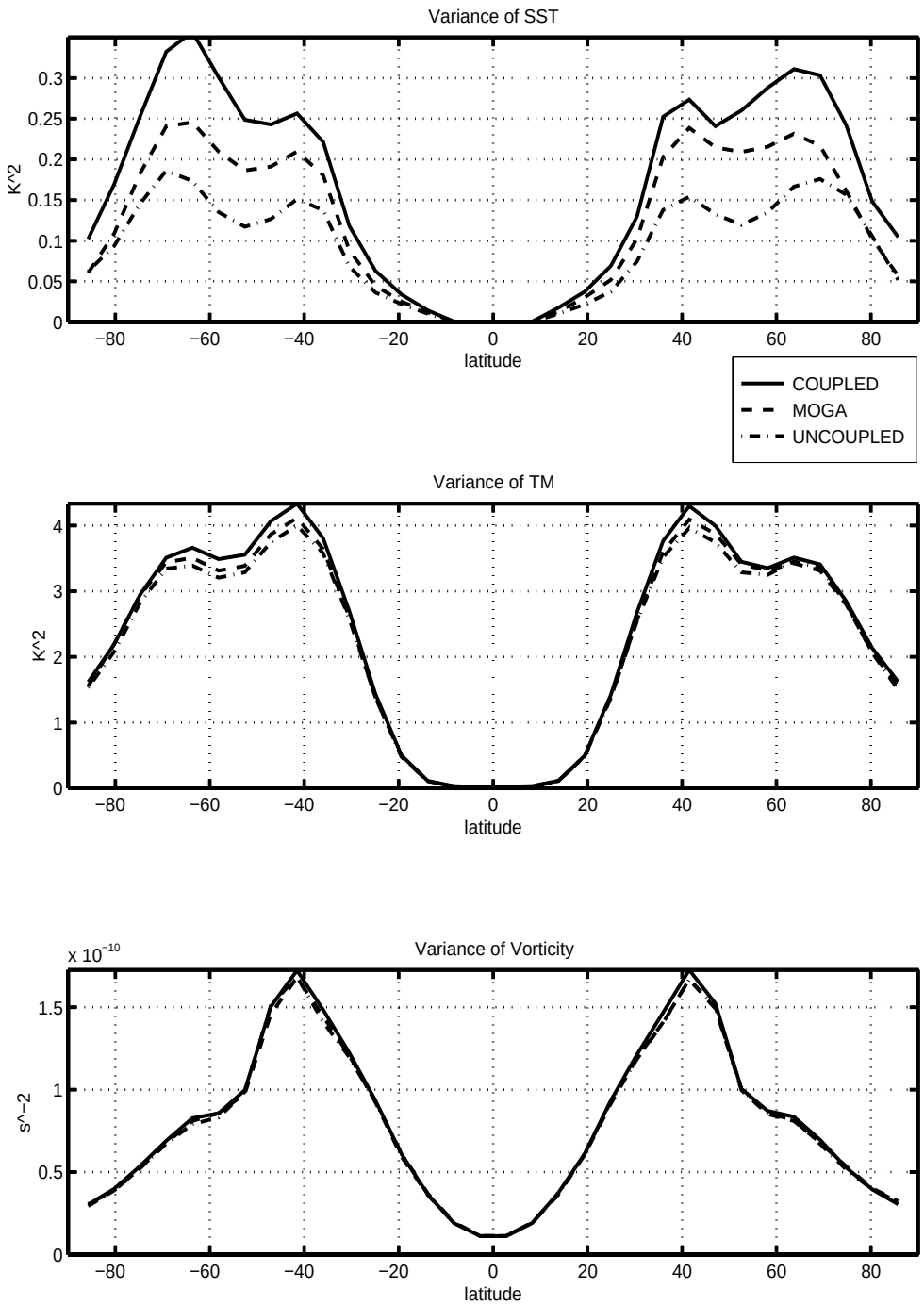

Figure 4.4. Variance of SST, $\bar{\theta}$, and $\bar{\zeta}$ as a function of latitude. Run4 (previous 6000 day run with completely consistent climatologies)

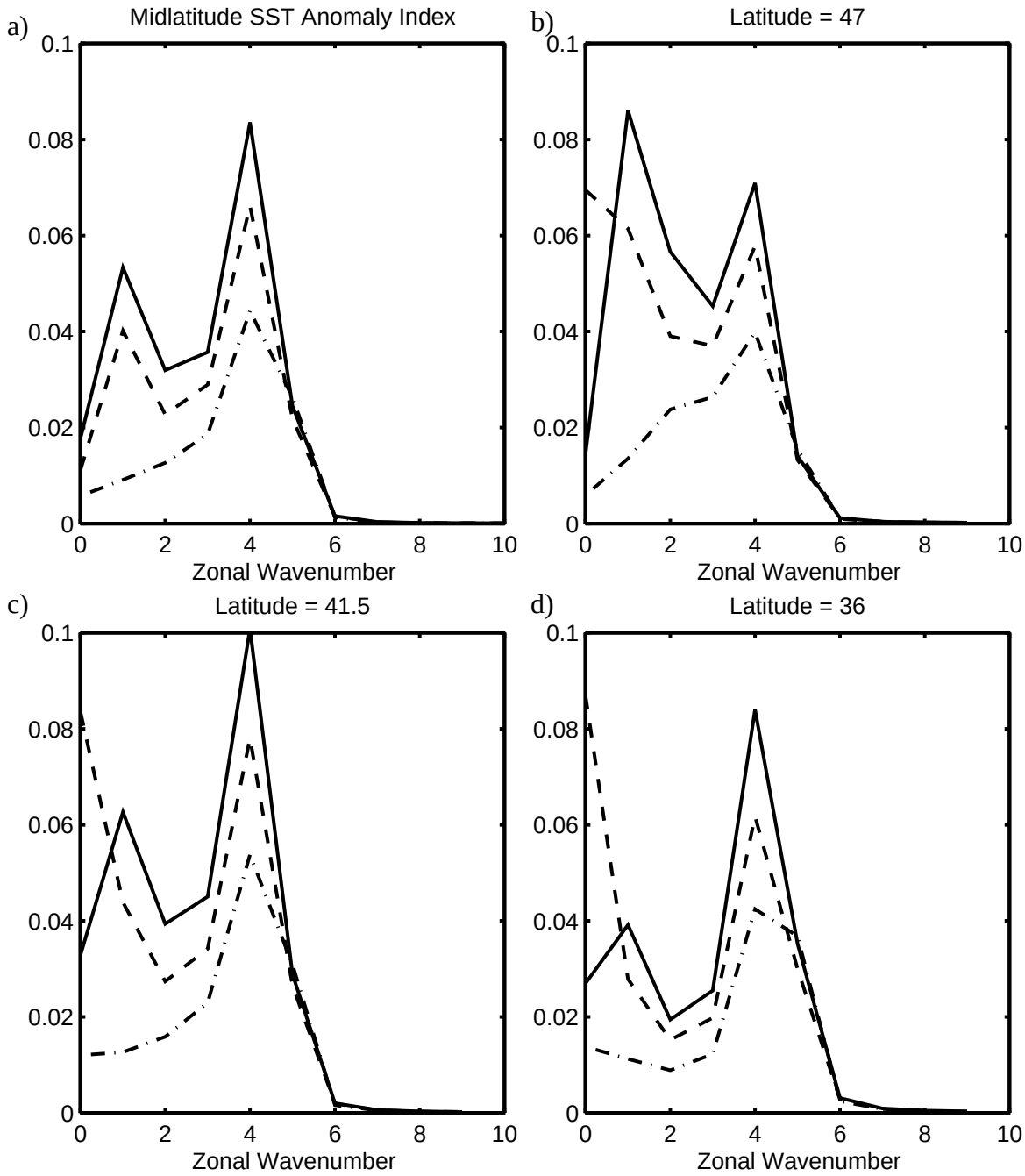

Figure 4.5. Variance of SST as a function of zonal wavenumber.a) Midlatitude SST anomaly index as defined in text. Average of Northern and Southern Hemisphere Indices; b) Average power at latitudes 47°N and 47°S; c) average power at latitudes 41.5°N and 41.5°S; d) average power at latitudes 36°N and 36°S. In all plots the lines are as follows: COUPLED (solid), MOGA (dashed) and UNCOUPLED (dash-dot). Units are K^2 . Plots are normalized so that the sum over all wavenumbers equals the total variance.

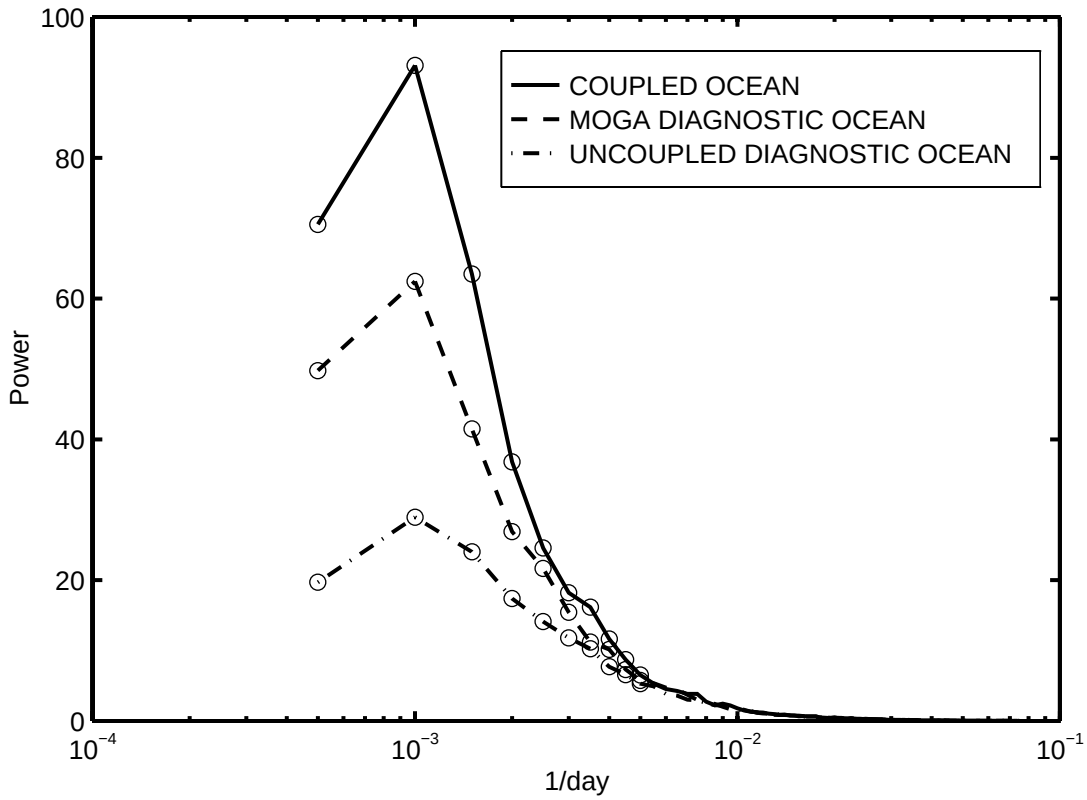

Figure 4.6. Power spectrum for midlatitude SST index. Mean of power spectral estimates at all longitudes for Northern Hemisphere and Southern Hemisphere SST indices is shown. Units are K^2day. Individual spectral extimates for first ten non-zero frequencies are indicated by open circles. Frequency scale is logarithmic, so that the area under the spectrum does **not** correspond to total variance.

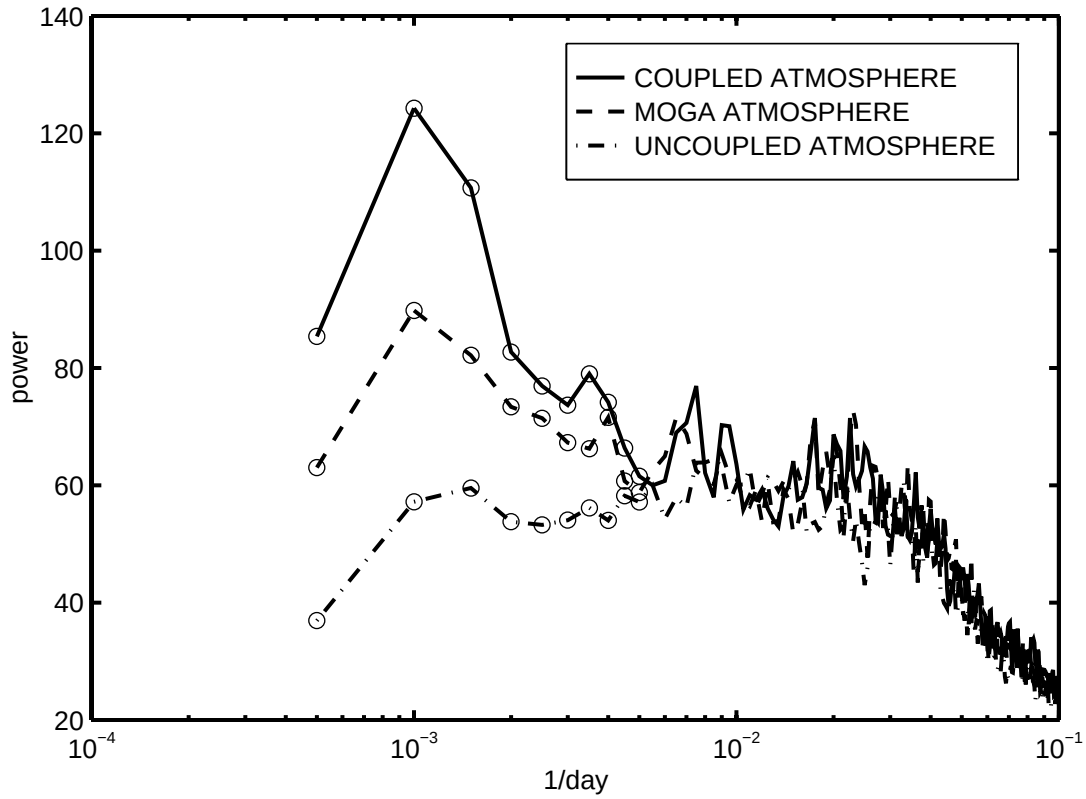

Figure 4.7. Power spectrum for $\bar{\theta}$ at latitudes 41.5 N and 41.5 S. Plot shows mean of power spectral estimates at all longitudes for the given latitudes. Units are K^2day. Individual spectral extimates for first ten non-zero frequencies are indicated by open circles.

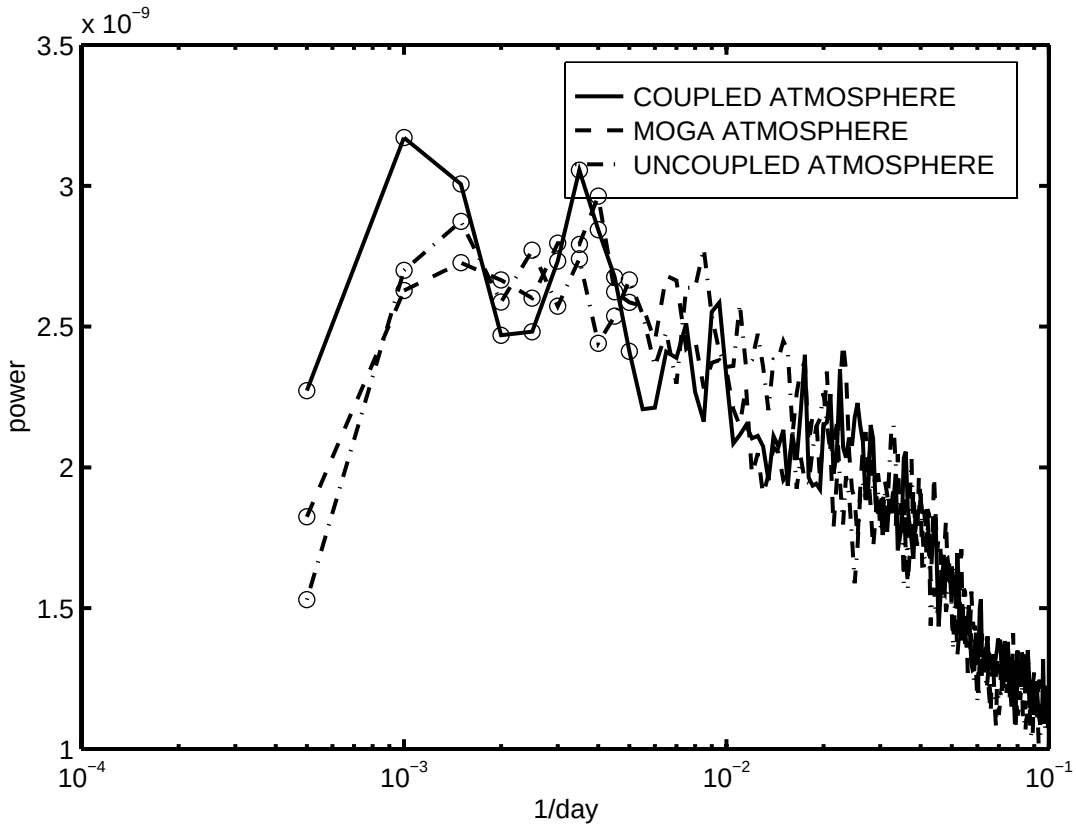

Figure 4.8. Power spectrum for $\bar{\zeta}$ at latitudes 41.5 N and 41.5 S. Plot shows mean of power spectral estimates at all longitudes for the given latitudes. Units are s^{-2}day. Individual spectral extimates for first ten non-zero frequencies are indicated by open circles.

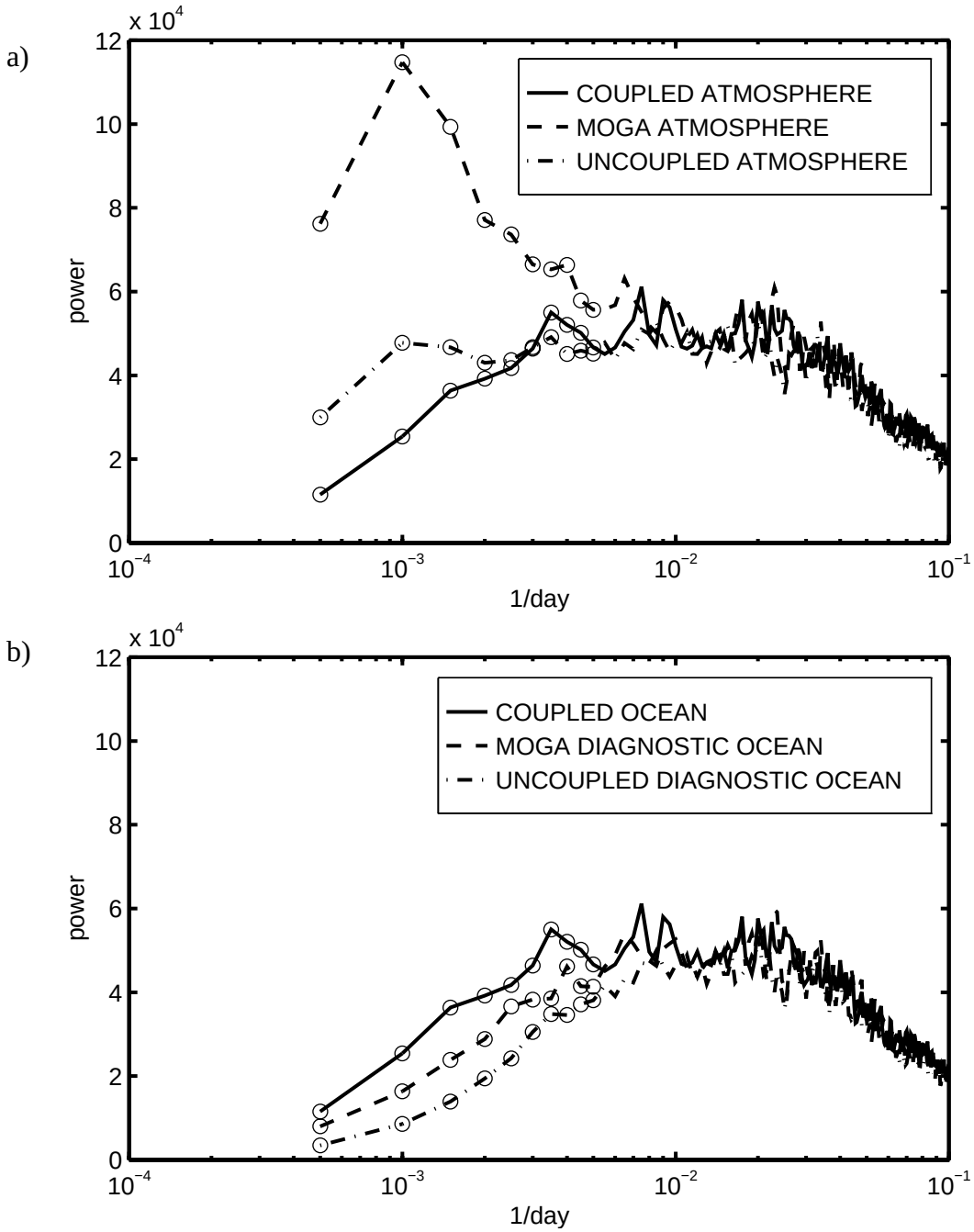

Figure 4.9. Power spectrum for total surface fluxes. a) Fluxes into atmosphere. In the MOGA and UNCOUPLED cases these are the fluxes between the specified SST and the atmosphere; b) Fluxes into diagnostic ocean. The coupled ocean spectrum is duplicated from part a) for comparison. Units are W^2m^{-4} day.

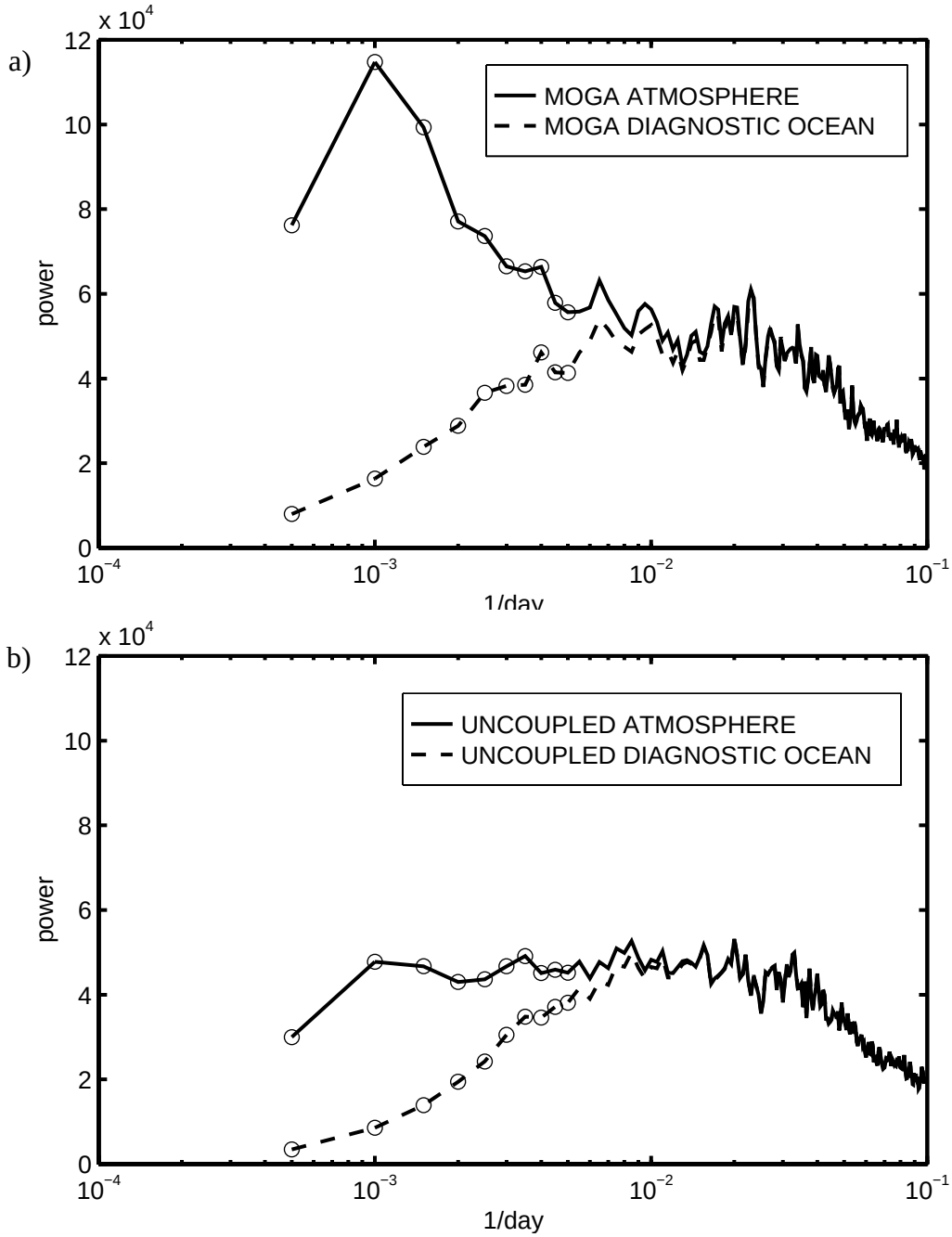

Figure 4.10. Power spectrum for total surface fluxes. a) fluxes into atmosphere (solid) and fluxes into diagnostic ocean (dashed) for MOGA run; b) same as in a) but for the UNCOUPLED run. Units are W^2m^{-4} day.

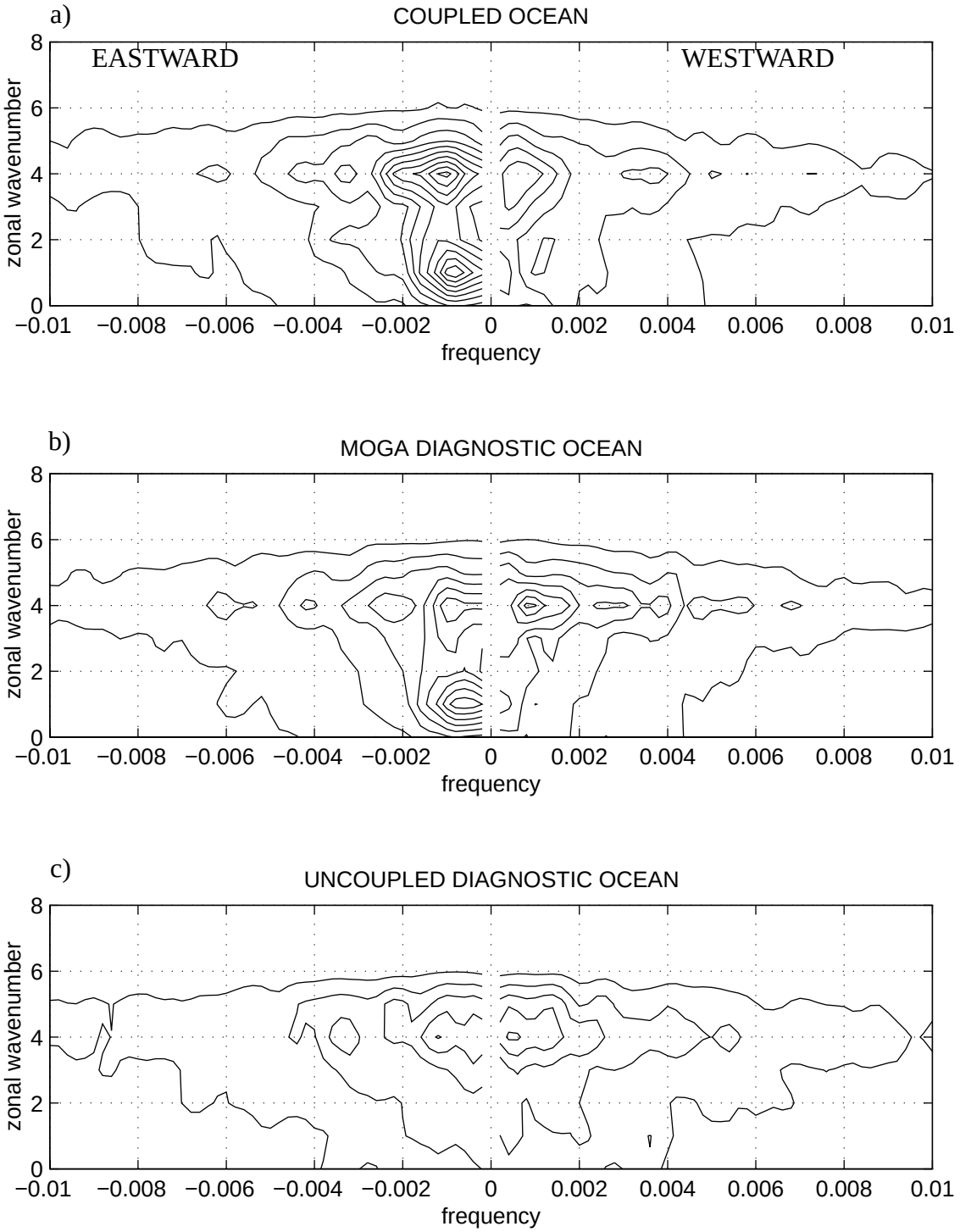

Figure 4.11. Square root of power (RMS amplitude) in frequency-wavenumber domain of SST for a) COUPLED ocean; b) MOGA DIAGNOSTIC ocean; and c) UNCOUPLED DIAGNOSTIC ocean. Units are $(K^2\ day)^{1/2}$. Contour interval is 0.5 in these units. The field is normalized so that the integral over the upper half-plane of the square of amplitude in the units shown is equal to the mean variance.

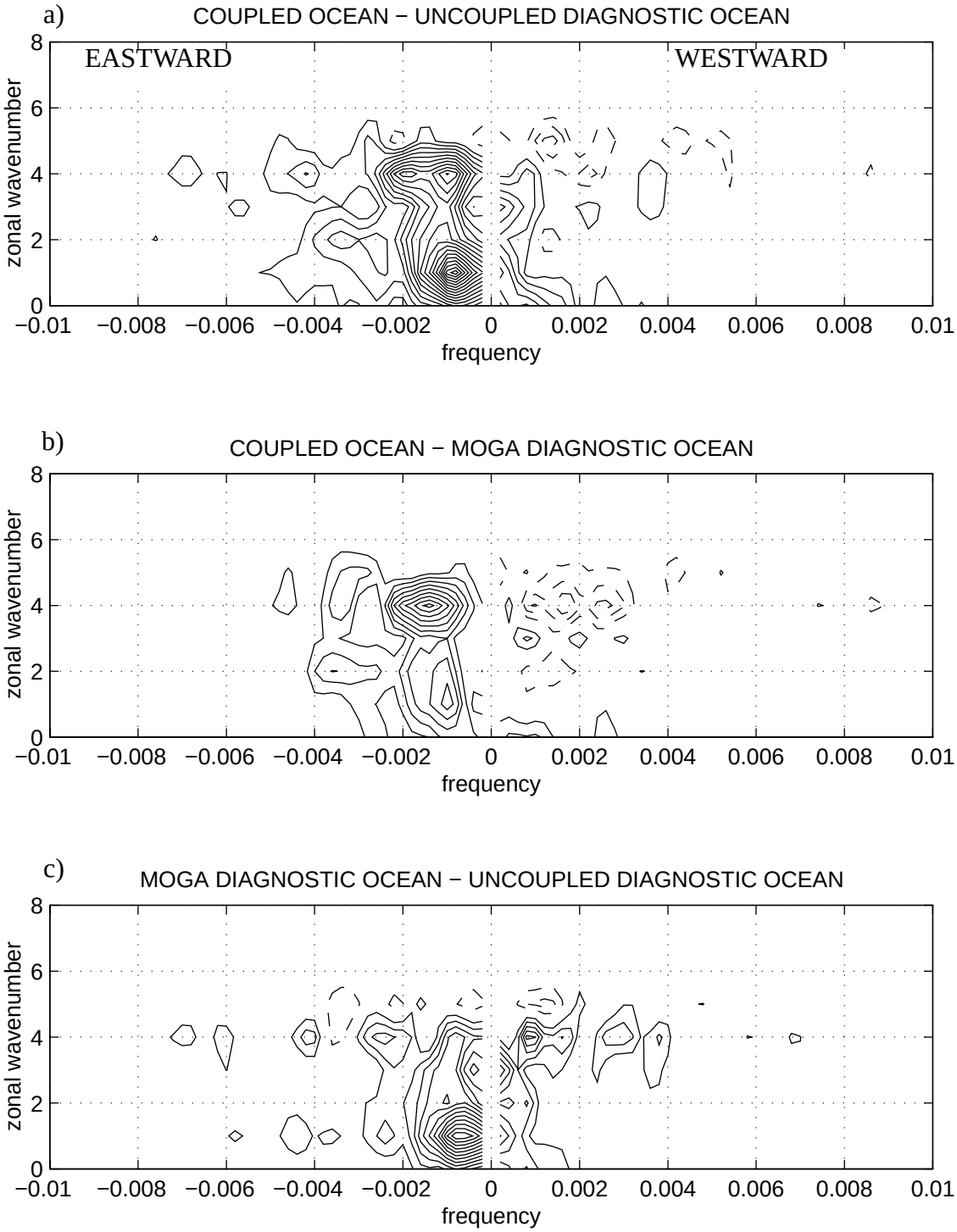

Figure 4.12. As in figure 4.11 except for differences between runs. a) COUPLED - UNCOUPLED DIAGNOSTIC ocean; b) COUPLED - MOGA DIAGNOSTIC ocean; and c) MOGA DIAGNOSTIC - UNCOUPLED DIAGNOSTIC ocean. Units are $(K^2\ day)^{1/2}$. Contour interval is 0.25 in these units. Negative contours are dashed.

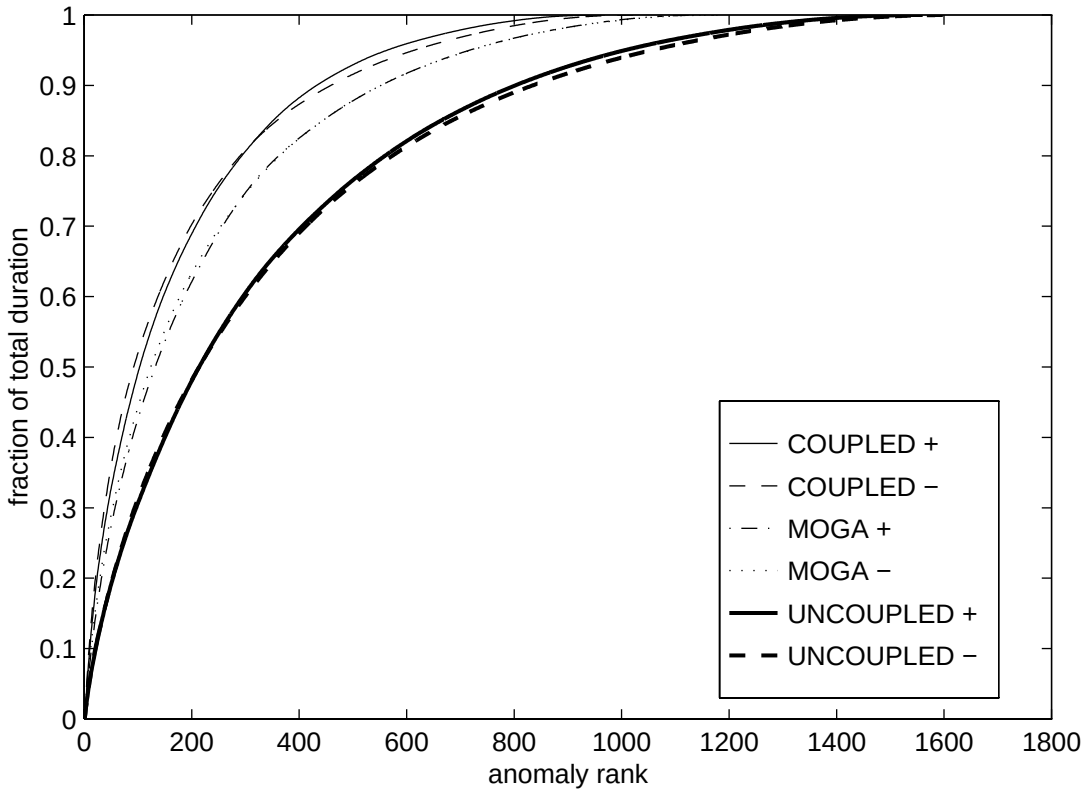

Figure 4.13. Normalized measure of SST anomaly persistence. SST anomalies defined as in text are ranked by duration. The fraction of the total duration accounted for by all anomalies up to a given rank is shown here. The individual cases plotted are as folows: COUPLED OCEAN positive (thin solid) and negative (thin dashed) anomalies, MOGA diagnostic ocean positive (dash-dot) and negative (dotted) anomalies,and UNCOUPLED diagnostic ocean positive (thick solid) and negative (thick dashed) anomalies. Northern and Southern Hemisphere anomalies have been pooled for this analysis.

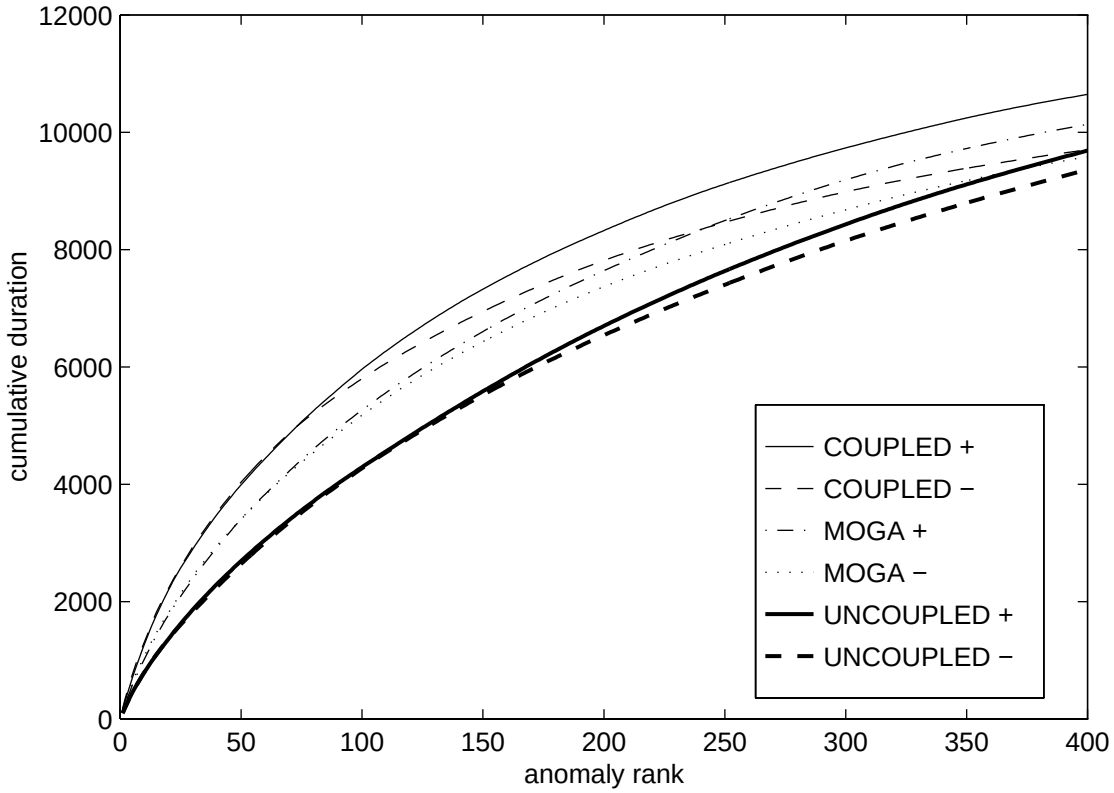

Figure 4.14. Unnormalized measure of SST anomaly persistence. SST anomalies defined as in text are ranked by duration. The cumulative duration accounted for by all anomalies up to a given rank is shown. The cumulative duration function is shown only for anomaly rank < 400. Line styles are as in figure 4.13.

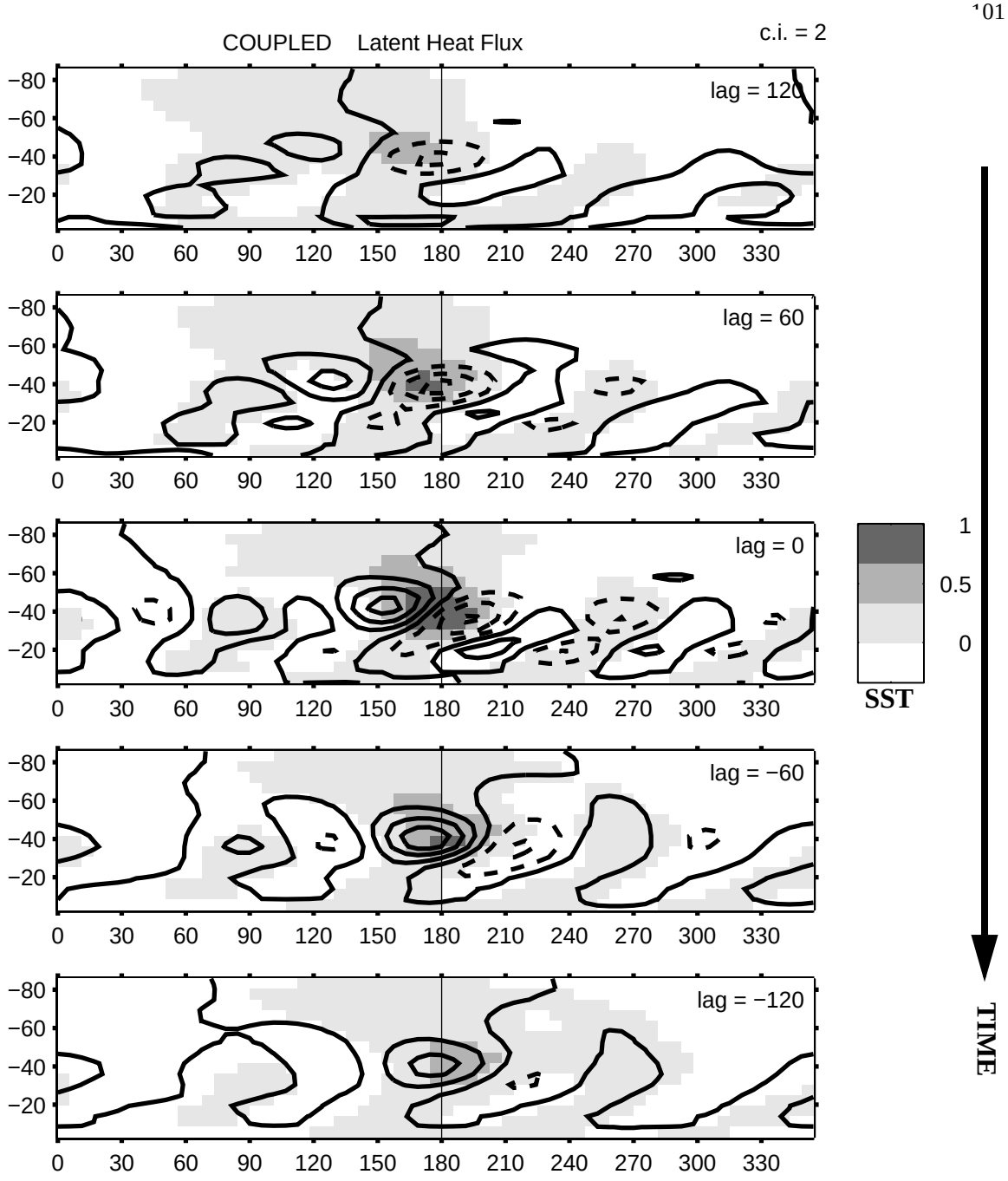

Figure 4.15. Lag Regression maps for COUPLED run surface latent heat flux. Contour interval is 2 W m^{-2} (per K of SST anomaly). Background maps indicate lag regressions of sea surface temperature. Gray scale is the same in every frame and is in units of K(of SST anomaly)/K(of SST anomaly at reference point). Longitude is the horizontal axis and latitude the vertical axis. Data from the Southern Hemisphere has been inverted to provide a Nothern Hemisphere orientation. The sense of time goes downward. In this and the following plots only the units of the “target” field are given. The phrase “per K of SST anomaly” is understood.

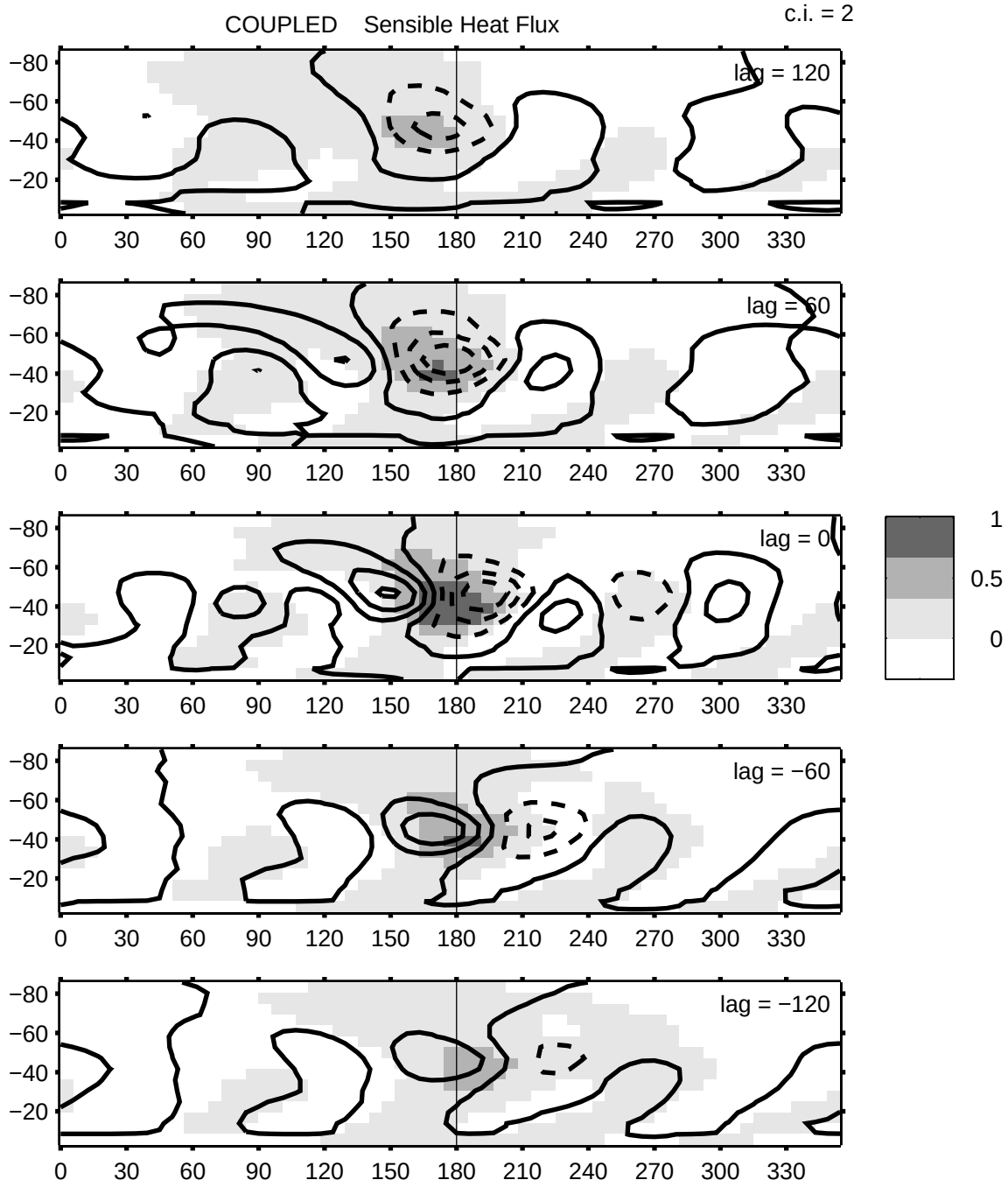

Figure 4.16. Lag regressions for COUPLED run surface sensible heat flux. See figure 4.15 caption for more detail.

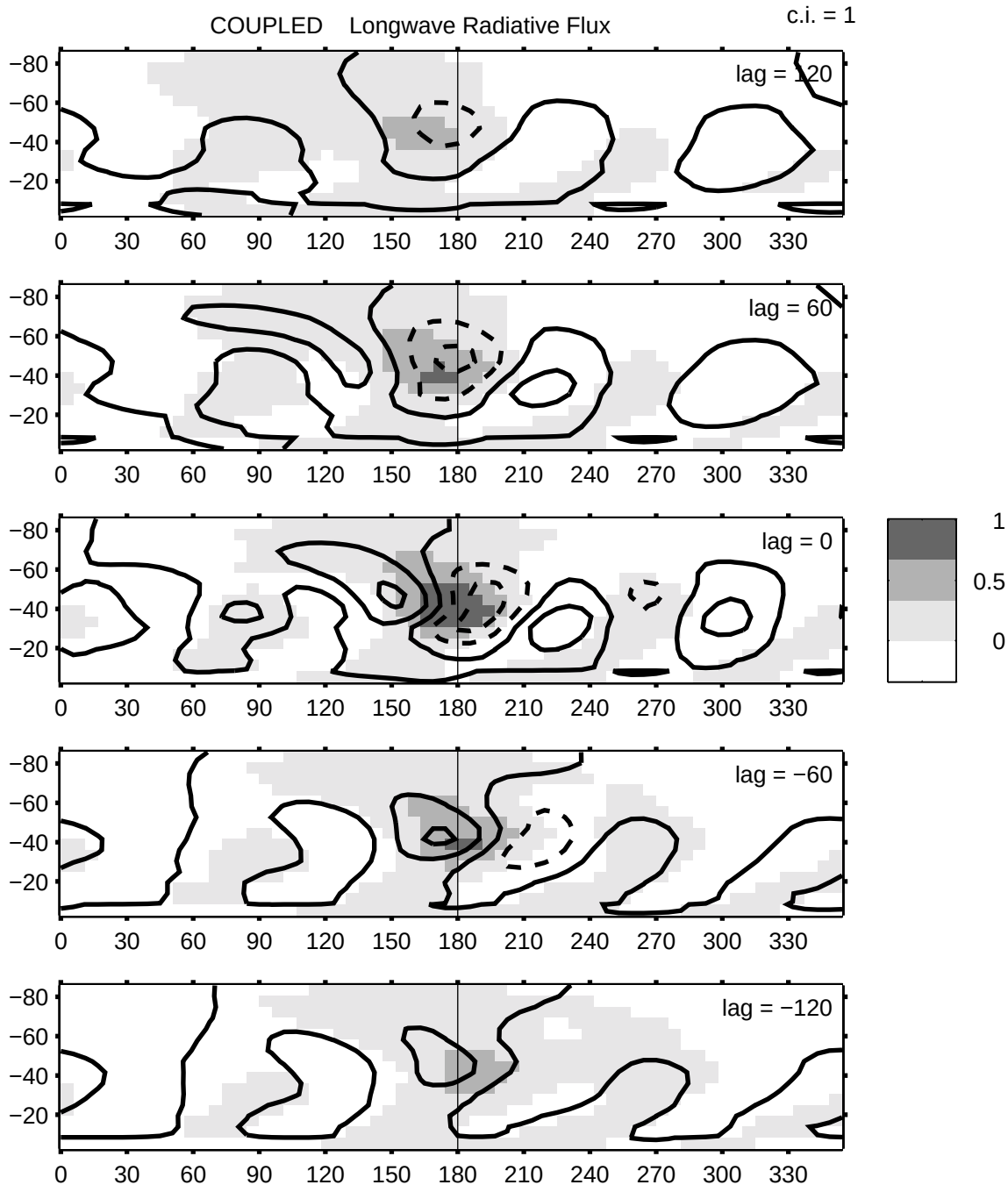

Figure 4.17. Lag regression maps for COUPLED run surface net longwave flux. Contour interval is 1 W m^{-2}.

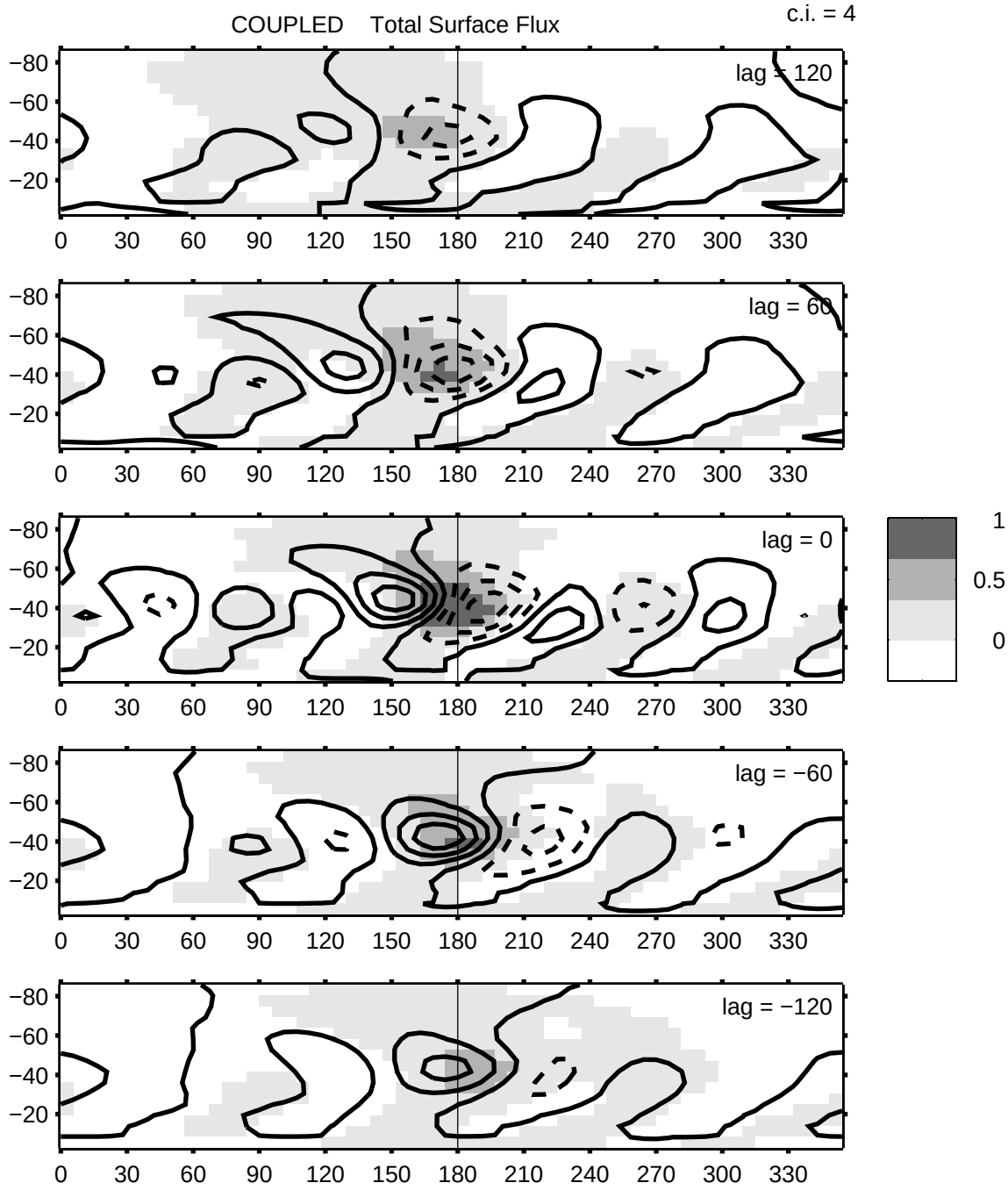

Figure 4.18. Lag regression maps for COUPLED run total surface heat flux. Contour interval is 4 W m^{-2}.

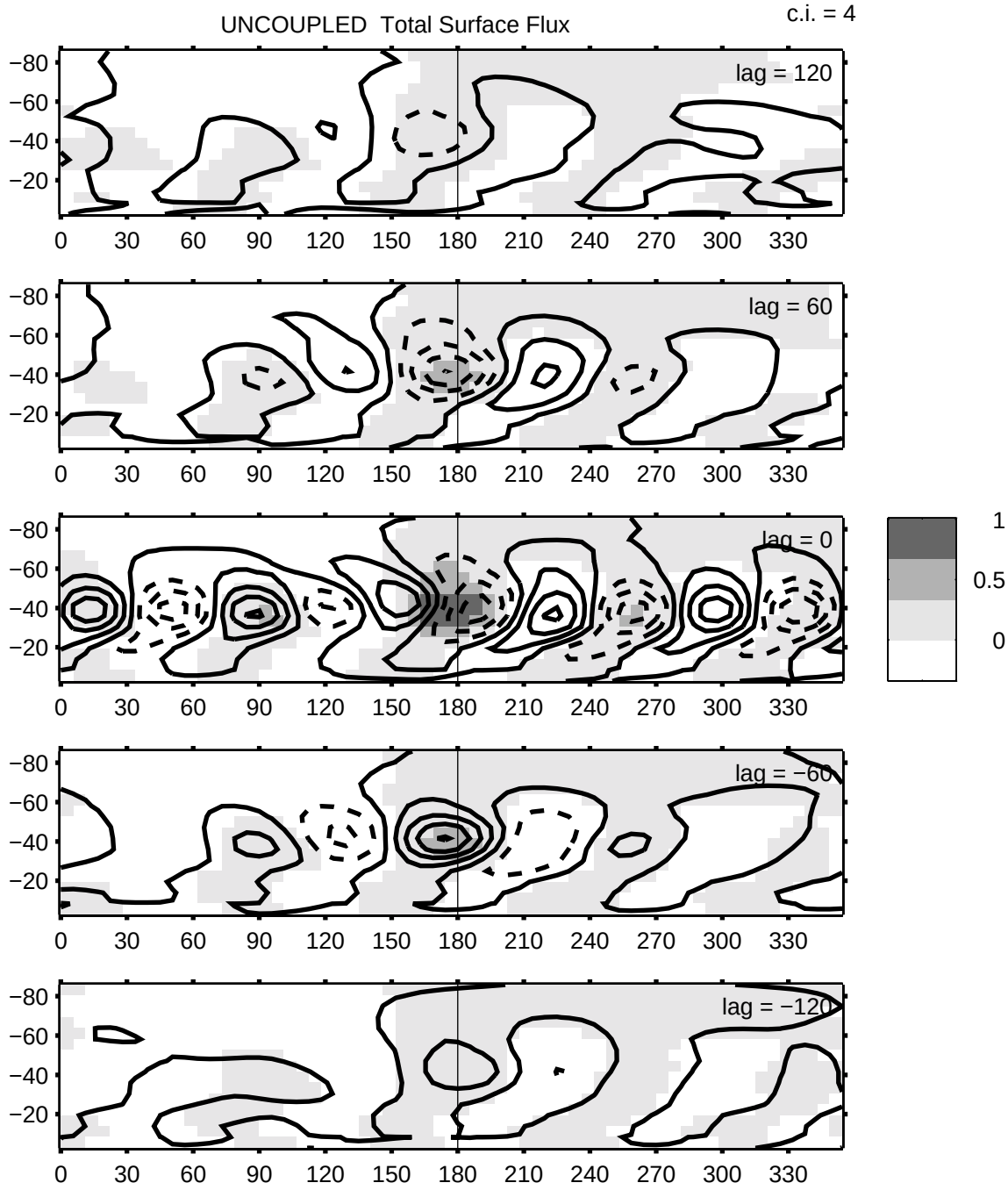

Figure 4.19. As in Figure 4.18 except for UNCOUPLED run total surface heat flux.

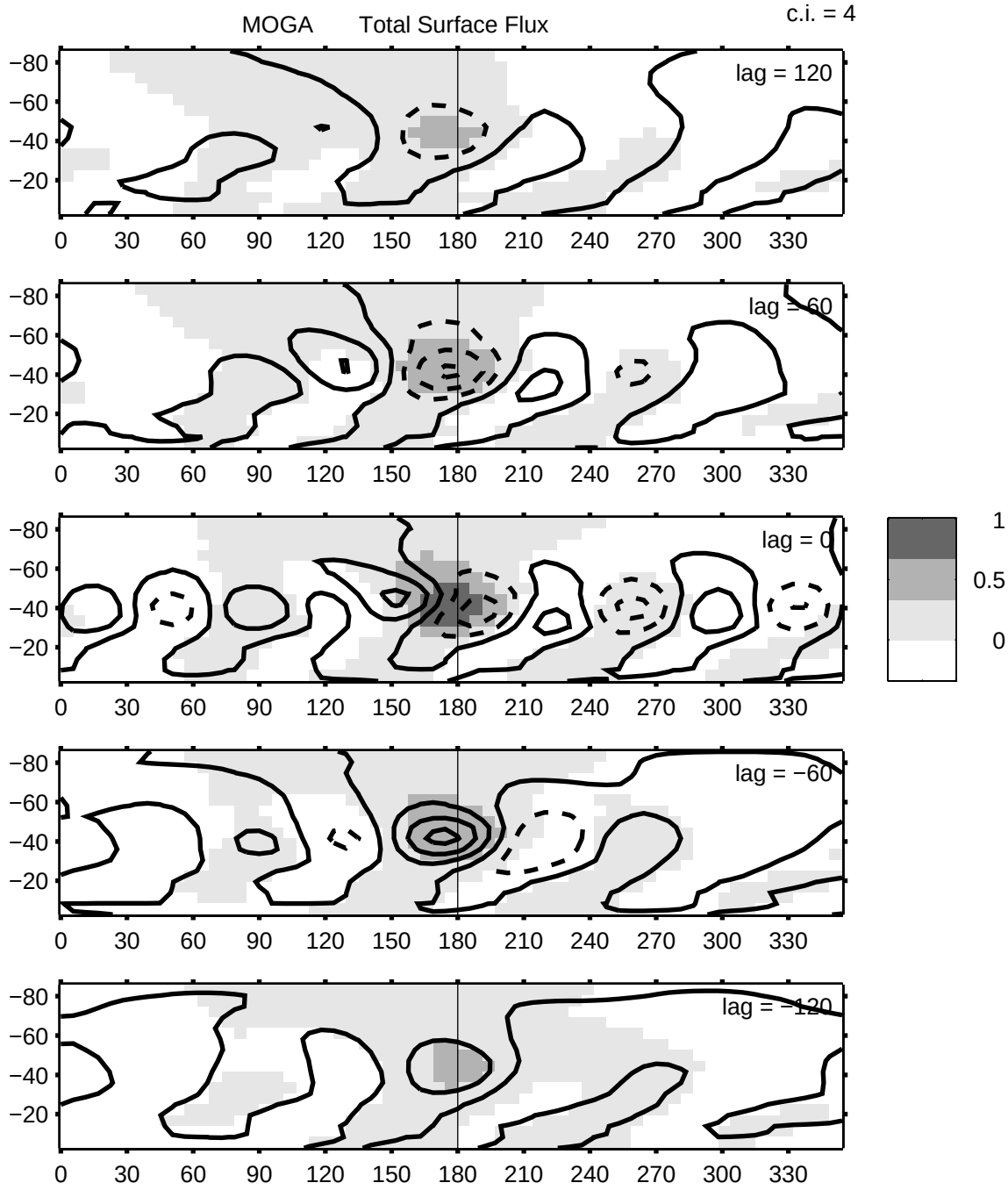

Figure 4.20. As in Figure 4.18 except for MOGA DIAGNOSTIC OCEAN run total surface heat flux

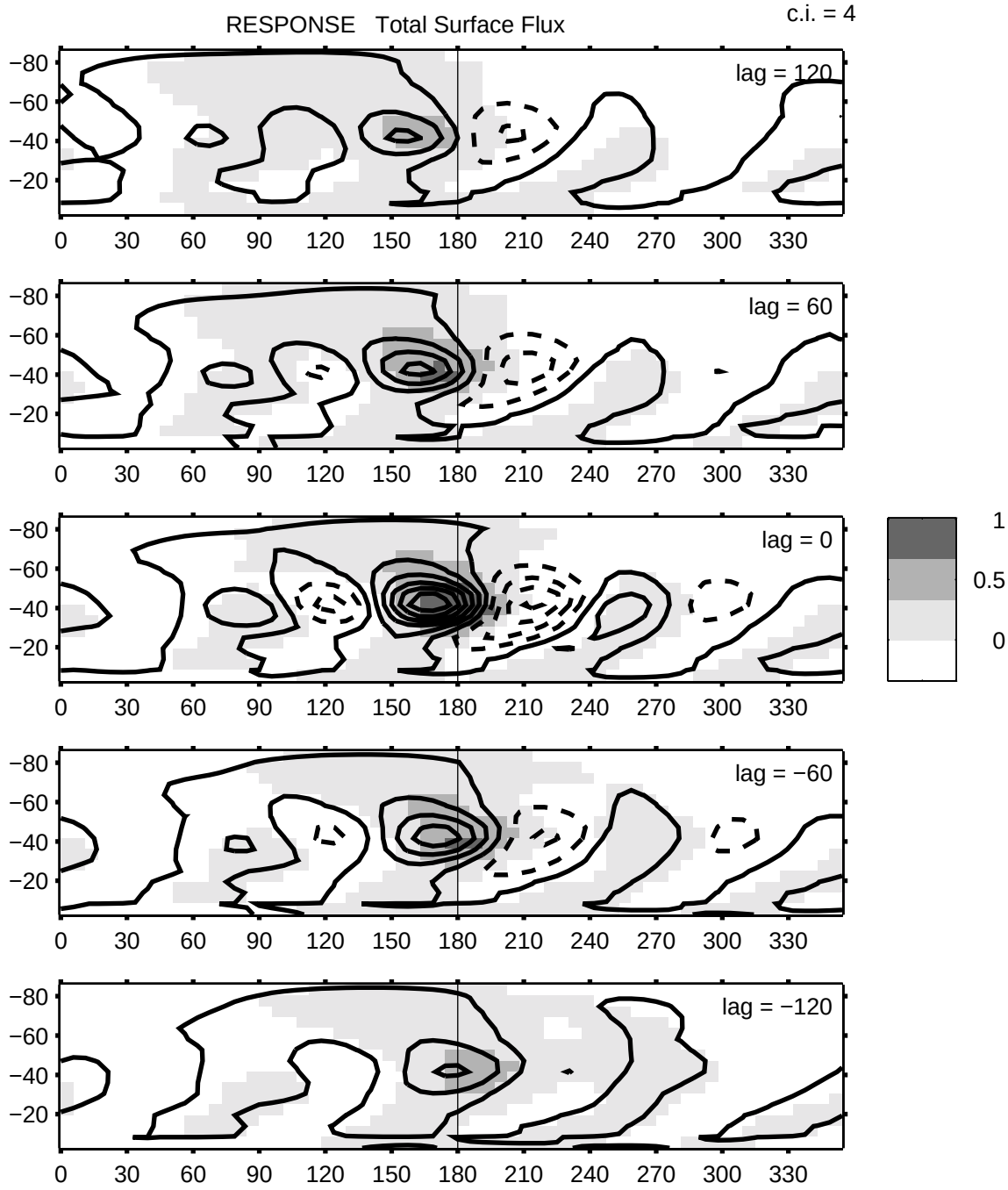

Figure 4.21. As in Figure 4.18 except for MOGA-RESPONSE run total surface heat flux

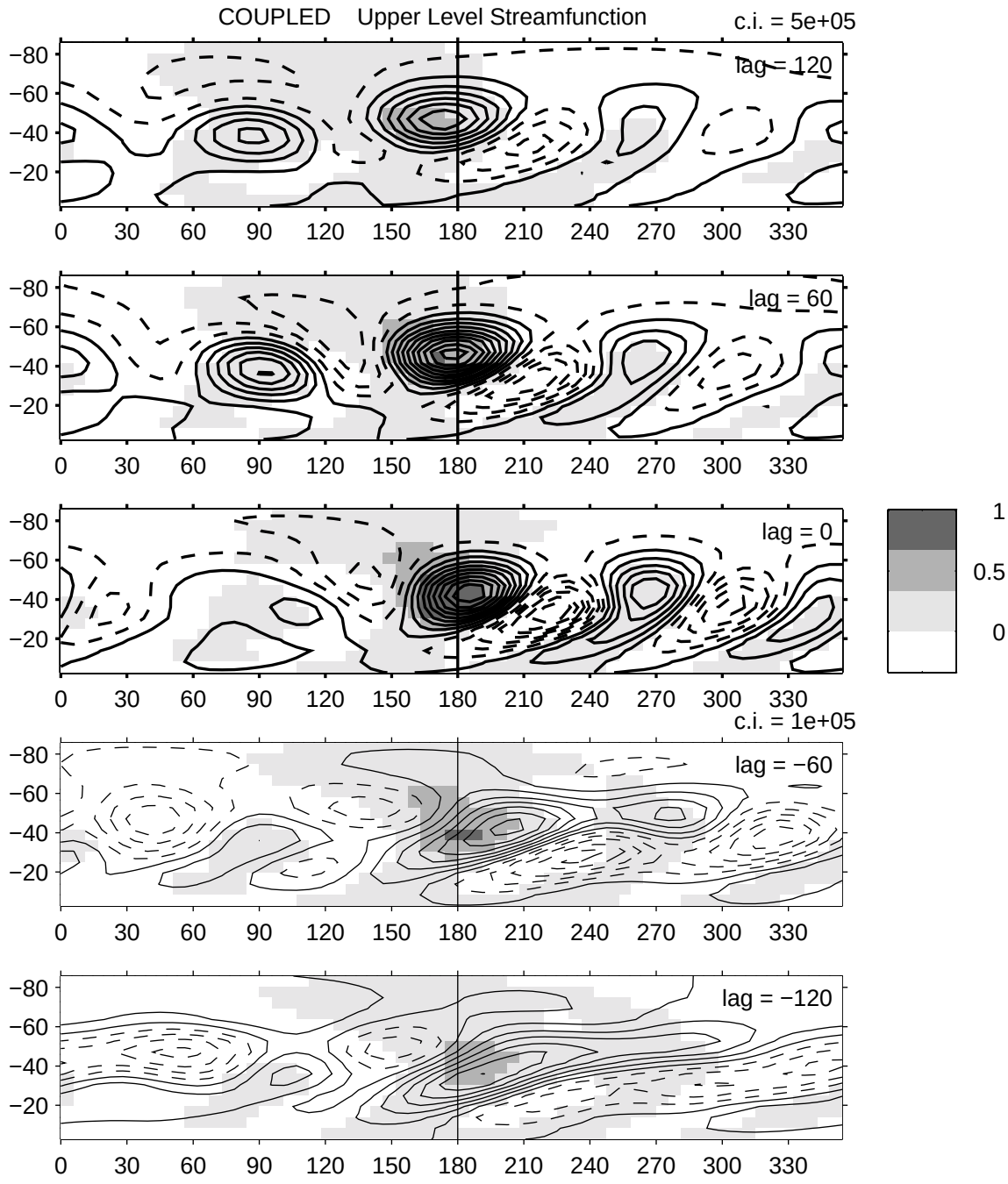

Figure 4.22. Lag regression maps for COUPLED 250 mb streamfunction. Contour inteval is 5×10^5 $m^2 s^{-2}$ for lags 0, 60, and 120 days, and 1×10^5 for lags -60 and -120 days. The latter is the same contour interval used for the MOGA-RESPONSE plots. These two plots are drawn in thin lines to highlight the different contour interval. .

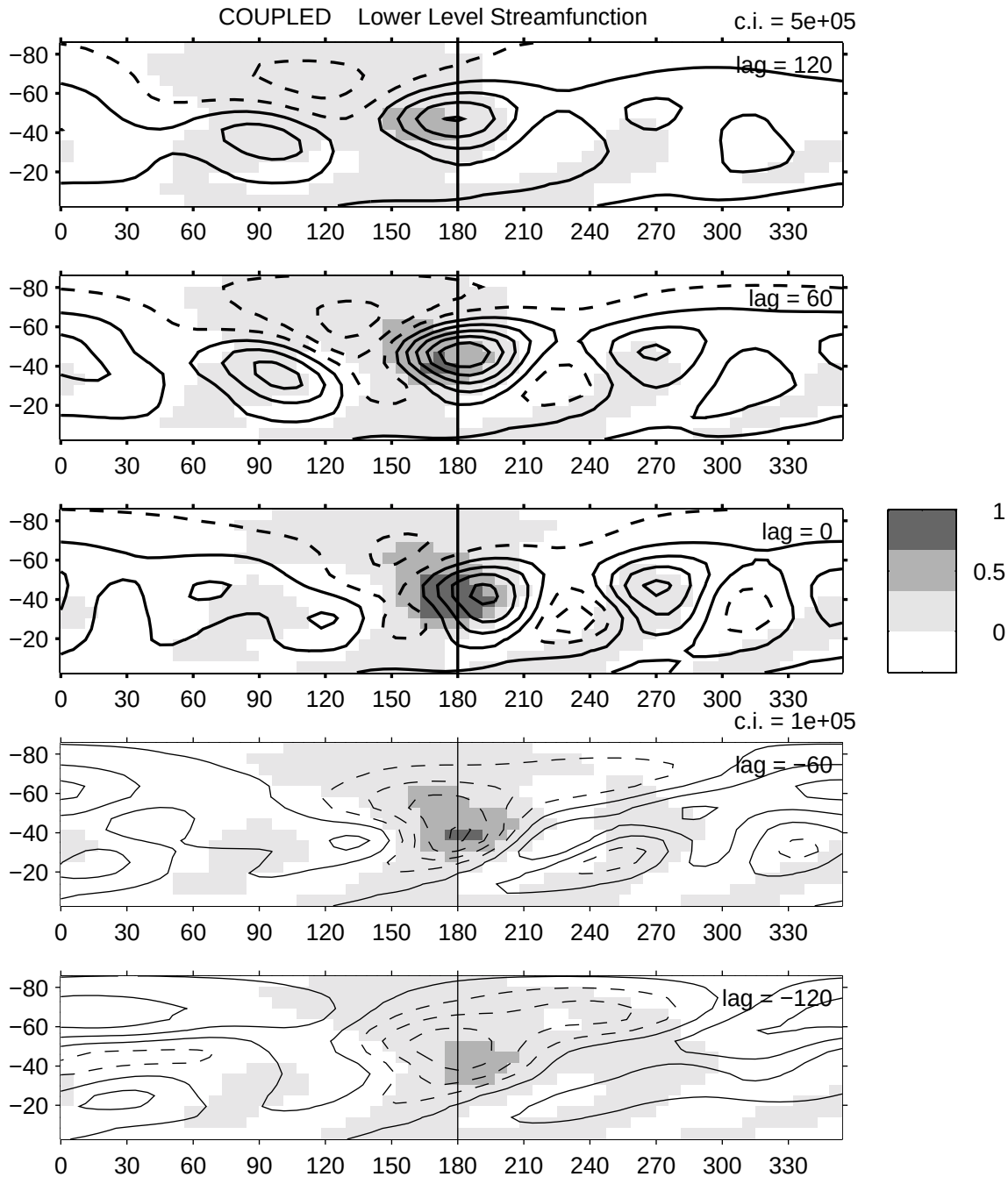

Figure 4.23. Lag regression maps for COUPLED 750 mb streamfunction. Contour inteval is 5×10^5 m^2 s^{-2}. Lower two plots use smaller contour interval. See figure 4.22 caption.

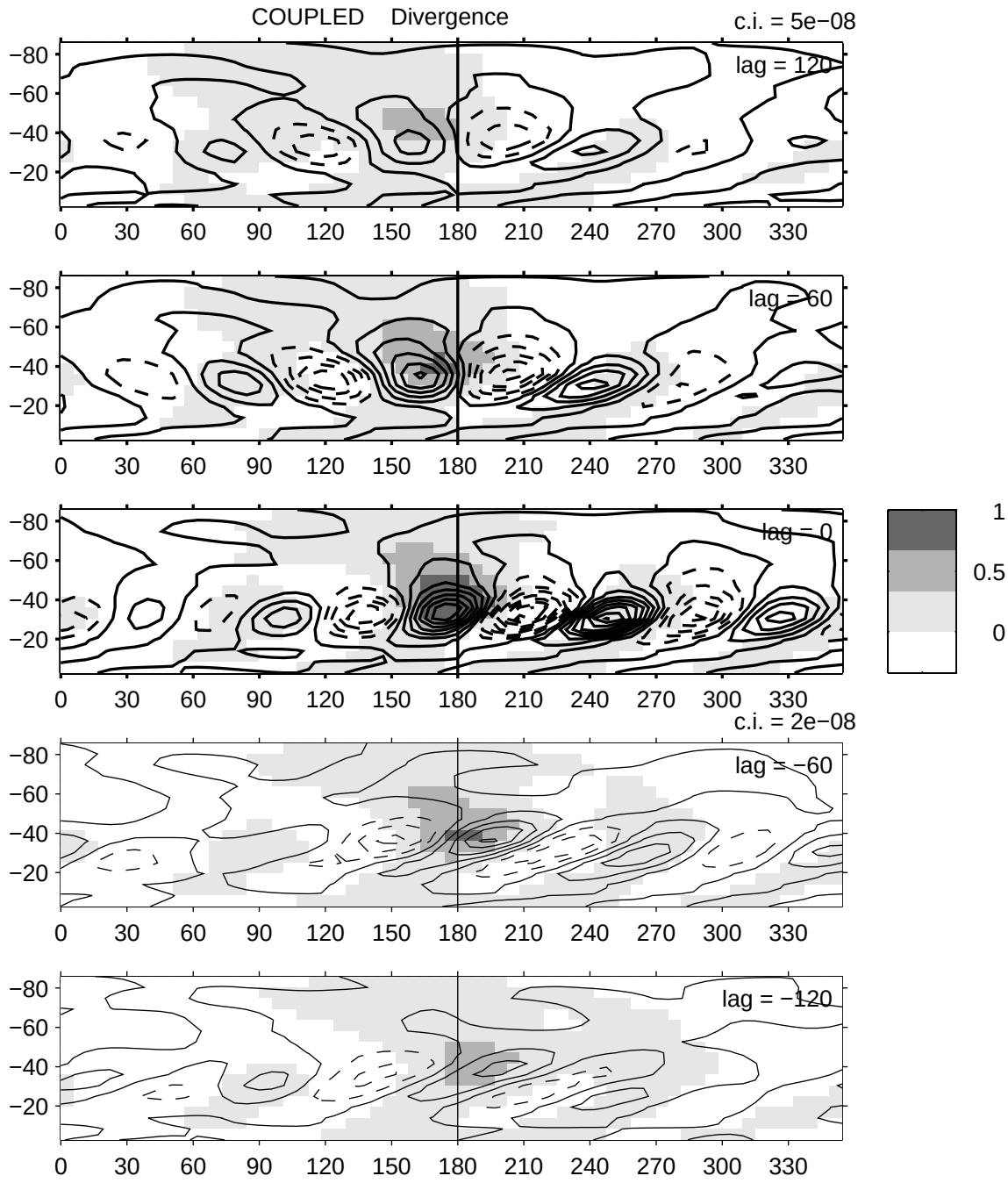

Figure 4.24. Lag regression maps for COUPLED 250 mb divergence. Contour inteval is 5×10^{-8} s^{-1}. Lower two plots use smaller contour interval. See figure 4.22 caption.

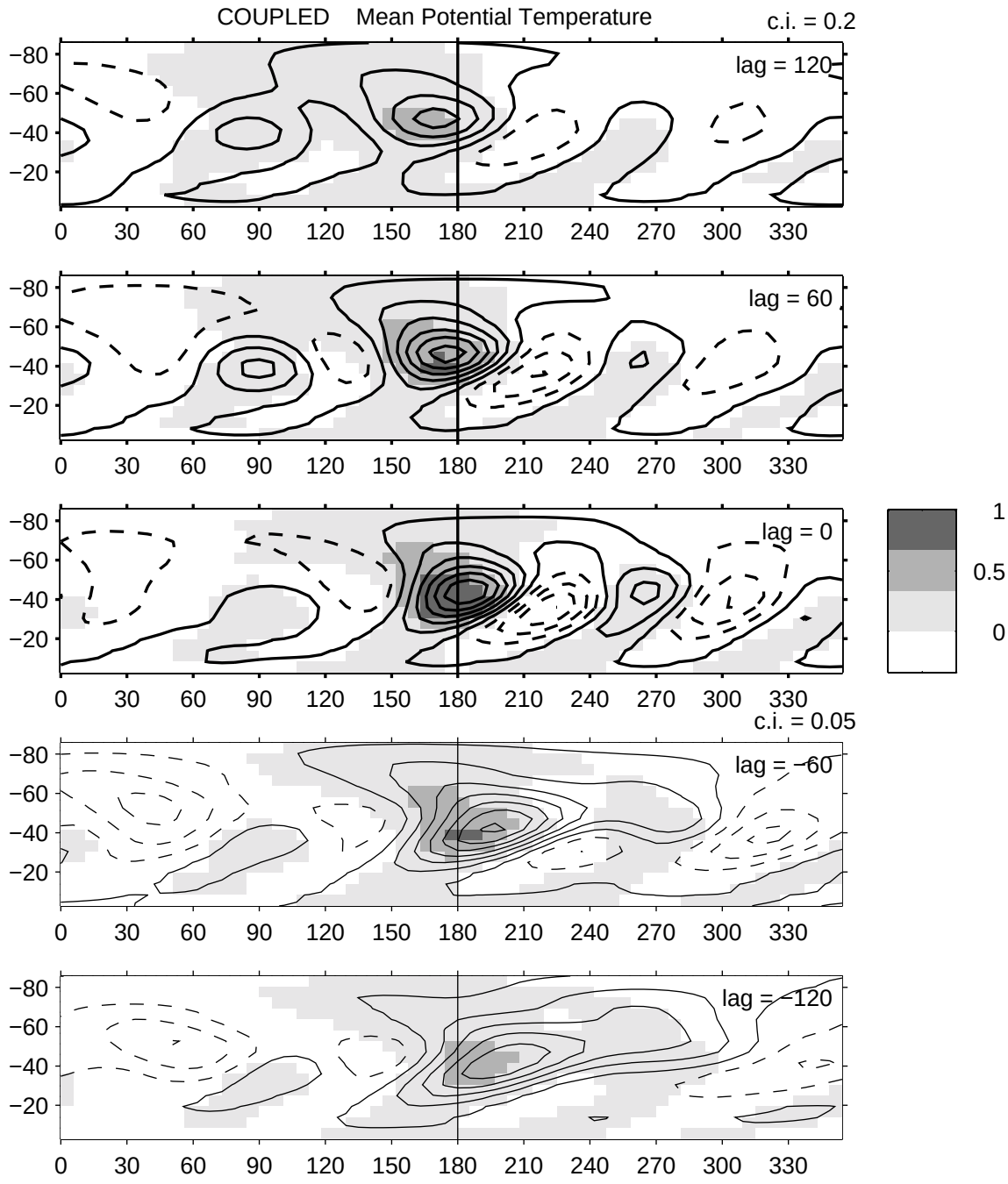

Figure 4.25. Lag regression maps for COUPLED vertical mean potential temperature $\bar{\theta}$. Contour inteval is 0.2 K. Lower two plots use smaller contour interval. See figure 4.22 caption.

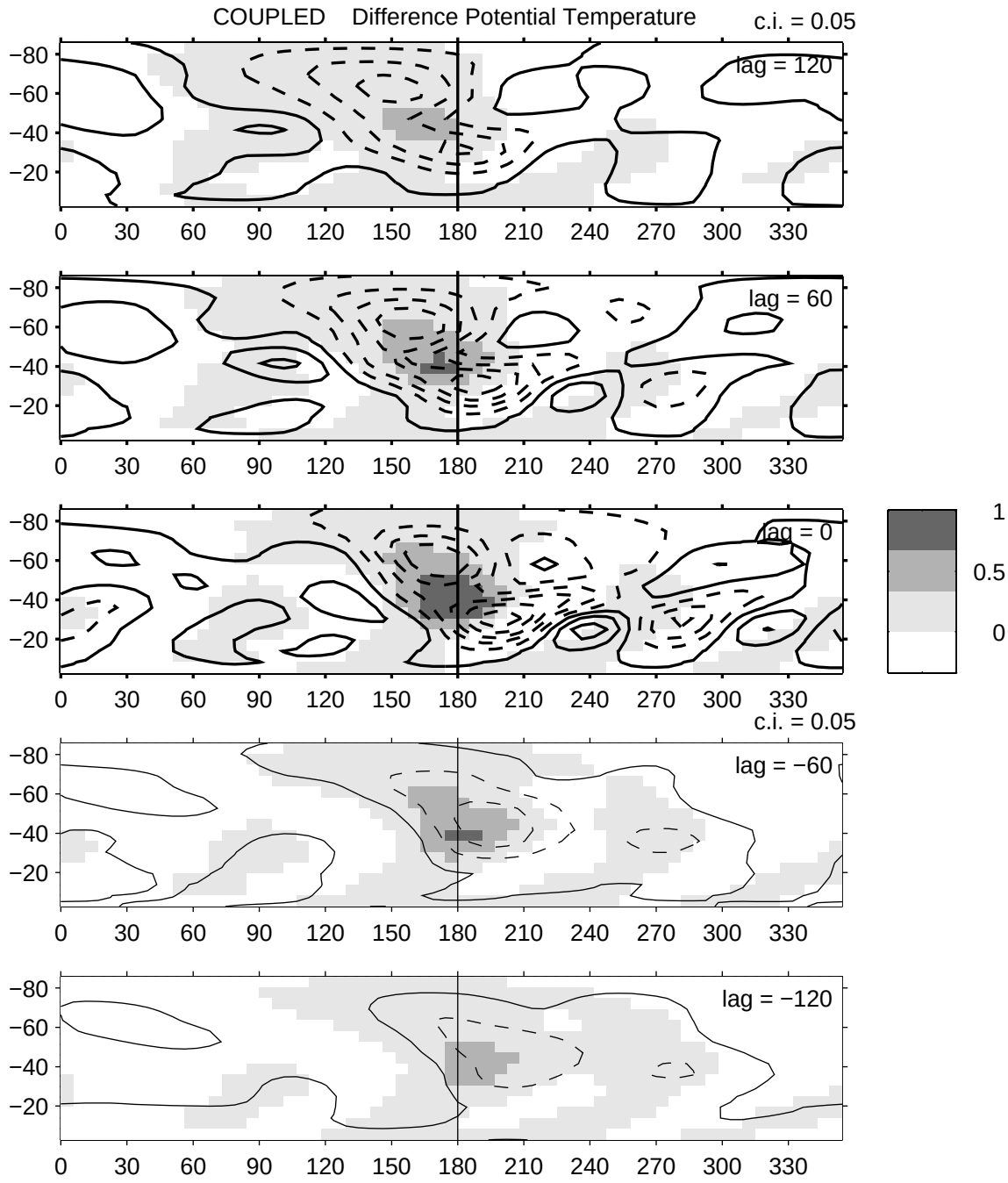

Figure 4.26. Lag regression maps for COUPLED vertical difference potential temperature $\hat{\theta}$. Contour inteval is 0.05 K in all plots. See figure 4.22 caption.

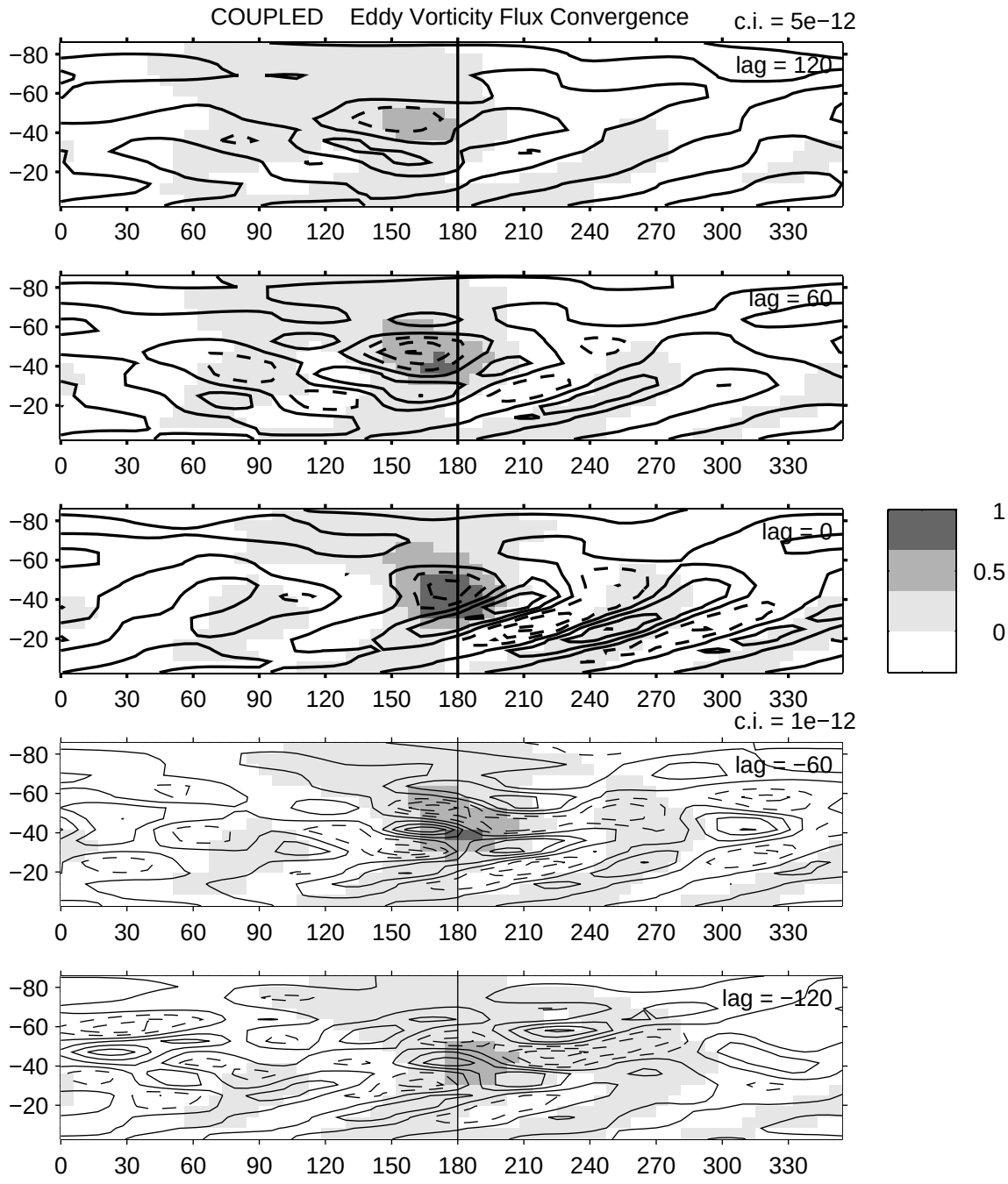

Figure 4.27. Lag regression maps for COUPLED 250 mb eddy vorticity flux convergence. Contour interval is 5×10^{-12} s^{-2}. In the Northern Hemisphere view I have adopted, a negative value indicates here indicates forcing of anticyclonic circulation. Lower two plots use smaller contour interval. See figure 4.22 caption.

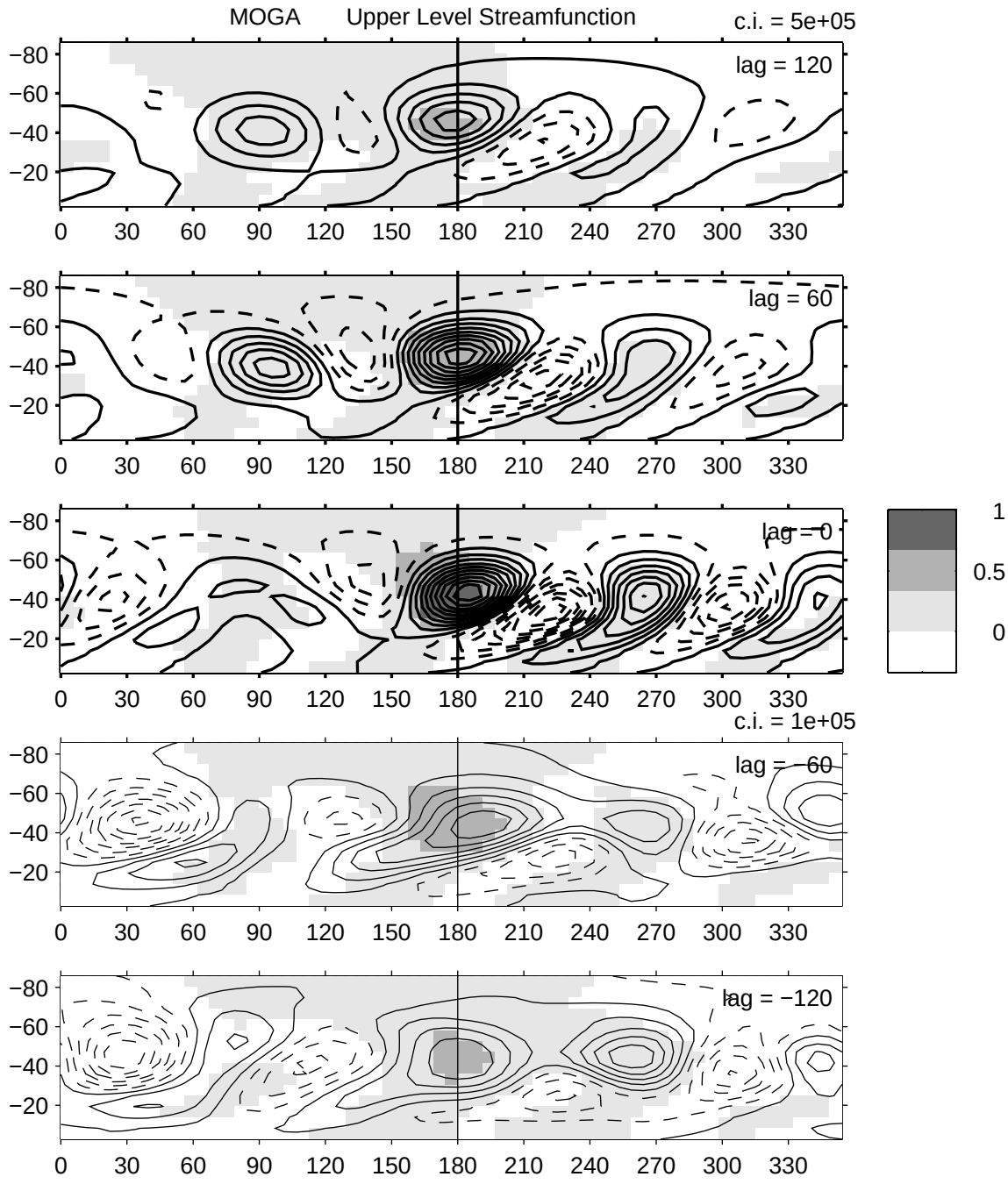

Figure 4.28. Lag regression maps for MOGA 250 mb streamfunction. Contour inteval is 5×10^5 m^2 s^{-2}. Lower two plots use smaller contour interval. See figure 4.22 caption.

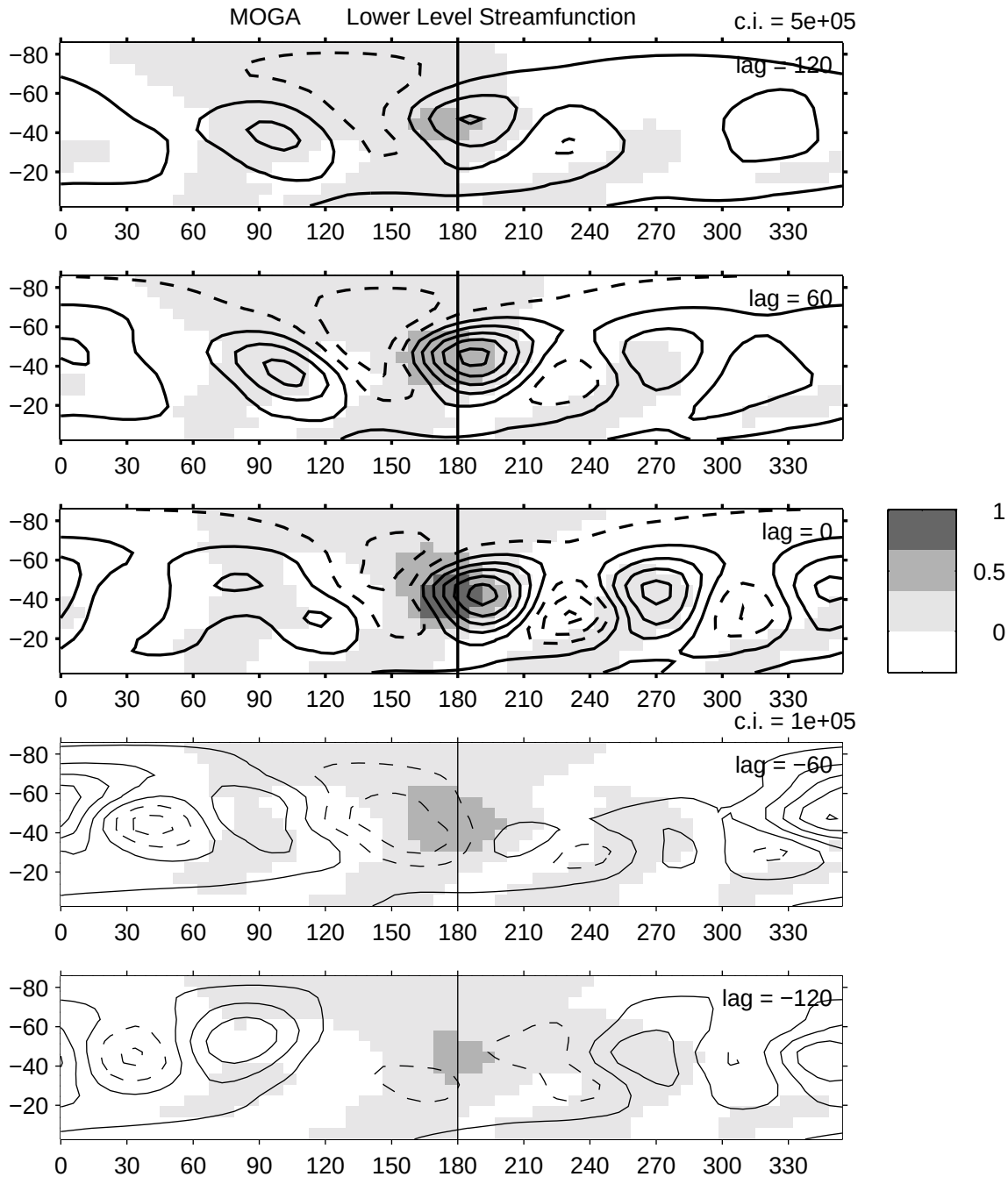

Figure 4.29. Lag regression maps for MOGA 750 mb streamfunction. Contour inteval is 5×10^5 m^2 s^{-2}. Lower two plots use smaller contour interval. See figure 4.22 caption.

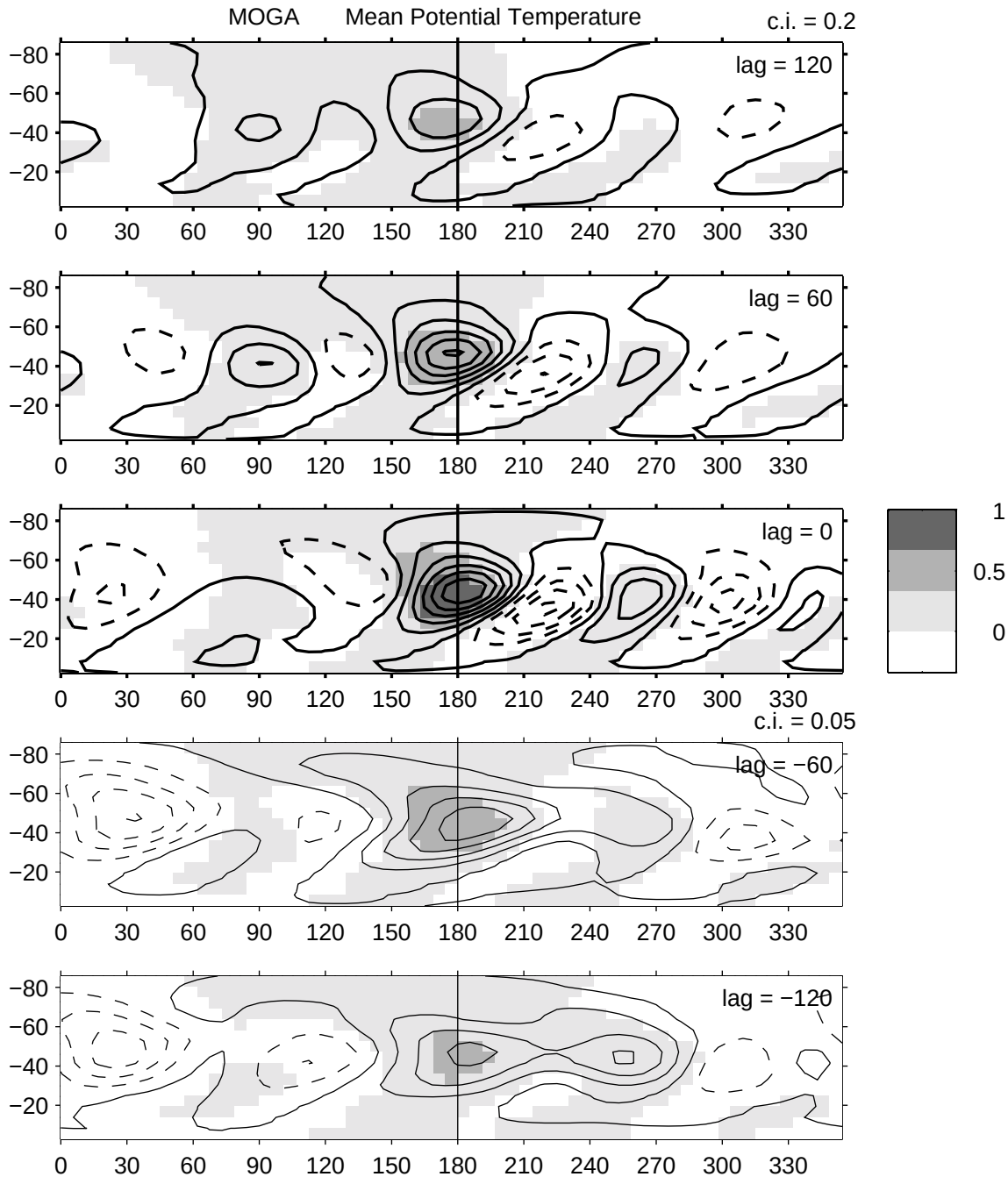

Figure 4.30. Lag regression maps for MOGA vertical mean potential temperature, $\bar{\theta}$. Contour inteval is 0.2 K. Lower two plots use smaller contour interval. See figure 4.22 caption.

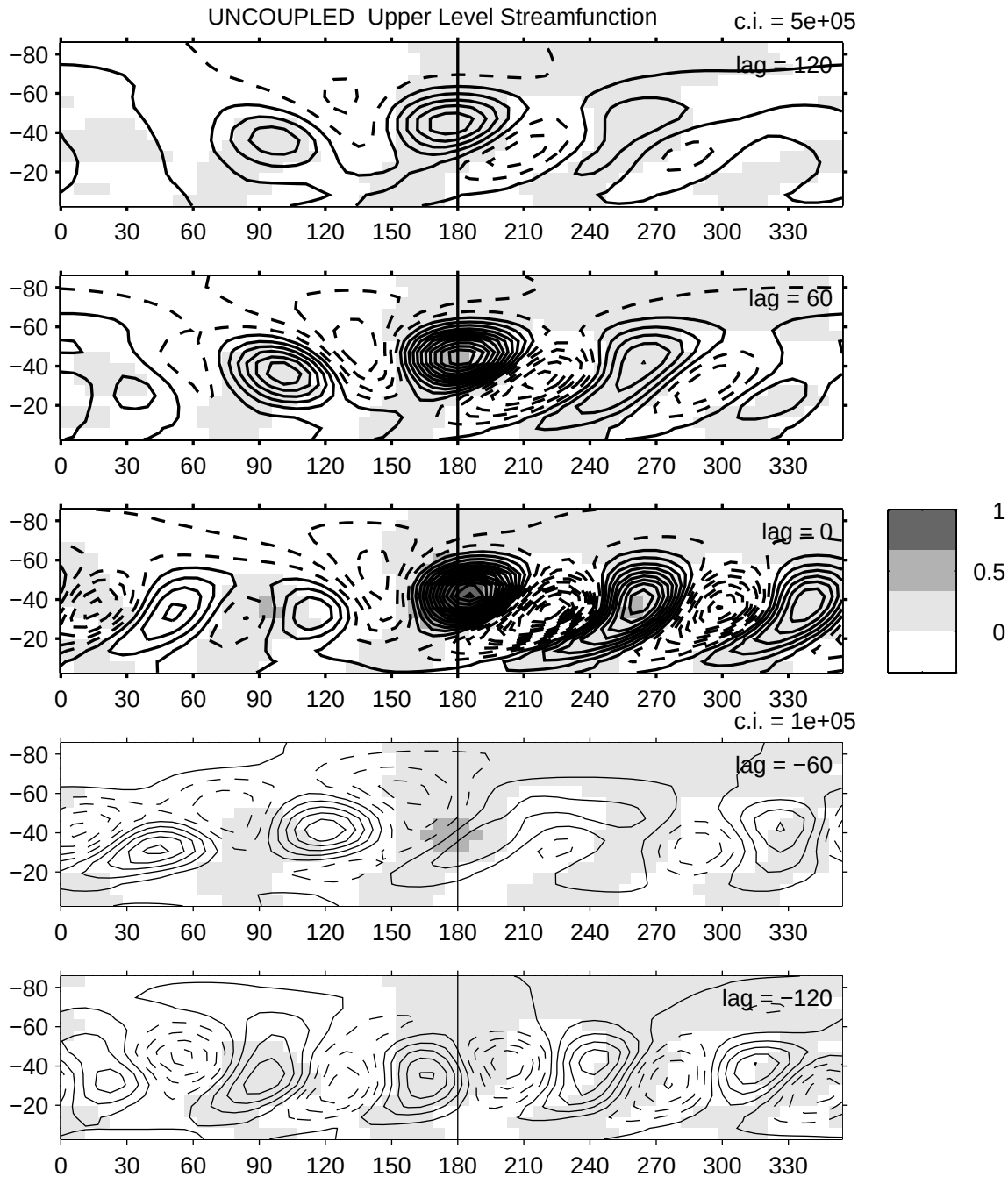

Figure 4.31. Lag regression maps for UNCOUPLED 250 mb streamfunction. Contour inteval is 5×10^5 m^2 s^{-2}. Lower two plots use smaller contour interval. See figure 4.22 caption.

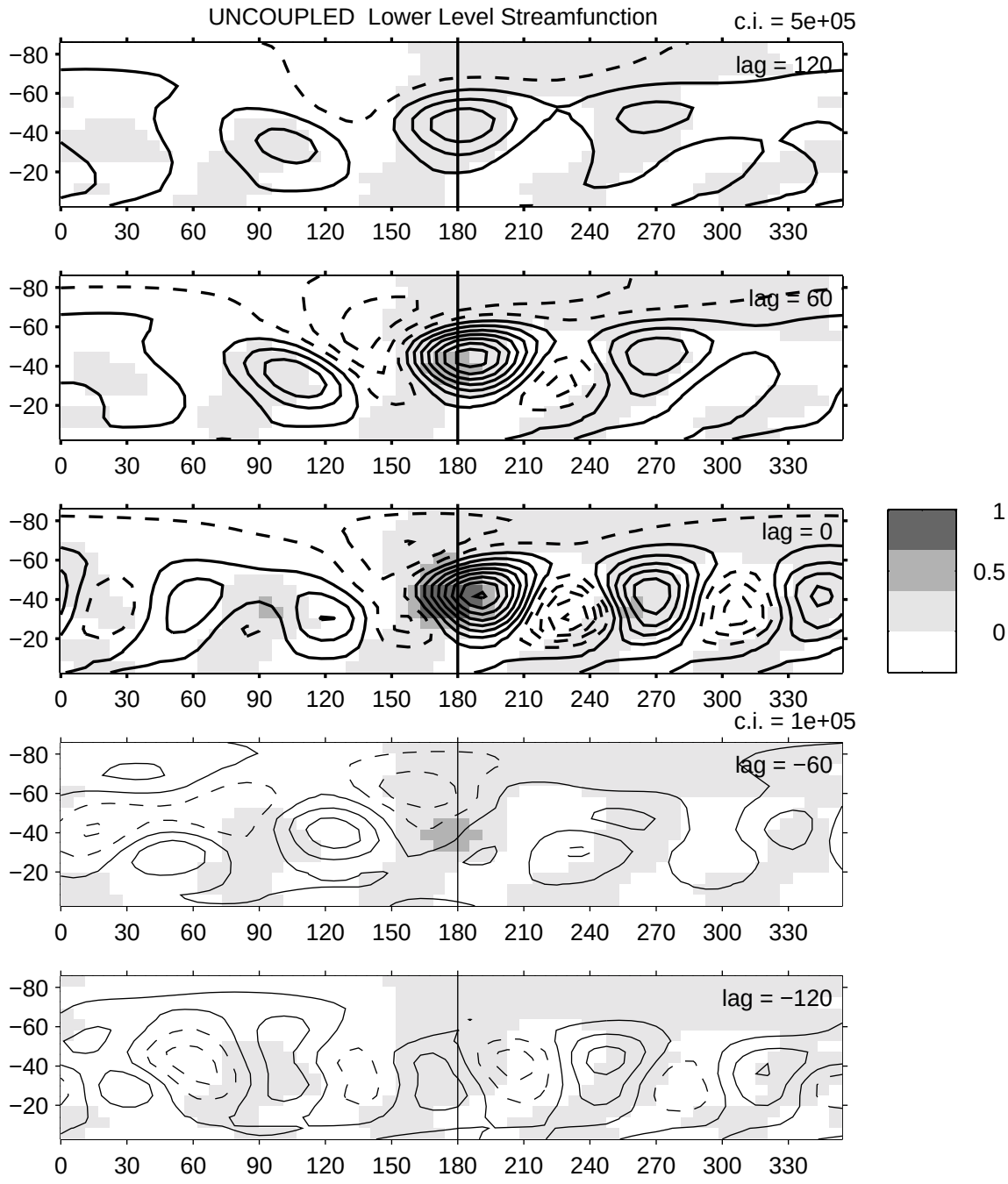

Figure 4.32. Lag regression maps for UNCOUPLED 750 mb streamfunction. Contour inteval is 5×10^5 m^2 s^{-2}. Lower two plots use smaller contour interval. See figure 4.22 caption.

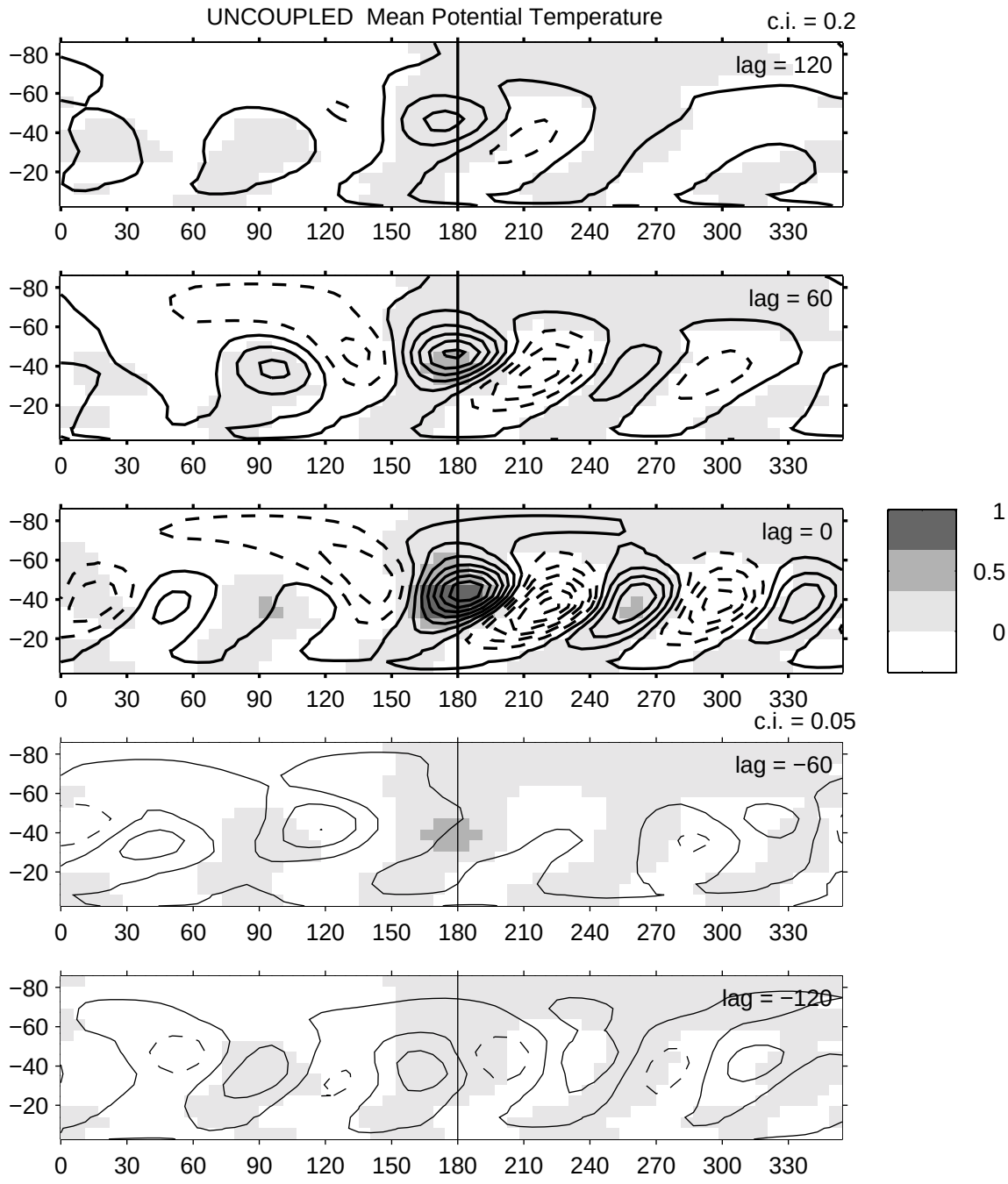

Figure 4.33. Lag regression maps for UNCOUPLED vertical mean potential temperature, $\bar{\theta}$. Contour inteval is 0.2 K. Lower two plots use smaller contour interval. See figure 4.22 caption.

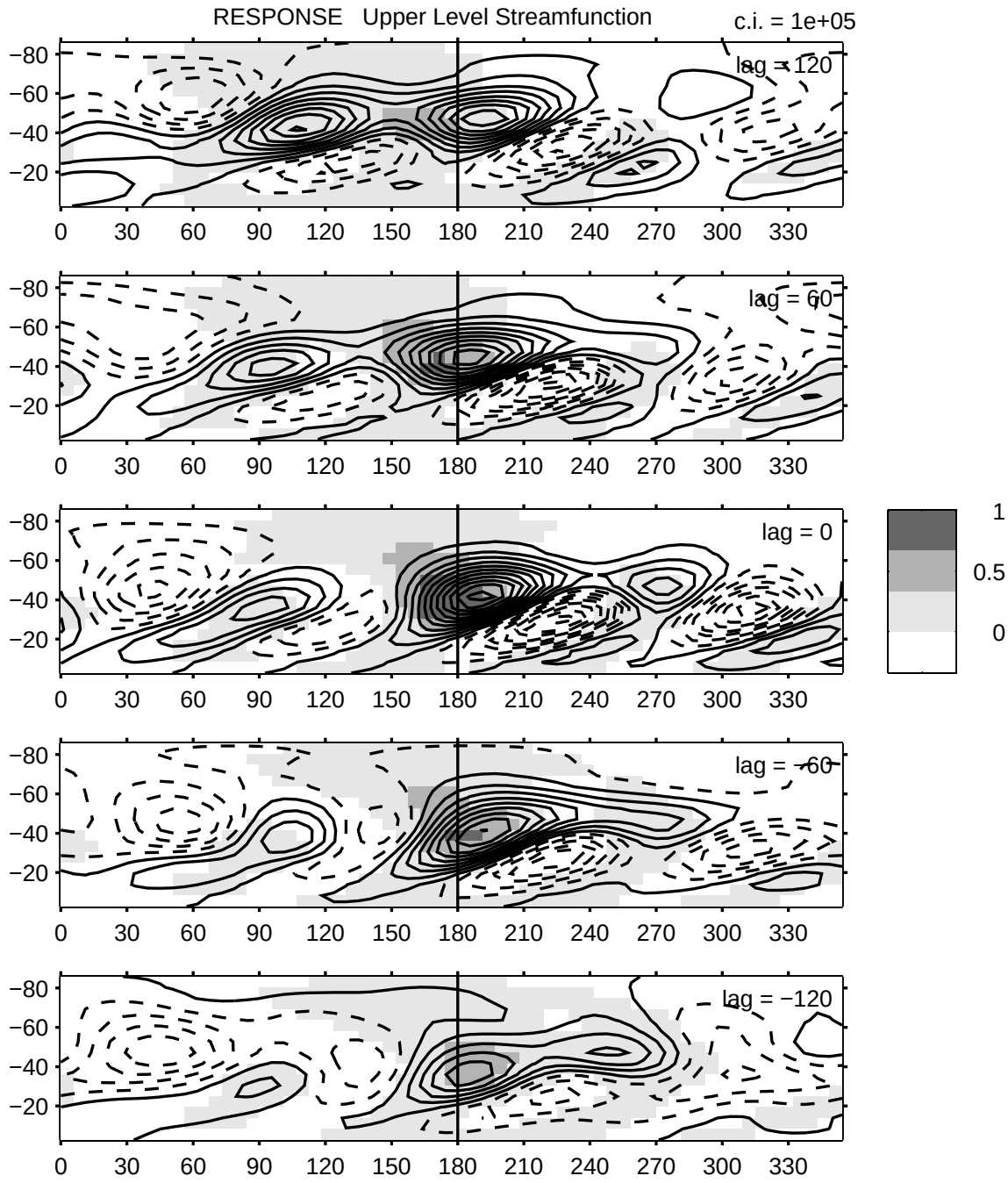

Figure 4.34. Lag regression maps for MOGA-RESPONSE 250 mb streamfunction. Contour inteval is 1×10^5 m^2 s^{-2} in all plots.

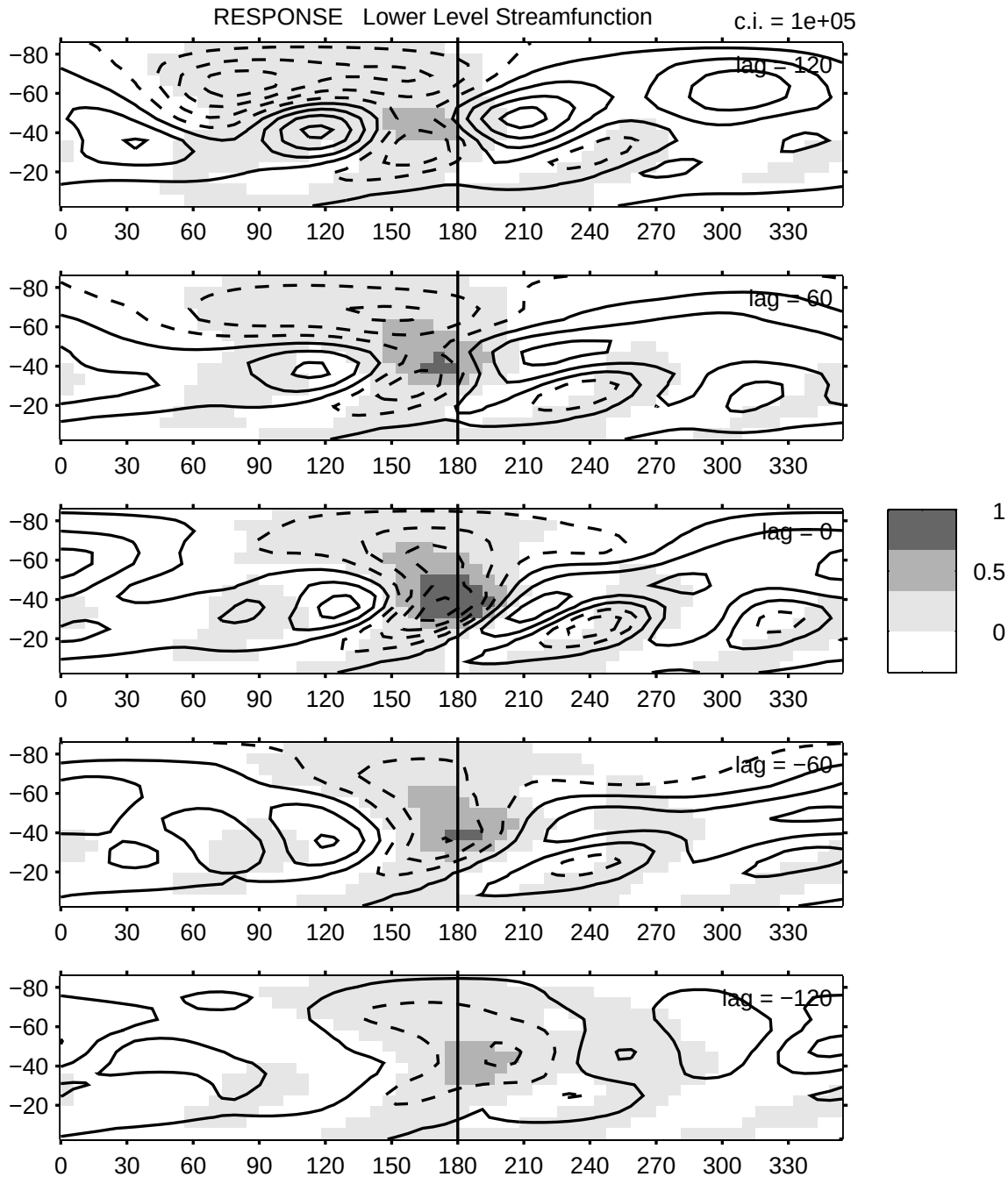

Figure 4.35. Lag regression maps for MOGA-RESPONSE 750 mb streamfunction. Contour inteval is 1×10^5 m^2 s^{-2}.

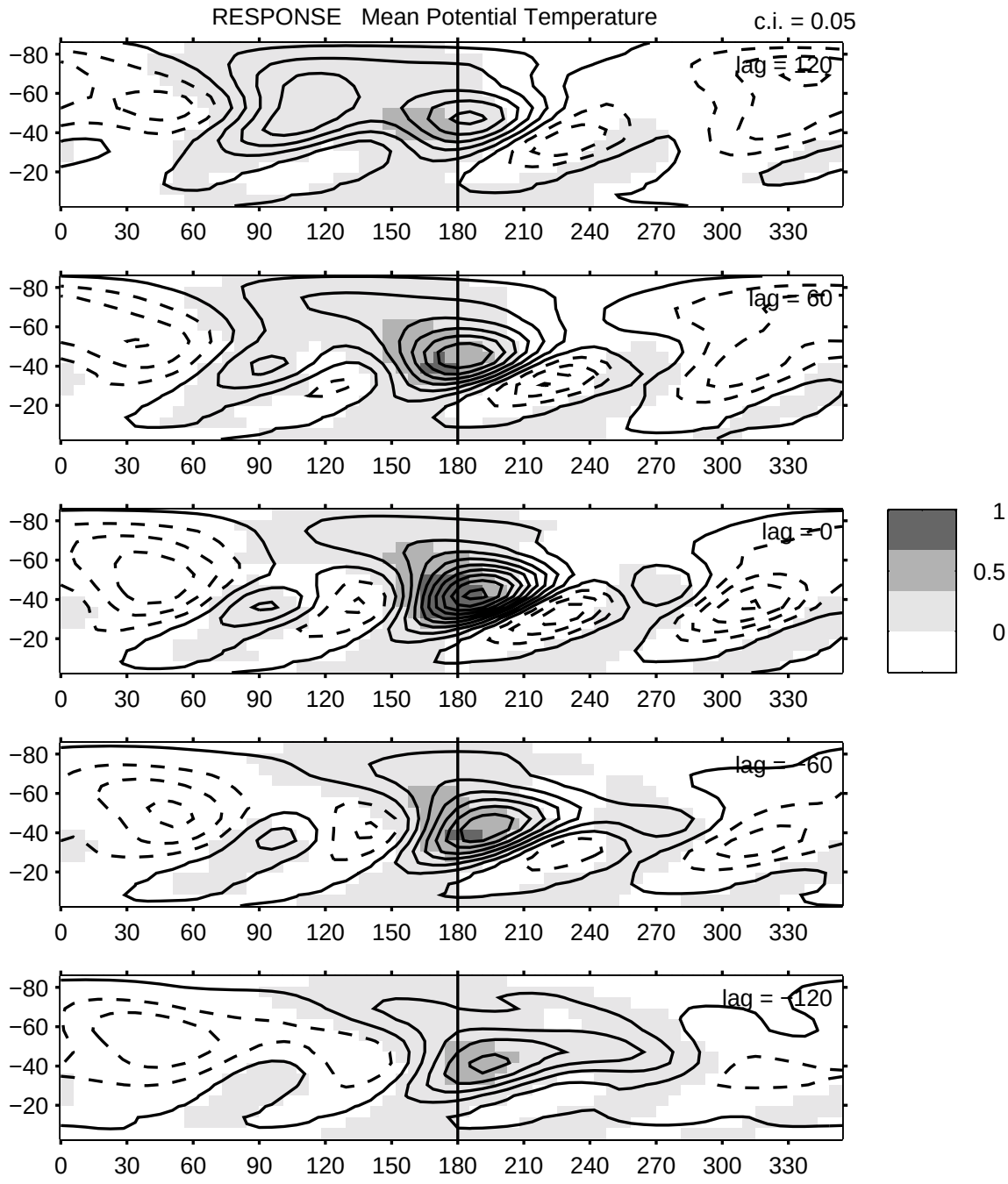

Figure 4.36. Lag regression maps for MOGA-RESPONSE vertical mean potential temperature, $\bar{\theta}$. Contour inteval is 0.05 K.

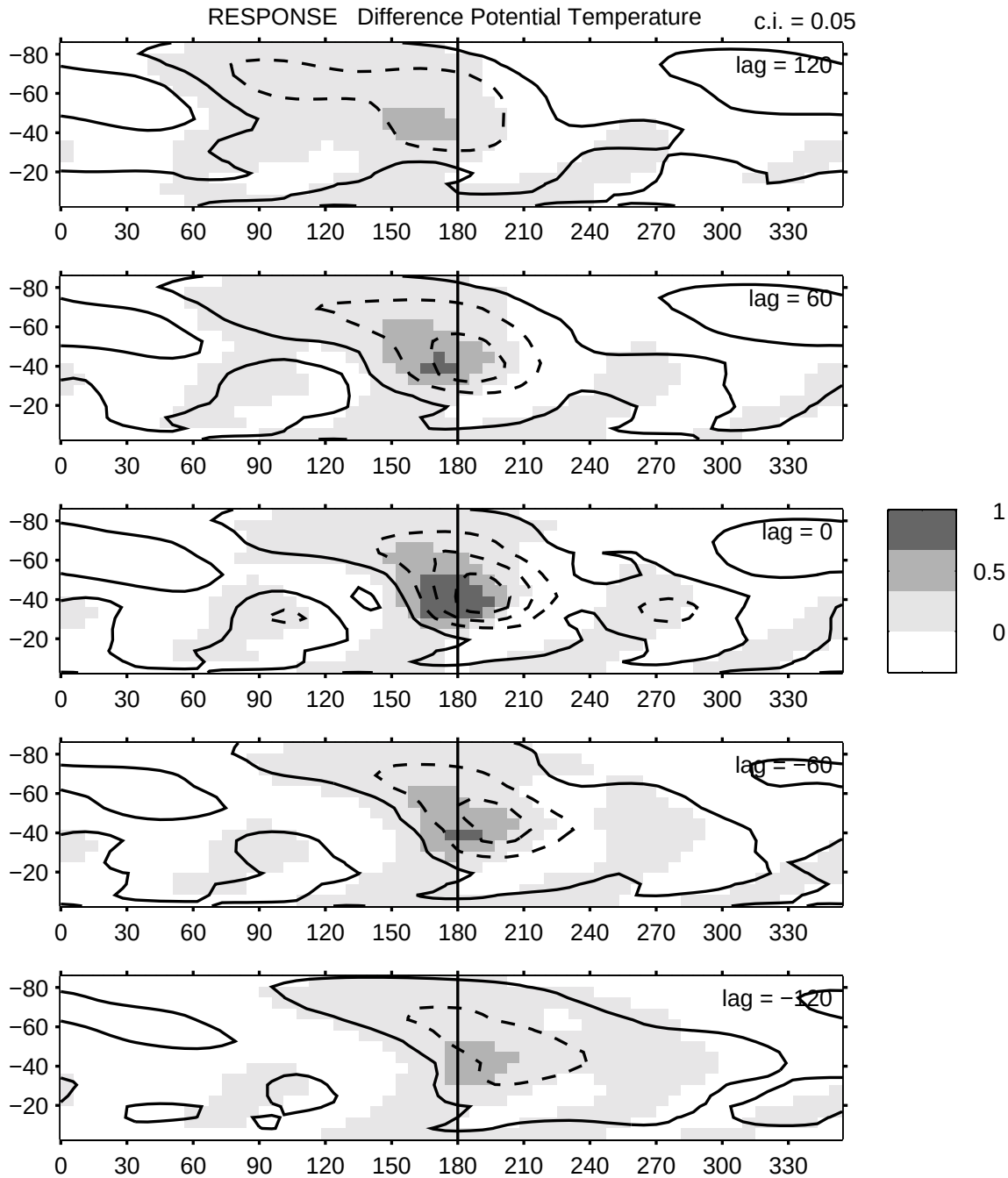

Figure 4.37. Lag regression maps for MOGA-RESPONSE vertical difference potential temperature, $\hat{\theta}$. Contour inteval is 0.05 K.

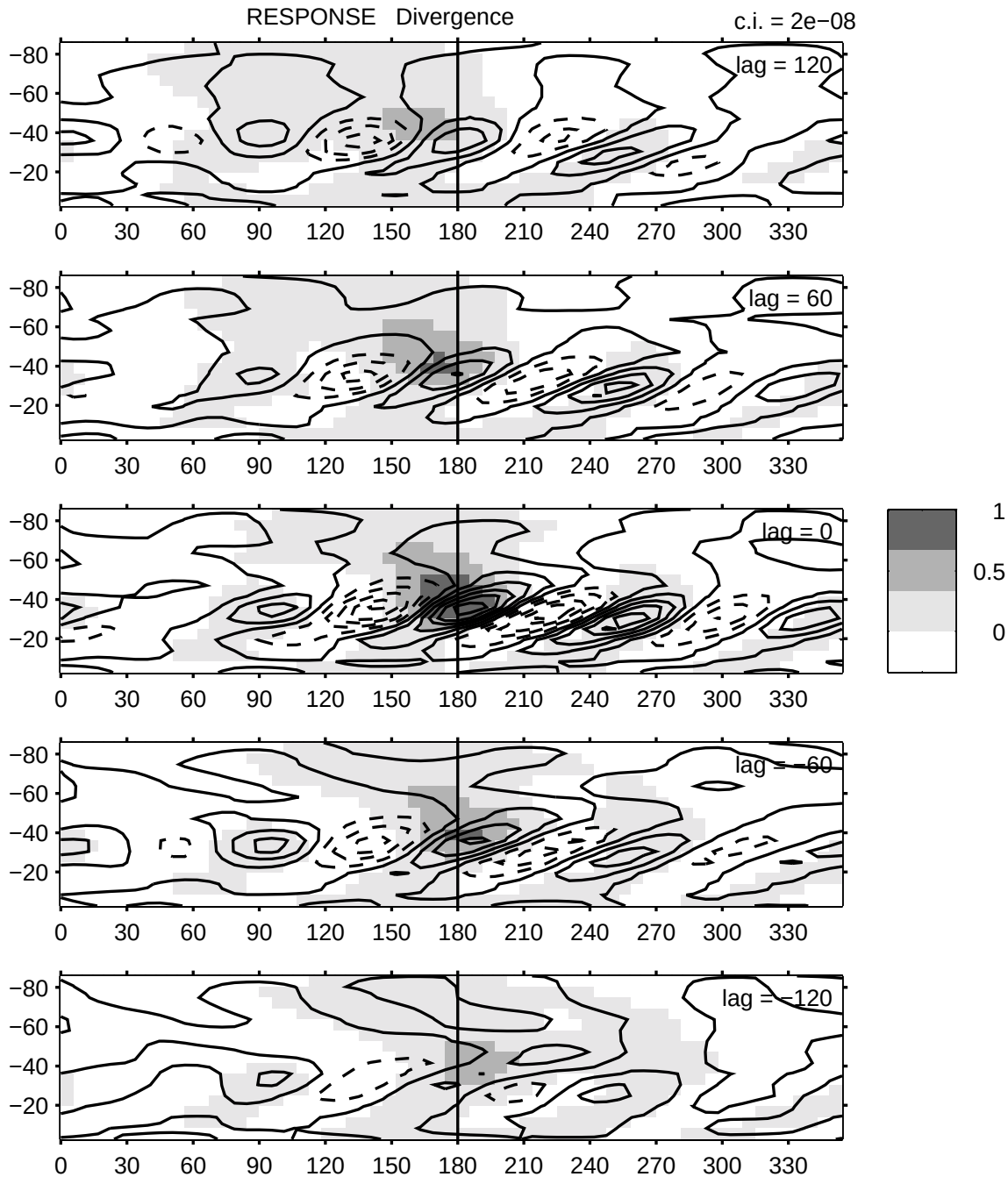

Figure 4.38. Lag regression maps for MOGA-RESPONSE 250 mb divergence. Contour inteval is 2×10^{-8} s^{-1}.

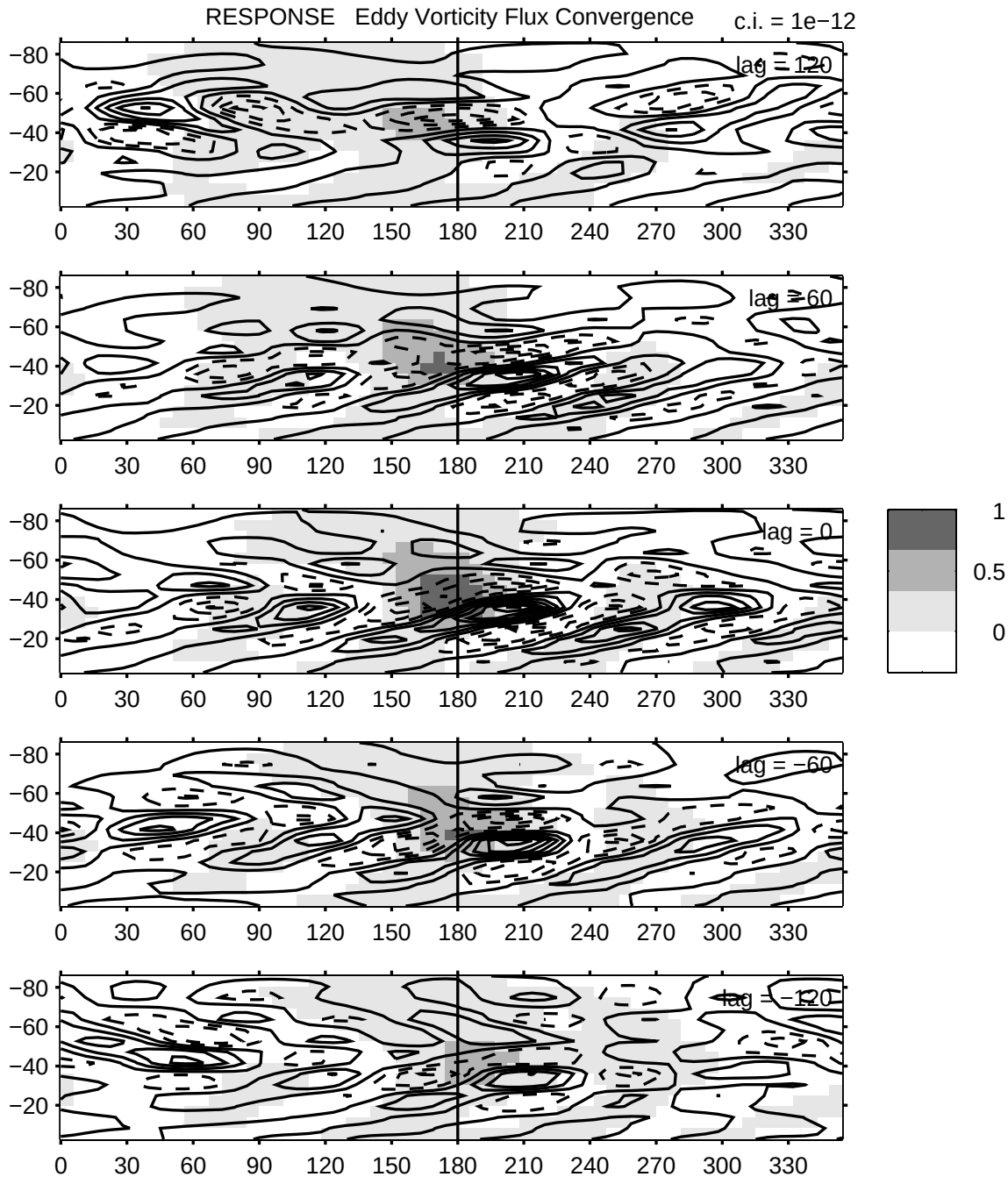

Figure 4.39. Lag regression maps for MOGA-RESPONSE 250 mb eddy vorticity flux convergence. Contour interval is 1×10^{-12} s^{-2}. In the Northern Hemisphere view I have adopted, a negative value indicates here indicates forcing of anticyclonic circulation.

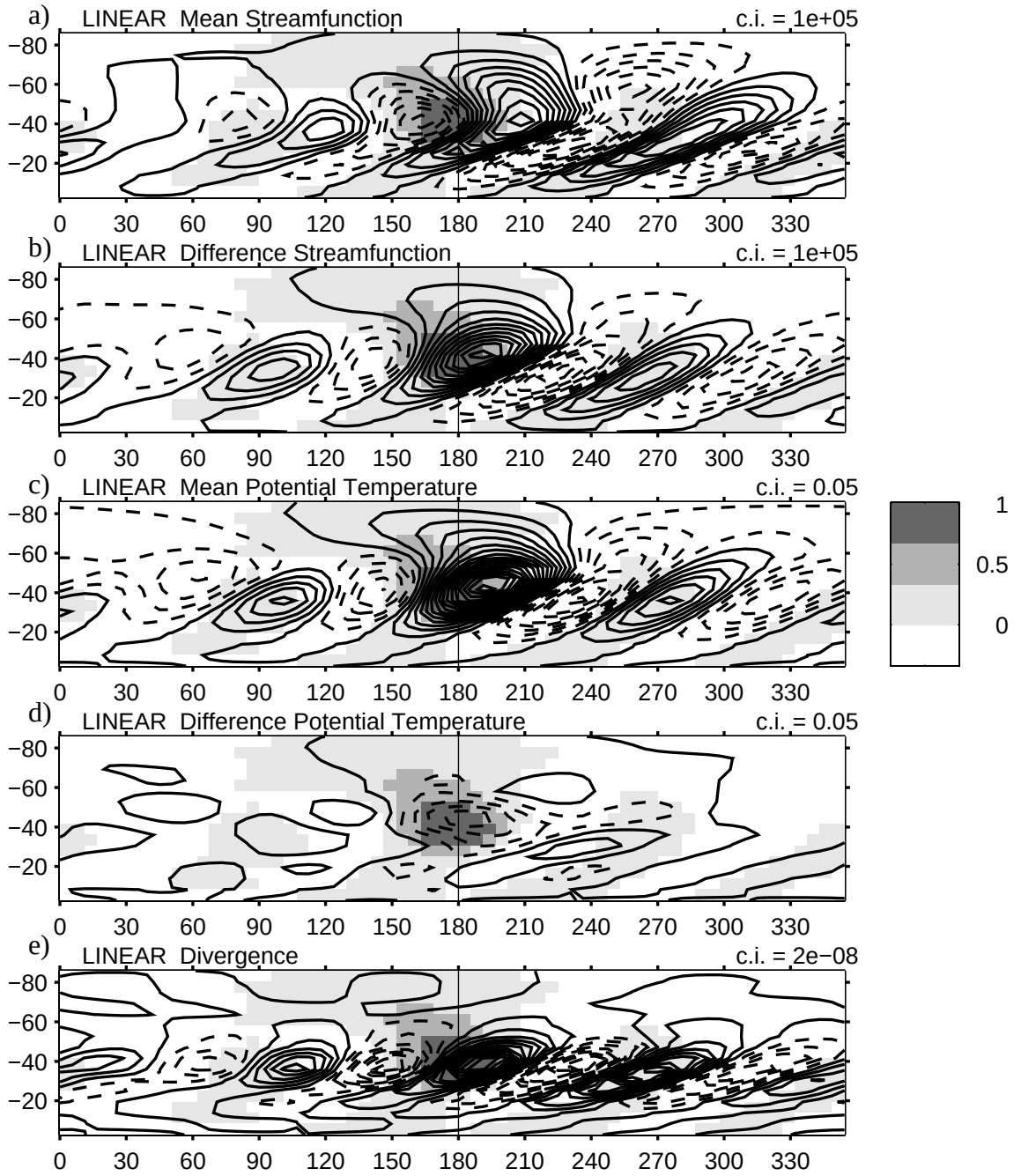

Figure 4.40. Steady LINEAR response to coupled sea surface temperature forcing. a) vertical mean streamfunction, $\bar{\psi}$; b) vertical difference stramfunction, $\hat{\psi}$; c) vertical mean potential temperature $\bar{\theta}$; d) vertical difference potential temperature $\hat{\theta}$; e) divergence. The contour intervals are same as in MOGA-RESPONSE figures. The untis are customary, the contour interval is noted in each figure.

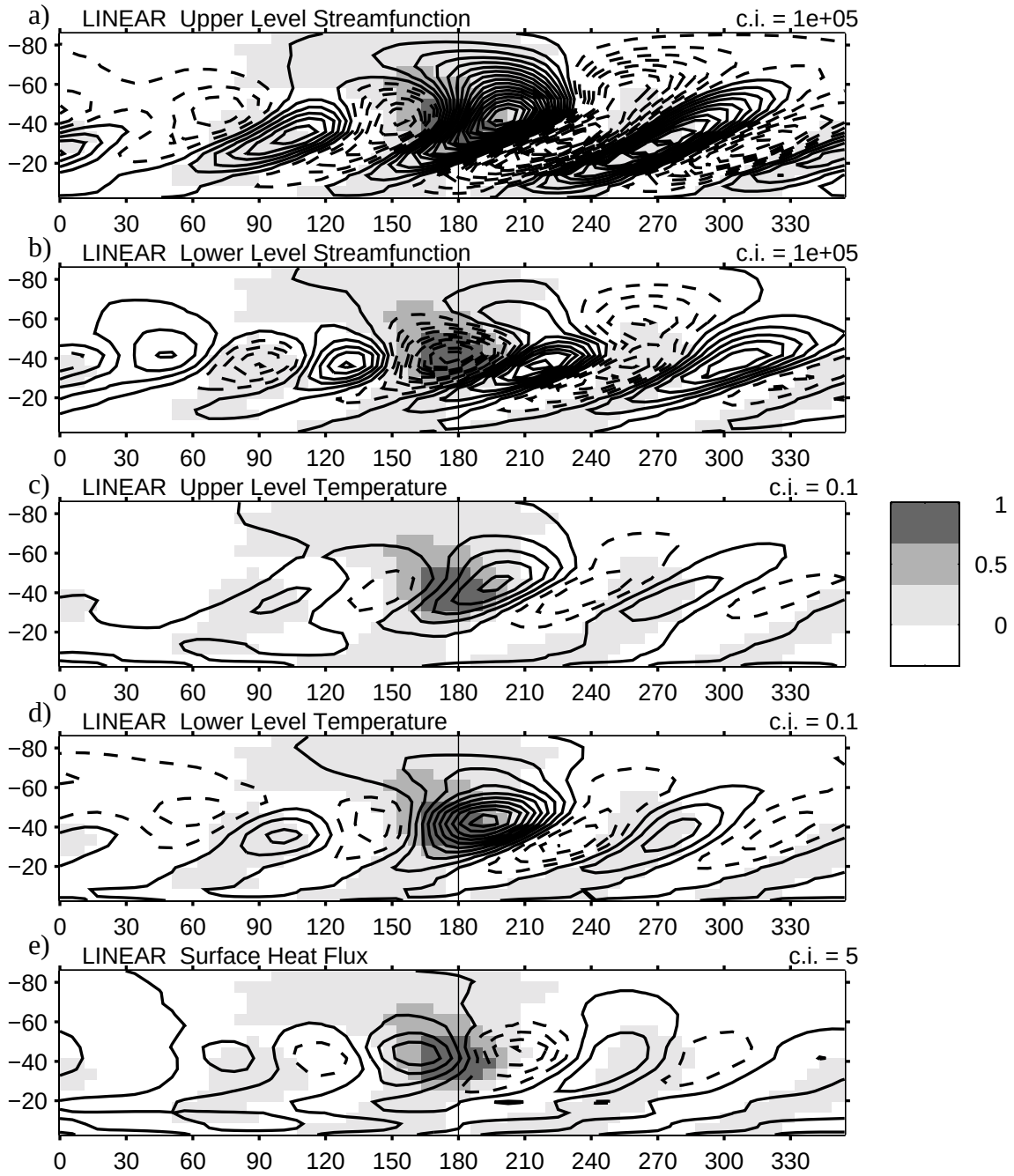

Figure 4.41. Steady LINEAR response to coupled sea surface temperature forcing. a) 250 mb streamfunction; b) 750 mb stramfunction; c) 250 mb temperature; d) 750 mb temperature; e) total surface heat flux (positive upwards). Contour intervals are same as in MOGA-RESPONSE figures (Figs. 4.37-4.39). The untis are customary. The units for figure e) are W m^{-2}. The contour interval is noted in each figure.

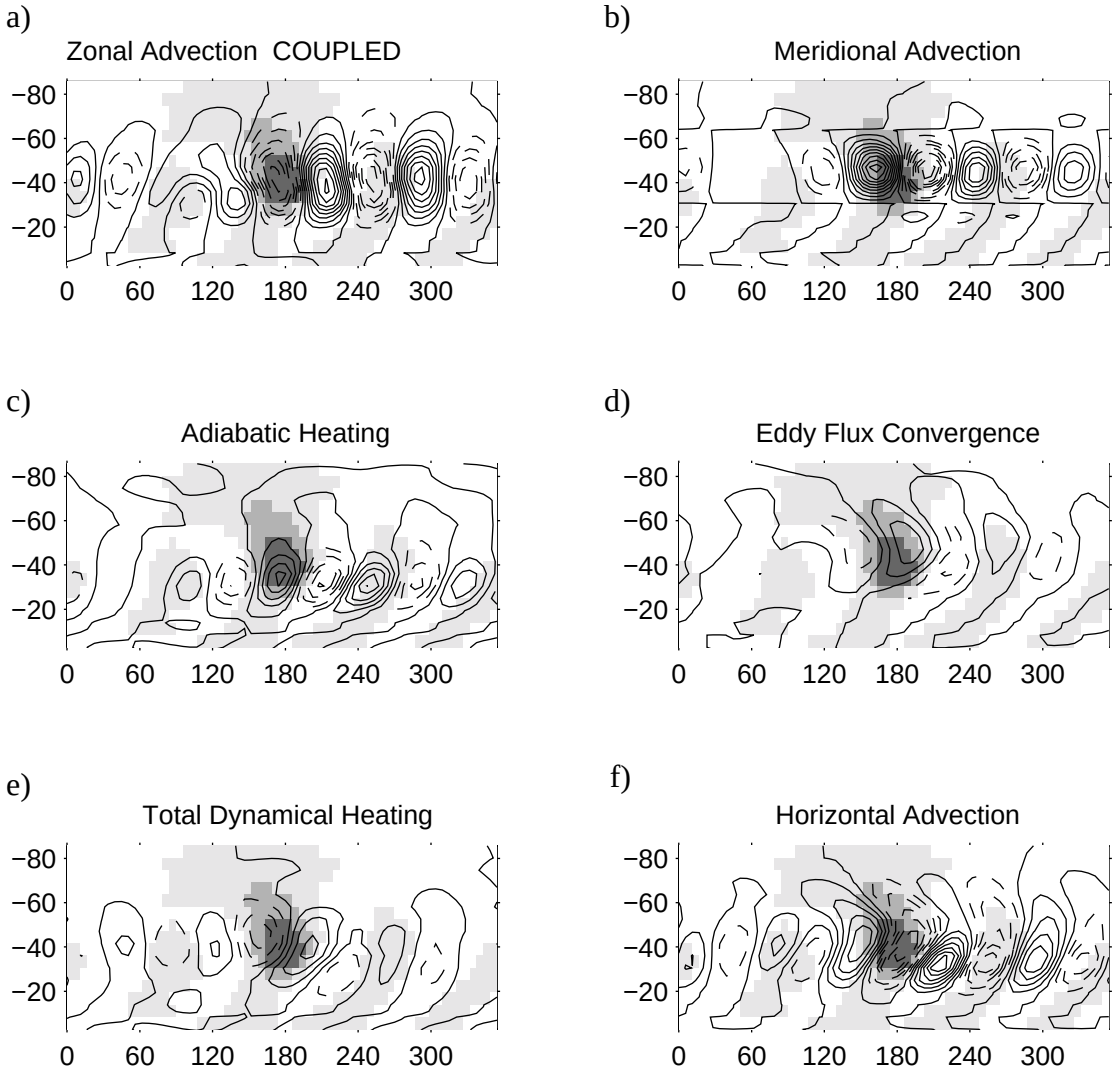

Figure 4.42. 750 mb heat budget using linear regression of COUPLED atmosphere versus normalized Southern Hemisphere COUPLED SST index. a) linear advection by the mean zonal wind $(1/a\ \cos\phi)\bar{u}\tilde{\theta}_\lambda$; b) linear advection by perturbation meridional wind $(1/a)\tilde{v}\bar{\theta}_\phi$; c) adiabatic heating by anomalous vertical motion, $\tilde{D}\bar{\hat{\theta}}$; d) eddy heat flux convergence; e) total dynamical heating; and f) linear horizontal advection, defined as the sum of the terms shown in figures a and b. Contour interval is 5e-7 Ks^{-1}. SST anomalies depicted by shading as in lag-regression plots.

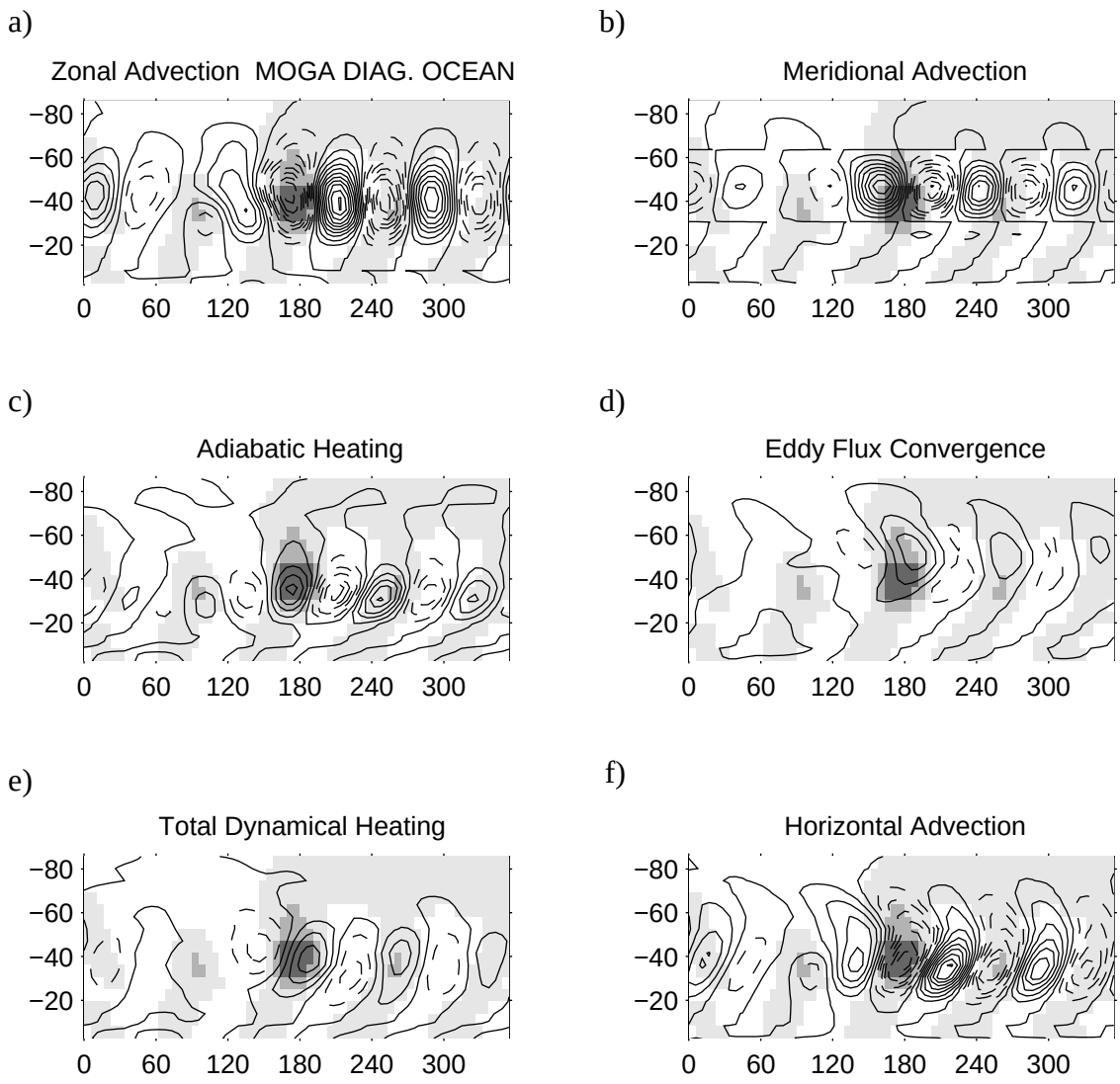

Figure 4.43. As in figure 4.42 except for linear regression of MOGA atmosphere versus MOGA diagnostic ocean.

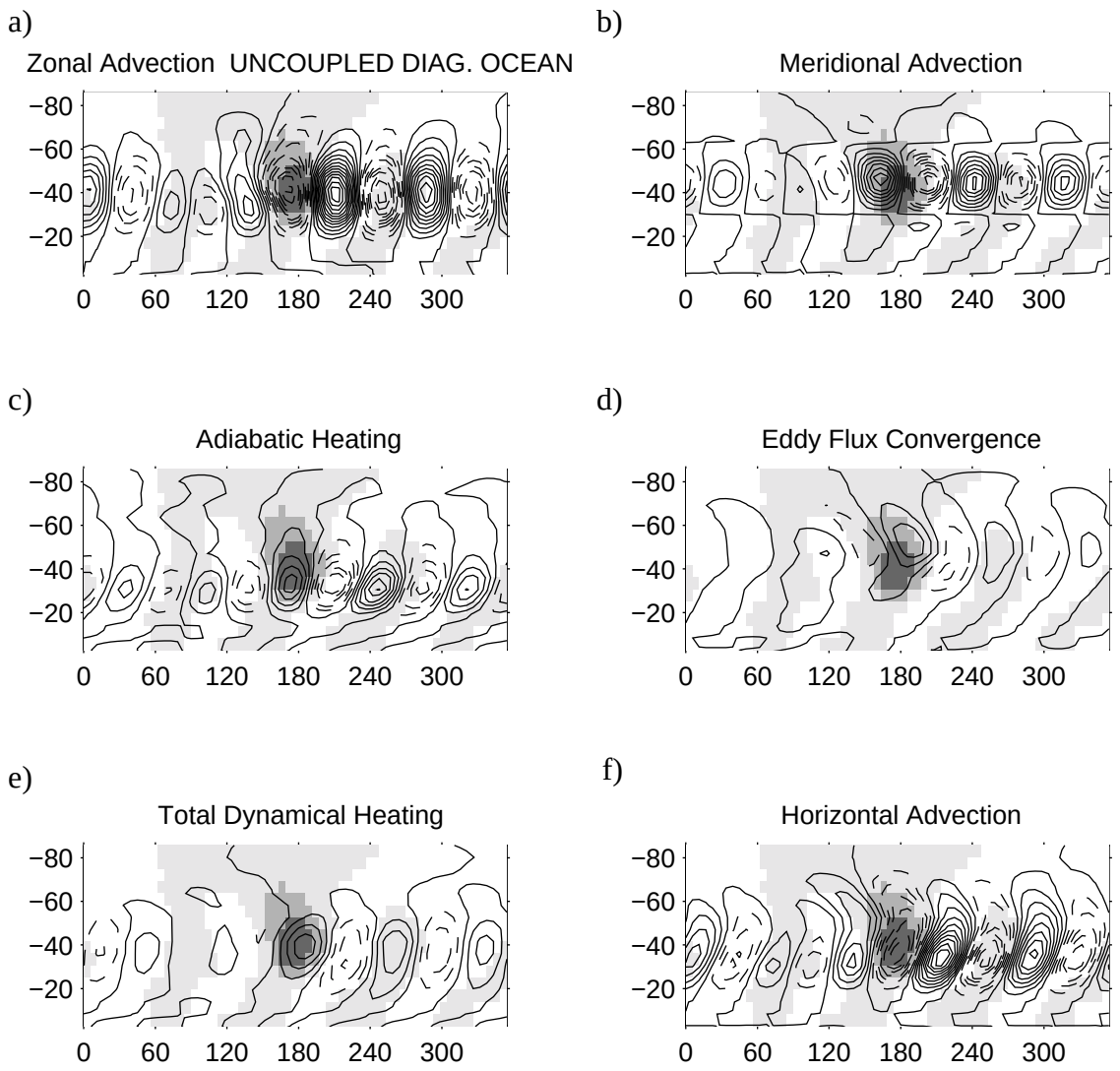

Figure 4.44. As in figure 4.42 except for linear regression of UNCOUPLED atmosphere versus UNCOUPLED diagnostic ocean.

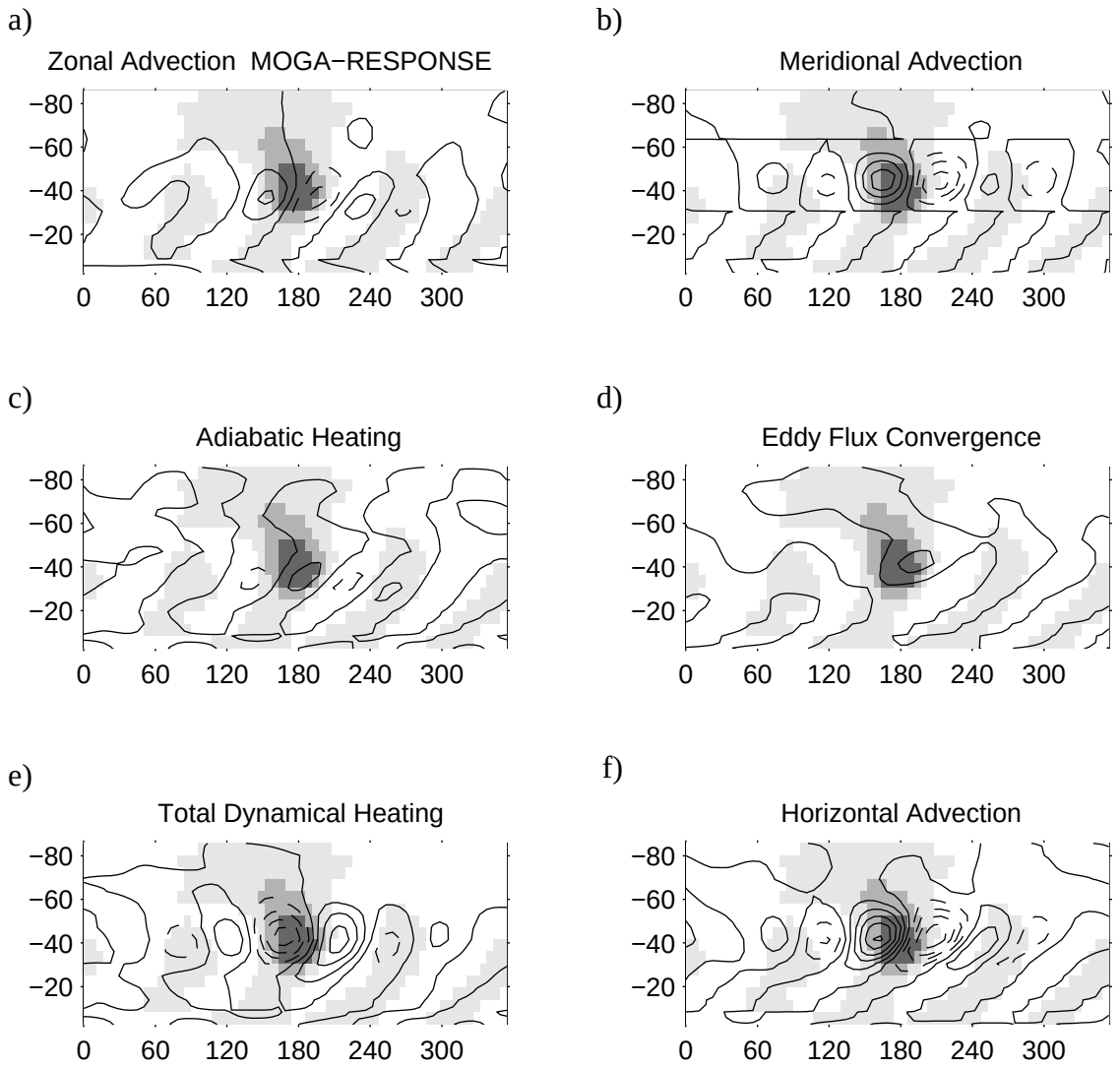

Figure 4.45. As in figure 4.42 except for MOGA-RESPONSE regressions.

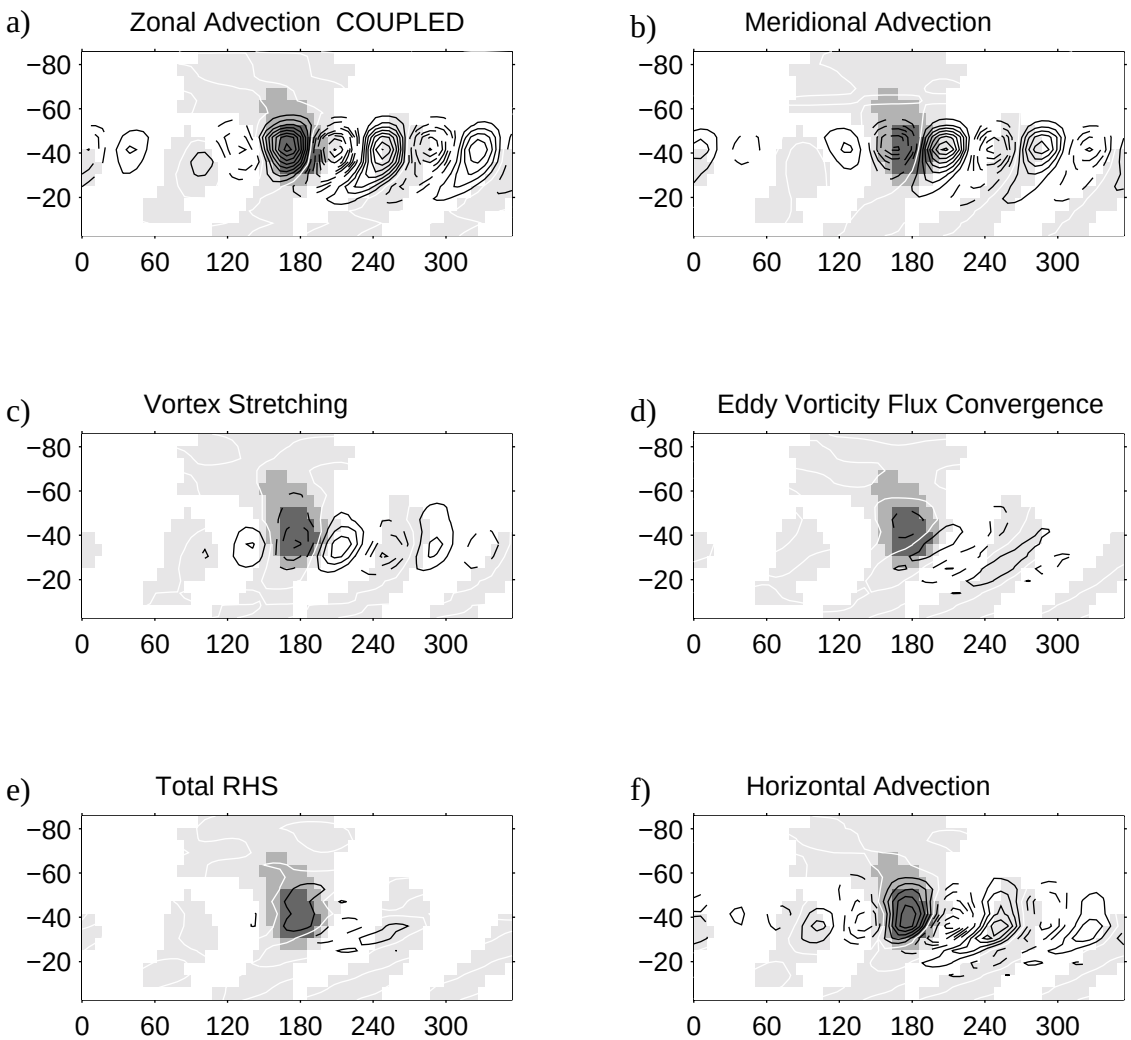

Figure 4.46. 250 mb vorticity budget for COUPLED run using linear regression with Southern Hemisphere SST index. a) linear advection by the mean zonal wind $(1/a\ \cos\phi)\bar{u}\tilde{\zeta}_\lambda$; b) linear advection by perturbation meridional wind $(1/a)\tilde{v}\overline{(\zeta + f)}_\phi$; c) vortex stretching by anomalous vertical motion, $\tilde{D}\overline{\zeta}$; d) eddy flux convergence; e) total of right hand side terms; and f) linear horizontal advection, defined as the sum of the terms shown in figures a and b. Contour interval is $8\text{x}10^{-12}$ s^{-2} in figures a and b, and $4\text{x}10^{-12}$ s^{-2} in c-f.

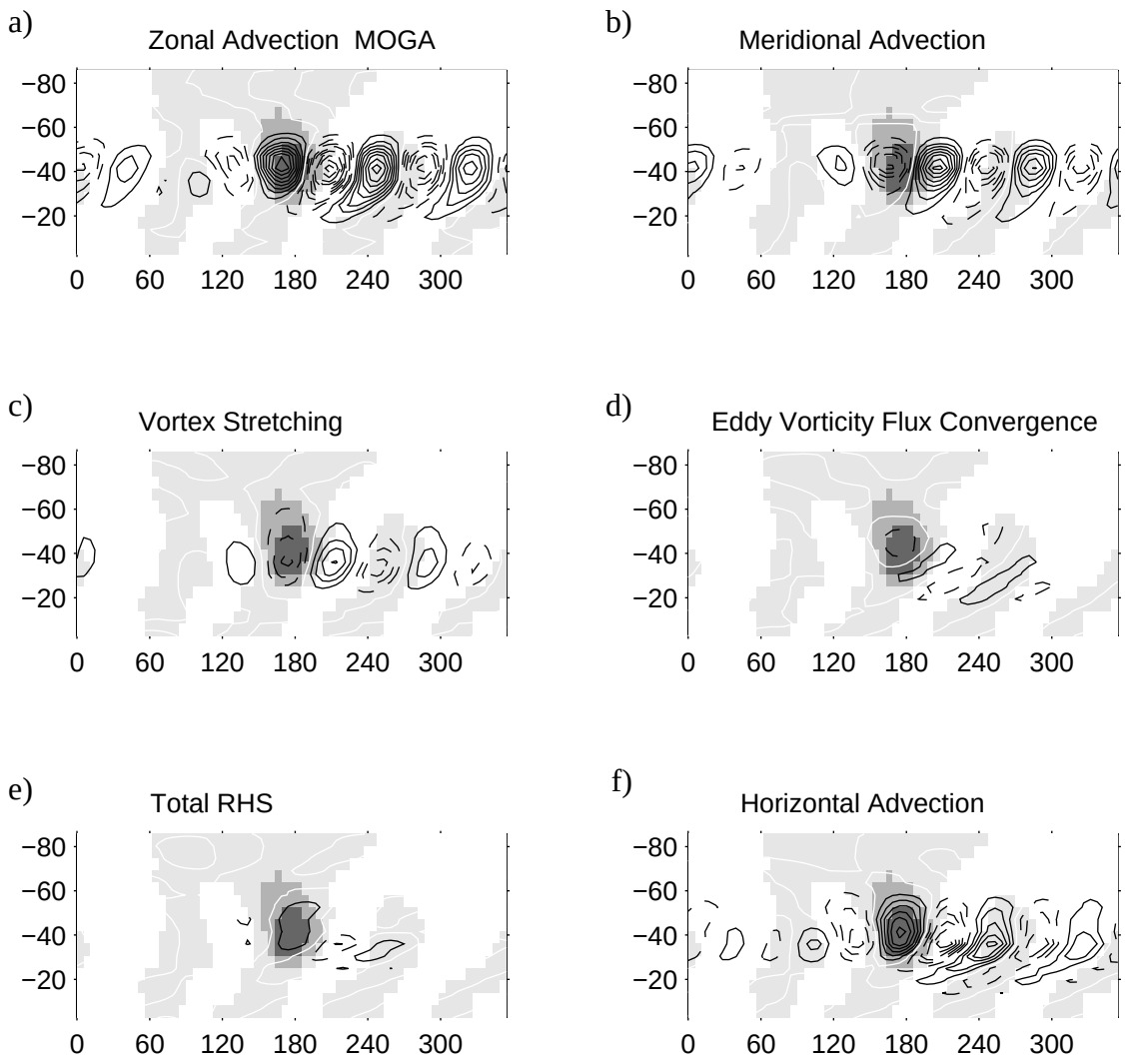

Figure 4.47. Same as figure 4.46 except for linear regression of MOGA atmosphere with MOGA diagnostic ocean. Contour interval is 8×10^{-12} s^{-2} in figures a and b, and 4×10^{-12} s^{-2} in c-f.

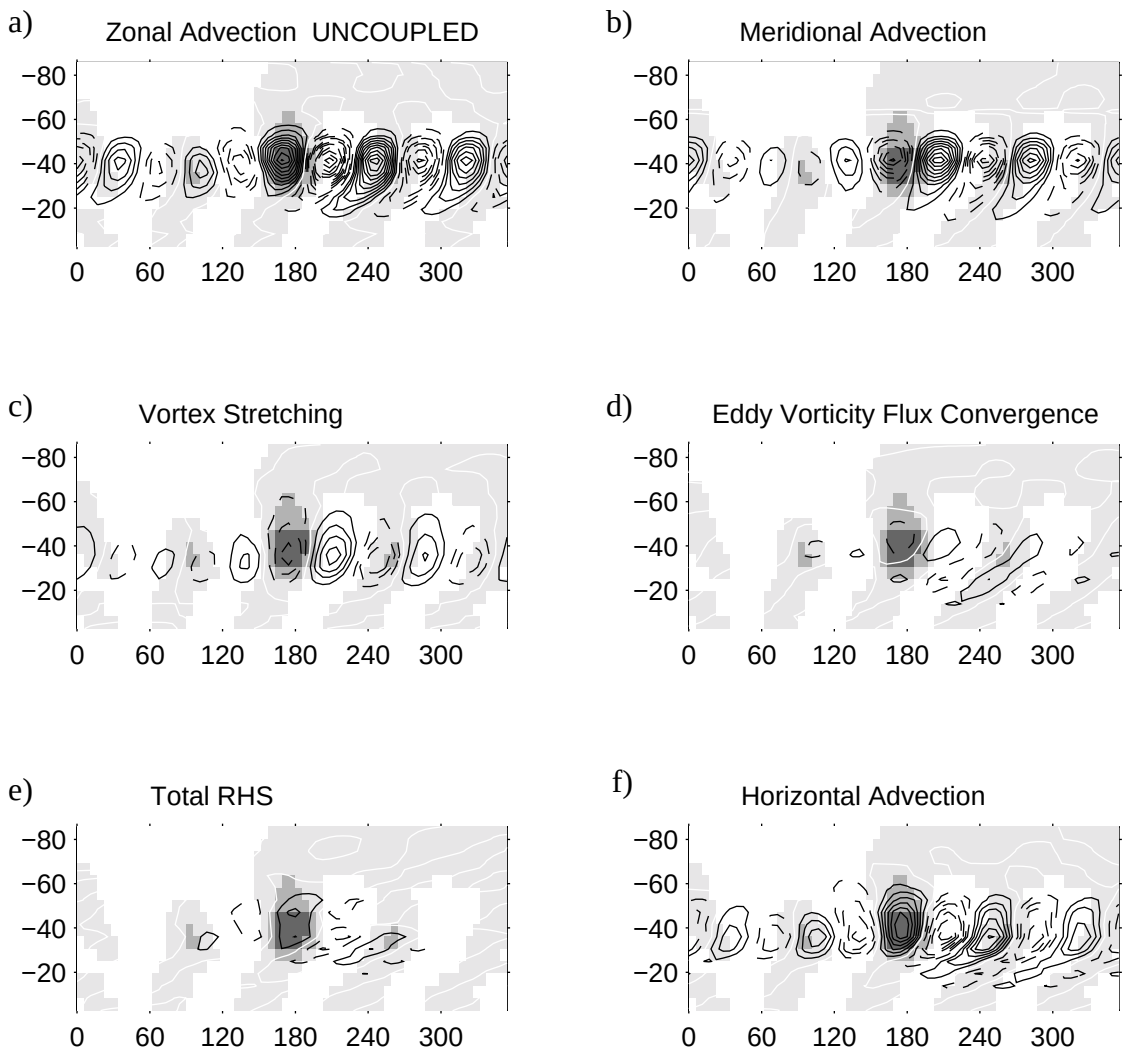

Figure 4.48. Same as figure 4.46 except for linear regression of UNCOUPLED atmosphere with UNCOUPLED diagnostic ocean. Contour interval is 8×10^{-12} s^{-2} in figures a and b, and 4×10^{-12} s^{-2} in c-f.

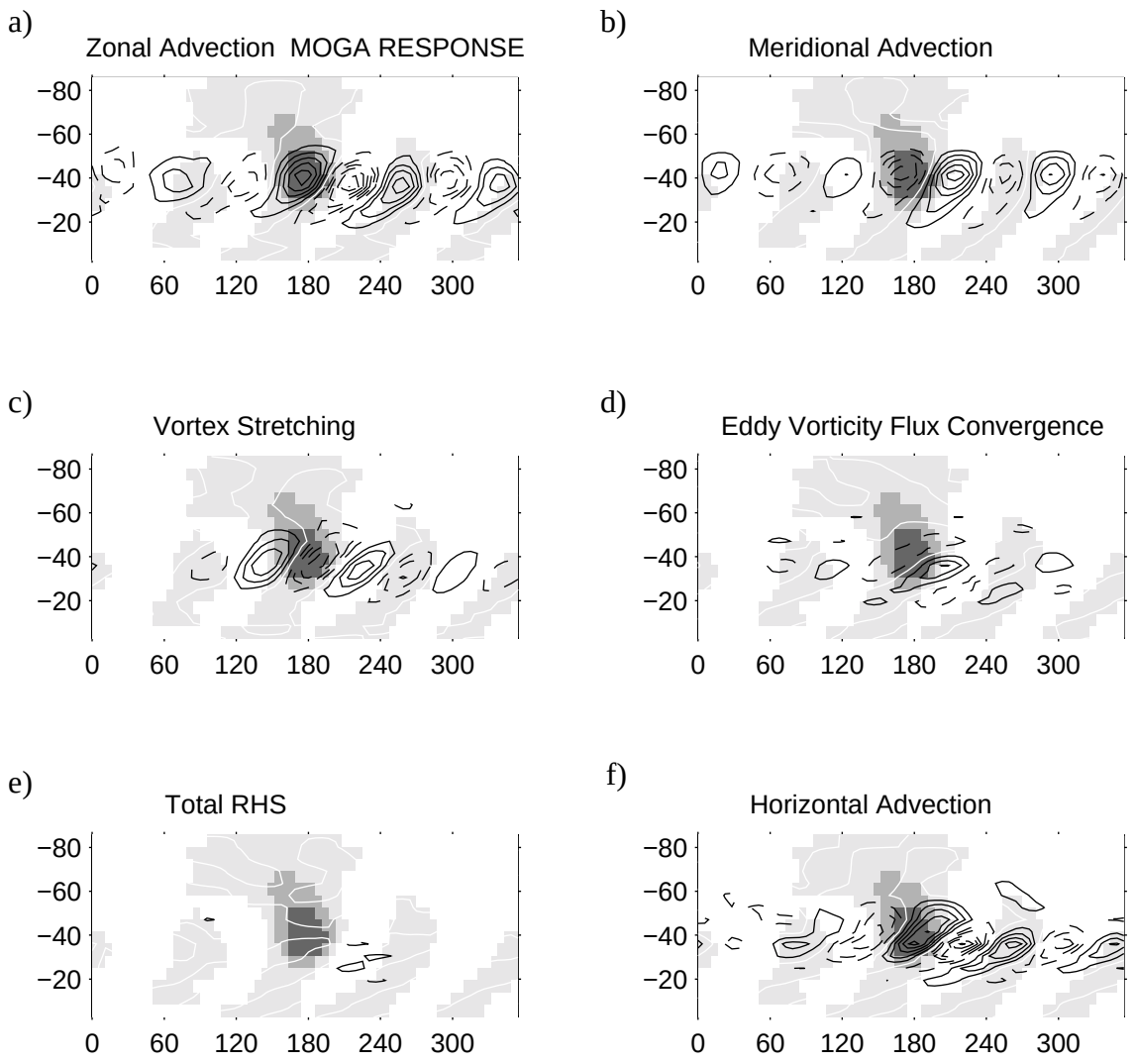

Figure 4.49. Same as figure 4.46 except for MOGA-RESPONSE regressions. Contour interval is $4x10^{-12}$ s^{-2} in figures a and b, and $2x10^{-12}$ s^{-2} in c-f.

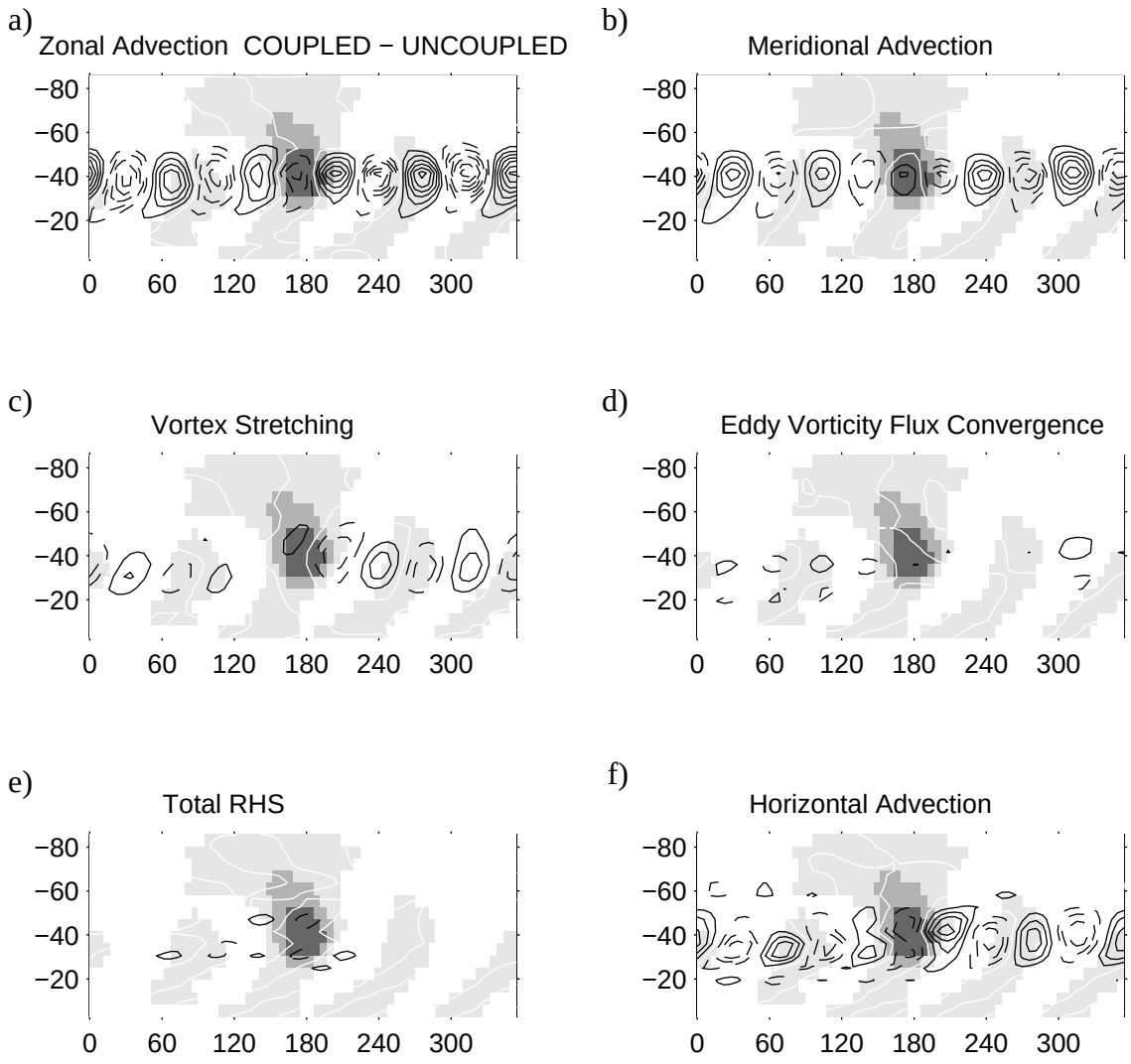

Figure 4.50. Same as figure 4.46 except for difference between COUPLED and UNCOUPLED (diagnostic) runs. Contour interval is $4x10^{-12}$ s^{-2} in figures a and b, and $2x10^{-12}$ s^{-2} in c-f.

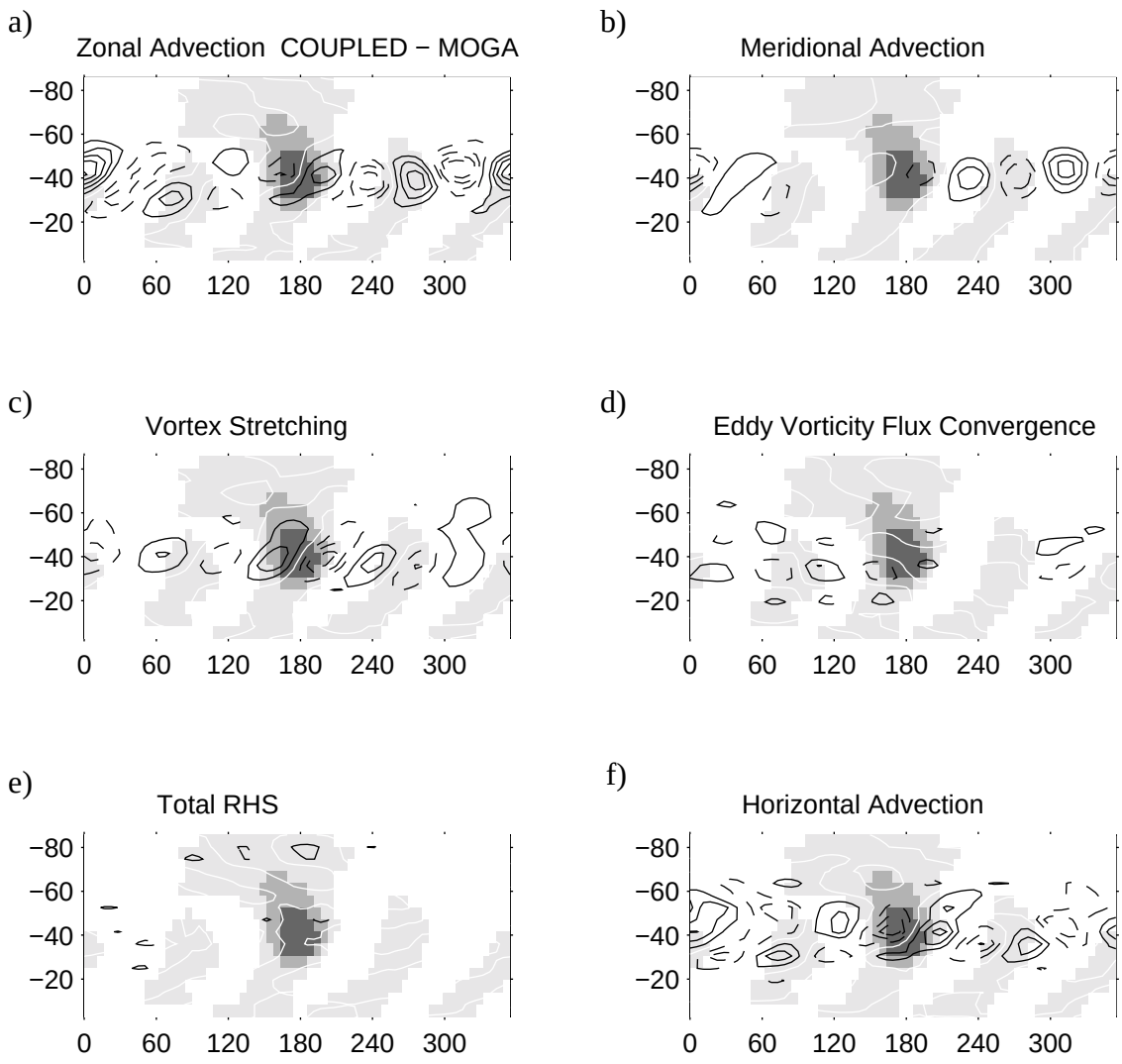

Figure 4.51. Same as figure 4.46 except for difference between COUPLED and MOGA (diagnostic) runs. Contour interval is 4×10^{-12} s^{-2} in figures a and b, and 2×10^{-12} s^{-2} in c-f.

Chapter 5: Coupling and Low-Frequency Variability on an All-Ocean Planet: Discussion.

5.1 Introduction

Chapter 4 described the following phenomena associated with coupling: increased variance, increased persistence, and eastward SST anomaly propagation. In this section we discuss possible mechanisms for these phenomena. Briefly, the main lesson is that coupling selectively enhances[1] certain structures present in the natural low-frequency variability of the model atmosphere, and that this enhancement occurs because coupling reduces the damping of the favored structures.

5.2 Coupled Random Walks and the Effect of Coupling on Variance

The variance in the SST from the COUPLED ocean is over twice that in the UNCOUPLED diagnostic ocean. Such a large and robust signal should have a simple explanation. In fact, a local thermodynamic argument goes a long way toward explaining the increased variance. Locally, one can think of SST as determining a 'baseline' temperature about which the atmosphere temperature fluctuates in a random walk. The random low-frequency forcing is generated from the higher frequencies in the atmosphere by nonlinearity. If left unchecked, the atmospheric temperature variance would increase indefinitely. The random walk is counteracted by two damping processes, a relatively slow thermal damping to space and a relatively fast damping due to surface fluxes, and the result is a statistical equilibrium. In the UNCOUPLED run this baseline is fixed by the specification of SST, and the atmospheric temperature variance is tightly constrained. In

1. The term "selective enhancement" to describe this effect was suggested to me by Prof. J. M. Wallace at the University of Washington.

the COUPLED run this baseline itself undergoes a random walk forced by the heat fluxes from the atmosphere. The entire coupled ocean-atmosphere system is damped back to the coupled climatology by relatively slow process of radiation to space by the ocean and the atmosphere, resulting in a larger atmospheric temperature variance. In this manner the low frequency variance of the system is increased due to coupling.

Plots of coupled, damped random walks which qualitatively illustrate the effect of coupling on variance are shown in figure 5.1. Although these plots were derived from an actual stochastic model, they are presented here only to illustrate graphically the relationship between coupling, damping, and variance. The upper panel shows a system where slow and fast time scales are well separated. The lower panel shows the subtler, but more realistic, effect when the slow and fast time scales are not as well separated. The standard deviation of the coupled and uncoupled "atmosphere" time series are shown in the figure legend for the latter case. Note that in both cases shown in figure 5.1 the "coupled" atmosphere temperature has greater variance than the "uncoupled" atmosphere temperature. Equivalently, one can view the effect of coupling in the frequency domain as reducing thermal damping at low frequencies by allowing the adjustment of SSTs to the natural low-frequency variability of the atmosphere. In fact, it is the *near absence* of surface fluxes into and out of the atmosphere at the lowest frequencies which is the tell-tale sign of coupling in these numerical model runs.

The "coupled random walk" mechanism is examined in greater depth in Chapter 6 for a simple stochastically forced energy balance model which is able to reproduce the power spectra of atmosphere and ocean temperature in the two-level model reasonably well. The stochastic energy balance model also allows us to investigate the role of damping and direct forcing in the MOGA run, which is difficult to do in the purely qualitative

discussion given here.

5.3 Persistence and Propagation: Selective Enhancement of Natural Variability by Coupled Linear Modes.

COUPLED SST anomalies show enhanced persistence and a preferred direction of propagation compared to the UNCOUPLED diagnostic SST. An extension of the “coupled random walk” yields a plausible mechanism for both these effects. The reduction of damping at low frequencies due to coupling will selectively enhance those structures of the natural variability of the atmosphere for which the damping is reduced the most.

For the parameter range investigated in this study, the 2-level model atmosphere responds to anomalous heating through anomalous northerly (cold) advection, much as predicted in Hoskins and Karoly (1983) for heating anomalies in a zonal flow. In the COUPLED model this response is manifested not as a lower level cyclone, but rather as a statistical reduction in the lower-level anticyclonic circulation associated with the uncoupled variability. Close-up views of simultaneous regressions maps performed with normalized SST time series for COUPLED 250 mb streamfunction (Fig. 5.2a) and COUPLED 750 mb streamfunction (Fig 5.2b) compared to similar maps for the UNCOUPLED DIAGNOSTIC run (Fig. 5.3a and 5.3b, respectively) confirm the increased baroclinic/barotropic ratio in the COUPLED run. In fact the low-level anticyclonic winds are weaker in the COUPLED run than in the UNCOUPLED run. Therefore coupling, in addition to reducing thermal damping at low frequencies, also has the effect of reducing frictional damping due to Ekman pumping, a somewhat surprising result.

Eastward propagation is consistent with the Frankignoul’s (1985) results from a coupled linear model. Using a 2-layer, quasi-geostrophic beta-plane, channel model coupled to a slab mixed layer[1], he found eastward propagating coupled modes with phase

speeds varying from a few cm s^{-1} to 20 cm s^{-1}. Away from the linear channel model's resonance, lower zonal wavenumber modes have faster phase speeds and lower damping. Although in the coupled linear model the longest zonal wavenumbers are the least damped, the small projection of the natural atmospheric variability onto these modes due to a mismatch of phase speed will prevent the low wavenumber modes from showing the greatest enhancement. Instead, the quasi-stationary waves of natural atmospheric variability -- zonal wavenumbers 4 and 5 in the present study -- are most closely matched in phase speed to the slow, coupled linear modes and will probably project most strongly onto them.

One would not expect the linear coupled modes to survive completely intact in the nonlinear simulation. Recall that the linear coupled modes were calculated by letting the steady linear atmospheric response to a SST anomaly feed back on the SST anomaly through surface fluxes. The similarity of the MOGA atmosphere's response to the steady LINEAR response described in the previous chapter, and in particular the similarity in the surface flux field, is a strong indication that a similar feedback could occur in the COUPLED model run. It seems that coupling selectively enhances structures which are quite similar in structure to the coupled modes of the linear model.

5.4 Response to externally imposed forcing

The main practical reason for studying intrinsic midlatitude variability is to better understand the midlatitude response to externally imposed forcing, particularly forcing

---

1. Note that Frankignoul used a 100 m deep mixed layer and a surface flux parameterization of 40 W m^{-2} per degree of air-sea temperature difference, while I use a 50 m deep mixed layer, and 20 W m^{-2} is a more appropriate value of the surface flux proportionality constant for the midlatitudes of my model. The two effects cancel, so that the mixed-layer time scale is roughly 4 months in both models.

from anomalous tropical heating. What do the results in this dissertation have to say about the response to extermal forcing? First of all that the main role of open-ocean midlatitude SST anomalies is to modulate the damping of low-frequency atmospheric anomalies.

The relationship between the results from past studies of the response of the atmosphere to prescribed SST anomalies and the MOGA atmospheric response is problematic. A barotropic anticyclonic signal is commonly seen downstream from warm SST anomalies in numerical modeling studies, as in Palmer and Sun (1985). This signal is often interpreted as a response to the prescribed SST anomaly. However the similarity between the natural uncoupled variability of the atmosphere and the so-called “response” seen in other studies is striking, leading one to question whether what is called a “response” can be more accurately described as a spatial reorganization of the the natural, uncoupled variability of the atmosphere.[1] Yet the MOGA runs presented in this dissertation show little, if any, sign of a barotropic signal, indicating that reorganization is not a major factor in the present model’s response to SST anomalies. An attempt to unify these two viewpoints -- “response” and “reorganization” -- can be made by hypothesizing that under certain circumstances SST forcing is able to organize low-frequency variability much more effectively than in the present simulations. For example, the need for many early modeling studies to specify unrealistically large SST anomalies (“superanomalies”) of up to 8 K in order to produce a realistic barotropic “response” might have been due to the need to force the model into a regime where efficient reorganization of the natural variability could take place, and not due to poor model physics as was commonly supposed.

In a realistic GCM with zonal asymmetry the geographic location of the SST anom-

1. The general consistency in the sign of the atmospheric “response” from run to run both among the small ensemble of runs performed by Palmer and Sun(1988) and from study to study, leads me to discount the possibilty that the batotropic structure is the result of sampling error.

aly might also effect its ability to organize natural atmospheric variability. In a zonally symmetric model the geographic regions of greatest atmospheric low-frequency dynamical variability (measured by, say, 250 mb lowpass filtered streamfunction variance) will also have the greatest SST variance. However, in the real midlatitudes, there can be large SST anomalies off the east coasts of continents due to advection across the strong temperature gradient formed by land-ocean contrast. Palmer and Sun (1985), for example, chose to specify a SST anomaly based on observations of a large anomaly off the coast of Newfoundland. This region is upstream from the region of largest atmospheric low-frequency variance in the North Atlantic. Presumably the North American continent was the source of cold air which was responsible for the generation of this SST anomalies to begin with. In that sense, zonal asymmetries in the surface properties of the Earth can force large SST anomalies in regions of relatively low atmospheric variability. The “response”, or “reorganization” of variability may be much larger than to SST anomalies formed in regions of high atmospheric variance.

SST variability in the eastern North Pacific Ocean is probably more akin to the present model than is North Atlantic variability. The basic patterns of SST variability are formed in a region of high atmospheric variability (though advection of cold air from Alaska and Canada can sometimes play an important role as in the North Atlantic). ENSO forcing plays a major role in the low-frequency variability of North Pacific SST. Given N.-C. Lau’s preliminary result described in Chapter 1 that a midlatitude slab mixed-layer model resulted in a strongly favored polarity of the PNA pattern in the atmosphere, it seems reasonable to hypothesize that a “selective enhancement” mechanism helps determine the North Pacific response to ENSO forcing.

5.5 Summary

A simple thermodynamic argument explains the increased variance in the COUPLED run. The “selective enhancement through reduced damping” mechanism gives a plausible explanation for the persistence and propagation effects seen in this study. However, it would be desirable to find a more detailed mechanism that describes the way in which the natural atmospheric variability couples to SST anomalies, and to investigate the relative role of high frequency transient eddies and low frequency circulation circulation anomalies.

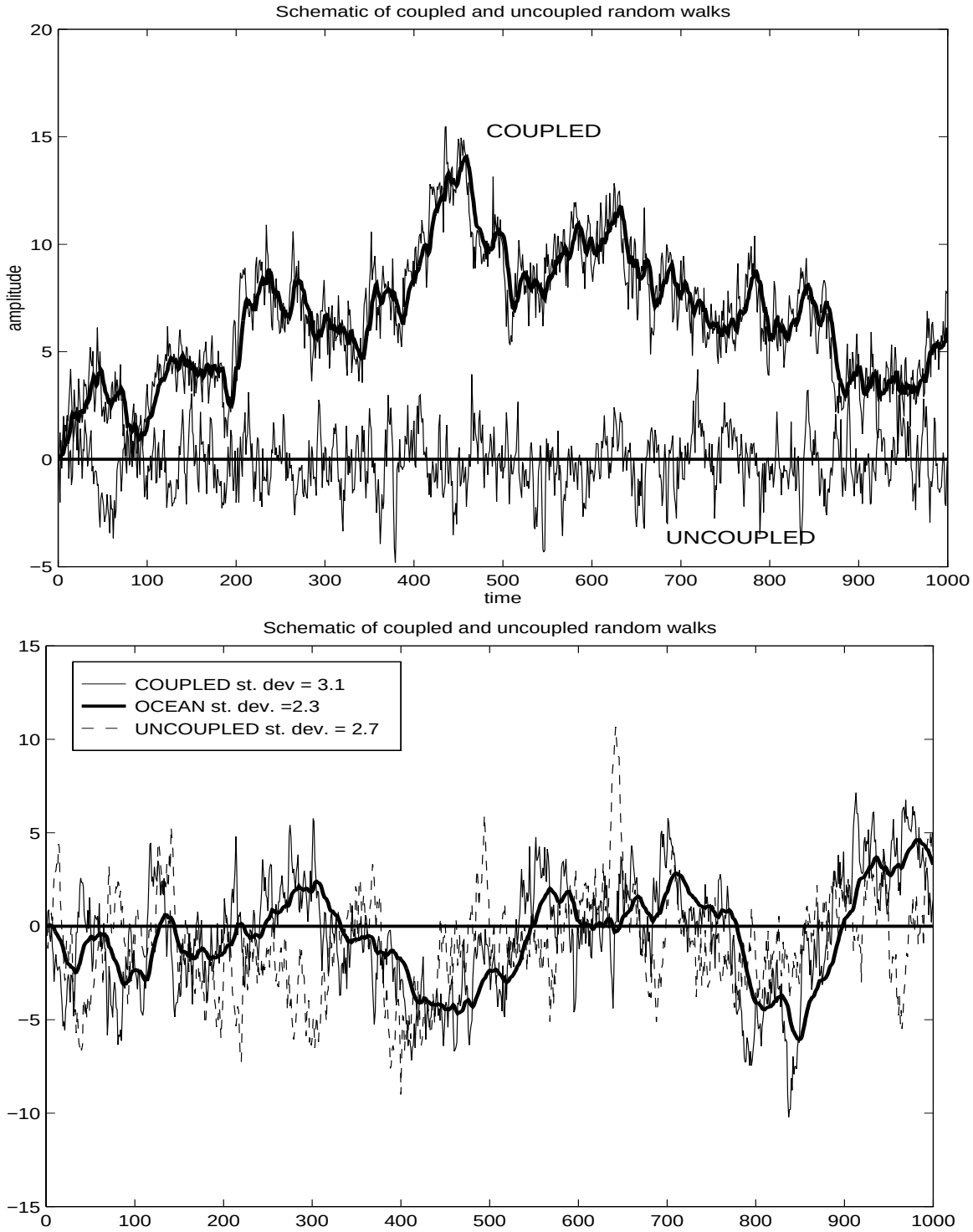

Figure 5.1. Coupled and uncoupled random walks. a) large separation between slow and fast variance, b) small separation between slow and fast variance. Standard deviations are shown in legend.

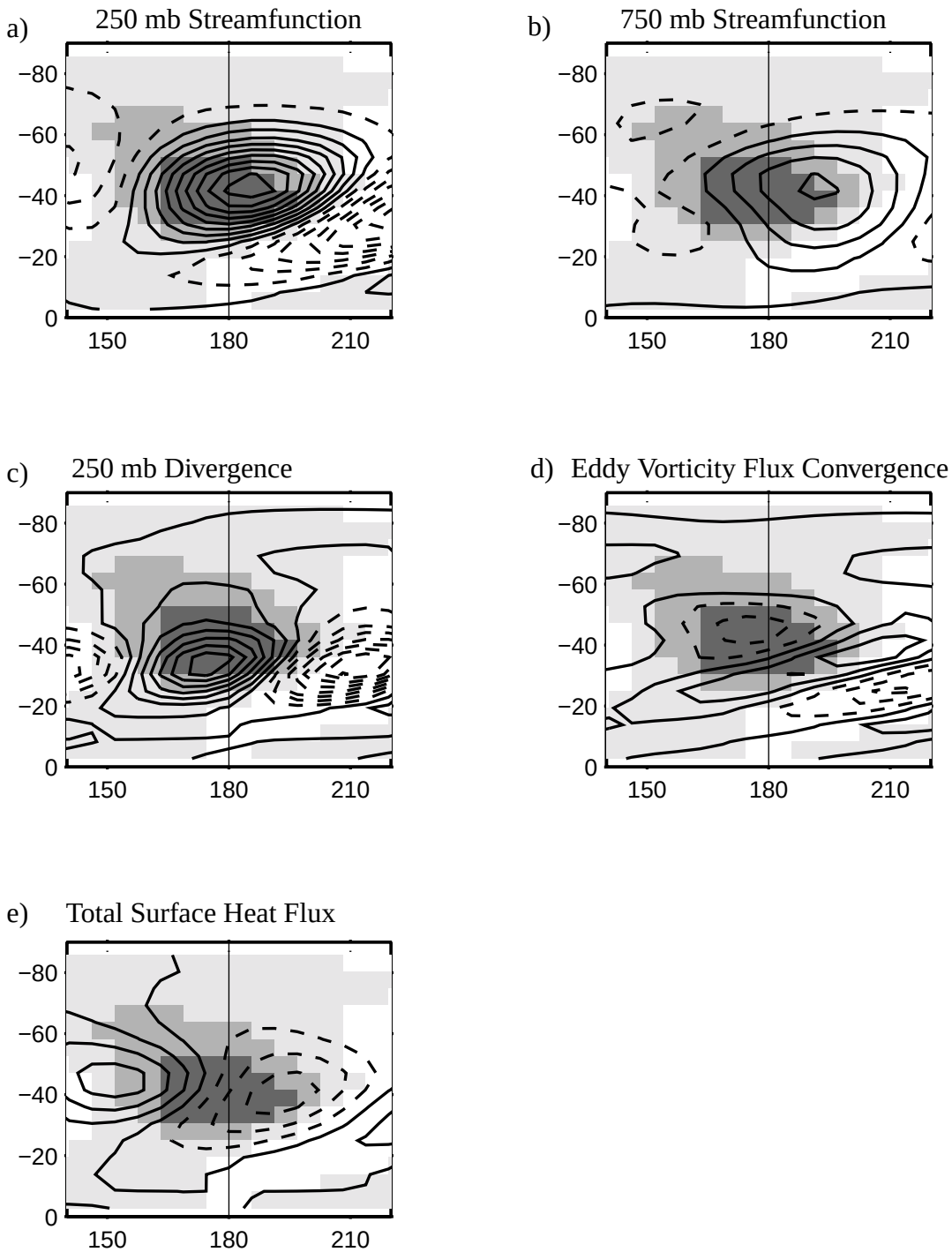

Figure 5.2. COUPLED run simultaneous regression against normalized Southern Hemisphere SST index. Close-up in region of maximum SST anomaly. a) 250 mb streamfunction; b) 750 mb streamfunction; c) 250 mb divergence; d) 250 mb eddy vorticity flux convergence; e) total surface heat flux. Units are as in unzoomed lag regression maps for the same variables (Figs. 4.22, 4.23, 4.24, 4.27, and 4.18 respectively).

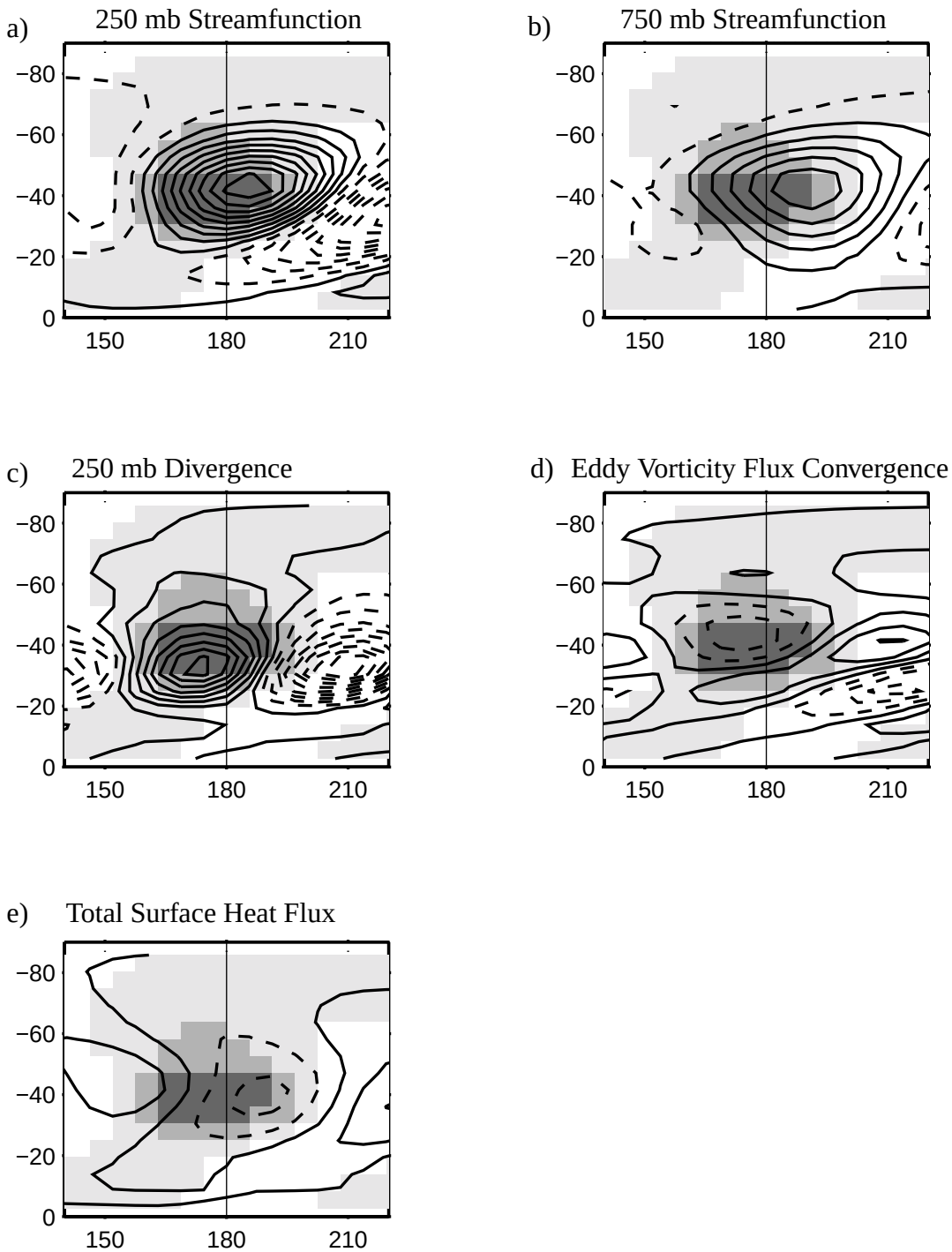

Figure 5.3. UNCOUPLED run simultaneous regression against normalized Southern Hemisphere SST index . Close-up in region of maximum SST anomaly. Units are as in Fig. 5.2

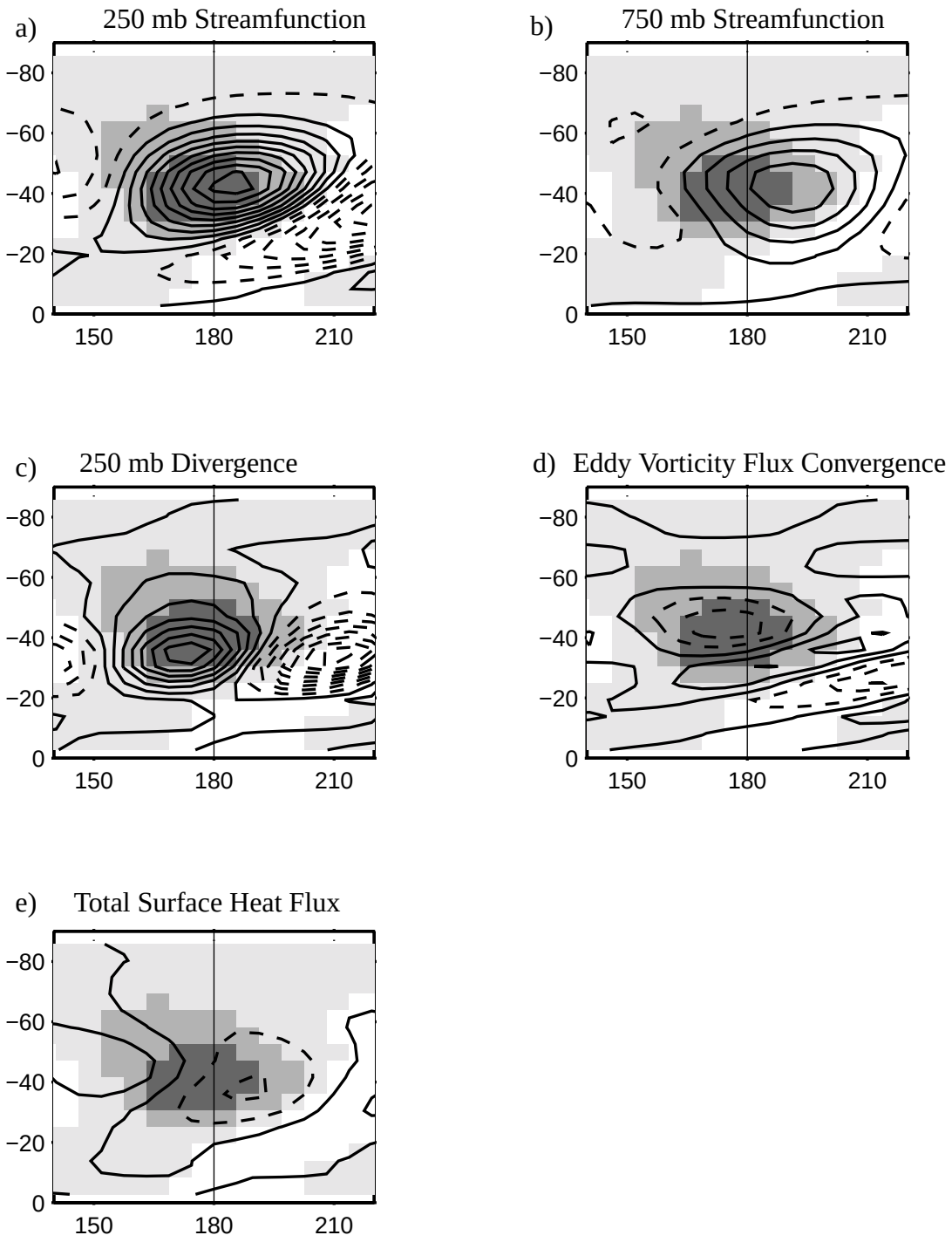

Figure 5.4. MOGA run simultaneous regression against normalized Southern Hemisphere SST index from MOGA diagnostic ocean. Close-up in region of maximum SST anomaly. Units are as in Fig 5.2.

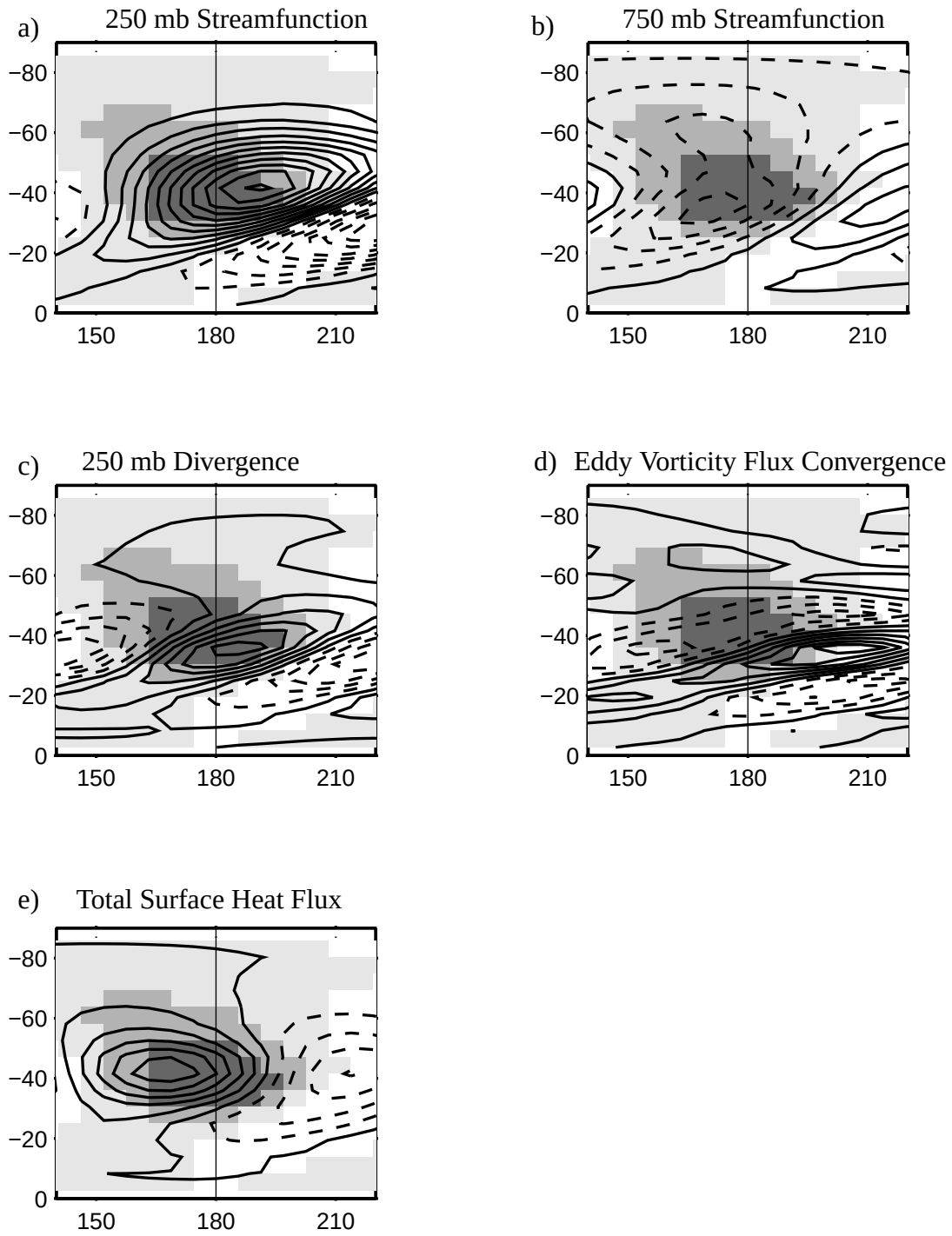

Figure 5.5. MOGA RESPONSE run simultaneous regression against normalized Southern Hemisphere SST index from COUPLED run. Close-up in region of maximum SST anomaly. Units are as in unzoomed lag regression maps for the same variables (Fig 4.34, 4.35, 4.38, 4.39, and 4.21 respectively).

Chapter 6: Variance and Coupling in a Stochastically Forced Energy Balance Model

6.1 Introduction

The previous chapters analyzed the low frequency variability in a two-level atmospheric General Circulation Model (GCM) with zonally symmetric boundary conditions coupled to a 50 meter deep mixed-layer ocean. The coupled model run was compared with an uncoupled atmosphere run where the sea surface temperature (SST) was prescribed to be the zonal mean of the climatology from the coupled run. I refer to this as the UNCOUPLED run. These two runs were compared to at third in which SST was prescribed to be the time-dependent SST field from the coupled run. In reference to similar experiments done by Lau (1994), I refer to this as the MOGA (Midlatitude Ocean, Global Atmosphere) run. A mixed layer ocean model was forced in diagnostic mode with the atmospheric temperatures and winds from the uncoupled and MOGA runs in order to produce SST fields for comparison with the coupled model SST. A more detailed description of these model runs is given in Chapters 3-5. A schematic illustration of the coupling in these runs is shown in figure 3.1.

One of the most striking features of these model runs is the strong enhancement of variance in the ocean due to coupling. This difference occurs mainly for time scales longer than the mixed-layer time scale, which is approximately 4 months. As shown in chapter 4, this enhancement occurs throughout the midlatitudes and for all zonal wavenumbers where there is significant SST variance (wavenumbers less than 7). There is a corresponding enhancement of atmospheric temperature variance at those time scales.

The strength and robustness of the above result leads one to speculate: Can a general principle be formulated that relates coupling to low frequency variance in an atmospheric GCM coupled to dynamically passive ocean? This chapter is directed at answering that question. I begin with a qualitative explanation which centers on the role of thermal damping. I then briefly summarize some work by others in stochastic modeling and then describe and analyze a new stochastically forced energy balance model that captures the essence of the effect of coupling on low frequency variance. In addition to explaining some results from Chapter 4, the stochastic model also provides a simple quantitative framework for understanding coupling in more complicated models where one system is dynamically passive. This understanding is especially relevant to current climate modeling research, as the coupled, uncoupled, and MOGA experimental designs are in common use.

6.2 Coupling, Damping, and Variance: A Qualitative Explanation

I begin with a qualitative argument that centers on the role of thermal damping in coupled models. First I relate coupling and the nature of the atmosphere-ocean boundary condition to thermal damping. Consider an atmospheric GCM coupled to a slab mixed-layer ocean of constant depth h. The value of h determines the nature of the lower boundary condition on the atmospheric thermodynamic equation. In the extreme case of $h \to 0$ we have instantaneous surface energy balance (SEB) as lower boundary condition of the atmosphere. In the 2-level atmosphere model used in chapters 3-5, this is nearly equivalent to specifying a constant heat flux from the surface into the lower layer, independent of the state of the atmosphere. This is because the downward shortwave flux in this model is nearly constant, and the latent heat flux is released locally. Therefore, atmospheric temperature anomalies are not damped by surface fluxes. The other extreme, $h \to \infty$, corre-

sponds to fixed SST. Atmospheric temperature anomalies of all frequencies are damped equally by surface fluxes. This case should exhibit the most damping due to surface fluxes when integrated over all frequencies, assuming that fluxes behave linearly for the frequency range of interest. For h finite, for example $h = 50$ meters, the coupling acts to damp only high frequency atmospheric temperature anomalies. For frequencies lower than the time scale associated with the mixed layer the SST can adjust to atmospheric temperature anomalies and the surface fluxes are reduced to near zero.

The general principle I propose is that, all else being equal, lower damping corresponds to higher variance. If this is true we expect that the fixed SST case will have the least variance, the coupled finite depth mixed-layer case more variance, and the SEB case the most variance. Consider the following thermodynamic argument. Start with the assumption that low frequency variability in the atmosphere is due to dynamical effects alone (e.g. geostrophic turbulence) and drives the system in a random walk about the long-term climatology. This drift away from the mean is balanced by thermal damping. The heat fluxes between atmosphere and ocean provide considerably faster damping than the radiative damping of the system to space. If we fix SST, the atmosphere temperature is strongly constrained by SST, and so will the temperature of a diagnostic ocean model driven by this atmosphere. However if we let the SST change, the whole system is allowed to drift further from climatology, due to the weaker damping.

Where does the MOGA run fit in to this scheme? It is important to note that because the slab mixed layer ocean is strictly linear, the dynamics of the atmosphere is the only source for low frequency variability in the coupled model. In the MOGA runs however, the prescribed SST are an additional external source of low frequency variability, so we can be confident that the MOGA run will have more variance than the uncoupled run with

its fixed, zonally symmetric SST. The MOGA atmosphere will respond to the prescribed SST anomalies, but it seems reasonable to assume that the bulk of the nonlinear atmospheric variability will be uncorrelated with the prescribed SST anomalies, at least for the modest SST anomalies (1-2K) in these simulations. Thus it is reasonable to expect that the variance in the MOGA atmosphere temperature to be less than that in the coupled atmosphere. The evidence from Chapter 4 indicates that the MOGA runs have significantly less variance that the coupled runs, so that the assumption that the bulk of atmospheric variability is uncorrelated with SST is supported.

In situations where the ocean is dynamically active the above argument, and the stochastic model I will present, are not applicable. In regions of very active ocean dynamics such as the tropical Pacific Ocean and the oceanic western boundary currents, or at extremely long time scales involving the thermohaline circulation, the ocean strongly forces the atmosphere, and coupling may produce instabilities.

A complication arises even for a passive ocean, as the mixed-layer depth $h \to 0$. As $h \to 0$ the time scale of the mixed layer becomes comparable or shorter than the synoptic time scale. Since baroclinic conversion is the ultimate source of much of variability in the model, the entire spectrum will be affected. Since I wish to avoid consideration of the effect of lower boundary conditions on baroclinic waves, I will not discuss the SEB case. Here I will chose the other extreme, $h \to \infty$ (the “uncoupled” run, with fixed SST) as the basis for comparison with the other runs.

6.3 Some Previous Results with Stochastic Models of Atmosphere-Ocean Interaction

Frankignoul (1985) reviews some of the work on stochastic modeling of atmosphere-ocean interaction in midlatitudes up to that time. Since the model I will formulate

in the next section is an extension of the models presented there, I will summarize some results shown in that paper. In this section the notation follows Frankignoul (1985), and differs somewhat from the notation in the rest of this chapter.

Frankignoul and Hasselmann (1979) considered the simplest stochastic model of SST variability, $\frac{dT}{dt} = F - \lambda T$, where F represents mixed-layer forcing anomalies, T the ocean temperature, and λ a feedback parameter. They assume F to be white at the frequencies of interest, yielding a red spectrum for T. The fit to spectra from data in the northern Pacific Ocean is quite good, at least away from dynamically active regions. They are also able to derive the correlation between forcing and SST, denoted R_{FT}, which is shown as curve *c* in figure 6.1. R_{FT} is strongly asymmetric in lag, with the correlation peaking when the atmosphere leads the ocean by about one month. The correlation is negligible for the ocean leading the atmosphere.

In a short note, Gill (1979) pointed out that the observed forcing already includes the effects of feedback. Frankignoul and Reynolds(1983) took this into account by specifying that some of the feedback be grouped with the stochastic forcing term. They define a new "known" forcing term $H' = q' - \lambda_a T'$, where q' represents a portion of the total stochastic forcing, and λ_a a portion of the feedback. They then calculate the lag-correlation between the "known" forcing and the SST, $R_{HT} = R_{qT} - \lambda_a R_{TT}$, which shows a more antisymmetric shape for typical parameter values. I would like to note here that this follows from their definition of H'. For the parameters they use, $R_{qT} \sim R_{FT}$ and $R_{TT} \sim e^{-\lambda|\tau|}$, and one is essentially subtracting a symmetric function peaked at the origin from the "uncorrected" lag-correlation. This changes the shape of the lag-correlation function to make it more anti-symmetric for positive values of λ_a (negative feedback). Plots of these

quantities can be found in Frankignoul(1985) and are reproduced in figure 6.1, curves a, b, and d.

I approach the problem differently. Rather than focusing only on oceanic variance and partitioning the variance and feedback terms, I create a stochastically forced *coupled* model.The model is shown schematicaly in figure 6.2. Instead of specifying the forcing of the oceanic as the stochastic variable as in Frankignoul and Hasselmann (1977), I let the dynamical forcing of the free atmosphere temperature be the stochastic variable. Therefore the feedback due to surface heat fluxes will be built in to the model. In addition, I will be able to consider feedback due to the atmospheric *dynamical* response to SST anomalies, albeit in a very approximate manner. The coupled stochastic model can be easily modified to represent the coupled, uncoupled and MOGA experimental designs presented in Chapter 3.

A similar system of coupled equations to Eq. 6.1, though without stochastic forcing, has been used by Sausen and Lunkeit (1990) to investigate climate drift. North and his colleagues have used various stochastically forced energy balance models, including a one-dimensional surface energy balance model coupled to a deep ocean. Kim and North (1991) also contains a list of some more recent references. Recently I have become aware of the work of Zubarev and Demchenko (1992). They investigated the predictability in a stochastic model almost identical to the one used here, however lacking the dynamical feedback term which I introduce. Their results support the notion that the uncoupled random walk of the atmosphere, and in their case of the ocean as well, are modified through coupling. However, their results are extremely sensitive in the parameter range which they claim corresponds to the Earth’s climate.

6.4 A Simple Stochastically Forced Energy Balance Model of Coupled Variability

The purpose of this stochastic model is heuristic: to interpret the modeling results from Chapters 3-5 in a simple framework. We start with the following equations which represent the perturbation energy balance at a given point on earth:

$$\begin{aligned} \gamma_a \frac{d\tilde{T}_a}{dt} &= \gamma_a \tilde{f} - (c_a + \lambda)(\tilde{T}_a - \tilde{T}_o) - \lambda_a \tilde{T}_a, \\ \gamma_o \frac{d\tilde{T}_o}{dt} &= (c_o + \lambda)(\tilde{T}_a - \tilde{T}_o) - \lambda_o \tilde{T}_o \ . \end{aligned} \qquad \text{(EQ 6.1)}$$

Subscripts "*a*" and "*o*" refer to atmosphere and ocean respectively. T is the temperature, γ the heat capacity, λ (no subscripts) the linearized coefficient from a bulk aerodynamic formulation of combined latent and sensible heat flux, c the portion of the longwave flux proportional to the air-sea temperature difference, and λ_a, λ_o the radiative damping of each component to space. f represents the dynamical component of the forcing, which we take to be the stochastic variable. We then take the Fourier transform of Eq. 6.1 ($t \rightarrow \omega$). divide through by $\lambda + c_a$ to yield:

$$\begin{aligned} i\sigma T_a &= F(\omega) - (T_a - T_o) - aT_a \\ i\sigma\beta T_o &= (T_a - T_o) - bT_o \end{aligned} \qquad \text{(EQ 6.2)}$$

We have made the following substitutions: $a = \lambda_a/(\lambda + c_a)$, $b = \lambda_o/(\lambda + c_o)$, $\beta = (\gamma_o/\gamma_a)((\lambda + c_a)/(\lambda + c_o))$, $\sigma = \gamma_a\omega/(\lambda + c_a)$,$F = \gamma_a f/(\lambda + c_a)$. In this chapter a tilde denotes a time-domain variable, and an unadorned variable the Fourier transform variable. In addition explicit reference to the independent variable t or σ will be used to avoid confusion. A derivation of Eq. 6.1 from a more detailed energy balance model is presented in Appendix C, where reasonable values of these parameters are also justified. These parameter values, shown in Table 6.1, will be referred to as the "standard

parameters".

Equation 2 can be rewritten as follows:

$$\begin{aligned} \sigma_a T_a &= F + T_o, \\ \sigma_o T_o &= T_a, \end{aligned} \qquad \text{(EQ 6.3)}$$

where $\sigma_a = (i\sigma + 1 + a)$, and $\sigma_o = (i\beta\sigma + 1 + b)$. Equations 6.3 as they stand are not suitable for comparing coupled and uncoupled systems. This is because the dynamical forcing term F includes the effects of coupling and will differ between coupled and uncoupled runs. To see this more clearly I calculate the power spectrum of T_a in response to the forcing F. From Equation 6.3 we have

$$|\sigma_a|^2 |T_a|^2 = |F|^2 + |T_o|^2 + F T_o^* + T_o F^*, \qquad \text{(EQ 6.4)}$$

where * represents complex conjugation. Note that $F T_o^*$ is just the Fourier transform of the lag-covariance function between F and T_o. From equation 6.4 we see that there are two contributions by SST anomalies to atmospheric variance: the direct effect of the SST anomaly and the indirect effect due to the lag-covariance between F and T_o.

In the analysis that follows it will be useful to split the forcing into two parts, $F = N + L$, where L is the direct low frequency response to SST anomalies and N is the natural low frequency variability inherent to the atmosphere. I will assume that the direct response is proportional to the SST anomaly at the low frequencies of interest, so that $L(\sigma) = \alpha T_o(\sigma)$, where α is a real constant. With these assumptions about atmospheric response, Eq. 6.3 :

$$\boxed{\begin{aligned} \sigma_a T_a &= N + (1 + \alpha) T_o, \\ \sigma_o T_o &= T_a. \end{aligned}} \qquad \text{(EQ 6.5)}$$

which is the form which will be used for the rest of the calculations in this chapter.

I expect the dynamical response to act as a negative feedback, with atmospheric heat fluxes partially offsetting the diabatic effects of a SST anomaly. That is, I expect that $-1 < \alpha < 0$.

Equations 6.5 can be used to model the coupled, uncoupled and MOGA experiments described in chapter 3 as follows. The "coupled" model (denoted by superscript C) solves equations 6.5 as a coupled set. Therefore, given N one can solve for T_a^C and T_o^C. For the "uncoupled" model, denoted by superscript U, I set $T_o = 0$ in the first equation of 6.5. Given N one can solve for T_a^U. The second equation in 6.5 then becomes the diagnostic equation for a "slave" ocean driven by the uncoupled atmosphere, from which we get T_o^U. Finally, to model the MOGA experiment (denoted by superscript M) I set $T_o = T_o^C$ in the atmosphere equation, and assume that N and T_o^C are uncorrelated. That is, the SST which forces the atmosphere is prescribed to be the SST from a coupled run, but natural variability of the atmosphere, N, is assumed to be unaffected by SST anomalies. This latter assumption will simplify the calculation of power spectra for the MOGA model. As in the "uncoupled" case, the MOGA atmosphere is used to force a "slave" mixed-layer ocean.

The quantities $N(\sigma)$ and α represent the distillation of complicated atmospheric dynamics and deserve further comment. The spectrum of the stochastic forcing, $|N(\sigma)|^2$, can be estimated directly from the uncoupled run of the 2-level model. In this run the SST is specified to be zonally symmetric and constant in time, so that the response to SST anomalies, $L(\sigma)$, is identically zero. In bridging the gap between the 2-level model and the stochastic model one needs to choose an appropriate measure of the free atmospheric temperature. I choose the vertical mean potential temperature in the 2-level model, interpreted as the 500 mb potential temperature to be the quantity which corresponds to the stochastic model's T_a. That is, I let $(1/2)^{\kappa/c_p}\bar{\theta} \leftrightarrow T_a$. From Eq. 2.2d and the definition of

F found below equation 6.2 we get the following expression for the estimate of stochastic forcing:

$$N_{est}(t) = F^{U}_{est}(t) = -\frac{\gamma_a}{\lambda + c_a}(1/2)^{\kappa/c_p}\nabla\bullet(\bar{\theta}\bar{\underset{\sim}{V}} + \hat{\theta}\hat{\underset{\sim}{V}}) \quad . \qquad \text{(EQ 6.6)}$$

The power spectrum of N_{est} from the UNCOUPLED run of chapters 3-5 is shown in figure 6.3 for selected latitudes. To calculate this spectrum, the 2-level model variables $\bar{\theta}$, $\bar{\underset{\sim}{V}}$, $\hat{\theta}$, and $\hat{\underset{\sim}{V}}$ were sampled daily from the 6000 day "uncoupled" run described in chapter 3. An estimate of the spectrum at each gridpoint was computed using overlapping 2000 day Hanning windows in the time domain with 1000 day overlap. Spectral estimates at each of the gridpoints around a latitude circle were then averaged to produce the averaged spectrum shown in figure 6.3. The power declines at higher frequencies, but does not appear to go to zero. The blueness of the spectrum is the result of the quadratic nonlinearity in the temperature advection terms. This forcing spectrum, when integrated in time and subjected to the damping processes in the atmosphere, leads to a red spectrum for atmospheric temperature. I have also estimated N using the total heat capacity of the 2-level atmosphere (which is proportional to $T_1 + T_2$) along with the corresponding dynamical forcing. the resulting estimates are very similar to those shown here. For simplicity, in some of the analytic calculations in this chapter I will assume N to be white noise of unit amplitude.

The dynamical response parameter, α, is not so simple to interpret. At present I have no formal derivation. Keep in mind that α is an estimate for the dynamical response in an averaged sense over the midlatitudes. We do not want to capture the mere reorganization of variance. Therefore α probably does not represent the covariance between local SST and atmospheric dynamical fluxes, as SST and fluxes are nearly in quadrature. In

addition it is probably not the correlation between surface fluxes and the atmospheric dynamical fluxes either, as these have to be nearly in balance. The best way to clarify the interpretation of α in future work will probably involve building a two-dimensional stochastic model, as suggested in chapter 7. For the purposes of the analytic calculations which follow I will take $\alpha = -0.5$.

6.5 Power in the Coupled, Uncoupled, and MOGA Models

As noted above, the stochastic model can be used to interpret the COUPLED, UNCOUPLED, and MOGA experiments of Chapter 3. The stochastic model allows us to predict from a simple model how coupling affects variance (power) in the three runs. In the coupled run (superscript C) we solve the coupled set in equation 6.5 for the power spectrum:

$$\left|T_a^C\right|^2 = \frac{\left|\sigma_o\right|^2 |N|^2}{\left|\sigma_a\sigma_o - (1+\alpha)\right|^2}$$
$$\left|T_o^C\right|^2 = \frac{|N|^2}{\left|\sigma_a\sigma_o - (1+\alpha)\right|^2} \qquad \text{(EQ 6.7)}$$

For the uncoupled (superscript U) run I set $T_o = 0$ in the atmosphere equation to calculate the power spectrum for T_a^U. I then calculate the “slave” ocean power T_o^U from the diagnostic ocean equation. In that case we get for the power spectrum:

$$\left|T_a^U\right|^2 = \frac{|N|^2}{\left|\sigma_a\right|^2} ,$$
$$\left|T_o^U\right|^2 = \frac{|N|^2}{\left|\sigma_a\sigma_o\right|^2} . \qquad \text{(EQ 6.8)}$$

For the MOGA run (superscript M) we set $T_o = T_o^C$ in the atmosphere equation, and

assume that N and T_o^C are uncorrelated. Thus, when we calculate the power spectrum of T_a^M the cross-terms between N and T_o^C are zero. As in the "uncoupled" case, the MOGA atmosphere is used to force a "slave" mixed-layer ocean. The power spectrum of the MOGA case is as follows:

$$\left|T_a^M\right|^2 = \frac{|N|^2}{\left|\sigma_a\right|^2}\left(1 + \frac{|1+\alpha|^2}{\left|\sigma_a\sigma_o - (1+\alpha)\right|^2}\right)$$
$$\left|T_o^M\right|^2 = \frac{|N|^2}{\left|\sigma_a\sigma_o\right|^2}\left(1 + \frac{|1+\alpha|^2}{\left|\sigma_a\sigma_o - (1+\alpha)\right|^2}\right) . \qquad \text{(EQ 6.9)}$$

Plots of these quantities are shown in Figure 6.4 for N assumed to be white noise with unit amplitude, for the standard parameters. Note that in this case, the uncoupled atmosphere variance is pure "red-noise". We are now in a position to draw some general conclusions about variance in coupled and uncoupled runs. The variance in the MOGA run can be expressed in terms of the variance in the coupled and uncoupled runs as follows:

$$\left|T_o^M\right|^2 = \left|T_o^U\right|^2\left(1 + \frac{|1+\alpha|^2}{\left|\sigma_a\sigma_o - (1+\alpha)\right|^2}\right)$$
$$= \left|T_o^C\right|^2\frac{\left|\sigma_a\sigma_o - (1+\alpha)\right|^2 + |1+\alpha|^2}{\left|\sigma_a\sigma_o\right|^2} \qquad \text{(EQ 6.10)}$$

Note that we haven't assumed anything about the shape of the spectrum of the forcing term N. We can see that at all frequencies, the both the coupled and MOGA runs have more variance than the uncoupled run, at least for reasonable values of α. The comparison of the MOGA and coupled runs is more complicated. For low frequencies, $\beta\sigma^2 < (1+a)(1+b)$, the Coupled variance exceeds the MOGA variance. For high frequencies, the direct forcing by the SST anomalies exceeds the internal variance. However, due to the long time scales associated with the ocean there is little power at these

higher frequencies.

It is instructive to consider the ratio of variance between the different models in the limit as $\sigma \to 0$ (or equivalently, $\omega \to 0$). Note that this ratio is the same for the atmosphere and ocean variables, so I have dropped the subscripts in the following equation.

$$\delta^{C,U} = \frac{|T^C|^2}{|T^U|^2} = \frac{z_0^2}{(z_0 - 1)^2}$$
$$\delta^{M,U} = \frac{|T^M|^2}{|T^U|^2} = 1 + \frac{1}{(z_0 - 1)^2}, \qquad \text{(EQ 6.11)}$$
$$\delta^{C,M} = \frac{|T^C|^2}{|T^M|^2} = \frac{z_0^2}{(z_0 - 1)^2 + 1}$$

where $z_0 = (1 + a)(1 + b)/(1 + \alpha)$. The ratio of power at a given frequency depends only on the parameter z_0, the product of the atmospheric and oceanic damping coefficients divided by the dynamical feedback. A plot of these power ratios as a function of z_0 is shown in figure 6.5. The standard parameters correspond to $z_0 = 2.56$, and is indicated by a vertical line in the plot. Large z_0 corresponds to either large damping or large negative atmospheric feedback. In this case the MOGA variance approaches the uncoupled variance, while the coupled variance approaches the uncoupled variance much more slowly. In the limit as $z_0 \to 1$, which is off the scale of figure 6.5, we see that the coupled and MOGA variance becomes the same, and both become infinite. This limit corresponds to the unrealistic case where positive atmospheric feedback counteracts damping. Even in the case where we allow no atmospheric feedback, $\alpha = 0$, so that $z_0 = 1.25$ for the standard parameters, we get excessively large ratios between coupled and uncoupled runs. The balance in the model ocean at low frequencies is essentially between a “random walk” forced by the atmospheric variance and radiative damping. Because the damping in this

model is rather small the ocean temperatures are allowed to drift very far before damping can balance the drift.

The differing effect of coupling on the atmosphere and ocean can be seen if we take the integral over all frequencies to get the total power. For white noise forcing of unit amplitude, the indefinite integrals of the quantities in equations 6.8, 6.9, and 6.10 can be performed via a partial fraction decomposition. Ideally we would like to prescribe some upper cutoff in our integration at high frequencies. However if one is willing to approximate the total variance by integrating over all frequencies from $0 \rightarrow \infty$, then it is simpler to consider these definite integrals as being in the complex plane and to evaluate them by summing over the residues at the poles of the integrand in the upper half-plane. The results for the uncoupled case are the simplest (see for example, CRC Math Tables):

$$\begin{aligned} \int_0^\infty \left|T_a^U\right|^2 d\sigma &= \frac{\pi|N|^2}{2\tilde{a}} \\ \int_0^\infty \left|T_o^U\right|^2 d\sigma &= \frac{\pi|N|^2}{2\tilde{a}\tilde{b}(\tilde{a}+\tilde{b})} \end{aligned} \qquad \text{(EQ 6.12)}$$

where $\tilde{a} = 1 + a, \tilde{b} = (1 + b)/\beta$. The integrals for the coupled variance are more tedious. If we perform the definite integral first and then expand the result in the small parameter $1/\beta$, keeping only the leading order, we get:

$$\Delta_a^{C,U} = \frac{\int_0^\infty \left|T_a^C\right|^2 d\sigma}{\int_0^\infty \left|T_a^U\right|^2 d\sigma} = \left(1 + \frac{1}{z_0}\frac{\tilde{b}}{\tilde{a}}\right)$$

$$\Delta_o^{C,U} = \frac{\int_0^\infty \left|T_o^C\right|^2 d\sigma}{\int_0^\infty \left|T_o^U\right|^2 d\sigma} = \left(1 + \frac{1}{z_0}\right) \qquad \text{(EQ 6.13)}$$

where z_0 is as before. $\Delta_o^{C,U}$ has been plotted on figure 6.6. For the standard parameters, $\Delta_a^{C,U} = 1.02$ and $\Delta_o^{C,U} = 1.40$. Because the bulk of atmospheric variability lies in higher frequencies where coupling has little effect, the ratio of coupled to uncoupled total variance is near unity. On the other hand, the bulk of model oceanic variance is at low frequencies where the effect of coupling is strong, so the ratio is substantial. This reflects what happens in the 2-level model, as the atmospheric variance is only slightly effected by coupling, but the oceanic variance is substantially increased by coupling. I have not analyzed the MOGA runs here, as the math is more tedious and one can see by visual inspection of the power spectra that the total MOGA variance will lie between the coupled and uncoupled cases for the parameters used here. We can use equation 6.14 to estimate z_0 and hence α directly from the ratio of SST variance between the coupled and uncoupled runs. In this case we would estimate that $\alpha = -0.56$.

6.6 A Note About MOGA Runs

The comparison between the coupled and MOGA runs is especially intriguing. Suppose we look at the coupled run from the somewhat artificial perspective that it is simply another MOGA run, but with very special atmospheric initial conditions. That is, I could

create a MOGA run which exactly reproduces the coupled run as follows. Prescribe the SST to be that from the history file of a coupled run. Prescribe the atmospheric initial conditions to be identical to the initial conditions of the coupled run. The slave SST forced by the atmosphere will be identical to the coupled SST. This leads to a question: Can we find a general principle which distinguishes the "coupled" initial condition from all other initial conditions? For example, does the "coupled" initial condition maximize variance in the slave ocean compared to all other initial conditions?

Phrased another way, does a sufficiently long coupled run produce more variability than MOGA runs with all other possible atmospheric initial conditions? If one accepts the assumptions of the stochastic model, then the answer is yes (for all reasonable parameters), as indicated by the variance ratio in equation 6.11. This would indicate that for small amplitude SST anomalies and zonally homogeneous lower boundary conditions such a condition is likely to hold in a full atmospheric GCM coupled to a slab mixed layer model. I suspect that under these assumptions it *may* be possible to make a much stronger proof directly from the equations of motion. However, large amplitude SST anomalies may violate the assumption of the linearity of the atmospheric response. Zonal asymmetries, the presence of orographically forced waves and the effects of strong tropical-extratropical interaction complicate matters greatly in more realistic models and in the real world.

6.7 Summary

The coupled stochastic model is able to qualitatively reproduce the ratio of total variance between COUPLED, MOGA, and UNCOUPLED runs. The spectra are also qualitatively reproduced without much tuning of the model. The results point out that the reduction of thermal damping and thereby leads to an increase in the variance of the sys-

tem. These results with the simple stochastic model are consistent with the conclusion from chapter 5 that coupling is able to enhance variance by reducing thermal damping.

Table 6.1: Standard Parameter for Stochastic Model

Parameter	Value	Parameter	Value
c_a	3.9 W m^{-2} K^{-1}	γ_a	1×10^{7} J m^{-2} K^{-1}
c_o	3.4 W m^{-2} K^{-1}	γ_o	1×10^{8} J m^{-2} K^{-1}
λ_a	2.8 W m^{-2} K^{-1}	β	20.5
λ_o	1.9 W m^{-2} K^{-1}	a	.15
λ	20 W m^{-2} K^{-1}	b	.10

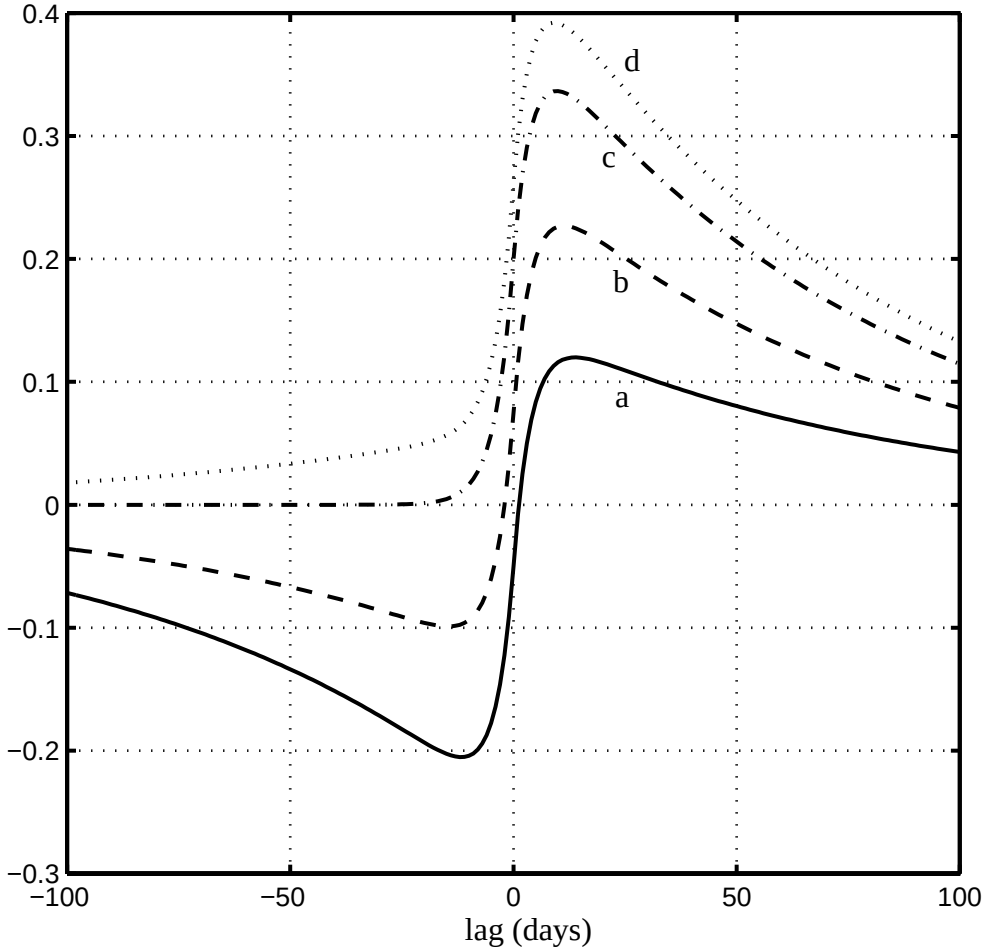

Figure 6.1. Predicted lag-correlation for stochastic SST equation with simple atmospheric feedback, as in figure 21 of Frankignoul (1985). Strong negative atmospheric feedback (curve a), weaker negative atmospheric feedback (curve b), no atmospheric feedback (curve c), and weak positive atmospheric feedback (curve d). Parameters are the same as in Frankignoul's figure except for the inclusion here of the "no feedback" case.

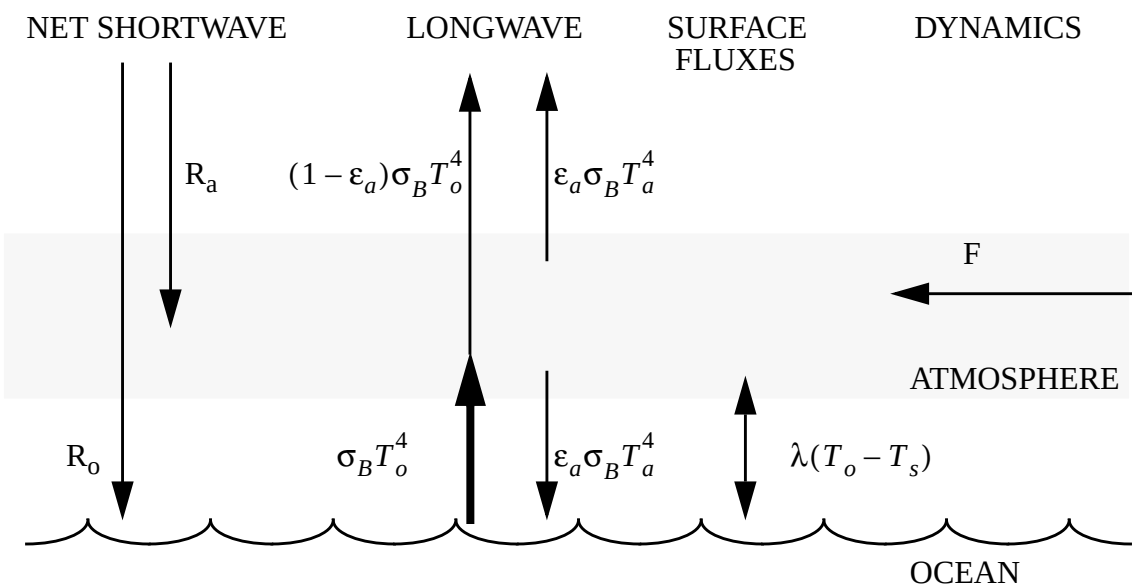

Figure 6.2. Diagram of simple energy balance model on which Equations 6.1 are based. See Appendix Cfor definition of symbols.

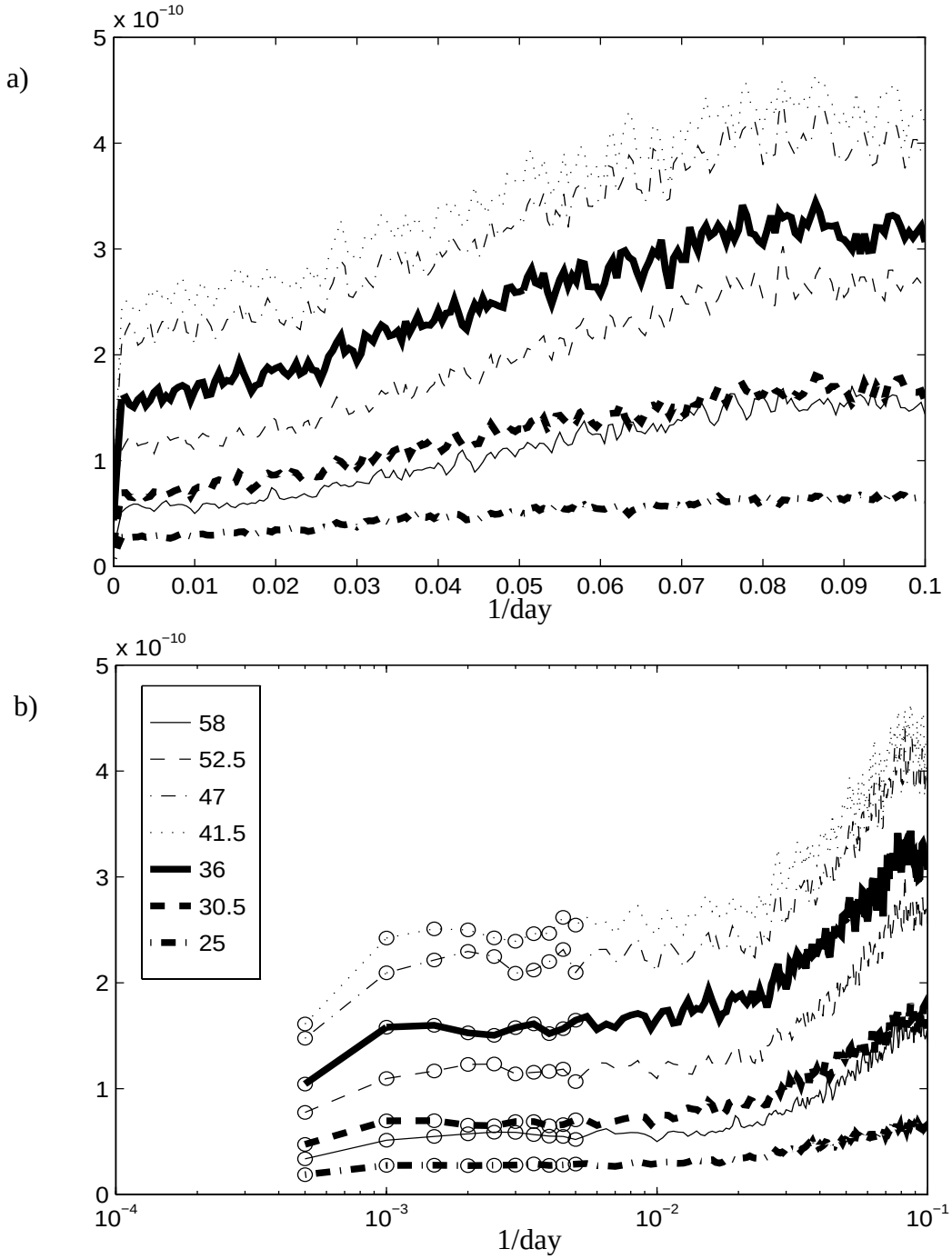

Figure 6.3. Averaged power spectrum of advective forcing term $\nabla\bullet(\bar{\underset{\sim}{v}}\bar{\theta} + \hat{\underset{\sim}{v}}\hat{\theta})$ in UNCOUPLED run at various latitudes. a) linear frequency scale, b) logarithmic frequency scale. Spectrum shown in both plots is the average power at all gridpoints along a latitude circle in both hemispheres for the latitudes indicated in the legend in figure b. In b, the ten lowest frequencies are highlighted by circles. The lowest frequency estimate is strongly affected by averaging inherent in use of a window.

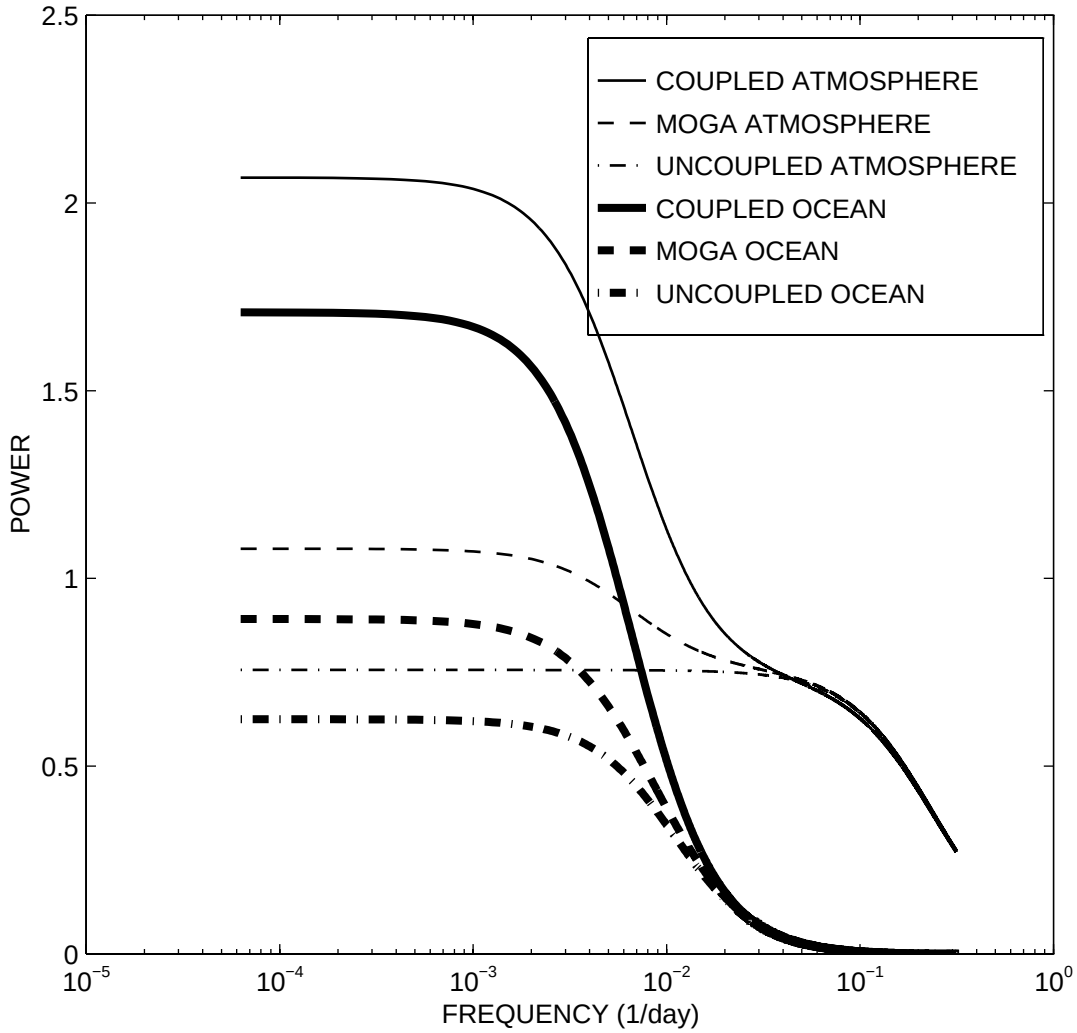

Figure 6.4. Stochastic model power spectra for white noise forcing with unit amplitude. The feedback parameter α = -0.5.

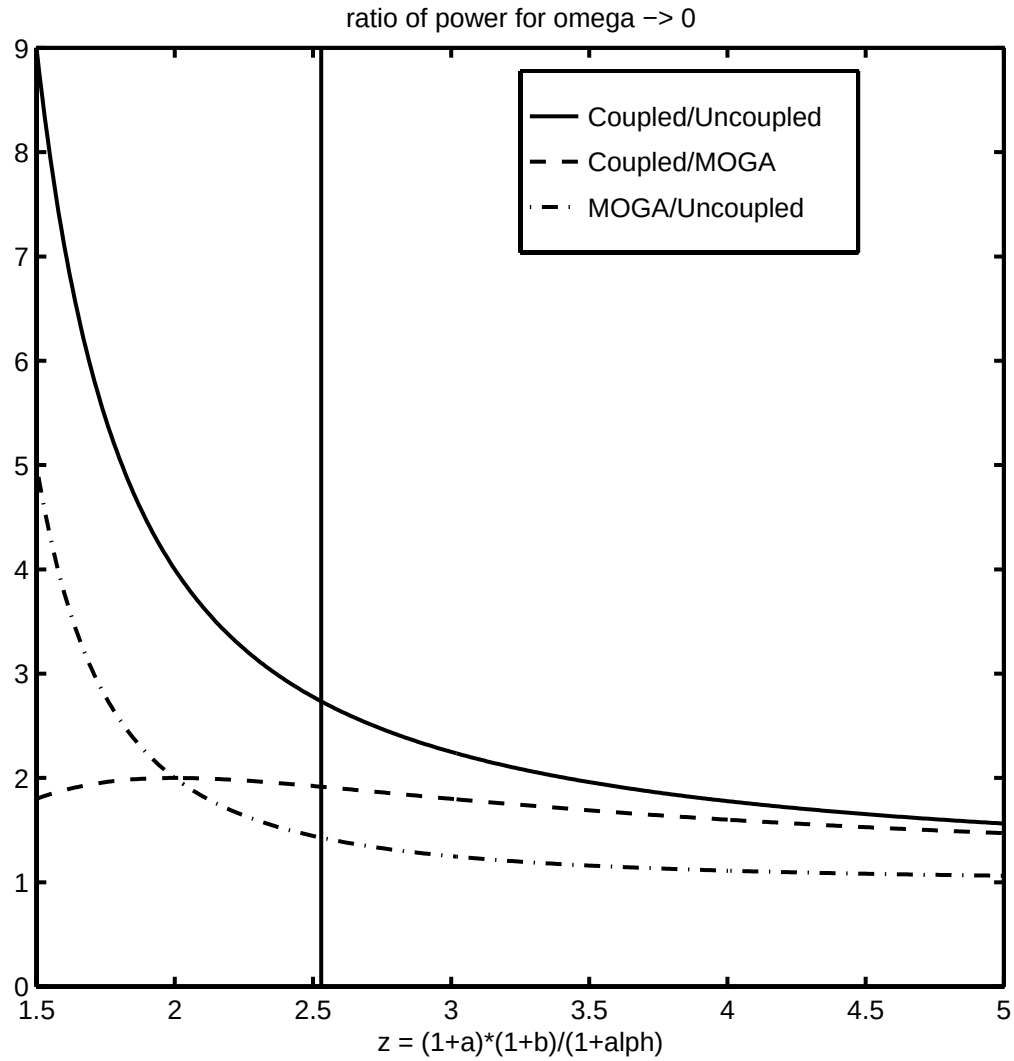

Figure 6.5. Ratio of power in ocean temperature between COUPLED and UNCOUPLED (solid line), COUPLED and MOGA (dashed line), and MOGA and UNCOUPLED (dash-dot line) in the limit as the frequency ω approaches zero. The thick vertical line at $z_0 = 2.53$ indicates the standard parameters discussed in the text.

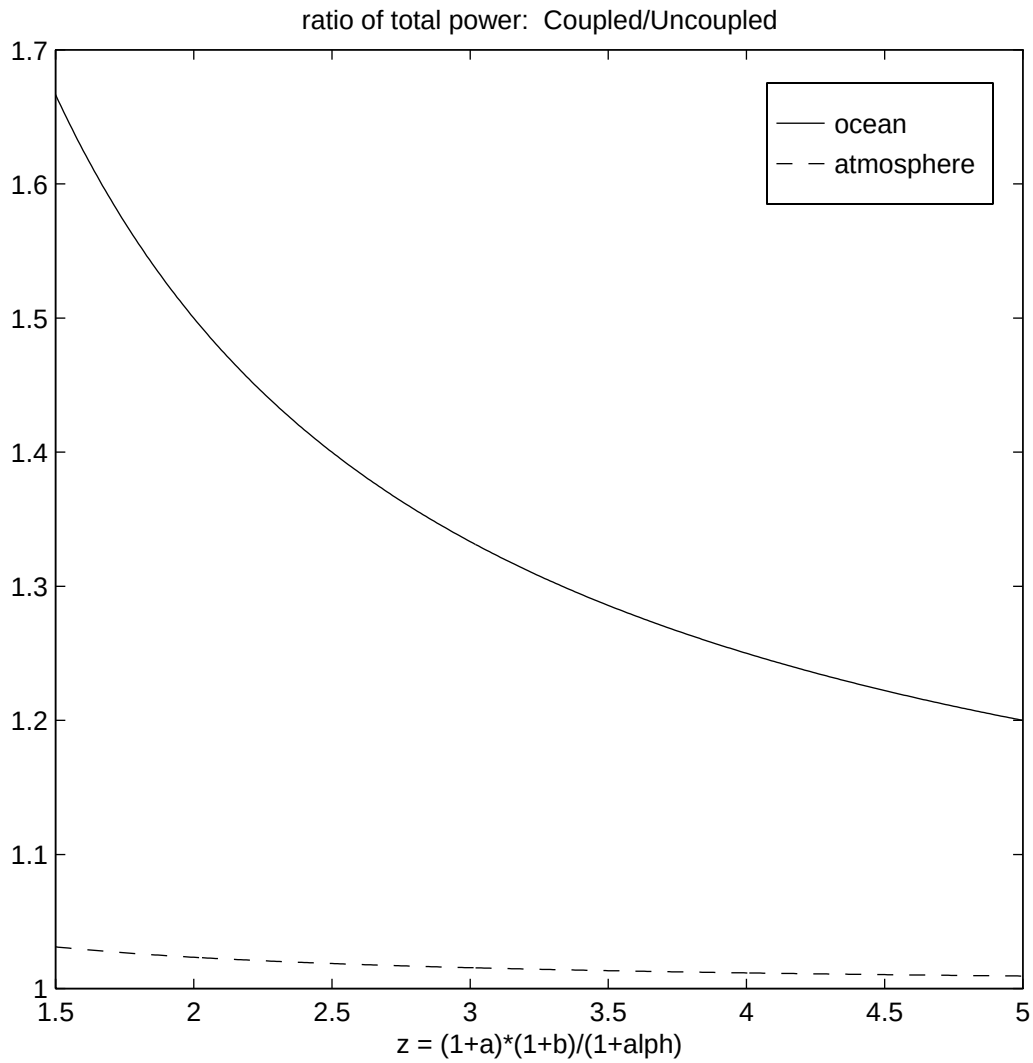

Figure 6.6. Ratio of total power between COUPLED and UNCOUPLED runs. Ocean Temperature (solid line), atmospheric temeprature(dashed line).

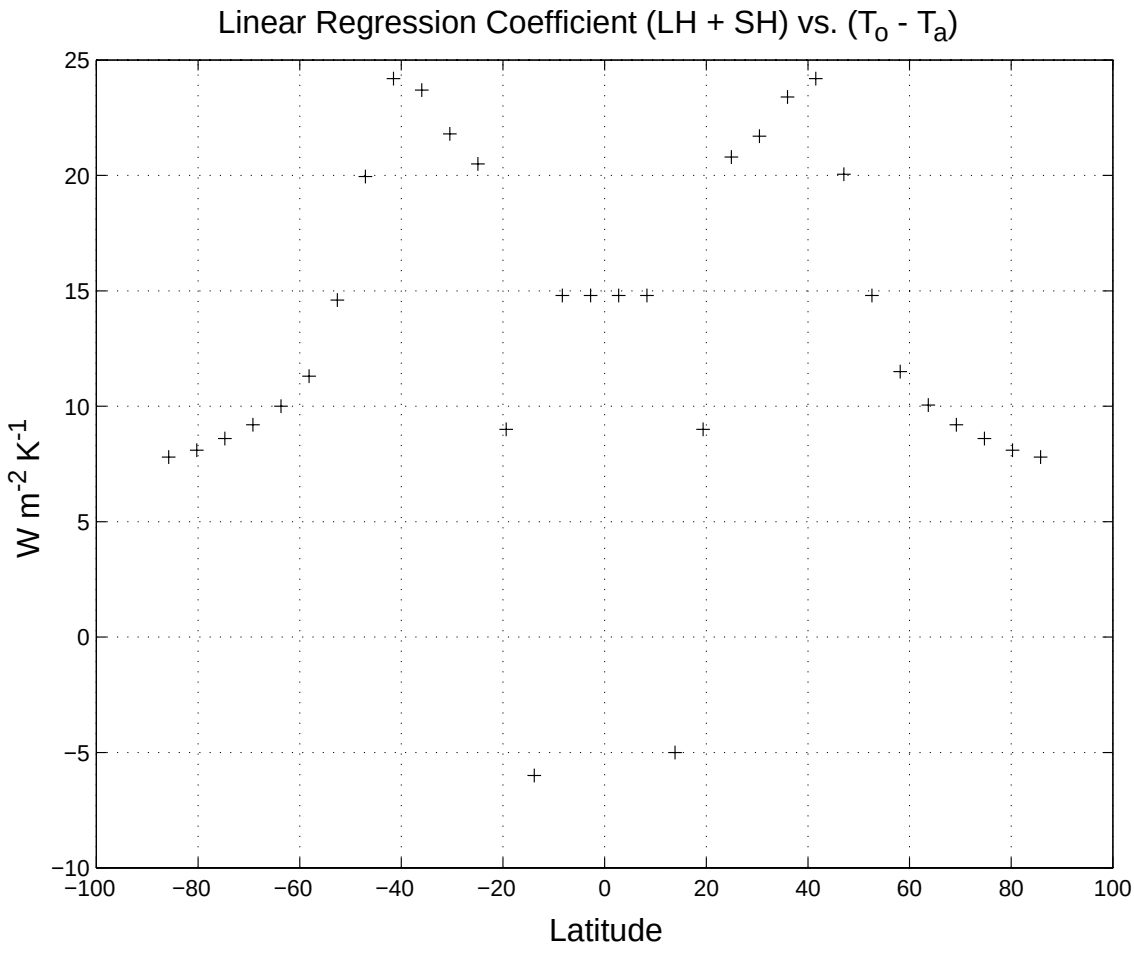

Figure 6.7. Linear regression coefficient as a function of latitude for regression of latent plus sensible surface heat flux vs. ocean-atmosphere temperature difference.

Chapter 7. Conclusion

7.1 Summary of Main Results

We have shown that in this model coupling qualitatively changes low-frequency variability even though the direct response of the model to SST anomalies is small. The main effects of coupling are an increase the variance in SST, atmospheric temperature, and baroclinic streamfunction, an increase in SST anomaly persistence, and a preference for eastward propagation. We have also shown that coupling has an effect on the atmosphere above and beyond the effect of direct forcing by the SST anomalies. The mechanism for all these phenomena is the selective enhancement of the components of natural uncoupled atmospheric variability that project strongly onto structures that are very similar to linear coupled modes. These preferred structures are distinguished by their decreased damping relative to other possible structures. The role of coupling in reducing thermal damping is paramount, and is well illustrated by the one-dimensional stochastically forced energy-balance model of chapter 6. In addition there appears to be a reduction in frictional damping associated with the thermal coupling that also contributes to the enhancement of low-frequency variability. Though the above results were found in an all-ocean model, the mechanism of selective enhancement is so basic that these phenomena are likely to be found, in one form or another, in more realistic GCMs, and possibly in nature as well.

7.2 Implications

Many present-day climate models include at least a slab mixed-layer ocean model in order to be able to model long term trends in globally averaged temperature. While the effect on the model climatology has long been understood, it is not clear whether the effect that a slab mixed-layer can have on low-frequency variability is well appreciated, and this

effect has not been investigated in depth. However, many coupled models use flux correction schemes in order to prevent climate drift. The effects of flux correction on the phenomena presented in this thesis has not been investigated.

Shorter-term climate variability studies are often performed with prescribed SSTs. In such studies, the introduction of simple slab mixed-layer, possibly with flux correction, would probably be a simple, cost-effective improvement, particularly for studies of interannual and intraseasonal variability. More sophisticated, prognostic-depth mixed-layer models such as described by Gaspar (1988) would be suitable for inclusion in models with a seasonal cycle, and would also be cost-effective.

Another significant modelling question regards the interpretation of MOGA-type numerical experiments. We can say with certainty that the direct forcing of the atmosphere by the ocean does not represent the entire midlatitude contribution from the ocean in the present modeling studies. The small response seen in MOGA experiments such as in Lau and Nath (1994) is not an indication of the unimportance of the midlatitude oceans. However, MOGA-type experiments may be more appropriate in limited geographic regions where midlatitude SST anomalies are forced rapidly by processes which are external to those considered in the present study, such as in the lee of continents in winter or in places where rapid mixed-layer entrainment causes rapid cooling. It remains to be seen whether the results demonstrated in this study extend to more realistic simulations including a seasonal cycle, climatological stationary waves, land-ocean contrast, or a prognostic-depth mixed layer.

7.3 Further Work

I feel the most promising avenues of research suggested by this study are the follow-

ing. First, to determine in more detail the mechanism for selective enhancement at work in this model, in particular regarding the relative role of high-frequency eddies vs. low-frequency nonlinear dynamics in providing feedback in coupling the barotropic and baroclinic circulations. Second, to investigate whether the selective enhancement mechanism operates similarly to the way it does in the present model in wintertime situations with an equatorially asymmetric climatology or for a model configuration with an orographically or thermographically forced zonally asymmetric climate. Third, to construct a two-dimensional stochastically-forced, coupled linear model.

7.4 Conclusion

Common views of midlatitude atmosphere-ocean interaction look at the two halves of the interaction separately. The forcing of the ocean by the atmosphere is rather straightforward. The forcing of the atmosphere by SST anomalies is less clear-cut. This thesis argues for adopting an alternate view of the midlatitude system: the stochastically forced coupled linear system. In more general terms it suggests that the variability associated with SST anomalies may be seen as a reorganization of the natural midlatitude variability. The efficiency of this reorganization may depend on many factors in the real world or in more realistic simulations.

Finally this dissertation also demonstrates the difficulty, even in numerical modeling studies, of unambiguously separating forcing from response in nonlinear systems. This is a complex problem, and no one viewpoint will serve all purposes or describe all regimes. The hope here is to stimulate thought and suggest the possibility of a more unified approach to the interpretation of atmosphere-ocean interaction in the midlatitudes.

BIBLIOGRAPHY

Alexander, M. A., 1990: Simulation of the response of the North Pacific Ocean to the anomalous atmospheric circulation associated with El Niño. *Climate Dyn.*, **5**. 53-65.

Alexander, M. A., 1992a: Midlatitude atmosphere-ocean interaction during El Niño. Part I: The North Pacific Ocean. *J. Climate.*, **5**, 944-958.

Alexander, M. A., 1992b: Midlatitude atmosphere-ocean interaction during El Niño. Part II: The northern hemisphere atmosphere. *J. Climate.*, **5**, 959-972.

Beyer, W. H., Ed., 1984: *CRC Standard Mathematical Tables, 27th Edition*. Akron, Ohio. 615 pp.

Chervin, R. M., W. M. Washington, and S. H. Schneider, 1976: Testing the statistical significance of the response of the NCAR general circulation model to North Pacific Ocean surface temperature anomalies. *J. Atmos. Sci.*, **33**, 413-423.

Davis, R. E., 1976: Predictability of sea surface temperature and sea level pressure anomalies over the North Pacific Ocean. *J. Phys. Oceanogr.*, **6**, 249-266.

Durran, D. R., 1991: The third-order Adams-Bashforth method: An attractive alternative to leapfrog time differencing. *Mon. Wea. Rev.*, **119**, 702-720.

Esbensen, S. K., and Y. Kushnir, 1981: *The Heat Budget of the Global Ocean: An Atlas B.ased on Estimates from Surface Marine Observations*. Climatic Research Institute, Corvallis, Oregon, Report No. 29, 27 pp.

Egger, J., 1977: On the linear theory of the atmospheric response to sea surface temperature anomalies. *J. Atmos. Sci.*, **34**, 603-614.

Frankignoul, C., 1985: Sea surface temperature anomalies, planetary waves, and air-sea feedback in the middle latitudes. *Rev. Geophys.*, **23**, 357-390.

Frankignoul, C., and K. Hasselmann, 1977: Stochastic climate models. Part 2. Application to sea-surface temperature anomalies and thermocline variability. *Tellus*, **29**, 284-305.

Frankignoul, C., and R. W. Reynolds, 1983: Testing a dynamical model for mid-latitude sea surface temperature anomalies. *J. Phys. Oceanogr.*, **13**, 1131-1145.

Gaspar, P., 1988: Modeling the seasonal cycle of the upper ocean. *J. Phys. Oceanogr.*, **18**, 161-180.

Gill, A. E., 1979: Comments on stochastic models of climate variability. *Dyn. Atmos. Oceans,***3**, 481-483.

Haney, R. L., 1985: Midlatitude sea surface temperature anomalies: a numerical hindcast. *J. Phys. Oceanogr.*, **15**, 787-799.

Hasselmann, K., 1976: Stochastic climate models, I, Theory. *Tellus*, **28**, 473-485.

Held, I. M., 1983: Stationary and quasi-stationary eddies in the extratropical troposphere: theory. *Large Scale Dynamical Processes in the Atmosphere*, B. J. Hoskins and R. P. Pearce, Eds, Academic Press, New York, 127-168.

Held, I. M., and M. J. Suarez, 1978: A two-level primitive equation atmospheric model designed for climatic sensitivity experiments. *J. Atmos. Sci.*, **35**, 206-229.

Held, I. M., D. I. Linder, and M. J. Suarez, 1981: Albedo feedback, the meridional structure of the effective heat diffusivity, and climatic sensitivity: Results from dynamic and diffusive models. *J. Atmos. Sci.*, **38**, 1911-1927.

Hendon, H. H., and D. L. Hartmann, 1982: Stationary waves on a sphere: Sensitivity to thermal feedback. *J. Atmos. Sci.*, **39**, 1906-1920.

Hendon, H. H., and D. L. Hartmann, 1985: Variability in a nonlinear model of the atmosphere with zonally symmetric forcing. *J. Atmos. Sci.*, **42**, 2783-2797.

Hoskins, B. J., and D. J. Karoly, 1981: The steady linear response of a spherical atmosphere to thermal and orographic forcing. *J. Atmos. Sci.*, **38**, 1179-1196.

Kim, K. -Y., and G. R. North, 1991: Surface temperature fluctuations in a stochastic climate model. *J. Geophys. Res.*, **96**, 18,573-18,580.

Kim, K. -Y., and G. R. North, 1992: Seasonal cycle and second-moment statistics of a simple coupled climate system. *J. Geophys. Res.*, **97**, 20,437-20,448.

Kim, K. -Y., G. R. North, and J. Huang, 1992: On the transient response of a simple coupled climate system. *J. Geophys. Res.*, **97**, 10,069-10,081.

Kushnir, Y., and N. -C. Lau, 1992: The general circulation model response to a North Pacific SST anomaly: Dependence on time scale and pattern polarity. *J. Climate*, **5**, 271-283.

Lau, N. -C., and M. J. Nath, 1990: A general circulation model study of the atmospheric response to extratropical SST anomalies observed in 1950-79. *J. Climate.*, **3**, 965-989.

Lau, N. -C., and M. J. Nath, 1994: A modeling study of the relative roles of tropical and extratropical SST anomalies in the variability of the global atmosphere-ocean system. *J. Climate*, **7**, 1184-1207.

Lindzen, R. S., and A. Y. Hou, 1988: Hadley circulations for zonaly averaged heating centered off the equator. *J. Atmos. Sci.*, **45**, 2417-2427.

Luksch, U., H. v. Storch, and E. Maier-Reimer, 1989: *Modeling North Pacific SST Anomalies as a Response to Anomalous Atmospheric Forcing*. Max Planck-Institut für Meterologie, Hamburg, Report No. 37, 31 pp.

MacKay, R. M., and M. A. K. Khalil, 1991: Theory and development of a one dimensional time dependent radiative convective climate model. *Chemosphere*, **22**, 383-417.

Manabe, S., and R. F. Strickler, 1964: Thermal equilibrium of the atmosphere with a convective adjustment. *J. Atmos. Sci.*, **21**, 361-385.

Manabe, S., and R. Wetherald, 1967: Thermal equilibrium of the atmosphere with a given distribution of relative humidity. *J. Atmos. Sci.*, **24**, 241-259.

Manabe, S., J. Smagorinsky, and R. F. Strickler, 1965: Simulated climatology of a general circulation model with a hydrologic cycle. *Mon. Wea. Rev.*, **93**, 769-798.

Miller, A. J., 1992: Large-scale ocean-atmosphere interactions in a simplified coupled model of the midlatitude wintertime circulation. *J. Atmos. Sci.*, **49**, 273-286.

Miller, A. J., and J. O. Roads, 1990: A simplified coupled model of extended-range predictability. *J. Climate.*, **3**, 523-542.

Mitsudera, H., and F. Grimshaw, 1994: Capture and resonant forcing of solitary waves by the interaction of a baroclinic current with topography. *J. Phys. Oceanogr.*, **24**, 2217-2244.

Palmer, T. N., and Z. Sun, 1985: A modelling and observational study of the relationship between sea surface temperature in the north-west Atlantic and the atmospheric general circulation. *Quart. J. Roy. Met. Soc.*, **111**, 947-975.

Phillips, T. J., 1982: On the interaction of surface heating anomalies with zonally symmetric and asymmetric atmospheric flows. *J. Atmos. Sci.*, **39**, 1953-1971.

Phillips, T. J., 1992: An application of a simple coupled ocean-atmosphere model to the study of seasonal climate prediction. *J. Climate*, **5**, 1078-1095.

Pitcher, E. J., M. L. Blackmon, G. T. Bates, and S. Munoz, 1988: The effects of North Pacific sea surface temperature anomalies on the January climate of a general circulation model. *J. Atmos. Sci.*, **45**, 173-188.

Qin, J., and W. A. Robinson, 1992: Barotropic dynamics of interactions between synoptic and low-frequency eddies. *J. Atmos. Sci.*, **49**, 71-79.

Roads, J. O., 1989: Linear and nonlinear responses to middle latitude surface temperature anomalies. *J. Climate.*, **2**, 1014-1046.

Robinson, W. A., 1991a: The dynamics of low-frequency variability in a simple model of the global atmosphere. *J. Atmos. Sci.*, **48**, 429-441.

Robinson, W. A., 1991b: The dynamics of the zonal index in a simple model of the atmosphere. *Tellus*, **43A**, 295-305.

Rodgers, C. D., and C. D. Walshaw, 1966: The computation of infrared cooling rates in planetary atmospheres. *Quart. J. Roy. Meteor. Soc.*, **92**, 67-92.

Salmon, R., and M. C. Henderschott, 1976: Large-scale air-sea interactions with a simple general circulation model. *Tellus.*, **28**, 228-242.

Sausen, R., and F. Lunkeit, 1990: Some remarks on the cause of the climate drift of coupled ocean-atmosphere models. *Beitr. Phys. Atmosph.*, **63**, 141-146.

Schneider, K. K., and J. L. Kinter III, 1994: An examination of internally generated variability in long climate simulations. *Climate Dyn.*, **10**, 181-204.

Semtner, A. J., 1984: Development of efficient, dynamical ocean-atmosphere models for climatic studies. *J. Climate Appl. Meteor.*, **23**, 353-374.

Wallace, J. M., and M. L. Blackmon, 1983: Observations of low-frequency atmospheric variability. *Large Scale Dynamical Processes in the Atmosphere*, B. J. Hoskins and R. P. Pearce, Eds, Academic Press, New York, 55-94.

Wallace, J. M., and Z. Jiang, 1987: On the observed structure of the interannual variability of the atmosphere/ocean climate system. *Atmospheric and oceanic variability,* H. Cattle, Ed., Roy. Meteor. Soc., Bracknell, Berkshire, 17-43.

Wallace, J. M., C. Smith, and Q. Jiang, 1990: Spatial patterns of atmosphere-ocean interaction in the northern winter. *J. Climate*, **3**, 990-998.

Williamson, D. L., J. T. Kiehl, V. Ramanathan, R. E. Dickinson, and J. J. Hack, 1987: *Description of NCAR Community Climate Model (CCM1)*. NCAR Technical Note NCAR/TN-285+STR, Boulder, Colorado, 112 pp.

Yu, J-Y., and D. L. Hartmann, 1993: Zonal flow vacillation and eddy forcing in a simple GCM of the atmosphere. *J. Atmos. Sci.*, **50**, 3244-3259.

Zubarev, A. P., and P. F. Demchenko, 1992: Predictability of the average global air temperature in a simple stochastic atmosphere-ocean interaction model. *Izv. Atmos. Oc. Phys.*, **28**, 19-23.

Appendix A: Persistence Algorithm

In order to quantify persistence of sea surface temperature (SST) anomalies I have adopted the following method. First, a time-longitude section of the pentad-mean SST anomaly data is contoured at a level of one standard deviation above the mean. That is, only one contour level is drawn. An “event” is then defined to correspond to a single closed contour. For each unbroken contour line, the contour plotting routine in the numerical mathematics package MATLAB conveniently returns the coordinates of its constituent line segments in units of longitude and time. The durations of events, defined as the maximum time minus minimum time, are then computed and ranked in descending order of duration. (Note that for different purposes, contour width or area could also be used in place of duration). The process can be repeated using a contour value of one standard deviation below the mean.

The cyclic boundary condition in the zonal direction leads to a complication in making an accurate identification of closed contours. Contours that intersect the right or left edges of the plot and continue on the other side of the plot should be counted as a single contour. Contours that cross one of these edges (but which do not wrap around more than once) are accounted for correctly by first contouring augmented data which wraps around the globe twice in the zonal direction, and then throwing out the duplicate contours and any contours which intersect the left and right edges. Contours that intersect the top or bottom edges are closed along that edge. To quantify persistence, the contour durations are then binned and can be shown in a histogram of contour duration. Alternatively, a plot of the cumulative sum (or cumulative fraction) of event duration as a function of the rank of the anomaly produces a smoother function to display.

This procedure has yet to be subjected to a detailed sensitivity analysis. The proce-

dure is obviously sensitive to the choice of contour level used to define an event. For example, a long-lasting coherent feature will in general be split into several shorter segments if a larger contour level is chosen. In addition since we are looking only at a zonal slice, a localized SST anomaly that moves to the north or south may be seen as several shorter anomalies, or may be lost track of altogether. This latter effect is minimized for the current data by using the SSTA index, which is averaged over several latitudes, and because SST variability largely confined to the midlatitudes.

Appendix B: Budgets Using Linear Regression

In the course of this study I have used one-point linear regression maps extensively. The purpose of this section is to describe how to compute a consistent budget of a quadratically nonlinear equation using the same technique. For this example I will use a simplified equation of motion representing an advection term, as follows:

$$\frac{\partial q}{\partial t} = -vq_y. \qquad \text{(EQ B.1)}$$

Time means of a scalar variable x are denoted by an overbar, $\bar{x}$, and anomalies by a prime, x'. Zonal means are denoted by square brackets, $[x]$, and anomalies by an asterisk, x^*. I will also introduce an additional symbol, $\tilde{x} = \overline{z'x'}$, which is the linear regression of x with a time series $z(t)$ which has zero mean and unit variance. In this study, $z(t)$ is chosen to be the SST anomaly time series at a given grid point.

First we construct the regressed budget for time mean quantities by expanding the variables in Eq. B.1 in terms of time means and anomalies, and then regressing against z:

$$\widetilde{\frac{\partial}{\partial t}q'} = \frac{1}{T}\int_0^T z(t)\frac{\partial}{\partial t}q'dt = \overline{q_y}\tilde{v} + \bar{v}\tilde{q}_y + \widetilde{v'q'}_y. \qquad \text{(EQ B.2)}$$

The left hand side of this equation is problematic. Using integration by parts it can be written:

$$\frac{1}{T}\int_0^T z(t)\frac{\partial}{\partial t}q'dt = \frac{1}{T}(z'q')\Big|_0^T - \frac{1}{T}\int_0^T q(t)\frac{d}{dt}z'dt. \qquad \text{(EQ B.3)}$$

The first term on the RHS is presumed to be small for long time series. When a slowly varying quantity such as SST anomaly is chosen as “z”, then it is presumed that the second term is small as well, so that the budget essentially adds up to zero. These terms can be evaluated explicitly if desired as a check on the exactness of the balance.

If we expand all quantities in Eq. B.2 in terms of zonal means and anomalies we can construct an eddy budget for the regressed variable:

$$\widetilde{\frac{\partial q'}{\partial t}}^{*} = \bar{q}_y^{*}[\tilde{v}] + [\bar{q}_y]\tilde{v}^{*} + (\bar{q}_y^{*}\tilde{v}^{*})^{*} + \bar{v}^{*}[\tilde{q}_y] + [\bar{v}]\tilde{q}_y^{*} + (\bar{v}^{*}\tilde{q}_y^{*})^{*} + (\widetilde{v'q'_y})^{*} \quad . \qquad \text{(EQ B.4)}$$

For a long integration with zonally symmetric boundary conditions, the stationary wave terms should be negligible, reducing the budget to:

$$\widetilde{\frac{\partial q'}{\partial t}}^{*} = [\bar{q}_y]\tilde{v}^{*} + [\bar{v}]\tilde{q}_y^{*} + (\widetilde{v'q'_y})^{*} \quad . \qquad \text{(EQ B.5)}$$

If we wish, we can expand the final term on the RHS of Eq. B.5 into zonal mean and zonally asymmetric contributions:

$$\widetilde{(v'q'_y)}^{*} = \widetilde{[v']q'_y}^{*} + \widetilde{v'^{*}[q'_y]} + (\widetilde{v'^{*}q'^{*}_y})^{*} \quad . \qquad \text{(EQ B.6)}$$

Appendix C: Derivation of the Energy Balance Model

We wish to bridge the gap between the heuristic model presented in Equation 6.3 and more realistic models. This derivation will clarify the assumptions are behind Equation 6.3 and will guide us in estimating reasonable values for the free parameters in Equation 6.3, namely a,b,λ, and β. The main motivation was to explain the results of from the two-level model by using a simplified, vertically-averaged version of the model thermodynamic equations, and the assumptions used here are guided by the formulation and behavior of that model. One can also think of this model as relevant to the vertical average equations of the real atmosphere.

We treat the atmosphere as a single gray-body layer with effective temperature T_a, longwave emissivity $\varepsilon_a = 0.76$, and thermal capacity γ_a. The ocean is treated as a well-mixed layer with heat capacity γ_o. The resulting balance between shortwave, longwave, surface, and dynamical fluxes is shown in figure 6. 12, where the variables are defined. The equations are as follows:

$$\begin{aligned} \gamma_a \frac{\partial T_a}{\partial t} &= R_a + \varepsilon_a \sigma_B T_o^4 - 2\varepsilon_a \sigma_B T_o^4 + \lambda(T_o - T_s) + F \\ \gamma_o \frac{\partial T_o}{\partial t} &= R_o - \sigma_B T_o^4 + \varepsilon_a \sigma_B T_a^4 - \lambda(T_o - T_s) \end{aligned} \qquad \text{(EQ C.1)}$$

The combined surface turbulent latent and sensible heat fluxes are linearized, and λ is assumed to be constant. Latent heat is also assumed to be released locally. To close the system we need to specify a relation between T_a and T_s. Here we assume a constant atmospheric lapse rate and a constant effective longwave emission height, so that perturbation values $T_a' = T_s'$. This assumption is supported by the observation that at very low frequencies, temperature anomalies display a strongly barotropic vertical structure in the

troposphere.

We are interested only in the perturbations about the climatology, so the steady solution will not be shown. We construct perturbation equations by linearizing about the steady solution $\bar{T}_a$, $\bar{T}_o$. We also regroup terms so that the portion of the longwave flux which is proportional to the air-sea temperature difference is included with the other surface fluxes.

$$\gamma_a \frac{\partial T'_o}{\partial t} = R_a' + (\lambda + 4\varepsilon_a \sigma_B \bar{T}_o^3)(T_o' - T_s') - 4\varepsilon_a \sigma_B (2\bar{T}_a^3 - \bar{T}_o^3) T_a' + F'$$
$$\gamma_o \frac{\partial T'_o}{\partial t} = R_o' - (\lambda + 4\varepsilon_a \sigma_B \bar{T}_a^3)(T_o' - T_s') - 4\sigma_B (\bar{T}_o^3 - \varepsilon_a \bar{T}_a^3) T_o' \qquad \text{(EQ C.2)}$$

Note that Eq. C.2 is in the same form as Eq. 6.1, provided we assume that $R_a' = R_o' = 0$. This is an extremely good approximation in the 2-level model because the effects of clouds are not included.

The parameters may now be estimated. If we choose $T_a' = 270\text{K}$, and $T_o' = 285\text{K}$, we have (in units of $\text{Wm}^{-2}\text{K}^{-1}$): $c_a = 3.9$, $c_o = 3.4$, $\lambda_a = 2.8$, and $\lambda_o = 1.9$. The surface flux coefficient, λ, can be estimated from the linear regression of the sensible+latent fluxes vs. the ocean-atmosphere temperature difference. Estimates for λ as a function of latitude are shown in figure 6.7. I will choose $\lambda = 20\,\text{Wm}^{-2}\text{K}^{-1}$. The small and negative values in the tropics are due to the fact that at these latitudes in the 2-level model the surface fluxes are primarily determined by wind speed.

VITA

Joseph James Barsugli was born in Los Angeles, California on Sept. 2, 1960. He attended Cherimoya Avenue Elementary School, Walter Reed Junior High School, and North Hollywood High School. He received a B.A., *magna cum laude*, in Physics at Harvard University in 1982.